Towards Extracellular Vesicle Based Gene Therapy for Huntington's Disease



Aisling O'Loughlin

Thesis submitted for the degree of Doctor of Philosophy

Department of Physiology, Anatomy and Genetics, University of Oxford

University College

Hilary 2016

Towards Extracellular Vesicle Based Gene Therapy for Huntington's Disease

A Thesis Submitted for the Degree of Doctor of Philosophy, Hilary term 2016

Aisling O'Loughlin, University College, University of Oxford

Huntington's disease (HD) can be regarded as a model neurodegenerative disorder to screen potential genetic based therapeutics and their carriers. It is an autosomal dominant disorder caused by a mutation in a single gene that leads to progressive neurodegeneration caused in part by protein misfolding. The mutation codes for an expanded polyglutamine tract within the Huntingtin gene (*HTT*) which leads to neuronal loss through a pathological cascade of events. Current treatment strategies include symptom management but no disease-modifying therapies exist.

Research has shown that nucleic acid based therapeutics aimed at decreasing *HTT* expression can prevent, or reverse, the phenotype. Translating such therapies to the clinic is hindered by the blood brain barrier (BBB) and the lack of an easily administrable, non-toxic, immunologically inert delivery vehicle capable of bypassing the BBB. This study examines a range of nucleic acid based therapeutics for their potency and toxicity, and evaluates extracellular vesicles (EVs) as a delivery vehicle through investigation of the biodistribution of brain targeted EVs and an analysis of EV loading.

A small interfering RNA (siRNA) targeting a region upstream of the repeat induced potent non-toxic silencing of *HTT*. In examining EVs as a carrier for therapeutics for neurological diseases including HD, it was found that targeting can increase brain accumulation of EVs but that the physiological characteristics of EVs which make them susceptible to clearance by the reticuloendothelial system (RES) must be further evaluated to bioengineer modified EVs to avoid fast clearance. Lastly, loading by electroporation was found to induce siRNA aggregation which can lead to overestimation of loading by increasing siRNA content in an ultracentrifugation pellet, but cholesterol-conjugated siRNA mixed with EVs was capable of generating silencing *in vitro*.

This thesis examined EV based treatment for HD through the selection of a nucleic acid cargo to silence *HTT*, and examination of EVs as a delivery vehicle via biodistribution and loading studies. If the loading can be optimised and fast clearance avoided, there is promise in the use of EVs as a carrier of siRNA for HD.

Acknowledgements

Firstly, I would like to thank my Supervisor Professor Matthew Wood as well as Dr. Imre Mäger and Dr. Miguel Varela for their support, help and advice throughout this project. Their insightful comments and guidance have been invaluable in pursuing this work.

I am also grateful to the Wellcome Trust for their generous funding of the Doctoral Programme in Neuroscience at Oxford.

I would like to express my appreciation to every member of the Wood Lab for helping to make my time here one that I will never forget. I would like to thank Dr. Pieter Vader in particular for his important input with the exosome side of the project, and Dr. Samir El Andaloussi for advice throughout. Thank you also to Dr. Graham McClorey for guidance with the exon skipping project, to Dr. Corinne Betts and Dr. Suzan Hammond for performing injections, and to Fiona Lee for help with NTA.

I would also like to extend my thanks to all of the friends I have made in Oxford who have helped to ensure that I loved my time here. A special mention for my coffee/wine buddies Rozzy, Ellie, Laura and Damien for providing many laughs, celebrations and commiserations along the journey. Outside of Oxford my friends from home in particular the Loreto girls and the "Nerd Herd" from UCD have always listened when it seemed like things were not going quite as planned and also shared in a lot of fun along the way. To Paul and Theresa, we embarked on our PhDs together and I wish you could have finished yours, but as some of the first friends I made in Oxford I will never forget the times we shared, particularly Paul's infectious laugh and sheer love of Science.

I would like to thank my family for always believing in me and encouraging me to do my best. This thesis could not have been completed without their unwavering support amidst many calls to "keep your head". To Nana for keeping me in her thoughts and prayers. I wish my late grandparents could have seen the finished product.

Finally, I would like to thank Tom, for always brightening up my day and making me smile. Thank you for everything you have done over the last two years, and particularly for doing everything possible to support me and keep me sane in the final stretch!

Is fiú agus is féider.

Fanfaidh na cuimhní cinn liom go deo.

Declaration

The work presented in this thesis was undertaken at the Department of Physiology, Anatomy and Genetics, University of Oxford, in the laboratory of Professor Matthew Wood. All work presented is my own with the following exceptions where work was carried out in close collaboration: 1) The studies involving the LNAs and CRISPRi in Chapter 3 were performed in collaboration with Dr. Miguel Varela and Sabrina Heman-Ackah respectively, both members of the Wood Lab, University of Oxford. The design of the exon skipping oligonucleotides in the same chapter was carried out in collaboration with Dr. Graham McClorey, Wood Lab, University of Oxford. 2) The *in vivo* biodistribution study and *in vitro* blood brain barrier model uptake assay in Chapter 4 were carried out in collaboration with Oscar Wiklander and Joel Nordin of Karolinska Institutet, and Dr. Christopher Untucht of AbbVie respectively. In each case experimental design, cell culture and targeted EV production were performed in Oxford by Aisling O'Loughlin and EVs were shipped to these collaborators for injection or flow cytometry uptake assays. 3) The electron microscopy in Chapter 5 was performed in collaboration with Dr. Kariem Ezzat, Wood Lab, University of Oxford. This work has not been submitted for any other degree at this university or any other institution.

This thesis contains approximately 46,700 words.

List of Abbreviations

ACTB	β-Actin
AD	Alzhiemer's Disease
ANOVA	Analysis of Variance
ASO	Antisense Oligonucleotide
BBB	Blood Brain Barrier
cc-siRNA	Cholesterol Conjugated Small Interfering Ribonucleic Acid
cDNA	Complementary Deoxyribonucleic Acid
CNS	Central Nervous System
CRISPR	Clustered Regularly-Interspaced Short Palindromic Repeats
CRISPRi	Clustered Regularly-Interspaced Short Palindromic Repeats Interference
DC	Dendritic Cell
DiR	DiIC18(7); 1,1'-Dioctadecyl-3,3,3',3'Tetramethyl-indotricarbocyanine Iodide
dNTP	Deoxynucleotide Triphosphate
dsRNA	Double Stranded RNA
ELAVL1	Embryonic Lethal, Abnormal Vision, Drosophila like-1 (also known as HuR)
ESE	Exonic Splicing Enhancer
EV	Extracellular Vesicle
FBS	Foetal Bovine Serum
GAPDH	Glyceraldehyde 3-phosphate dehydrogenase
GFP	Green Fluorescent Protein
GM-CSF	Granulocyte Macrophage Colony Stimulating Factor
HD	Huntington's Disease
HDL	High Density Lipoprotein
HEK293	Human Embryonic Kidney 293 Cells
hESE-MSC	Human Embryonic Stem Cell Derived Mesenchymal Stem Cell
HTT	Huntingtin
HuR	Human antigen R (also known as ELAVL1)
IL	Interleukin
iPSC	Induced Pluripotent Stem Cell

IRDye	Infrared Dye
IVIS	In Vivo Imaging System
Lamp2b	Lysosome Associated Membrane Protein 2b
LB	Lysogeny Broth
LDL	Low Density Lipoprotein
LNA	Locked Nucleic Acid
miRNA	MicroRNA
MPS	Mononuclear Phagocyte System
mRNA	Messenger RNA
MSC	Mesenchymal Stem Cell
mTOR	Mechanistic Target of Rapamycin
N2A	Neuro2A Neuroblastoma Cells
NTA	Nanoparticle Tracking Analysis
PBS	Phosphate Buffer Solution
PCR	Polymerase Chain Reaction
PD	Parkinson's Disease
qPCR	Quantitative Polymerase Chain Reaction
RES	Reticuloendothelial System
rpBMEC	Rat Progenitor Brain Microvascular Endothelial Cells
RRM	RNA Recognition Motif
RT	Reverse Transcription
RVG	Rabies Virus Glycoprotein
SEM	Standard Error of the Mean
sgRNA	Single Guide RNA
shRNA	Short Hairpin RNA
siRNA	Small Interfering RNA
SR	Serine/Arginine-Rich Proteins
TEM	Transmission Electron Microscopy
TfR	Transferrin Receptor
TSS	Transcription Start Site
TrkB	Tropomyosin Receptor Kinase B
WB	Western Blot

List of Figures

Figure 1.1 Schematic of Healthy Neuron Expressing Wild Type Huntingtin ……..…24

Figure 1.2 Schematic of Diseased Neuron in HD Expressing Mutant Huntingtin …....31

Figure 1.3 Schematic of the Mechanism of Action of Nucleic Acid Based Therapeutics.....47

Figure 1.4 Components of the Blood-Brain Barrier……..……..…..…50

Figure 1.5 Exosome Biogenesis……..……..…56

Figure 2.1 Structure of Lamp2B-RVG Targeting Peptide ……..…….…77

Figure 2.2 Design of Novel Transferrin Targeting Constructs ……..……...…78

Figure 2.3 Schematic of EV Isolation and Treatment Methods ……....…82

Figure 3.1 Identification of Optimal *In Vitro* Reference Gene for Human Fibroblasts…….....109

Figure 3.2 Identification of Optimal *In Vitro* Reference Gene for Human HEK293 cells……111

Figure 3.3 Investigation of siRNA Treatments for Huntingtin Knockdown…..…...…113

Figure 3.4 Investigation of Antisense Oligonucleotide Treatments for Huntingtin Knockdown……...…116

Figure 3.5 Investigation of Multigene Oligonucleotide Treatments for Huntingtin Knockdown……...…118

Figure 3.6 Predicted Sequence Following Exon Skipping of Huntingtin Exon 3..…119

Figure 3.7 Determination of Potential Sequences for Exon Skipping Oligonucleotides to Skip Huntingtin Exon 3 using ESEFinder ……...121

Figure 3.8 Validation of Potential Sequences for Exon Skipping Oligonucleotides for Skipping Exon 3 using RESCUE-ESE……..124

Figure 3.9 Investigation of Exon Skipping Treatments for Huntingtin Knockdown...126

Figure 3.10 Gene Specific Reverse Transcription PCR ……..…128

Figure 3.11 Determination of N-terminal Fragment Generation Following Exon Skipping Treatment ……..……129

Figure 3.12 Investigation of shRNA Treatments for Huntingtin Knockdown…….131

Figure 3.13 Investigation of CRISPRi for Huntingtin Knockdown ……134

Figure 3.14 Quantification of Huntingtin Protein Following Treatments for Huntingtin Knockdown ……..137

Figure 3.15 Visualisation of Mutant and Wild-type Protein Levels following Treatments for Huntingtin Knockdown ……...……140

Figure 3.16 Investigation of Cell Viability following Treatments for Huntingtin Knockdown……...……142

Figure 4.1 DiR Labelling Co-Localizes with EVs and does not Alter EV Morphology……...157

Figure 4.2 Biodistribution of HEK293 and Dendritic Cell Derived EVs ……...…160

Figure 4.3 Characterisation of Bone Marrow Dendritic Cell Derived Extracellular Vesicles with and without RVG ……...…162

Figure 4.4 Characterisation of DiR labelled EVs Derived from Bone Marrow Dendritic Cells Transfected with RVG ……163

Figure 4.5 Biodistribution of RVG Targeted and Untargeted Bone Marrow Dendritic Cell Derived EVs ……..……165

Figure 4.6 RVG increases Targeting to Acetylcholine-Receptor Rich Tissues Including the Brain ……...……166

Figure 4.7 Biodistribution of RVG and non-RVG Bone Marrow Dendric Cell Derived EVs in Allogenic and Syngenic Recipients ……..……167

Figure 4.8 Distribution of RVG and non-RVG Bone Marrow Dendritic Cell Derived EVs in Allogenic and Syngenic Recipients in the Brain ……..……170

Figure 4.9 Characterisation of HEK293 Derived Extracellular Vesices …….……176

Figure 4.10 Characterisation of EVs from HEK293 Cells Transfected with pBa.TfR.GFP, pBa.TfR.GFP-EPRNEEK, pBa.TfR.GFP-G7 and pBa.TfR.GFP-RVG and confirmation of GFP expression ……179

Figure 4.11 Biodistribution of DiR Labelled EVs from HEK293 Cells Transfected with pBa.TfR.GFP, pBa.TfR.GFP-EPRNEEK, pBa.TfR-G7 and pBa.TfR-RVG ……...…181

Figure 4.12 Brain Distribution of DiR Labelled EVs from HEK293 Cells Transfected with pBa.TfR.GFP, pBa.TfR.GFP-EPRNEEK, pBa.TfR-G7 and pBa.TfR-RVG…...182

Figure 4.13 Dynamic Light Scattering of PKH26 or non-PKH26 labelled EVs ……184

Figure 4.14 Flow Cytometry Uptake Results on b.END3 Cells ……..…185

Figure 4.15 Flow Cytometry Analysis of rpBMECs Treated with EVs from Cells Transfected with Brain Targeting Constructs ……...…187

Figure 5.1 Schematic of Experimental Plan to Test Extracellular Vesicle siRNA Delivery ……202

Figure 5.2 Characterisation of Dendritic Cell Derived Extracellular Vesicles…..…..204

Figure 5.3 Characterisation of Neuro2A Derived Extracellular Vesicles ……...…205

Figure 5.4 Cholesterol Conjugated siRNA Retention Following Electroporation …..208

Figure 5.5 Identification of Optimal *In Vitro* Reference Gene for Murine Neuro2A cells……210

Figure 5.6 Identification of Optimal *In Vivo* Reference Gene ……211

Figure 5.7 Treatment of HD fibroblasts with Dendritic Cell Derived Extracellular Vesicles ……213

Figure 5.8 Treatment of Neuro2A cells with Dendritic Cell Derived Extracellular Vesicles ……..…..215

Figure 5.9 Treatment of Neuro2A cells with Neuro2A Cell Derived Extracellular Vesicles ……217

Figure 5.10 Treatment of HEK293 cells with Dendritic Cell Derived Extracellular Vesicles ……...….219

Figure 5.11 *In Vivo* Delivery of siRNA by RVG Targeted DC Derived EVs Loaded via Electroporation……..……...…….....222

Figure 5.12 Validation of Cholesterol Conjugated siRNA …….224

Figure 5.13 Levels of Fluorescent cc-siRNA Secreted in Cell Culture Medium.....226

Figure 5.14 Cholesterol Conjugated siRNA Retention Following Electroporation.…228

Figure 5.15 Treatment of HEK293 cells with Neuro2A-derived Extracellular Vesicles Mixed with Cholesterol Conjugated siRNA ……230

Figure 5.16 siRNA Retention in Pellet with Varying Extracellular Vesicle:Cholesterol Conjugated siRNA Ratio ……..……233

Figure 5.17 siRNA Retention in Pellet Following Mixing with Cholesterol Conjugated siRNA with Varying Incubation Temperature …….……236

Figure 5.18 siRNA Retention in Pellet Following Mixing with Cholesterol Conjugated siRNA with Varying Incubation Time ……..…238

Figure 5.19 siRNA Retention in Pellet Following Mixing with Cholesterol Conjugated siRNA with Varying Incubation Volume …….……240

Figure 5.20 siRNA Retention in Pellet Following Mixing with Cholesterol Conjugated siRNA at Optimised Conditions ……...…242

Figure 5.21 Characterisation of Neuro2A-derived Extracellular Vesicles Following Incubation with Cholesterol Conjugated siRNA ……..…243

Figure 5.22 Treatment of HEK293 cells with Neuro2A-derived Extracellular Vesicles Mixed with Cholesterol Conjugated siRNA at Optimised Conditions ……245

Figure 5.23 Dose Response of Treatment of HEK293 cells with Neuro2A-derived Extracellular Vesicles Mixed with Cholesterol Conjugated siRNA at Optimised Conditions……..…247

Figure 5.24 Duration of Silencing of Treatment of HEK293 cells with Neuro2A-derived Extracellular Vesicles Mixed with Cholesterol Conjugated siRNA at Optimised Conditions…….……249

List of Tables

Table 1.1 List of Drugs which are Undergoing or have Recently Undergone Clinical Trials……35

Table 1.2 Drugs in Preclinical Development for HD ……...…….37

Table 1.3 Subcategories of Membrane Vesicles ……...……54

Table 1.4 Currently used Gene Therapy Vectors and Associated Advantages and Disadvantages …….60

Table 2.1 List of siRNAs……...….72

Table 2.2 List of LNA ASOs……..73

Table 2.3 List of Exon Skipping Oligonucleotides……...…….74

Table 2.4 List of sgRNAs for CRISPRi plasmids……..75

Table 2.5 List of shRNA Insert Sequence……..……76

Table 2.6 List of Primary Antibodies for Western Blot……...…..88

Table 2.7 Primers for Gene Specific RT-PCR…….……..99

Table 2.8 List of Human qPCR Probes……101

Table 2.9 List of Murine qPCR Probes……101

Table 3.1 Table of Potency and Toxicity Profile of Best Candidate Nucleic Acid Based Therapeutics in Each Category……...……..151

Table 4.1 Proteomic Analysis of Transmembrane Proteins in EV Samples……174

Table of Contents

Chapter 1 Introduction 16
1.1 Neurodegenerative Disorders 16
1.2 Huntington's Disease 16
1.2.1 Genetic Mutation 18
1.2.2 Structure of Huntingtin 19
1.2.4 Disease Mechanism and Pathology 24
1.2.5 Current Treatment Options 32
1.2.6 Treatment Strategies in Development 33
1.2.7 Silencing Huntingtin as a Therapeutic Strategy 39
1.3 Gene Therapy 40
1.3.1 Small Interfering RNA 41
1.3.2 Antisense Oligonucleotides 43
1.3.3 Exon Skipping 44
1.3.4 CRISPR Interference 45
1.3.5 Short Hairpin RNA 46
1.5 Membrane Vesicles 51
1.5.1 Microvesicles 52
1.5.2 Apoptotic blebs 52
1.5.3 Exosomes 53
1.5.4 Exosome Biogenesis 54
1.5.5 Extracellular Vesicles as Natural Carriers of RNA 57
1.6 Drug Delivery Vehicles 59
1.6.1 Advantages of Extracellular Vesicles as Delivery Vehicles 62
1.6.2 Therapeutic use of Extracellular Vesicles as Delivery Vehicles for RNAi 63
1.6.3 Exploitation of Intrinsic Therapeutic Role of Extracellular Vesicles 68
1.7 Conclusion 71
1.8 Aims 71
Chapter 2 Materials and Methods 72
2.1 siRNA and ASO Sequences 72
2.1.1 siRNAs 72
2.1.2 ASOs 73
2.1.3 Exon Skipping Oligonucleotides 74
2.2 Plasmid Sequences for Therapeutic Silencing 75

2.2.1 CRISPRi Plasmid Sequences 75
2.2.2 shRNA Expression Plasmids 76
2.3 Brain Targeting Plasmids 77
2.3.1 Lamp2b-RVG Plasmid for Neuronal Cell Targeting 77
2.3.2 Transferrin Plasmids for Neuronal Targeting 78
2.4 Cell culture 81
2.4.1 Cell Lines 81
2.4.2 Dendritic cells 81
2.5 Transfections 83
2.5.1 Transfections of EV-Secreting Cells 83
Transfection of DCs with Targeting Plasmids 83
Transfection of Neuro2A Cells with Targeting Plasmids 83
Transfection of HEK293 Cells with Targeting Plasmids 84
2.5.2 Transfection with CRISPRi and shRNA Plasmids 84
2.5.3 Transfection of siRNAs and Antisense Oligonucleotides 85
2.6 Microscopy 86
2.7 Extracellular Vesicle Isolation 86
2.8 Extracellular Vesicle Characterisation 86
2.8.1 Nanoparticle Tracking Analysis 86
2.8.2 Western Blotting 87
2.8.2 Transmission electron microscopy (TEM) 88
2.9 Measuring Biodistribution of EVs 89
2.10 Flow Cytometry 90
2.11 Loading of siRNA by Electroporation into Extracellular Vesicles 90
2.11.1 For *In Vitro* Use 90
2.11.2 For *In Vivo* Use 91
2.12 Loading of Cholesterol-Conjugated siRNA by Treatment of Parent Cell 92
2.13 Loading of siRNA by Mixing Extracellular Vesicles with Cholesterol-Conjugated siRNA 92
2.13.1 Loading by Mixing - Varying Ratio of Extracellular Vesicles to cc-siRNA 92
2.13.2 Loading by Mixing – Varying Temperature 93
2.13.3 Loading by Mixing – Varying Incubation Time 93
2.13.4 Loading by Mixing – Varying Incubation Volume 93
2.14 Quantification of Loading Using Fluorescence 94
2.15 RNA Quantification 94

Cells 94

Tissues 95

Extracellular Vesicles and Supernatant 95

2.15.2 Quant-iT RiboGreen RNA Assay 96

2.15.3 cDNA Synthesis 96

2.15.4 Gene Specific Reverse Transcription 97

2.15.5 GeNorm Assays 99

2.15.6 Quantitative Real-Time PCR 100

For mRNA 100

For siRNA 101

2.16.1 Protein Extraction 102

2.16.2 Enzyme-Linked Immunosorbent Assays (ELISAs) 102

2.17 MTS Cell Proliferation Assay 103

2.18 Statistical Analysis 104

Chapter 3 Evaluation of Cargo for Suppression of Huntingtin Expression 105

3.1 Introduction 105

3.2 Results 107

3.2.1 Identification of Optimal *In Vitro* Reference Genes for Human Fibroblasts 107

3.2.2 Identification of Optimal *In Vitro* Reference Gene for HEK293 cells 110

3.2.3 Investigation of siRNA Treatments for Huntingtin Silencing 112

3.2.4 Investigation of LNA Treatments for Huntingtin Silencing 115

3.2.5 Investigation of Multigene Oligonucleotides for Huntingtin Silencing 117

3.2.6 Investigation of Exon Skipping Oligonucleotides for Huntingtin Silencing 119

3.2.7 Investigation of shRNAs for Huntingtin Silencing 129

3.2.8 Investigation of CRISPR Interference for Huntingtin Silencing 132

3.2.9 Protein Quantification and Visualisation Following Treatments to Reduce Huntingtin Expression 135

3.2.10 Measurement of Cellular Toxicity of Treatments to Silence Huntingtin 140

3.3 Discussion 144

Chapter 4 Investigation of the Biodistribution of Targeted Extracellular Vesicles 153

4.1 Introduction 153

4.2 Results 156

4.2.1 Investigation of DiR as a Means of Labelling Extracellular Vesicles 156

4.2.2 Biodistribution of Untargeted HEK293 and Dendritic Cell Derived Extracellular Vesicles 159
4.2.3 Characterisation of RVG Targeted and Untargeted Extracellular Vesicles 162
4.2.4 Characterisation of DiR Labelled RVG EVs 164
4.2.5 Biodistribution of RVG Targeted Extracellular Vesicles 165
4.2.6 Investigation of Differences in Biodistribution Arising from Allogeneic and Syngeneic Nature of the Primary Source Cells 168
4.2.7 Design of Novel Targeting Peptides 172
4.2.8 Characterisation of EVs from HEK293 Cells 176
4.2.9 Characterisation of the EVs Produced by HEK293 Cells Transfected with the Transferrin Receptor-Based Targeting Vectors. 178
4.2.10 Investigation of the Biodistribution of Transferrin Receptor Anchored Targeting Vectors 180
4.2.11 Investigation of Uptake of Extracellular Vesicles from Transferrin Receptor-Based Targeting Vector Transfected Source Cells 183
4.3 Discussion 188
Chapter 5 Loading of Extracellular Vesicles with siRNA 199
5.1 Introduction 199
5.2 Results 201
5.2.1 Characterisation of Extracellular Vesicles Derived from Different Cell Sources 201
5.2.2 Characterisation of siRNA Loading Following Electroporation 206
5.2.3 Identification of Optimal *In Vitro* and *In Vivo* Reference Gene 209
5.2.4 Dendritic Cell Extracellular Vesicle Delivered siRNA Failed to Silence Huntingtin *In Vitro* in Fibroblasts 212
5.2.5 Dendritic Cell Extracellular Vesicle Delivered siRNA Failed to Silence Huntingtin in Neuro2A cells 213
5.2.6 Neuro2A cell EV Delivered siRNA Failed to Silence Huntingtin in Neuro2A cells 215
5.2.9 Validation of Cholesterol Conjugated siRNA 222
5.2.10 Cells Transfected with Cholesterol Conjugated siRNA will Secrete siRNA 225
5.2.11 Quantification of Loading of Cholesterol Conjugated siRNA Following Electroporation 227
5.2.12 Loading by Mixing Extracellular Vesicles with Cholesterol Conjugated siRNA can Generate Knockdown *In Vitro* 228
5.2.14 Optimisation of Loading by Mixing by Varying Incubation Temperature 234

5.2.15 Optimisation of Loading by Mixing by Varying Incubation Time 236
5.2.16 Optimisation of Loading by Mixing by Varying Incubation Volume 238
5.2.17 Cholesterol Conjugated siRNA Retention Following Loading by Mixing Using Optimised Conditions 240
5.2.18 Characterisation of Extracellular Vesicles Following Incubation with Cholesterol Conjugated siRNA 242
5.2.19 Loading by Mixing Extracellular Vesicles with Cholesterol Conjugated siRNA at Optimal Conditions can Generate Knockdown *In Vitro* 244
5.2.20 Dose Response of Extracellular Vesicles Mixed with Cholesterol Conjugated siRNA at Optimised Conditions 245
5.2.21 Investigation of Duration of Silencing of Extracellular Vesicles Mixed with Cholesterol Conjugated siRNA at Optimised Conditions 248
5.3 Discussion 250
Chapter 6 Discussion 259
6.1 Summary of Results 259
6.1.1 Silencing Huntingtin 260
6.1.2 Investigation of the Biodistribution of Brain Targeted Extracellular Vesicles 262
6.1.3 Evaluation of Loading of Extracellular Vesicles with siRNA 265
6.2 Challenges in the Treatment of Huntington's Disease 268
6.3 Challenges in the Development of Extracellular Vesicle Based Therapeutics in a Clinical Setting for the Delivery of RNA 270
6.4 Concluding Remarks 277
References 279

CHAPTER 1 INTRODUCTION[i]

1.1 Neurodegenerative Disorders

In the Western world the population is aging and with it the prevalence of neurodegenerative disorders is increasing, while development of effective therapies is lagging behind[1]. Although significant progress has been made in elucidating the pathological processes responsible for neurodegeneration they are not yet fully understood. However, parallels among this group of devastating disorders have been found, including aggregation of specific proteins and oxidative stress[2,3]. Huntington's disease (HD) is one such neurodegenerative disorder and although it is not as prevalent as Alzheimer's disease (AD) or Parkinson's disease (PD), it is also not as complex in terms of the genetics behind the disease. It is caused by a mutation in a single gene and thus the nature of the mutation renders HD an excellent opportunity to develop and test targeted gene therapy and potential carriers of nucleic acid based cargos for a neurodegenerative disease.

1.2 Huntington's Disease

Also known as Huntington's Chorea, the first recorded epidemic of HD as "Dancing Mania" was in 1374, but it was not until 1872 that the first accurate description was made by George Huntington[4]. Today, the prevalence of HD is 5-10 in 100,000 in Western populations and the age of onset ranges from 25 to 85 with a mean age of onset of 40 years[5,6]. Death usually occurs 15-18 years following the manifestation of clinical

[i] Some of the information in this chapter is adapted from O'Loughlin *et al*., Exosomes and the emerging field of exosome-based gene therapy. Current Gene Therapy. 2012. Aug; 12(4):262-74 with permission.

symptoms[7]. A small subset of patients develop a juvenile form where symptoms appear before the age of 20[8]. These cases make up just 5% of HD cases and patients present with a more severe disorder and rapid progression[9].

The symptoms of HD are a triad of motor dysfunction, psychiatric disturbances and cognitive decline[10]. Motor symptoms early in the course of the disease include involuntary hyperkinetic choreiform movements with disturbances in gait, and later as the disease progresses bradykinesia and rigidity can become apparent, as well as difficulty with speech and swallowing[11]. Depression, apathy, mood swings, aggression, anxiety and social disinhibition are commonly associated psychiatric symptoms[12]. Deficits in cognition include lower mental flexibility, executive function, memory and attention[12]. These cognitive impairments, as well as the psychiatric disturbances, can occur years before the onset of the motor symptoms[13–15].

The search for the gene responsible for HD began in 1979 in an area with a high incidence of the disorder, Lake Maracaibo, Venezuela[16]. Since the disease follows an autosomal dominant pattern of inheritance, transmission through families was recorded, and blood samples were analysed. From these samples scientists identified a region on the short arm of chromosome 4; 4p16.3, which linked with HD[17]. A worldwide hunt for the gene lead to the discovery of the IT15 gene and mutation responsible for the disease over 10 years later[18].

1.2.1 Genetic Mutation

The IT15 gene, first cloned in 1993, contains 67 exons and codes for a 3144-amino acid protein huntingtin (HTT)[18]. Near the amino terminus is a dynamic polyglutamine stretch encoded by a CAG nucleotide repeat of variable length which is the site of the mutation responsible for the disease. This unstable CAG repeat is polymorphic with a range of 6-35 repeats in the healthy population. A CAG repeat length of 36-39 leads to reduced penetrance of the disease, that is only some individuals with CAG repeat lengths within this range develop the disease, but if over 39 repeats are present the disease is almost fully penetrant[10]. Within the normal population, an intermediate expandable repeat length of 27-35 CAG repeats is unstable through meiotic transmission, particularly during spermatogenesis and in such cases an allele within the disease range can be transmitted to offspring[19]. As well as the CAG repeat, the *HTT* gene has other polymorphisms such as single nucleotide polymorphisms (SNPs) and a CCG repeat which do not contribute to the disease but can link with the CAG triplet repeat[20–22].

The length of the CAG repeat, in addition to determining whether the disease will develop, is also responsible for most (50-70%) of the variation in age of onset, which correlates with repeat length[17,23]. Although clinical manifestation usually occurs in mid-life, cellular damage can precede this as induced pluripotent stem cells from patients develop phenotypic consequences of the repeat and alterations in cognitive function are detectable up to 15 years prior to diagnosis[14,24].

1.2.2 Structure of Huntingtin

The *HTT* gene encodes a 348-kDa protein. The high molecular weight has hindered efforts to determine the entire structure via crystallography and mass spectrometry so that details of only part of the structure are known. It is well conserved in mammals[25]. The N-terminal is the most studied portion as it contains the site of the HD mutation. 17 amino acids precede the polyglutamine expansion, which is in turn followed by a proline-rich domain (PRD). The N-terminal 17 amino acids forms an amphipathic α-helix[26]. This region is subject to a range of post-translational modifications (PTMs) including acetylation, ubiquitination and sumoylation at lysines 6, 9 and 15 and phosphorylation at serines 13 and 16 which alter HTT clearance and subcellular localisation[27]. Sea urchins express a primitive polyglutamine stretch indicating that in evolutionary terms this sequence appeared before the divergence of echinoderms and chordates, approximately 500 million years ago, and has expanded gradually in the latter since[28]. Humans have the longest and most polymorphic stretch. The structure of the polyglutamine stretch is flexible, and has been found by X-ray crystallography at atomic resolution to adopt several conformations including α-helix, random coil and extended loop[29]. The PRD forms a rigid proline-proline helix[29]. Due to the more recent occurrence of this domain in evolution it has been hypothesised that it may function to stabilise the expanded polyglutamine stretch and maintain it in a non-aggregated form, as well as being involved in the control of HTT turnover and protein-protein interactions[30,31].

The structure of the remaining portion of the HTT protein is less well characterised as the mutation occurs in exon 1, but consists of ordered clusters of α-helical ~40 amino acid consensus sequences known as Huntingtin elongation factor 3 protein phosphatise 2A and yeast kinase TOR1 (HEAT) repeats. Each HEAT repeat adopts the configuration of

antiparallel α-helices with a helical hairpin which act as binding sites for protein-protein interactions[32,33]. Together these HEAT domains may form a superhelical structure or α-rod with a continuous hydrophobic core[32]. Between individual HEAT repeats there are expanses of disordered structure which are potential sites for some of the many PTMs HTT undergoes including phosphorylation, sumoylation, ubiquitination, acetylation and palmitoylation offering a high level of complexity to HTT interactions[27]. In addition, there are putative nuclear localisation motifs though no classical nuclear localisation signal has been identified[34]. There are also nuclear export and cytoplasmic retention signals[35,36].

1.2.3 Physiological Function of Wild Type Huntingtin

HTT is ubiquitously expressed with highest levels of expression in the neurons of the central nervous system (CNS) and testes[37]. Within the brain, it is most enriched in cortical pyramidal neurons in layers III and V which project to striatal neurons and also in interneurons of the cortex, hippocampus and cerebellum[38]. Temporally, it is known to be expressed from before birth through to and throughout adulthood[39]. Subcellularly, it is mostly cytoplasmic and has been found in a number of regions and co-localised with organelles. These include the nucleus, endoplasmic reticulum, Golgi apparatus and endosomes, and within neurites at synapses associated with vesicular structures including clathrin-coated vesicles, caveolae and microtubules[40–43]. It is capable of shuttling between the nucleus and cytoplasm[40–43].

The physiological role of wild-type HTT is yet to be fully elucidated but it is implicated in many cellular processes which are summarised in Figure 1.1 and include roles from

early in the life of a neuron through to its role in inhibiting apoptosis[44]. Its role in neurogenesis includes a potential involvement in cell cycle progression where it is thought to be involved in spindle orientation as it is targeted to the spindle poles in neurogenesis[45]. It can also influence production of growth factors such as brain derived neurotrophic factor (BDNF)[46]. The role of HTT as an anti-apoptotic has been identified in both *in vitro* and *in vivo* studies. A pro-survival role of HTT can protect cells from toxic stimuli while cells with a reduction of wild type HTT are increasingly susceptible to apoptosis[44,47,48]. HTT prohibits formation of an apoptosome, thus preventing the subsequent activation of caspase-3 and caspase-9[44,48]. HTT can also interact with casepase-3 itself and prevent it performing proteolysis[49]. HTT has also been identified as a substrate for Akt, the serine/threonine kinase involved in activation of pro-survival pathways[50].

HTT is involved in transcriptional control where the polyglutamine stretch has been hypothesised to form a polar zipper structure which can bind transcription factors where polyglutamine tracts are also found[51]. HTT has been shown to bind to and interact with transcriptional activators and repressors including the cAMP-response element (CREB)-binding protein (CBP), p53 and RE1-Silencing Transcription factor (REST)[52,53]. Through these interactions, HTT is well placed to influence the transcription of many genes with far reaching cellular consequences. It has also been implicated in RNA trafficking[54].

HTT interacts with the molecular motor machinery involved in trafficking vesicles. It is not known whether this is through dynein directly or indirectly via Huntingtin-associated protein 1 (HAP1)[55,56]. Through these interactions, HTT is involved in the transport of organelles, axonal transport at synapses where it has been shown to associate with

microtubules, caveolae, synaptosomes, synaptic vesicle precursors and clathrin-coated vesicles[43]. Overexpression of HTT increases the transport efficiency within cells while knockdown reduces organelle transport[56,57]. HTT is involved in autophagy which could be a result of its role in transport as HTT influences the retrograde transport of autophagosomes[58]. HTT is also thought to be involved in synaptic activity. HTT binds post-synaptic density protein 95 (PSD95), a player in synaptic transmission and part of the family of proteins which bind N-methyl-D-aspartate (NMDA) and kainate receptors at the postsynaptic density[59].

HTT is also involved in endocytic recycling and trafficking. The interaction of HTT either directly or indirectly with dynamin 1 again aids in this process[60]. Through the study of transferrin uptake it was established that endocytosis is reduced if HTT cannot interact with dynamin 1[60]. HTT may interact with and be part of a complex mediating endocytosis and vesicle trafficking with dynamin, endophilin-A3, endophilin-B1 and amphiphysin and interacting with the GTPase Rab 11[61]. Rab11 has a known role in vesicle recycling during endocytosis and HTT silencing decreases the attachment of Rab11 to membranes and it's activity[62].

Over 350 proteins which interact with HTT have been identified to date and they can be divided into subgroups based on their functions including proteins involved in gene transcription, intracellular signalling, trafficking, endocytosis, RNA splicing and metabolism[63]. Some of these proteins interact selectively with either wild-type or mutant HTT (mHTT)[64].

The N-terminal portion of the protein plays a role in membrane targeting, chaperone binding, trafficking, retention in the endoplasmic reticulum, nuclear export and regulates PTMs[26,35]. The function of the polyglutamine stretch is not known although its deletion in mice increases autophagy and longevity[65]. The PRD is thought to be involved in protein-protein interactions but its deletion has no profound effect on mouse behaviour[66].

PTMs can affect the function of the protein. Ubiquitination at the amino terminus of lysines 6, 9 and 15 can destabilise the protein and target it to the proteasome while sumoylation at the same sites can increase stability and decrease aggregation[67,68]. Phosphorylation appears to be neuroprotective. Phosphorylation at Serine 421, 434, 1181 and 1201 by Akt or cylin-dependent kinase 5 alters intracellular transport and decreases caspase cleavage at residue 513 limiting aggregate formation and toxicity[69–71]. Phosphorylation of another site at serine 536 decreases calpain cleavage also reducing the toxicity of mHTT[72]. Phosphorylation at serines 13 and 16 can increase neuronal localisation and with regard to the mutant protein, phosphorylation of these sites is thought to decrease mHTT aggregation and the associated neurodegeneration. In mice where these serines are mutated to phosphomimetic aspartate the pathogenesis of mHTT is abolished, but it is retained if they are mutated to alanine which is resistant to phosphorylation[73,74]. Sumoylation can alter the subcellular localization, stability and activity of HTT[75]. Palmitoylation at cysteine 214 aids in vesicular trafficking[76]. In addition, acetylation of the mutant at lysine 444 has been proposed to direct mHTT towards clearance via the autophagic-lysosomal pathway[77].

To summarise, the functions of HTT are multifaceted **(Figure 1.1)**. It can affect the gene expression network, neurogenesis, transport and recycling of vesicles and apoptosis.

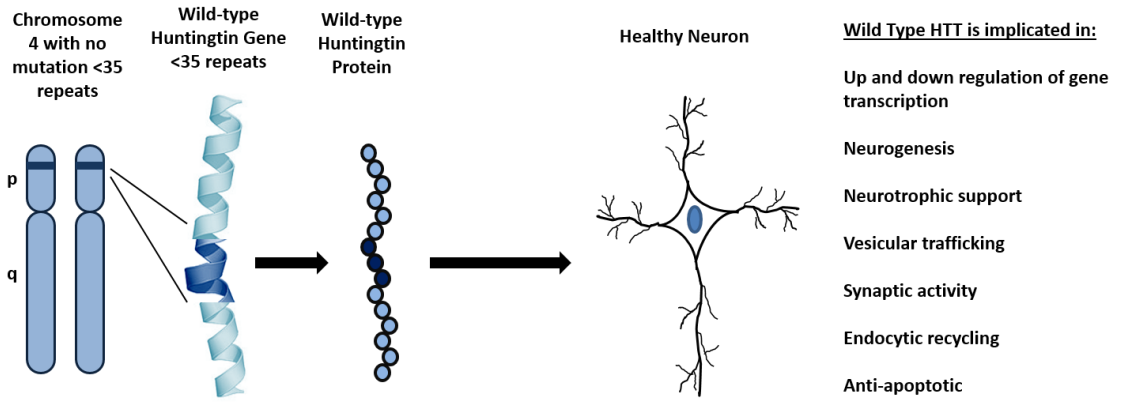


Figure 1.1 Schematic of a Healthy Neuron Expressing Wild Type Huntingtin. Wild type HTT with under 35 CAG triplet repeats on the short arm of chromosome 4 does not code for the mutant elongated polyglutamine (polyQ) stretch. The wild type protein is implicated in many physiological processes within the cell although its role is yet to be fully exemplified. It is thought to be involved in the control of gene expression, spindle orientation in neurogenesis, regulation of neurotrophic support particularly involving BDNF, vesicular and organelle trafficking, synaptic activity, endocytic recycling and is anti-apoptotic.

1.2.4 Disease Mechanism and Pathology

The CAG triplet repeat in HD encodes for a mutant HTT (mHTT) protein with an expanded polyglutamine tract close to the amino terminus. This tract causes aberrant folding of the protein which cannot be processed in the correct way by the cell. There has been debate regarding whether the nature of the pathology resulting from the mutation is due to a loss or gain of function. Complete deletion of wild-type HTT is embryonically lethal but there is evidence that suppression of expression is well tolerated in the adult[78,79]. However, even given an inability of mHTT to perform some of the functions of wild type HTT described above due to the expansion, the primary issue in HD seems to be a toxic gain of function by the mutant protein, or fragments thereof **(Figure 1.2)**[80,81]. This gain

of function causes cellular dysfunction, neuronal inclusions - a pathological hallmark of the disease - and brain atrophy[80].

The exact mechanism by which the toxic gain of function of mHTT leads to neuronal degeneration is not fully understood but HTT aggregation connects HD to other neurodegenerative diseases in which protein aggregation plays a role in pathology. These diseases include PD, AD, amyotrophic lateral sclerosis and spongiform encephalopathies[3]. The polyglutamine stretch in mHTT has the capacity to form abnormal conformations which increase the likelihood of aggregation. HTT rich inclusions have been identified in cells, animals models and patients expressing mHTT or mHTT fragments[82–85]. The inclusions vary in size from small clusters of amyloid fibrils to those of sufficient size to be viewed under a light microscope[84,86]. The inclusions are predominantly found in the nucleus, but also occur in the cytoplasm, dendrites and axon terminals[87].

The seeding of these aggregates is increasingly favourable as the repeat length increases which could contribute to the effect of the repeat length on age of onset described above[88]. There is evidence that small oligomers of mHTT monomers self-associate into α-helical clusters, which grow into non-β-oligomers[89]. These may then reorganise at a rate proportional to the repeat length into stable β-sheet rich amyloid fibrils[89]. The structure of the mHTT fragments which generate toxicity in HD are not known. Some research suggests that the presence of large inclusions causes toxicity, but more recent work indicates that these inclusions could actually be protective, sequestering the soluble toxic species[82,83]. A similar mechanism has gained weight in the field of AD where studies show that oligomers may be the toxic species involved in the neurodegeneration[90].

mHTT fragmentation is thought to play an important role in the pathogenesis of HD[91,92]. N-terminal fragments containing the abnormal polyglutamine stretch have been identified in all murine models expressing full-length mHTT and in human brains, and expression of a short fragment of mHTT has been shown to be sufficient to produce a HD phenotype in model animals[92,93]. Further evidence of N-terminal fragment involvement is the staining of neuronal inclusions with antibodies directed towards the N-terminus of mHTT but not the C-terminus and western blot analysis of short N-terminal fragments in patient and mouse model brains[85].

Another parallel to AD is the enzymatic generation of a pathogenic truncated fragment. Proteolytic cleavage of HTT occurs through cleavage by caspases and calpains and could play a role in the toxicity[72,94]. Perhaps the most studied fragment is a ~100 amino-acid N-terminal fragment consisting of the 17 N-terminal amino acids, the polyglutamine expansion and the PRD[95]. This fragment is involved in the formation of oligomers and alterations in its conformation due to the repeat expansion could be involved in the disease process, though the role is debated[89]. Some C-terminal fragments have also been identified and are thought to mediate toxicity through impaired interaction with dynamin 1 which could alter the homeostasis of the endoplasmic reticulum[60].

The fate of a cell may depend on whether accumulation of the mHTT protein or a mHTT fragment reaches a concentration threshold to trigger self-aggregation and associated pathological events. This is accelerated by hydrophobic interactions within the amphipathic α-helical structure of the 17 amino acids upstream of the repeat[96]. As mentioned, the CAG repeat length is thought to be important for initiating the aggregation in a seeding or nucleation effect as in juvenile HD cases there is more widespread

degeneration than in adults with fewer repeats[97]. The level of mHTT expression and the amount of fragmentation are also contributing factors. This seeding effect has led to the hypothesis of a prion-like mechanism of cell to cell transmission, another parallel with AD[98]. Small amyloid fibrils of polyglutamine proteins can be taken up *in vitro* through the plasma membrane and recruit endogenous polyglutamine proteins including mHTT exon 1 into aggregates[99]. This seeding is not limited to mHTT and also encourages the recruitment of other polyglutamine proteins which could contribute to the pathogenesis via sequestration and depletion of other vital proteins[100].

It is possible that the polyglutamine stretch alters PTMs as a change in the structure caused by the expansion could alter the accessibility to PTMs. PTMs of mHTT can alter the toxicity of mHTT through triggering changes in conformation, likelihood of aggregation, subcellular localisation and clearance[67,69,72,75,77]. As well as the PTMs mentioned above, phosphorylation at threonine 3 can alter toxicity[73].

mHTT and its fragments are increasingly localised to the nucleus in HD which increases its toxic effects partly through transcription modification[101]. Particular gene expression patterns have been found in animal models and HD brains in gene expression arrays[102]. *In vitro* data confirms that mHTT alters gene transcription[101,103,104]. This could be through the activators and inhibitors which also interact with the wild-type protein such as CBP or REST[53,104]. Direct interaction between mHTT and DNA has also been suggested[105]. This aberrant transcription could be responsible for another contributing factor to the pathogenesis of HD: a lack of neurotrophic support which has been reported with low transcription of BDNF in HD patients[106].

Due to the reported role HTT plays in vesicular trafficking, it is not surprising that part of HD pathogenesis is a dysfunction in trafficking. This further affects neurotrophic support as trafficking of BDNF has been found to be altered in HD[107]. In this role mHTT also impairs the correct functioning of the wild type protein[108].

Chronic expression of mHTT can overwhelm the physiological clearance mechanisms of the cell, the proteostasis network[109]. Levels of chaperones for the clearance machinery are limited as the disease progresses[110]. Endoplasmic reticulum recycling, the ubiquitin-proteasome system and autophagy are defective[111–113]. Alterations in function of the ubiquitin system have been noted in mouse models and human *post mortem* brain samples although it is not clear whether this is part of the disease mechanism or a normal response of the cell to the stress of the abnormal protein[114]. Evidence suggests it precedes inclusion formation[113]. Clearance by autophagy is decreased as mHTT can impede target recognition and hinder clearance[115]. In addition, a potentially stress relieving mechanism for the cell is inhibited, the heat shock response[116]. These systems require energy and can compromise cellular energy metabolism causing oxidative damage[117]. Mitochondrial dysfunction itself is implicated in HD with abnormalities in animal models and patients[118,119].

Once these toxic species are expressed, transcriptional regulation, ubiquitin proteasome activity, autophagy-lysosomal function and intracellular transport are altered; oxidative stress, mitochondrial dysfunction, neuroinflammation, excitotoxicity and apoptosis then follow[119]. These downstream resultant effects also play a role in other neurodegenerative diseases[120,121]. High levels of reactive oxygen species (ROS) have been identified in the HD brain and free radical production contributes to damage in animal models[118,122] .

Inflammatory markers of both the innate and adaptive immune response including cytokines and complement proteins are upregulated in HD[123,124]. Microglia are active in HD both prior to and post onset of symptoms and this correlates with the loss of neurons and disease severity[125]. Further evidence of glial cell involvement comes from expression of mHTT selectively in these cells co-cultured with neurons which can trigger neuronal death highlighting the role of mHTT in glial cells contributing to neuronal excitotoxicity[126]. Also, expression of mHTT in astrocytes in mice can cause a HD like phenotype alone or it can worsen a phenotype in an established model[127].

Most brain regions are affected in HD but the striatum and cortex are the most severely affected. A decrease in size of the striatum and cortical thinning have been reported 10 years prior to the onset of symptoms but worsen and can be predictive of clinical onset within 2 years of symptomatic development[128,129]. High levels of loss of striatal neurons have been reported, with up to 95% loss of GABAergic medium spiny neurons (MSNs), which project to the globus pallidus and substantia nigra[130]. Interneurons are mostly spared. There is also atrophy of the cerebral cortex, subcortical white matter, thalamus and certain hypothalamic nuclei[131].

The marked selective vulnerability of the striatal projection neurons to neurodegeneration in HD has sparked several hypotheses. A leading hypothesis is that they are most prone to damage from excitotoxicity from cortical glutamatergic projections. MSNs express different levels of NMDA receptor subunits compared with interneurons in the same brain region with MSNs expressing more NR2B/NR2A. Evidence to support this comes from the results of intrastriatal injection of glutamate agonists for NMDA and non-NMDA receptors (quinolinic acid and kainic acid respectively), which display the same

preferential toxicity to MSNs[132,133]. Prolonged NMDA receptor activation by glutamate in HD would increase exposure to intracellular calcium via NMDA associated calcium channels, leading to activation of calcium dependent enzymes and synthesis of nitric oxide[134]. Nitric oxide synthase triggers a cascade leading to neuronal damage. The reactive oxygen species (ROS) 3-nitropropionic acid can be administered to mimic a HD phenotype through inhibition of mitochondrial complex II. This facilitates increased ROS production and excitotoxic neuronal death selectively of MSNs in mouse models and patients which implicates oxidative stress in this preferential vulnerability[135].

MSNs are also thought to be more susceptible to decreases in neurotrophic support derived from projections from the cortex. As before, BDNF is implicated as MSNs have a high number of Tropomyosin receptor kinase B (TrkB) receptors, the receptors for BDNF[136]. One of the HTT interacting proteins, Ras homolog enriched in striatum (Rhes), is expressed mostly in the striatum and at lower levels in cortical areas affected in HD. It is thought to be involved in the selective vulnerability of MSNs, but it has not been clearly demonstrated to be expressed highly in MSNs compared to other striatal neurons while it is known to be expressed in some neurons which are less susceptible to degeneration in HD including granule cells of the cerebellum[137,138]. Although widely accepted that HD is a neurodegenerative disorder, certain pathological manifestations of the disease are mediated outside of the CNS such as muscle wasting, weight loss, metabolic impairments, endocrine dysfunction, cardiac problems and insulin sensitivity[124,139].

In summary, much of the pathogenesis of HD is caused by a toxic gain of function of the mutant elongated polyglutamine tract **(Figure 1.2)**. The toxic gain of function induces a pathological cascade of events including aberrant gene transcription, altered vesicular

signalling, aggregation, decreased neurotrophic support and is implicit in overwhelming the clearance mechanisms of the cell. These effects contribute to downstream excitotoxicity, mitochondrial dysfunction and oxidative stress. Most, but not all, of the pathology is in the brain. Therefore, when considering a therapy for HD, an ideal therapy would decrease HTT expression and target the brain preferentially, but not exclusively.

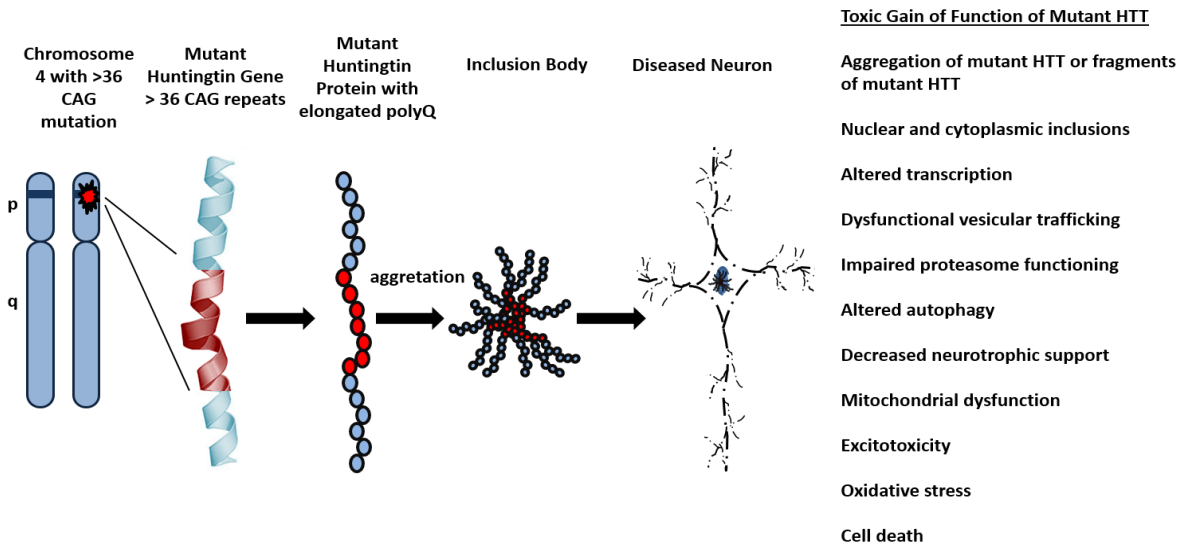


Figure 1.2 Schematic of a Diseased Neuron in HD Expressing Mutant Huntingtin. Mutant HTT with over 36 CAG triplet repeats on the short arm of chromosome 4 codes for a mutant elongated polyglutamine (polyQ) stretch. This causes cellular stress and toxicity through aggregation. Proteolytic cleavage generates short N-terminal fragments which are also susceptible to aggregation. These aggregates form intraneuronal, perineuronal and cytoplasmic inclusions. Mutant HTT alters gene transcription, affects vesicular trafficking, overwhelms the physiological clearance mechanisms of the cell including proteasome functioning and autophagy, decreases neurotrophic support and causes downstream mitochondrial dysfunction leading to excitotoxicity and oxidative stress. These pathological changes result in cell death and brain atrophy.

1.2.5 Current Treatment Options

It is now over 20 years since the mutation responsible for HD was identified but it is clear that even though HD is a monogenetic disorder, the multifaceted roles of HTT and the complex pathogenesis of HD mean that treatment is far from as simple as initially hoped. The drugs currently used are aimed at symptom management and although there are more in development, there is no treatment available which can halt the progression of HD.

The only FDA approved drug is tetrabenazine. It is thought to ameliorate the hyperkinetic symptoms such as chorea through inhibition of the vesicular dopamine transporter 2, but it has an unfavourable side effect profile[140]. Other aspects of the disease are managed solely by palliative care and require a collaboration between different fields including physiotherapy, speech therapy, nutritional therapy and occupational therapy[141]. Other drugs used for treating the symptoms of HD come from anecdotal clinical experience but several reports demonstrate the weak evidence supporting their use in managing HD and many are associated with side effects[142,143]. To choose the most effective treatments more systematically, in 2011 a number of instructions or algorithms for the treatment of certain aspects of HD; chorea, obsessive-compulsive behaviours and irritability were devised. However, they would recommend the same treatment for these symptoms regardless of the absence or presence of HD, and the specific recommendations depend on geographical location[144–146].

For chorea, this algorithm recommends tetrabenazine if there are no co-morbidities but an antipsychotic such as olanzapine or risperidone if the patient presents with the co-morbidities of psychosis, depression, aggressive behaviours or non-compliance[146]. Both

lines of symptom treatment are associated with side effects including sedation, apathy and swallowing impairment. If there is an inadequate response a combination of both treatments is advised. For irritability in HD, the guidelines recommend beginning treatment with an antipsychotic for aggressive behaviours or if the patient presents with psychosis and impulsivity, or alternatively a serotonin reuptake inhibitor if depression, anxiety or obsessive-compulsive behaviours are also indicated[144,145]. The antipsychotics recommended for this aggression and psychosis are the same as above for when the psychosis presents with chorea, and the antidepressants include citalopram, sertraline and paroxetine. Following dose optimisation the algorithm recommends adding adjuvant therapies if there is an insufficient response including benzodiazepines and mood stabilizing drugs. Since these drugs only target select symptoms, there is a need for development of new treatments to combat this disease.

1.2.6 Treatment Strategies in Development

Clinical trials have increased in recent years due to the lack of treatment options, however many fail to result in treatment recommendations[142]. The drugs in development for HD include drugs directed towards each stage in the pathogenic pathway. The drugs in clinical trials and preclinical development are summarised in Table 1.1 and 1.2 respectively.

The furthest in terms of phase of clinical trial are cysteamine (NCT02101957), co-enzyme Q10 (NCT00608881) and creatine (NCT00712426) all of which act to reduce excitotoxicity, as well as SD-809 ((NCT01795859), a derivative of the only approved drug for HD, tetrabenazine. The trials for creatine and coenzyme Q10 were the largest in

recruitment but closed early due to a lack of disease markers to identify efficacy. This deficiency of biomarkers and specific outcomes for studies in HD is a problem in implementing clinical trials and hinders the hunt for a therapeutic. The phase III study for RP103, delayed release cysteamine, is ongoing. Synthesised by Raptor Pharmaceuticals, it functions to increase synthesis and mobilization of cysteine, thereby increasing glutathione and limiting oxidative stress, inhibiting transglutaminase and heat shock protein response and increasing BDNF expression and secretion[147]. The phase III study by Auspex Pharmaceuticals of SD-809 (NCT01795859), a deuterated form of tetrabenazine and vesicular monoamine transporter 2 (VMAT2) inhibitor, is also ongoing.

So far, treatments are focused on the symptoms of HD. A different kind of therapy, based on antisense nucleic acid, which will be discussed later, is promising because it targets the expansion at the mRNA level and therefore tackles the cause of the pathology directly. A phase I/IIa safety trial of this nucleic acid based therapy, IONIS-HTT_{RX} , by Ionis Pharmaceuticals (NCT02519036) is the first therapy to reach clinical trials that is targeted to the first stage in the disease cascade, the decrease in expression of mHTT. The drug will be administered intrathecally. In addition to drugs, research is ongoing into foetal grafts, stem cell transplants and pallidal deep brain stimulation[148,149].

Trial Identifier	Mechanism of Action	Drug	Stage of Development	Outcome
NCT02519036	Targeting mHTT	IONIS-HTT_{RX}	Phase I/IIa	In recruitment
NCT00277355	Targeting caspases and mHTT proteolysis	Minocycline	Phase III	Treatment not futile as measured by TFC
NCT02074410	Correction of Transcriptional Dysregulation	OMS643762	Phase II	Well tolerated
NCT02197130		Sodium phenylbutyrate	Phase II	Indole metabolites detected in urine
NCT00608881	Targeting Mitochondrial Dysfunction, Antioxidants	Coenzyme Q10	Phase III	Study terminated due to futility
NCT00712426		Creatine	Phase III	Study terminated due to futility
NCT02101957		Cysteamine	Phase III	Change in UHDRS-TMS at 18 months
NCT00146211		Eicosapentaenoic acid	Phase II	Change in UHDRS-TMS at 18 and 36 months
NCT02336636		Resveratrol	Phase III	Change in caudate atrophy at 12 months
NCT01357681	Free Radical Scavenger	Epigallocatechin gallate	Phase II	Change in cognitive measures UHDRS at 12 months
NCT02231580	Targeting Excitotoxicity	BN82451B	Phase II	Safety and tolerability at 28 days
NCT01458470		Memantine	Phase II	No published results
NCT00277602		Riluzole	Phase III	No difference in outcome variables. Tolerability was acceptable

Trial Identifier	Mechanism of Action	Drug	Stage of Development	Outcome
NCT01795859	Inhibition of Monoamine Reuptake	SD-809	Phase III	Change in chorea scores at 2 weeks
NCT01451463		Tetrabenazine	Phase IV	Change in UHDRS, TMS and balance
NCT02006472	Targeting Behaviour	Pridopidine	Phase II	Change in UHDRS-TMS at 26 weeks
NCT01914965		Bupropion	Phase II	Decreased apathy
NCT01590888		PTB2	Phase II	Safe and well tolerated, potential benefit in executive function
NCT02215616	Immune Modulatory	Laquinimod	Phase II	Change in UHDRS-TMS at 1, 3, 6 and 12 month intervals
NCT00190450	Targeting Cell Loss	Foetal cells	Phase I	Mutant HTT aggregates found in neural grafts

Table 1.1 List of Drugs which are Undergoing or have Recently Undergone Clinical Trials. List of outcomes of clinical trials which are currently in progress or have recently ended. TFC (Total Functional Capacity score), Tinetti Mobility Test (TMT) and Unified Huntington's Disease Rating Scale (UHDRS) motor scores are routinely used to monitor progress in HD clinical trials.

Ref	Research Institute	Mechanism of Action	Drug	Outcome
[150]	Alnylam and Medtronic	Targeting mHTT	Non-allele selective siRNA with convection-enhanced delivery	Widespread, well tolerated distribution in the striatum and partial silencing of HTT in primates.
[79]	Medtronic		Non-allele selective siRNA with intrastriatal AAV delivery	Well tolerated partial suppression of wild type and mutant HTT long term (6 months) in primates.
[151]	Iowa University		Non-allele selective miRNA with intrastriatal AAV delivery	Partial well tolerated suppression of wild type and mutant HTT in the striatum in primates.
[152]	University of Masseteu-ssets and Alnylam		Non-alele selective intrastriatal AAV delivered cholesterol-conjugated siRNA	Less inclusions and increased survival in striatal neurons. Increased scores on motor tests following 1 dose in a murine model.
[153]	University Sangamo		Allele selective zinc finger protein intrastriatal AAV delivery	Dose dependent reduction in mHtt expression in the brain achieved, also less protein aggregation and improvement in motor performance measures in murine model.
[154]	A.B.Y. Fund Massachusetts General Hospital	Autophagy Enhancers/ Drugs which Increase Clearance	C2-8	Penetrates BBB. Less aggregates and atrophy and improved motor performance in murine model. Non-toxic.
[155]	RIKEN Brain Science Institute		Trehalose	Decreased aggregation, improved motor dysfunction and lifespan of murine model. Non-toxic.
[156]	CHDI	Correction of Transcription Dysregulation	HDACi 4b inhibition	Improved HD phenotypes. Also improved phenotype of offspring.
[157]	Aton Pharma		Suberoylanilide hydroxamic acid	Crossed the BBB, increased histone acetylation in the brain and improved motor deficit in murine model

Ref	Research Institute	Mechanism of Action	Drug	Outcome
[158]	McMaster University	Alteration of PTMs	GMI gangliosidase by intraventricular infusion	Decreased mHtt toxicity and 1restores normal function in murine model.
[159]	Irvine	Upregulation of Chaperone Proteins	ApiCCT1	Decreased toxicity in murine model.
[160]	Panjab University	Targeting Mitochondrial Dysfunction	4-HT	Decreased damage of 3-nitropropionic acid used to generate rat model. Improved cognitive function and motor deficits.
[161]	UCSF	Immune Modulatory	GW405833	Reduced CNS inflammation, synapse loss and improved motor impairments and lifespan in murine model.
[162]	Johns Hopkins Stanford	Increased Neurotrophic Support	TrkB agonists-7,8 – DHF and 4'-DMA-7,8-DHF	Chronic administration reduced brain atrophy, motor deficits and improved survival in murine model.
[163]	CHDI		TrkB agonst, LM22A-4	Reduced neurite degeneration, inflammation, aggregate formation and some motor function though other measures including survival were unchanged.

Table 1.2 Some of the Drugs in Preclinical Development for HD. List of drugs, the pathological processes they target and effects in animal models of HD. AAV (adeno-associated virus), CHDI (Cure Huntington's Disease Initiative), A.B.Y. Fund (Discovery of Novel Huntington's Disease Therapeutics Fund, Massachusetts General Institute for Neurodegenerative Disease).

1.2.7 Silencing Huntingtin as a Therapeutic Strategy

As described, HD is mostly a gain of function disease. It is autosomal dominant in inheritance pattern, aggregates known as inclusion bodies are a hallmark of the disease, and cells and mice engineered to overexpress one allele of mHTT or fragments thereof develop HD-like pathology and symptoms[93]. Most of the research into the development of therapies for HD, as described above, has focused on decreasing the downstream effects of the disease. However, a direct method of decreasing expression of mHTT would target the disease early in the pathogenic chain of events, before the issues further along the cascade such as excitotoxicity and cell death occur and theoretically could prevent these. Importantly, genetic tests are available for those at risk to identify the individuals who will develop symptoms. This makes intervention prior to disease manifestation possible[164]. If such an intervention can reduce mHTT expression it may be able to prevent the cascade of pathogenesis beginning and in this way inhibit any disease outcome. For those already displaying symptoms, this type of therapy should halt the disease progress and potentially allow for some improvement as a rescue of the phenotype of mice conditionally expressing mHTT has been shown once expression is turned off[165].

It is known that HTT is necessary for early embryonic development as silencing at this early stage is embryonically lethal with impaired gastrulation[39]. Mice expressing 50% wild-type HTT in development have severely impaired epiblast formation and deformations of the cortex and striatum and do not survive long after birth[166]. Later studies found that HTT is necessary for differentiation of neuroblasts into the cortex, striatum and thalamus[167]. Interestingly, mHTT expressed as a transgene can compensate for this loss during development[168].

Turning off mHTT expression in an inducible transgenic mouse system led to partial recovery of both behavioural and pathological symptoms[165]. It is not yet known exactly how significant a reduction in wild-type HTT can be tolerated long term in an adult, though reports in macaques show a decrease of 45% is well tolerated[151].There is however disagreement in the field as conditional deletion of HTT in the forebrain of adult mice has been shown to cause progressive neuronal pathology[169]. It is possible to selectively target the mutant allele by targeting the expanded repeat or SNPs which co-localise with the mutant[21,170].

Mechanisms to reduce mHTT expression vary from genome-editing techniques to post-transcriptional gene silencing using RNA interference (RNAi). By targeting the disease at the top of the pathogenic cascade in this way therapeutic intervention could prevent any damage to cells. There is also the advantage of transient rather than permanent silencing so that if the wild type protein is also targeted, the dose can be titrated if any adverse effect of reducing wild type HTT expression below a level required for physiological function were to become apparent.

1.3 Gene Therapy

There are several available methods to silence a gene which can be used to silence HTT including RNA interference (RNAi) with small interfering RNAs (siRNAs), antisense oligonucleotides (ASOs), exon skipping oligonucleotides, and the plasmid based strategies clustered regularly interspaced short palindromic repeats interference (CRISPRi) and short hairpin RNA (shRNA) **(Figure 1.3)**. They act at different stages of the gene expression pathway to repress transcription, alter splicing, degrade mRNA or

inhibit translation (Figure 1.3 and RNA processing pathway shown in section 5a of figure 1.5).

1.3.1 Small Interfering RNA

RNAi is a mechanism of gene silencing whereby a synthetic double stranded siRNA mimics endogenous microRNA (miRNA). miRNAs are short ~22 nucleotide RNAs which regulate endogenous gene expression by binding to complementary mRNA and downregulating expression of a target gene. Manipulation of this process has allowed the development of exogenous siRNAs which hijack the cell's own highly conserved miRNA regulatory machinery to elicit targeted gene silencing. siRNAs are designed to mimic these endogenous miRNAs and are small ~19-25 nucleotide double stranded RNAs which post-transcriptionally regulate gene expression. The guide strand of the siRNA or miRNA is loaded into the RNA-induced silencing complex (RISC) and the passenger strand is degraded[171]. The miRNA-RISC hybrid binds to the target mRNA through the binding of a seed sequence in the siRNA from nucleotide 2-8 to the 3' untranslated region (UTR) of target mRNA[172]. The catalytic core of Argonaute 2 (AGO2) of the RISC complex is thought to cleave the target mRNA if there is perfect complementarity between the siRNA and the cognate target. In the case of miRNA where there is often imperfect pairing with the corresponding mRNA, a translational repression is induced. This repression is independent of the endonuclease activity of AGO2 and it has been suggested this may be caused by an inhibition of translation through interference in the recruitment of the translation initiation factor eukaryotic initiation factor 4-E (eIF4-E) or through interaction with eIF6 which can prevent association of ribosomal subunits. Inhibition of the initiation of translation can lead to the accumulation of the corresponding

mRNA in cytoplasmic processing bodies (P-bodies) and as a consequence, mRNA degradation[173–175].

The sequence of the siRNA determines its specificity and in part its potency and efficacy, but chemical modifications of the molecule also play a role. There are a range of modifications that can be applied to siRNA to overcome its intrinsic limitations namely poor bioavailability, susceptibility to nucleases and hydrophobicity. Alteration of the backbone by phosphorothioate modification increases nuclease resistance[176], modification of the ribose 2'-OH to 2'-F significantly increases serum stability and also the binding affinity of the siRNA with an increase in melting temperature with every modification[177]. Additionally an siRNA can be modified via a hydrophobic tag to compensate for its hydrophilic nature[152]. Bioinformatic tools offer an opportunity to test for off-target effects[178]. *In vitro* testing must also be performed as the presence of a secondary or tertiary structure in the mRNA target may prevent the siRNA-RISC binding to the target sequence[178].

There are many siRNA based therapeutics in clinical trials from phase I to III including several for disorders where local delivery is possible such as for disorders of the eye where delivery is not limited by biological barriers. The first siRNA clinical trial in 2004 (NCT00722384) was directed against vascular endothelial growth factor (VEGF) to reduce neovascularization in patients with age related macular degeneration and diabetic macular oedema. It passed phase I and II trials (NCT00722384 and NCT00259753) but was halted at phase III for poor efficacy (NCT00557791). 12 siRNA therapeutics have been tested in clinical trials with systemic delivery via intravenous injections, mostly carried by stable nucleic acid lipid particles (SNALPs)[179]. For HD, several siRNAs have shown promise *in vitro* and *in vivo* in animal models in silencing HTT and reducing the

pathology and symptoms, but the challenge of safe delivery halts progress to the clinic[79,150–152,180].

1.3.2 Antisense Oligonucleotides

ASOs are single stranded 13-25 nucleotide nucleic acids complementary to the target mRNA so that it will bind via Watson-Crick hybridization and inhibit translation and expression of the target mRNA[181]. There are another class of ASOs which act through the recruitment of RNase H, a ubiquitous enzyme which hydrolyzes the RNA strand of an RNA:DNA duplex to degrade target mRNA[182].

The use of unmodified ASOs is hindered by rapid endonuclease and exonuclease mediated degradation in the same way as siRNAs are affected. There are also a number of chemical modifications that are regularly used to increase the efficacy of potential treatments. The chemistry of an ASO affects its binding affinity, stability, toxicity and mechanism of action. Intramolecular linkage of 2'-oxygen to 4'-carbon of the ribose ring creates a bridged nucleic acid known as locked nucleic acid (LNA), the ribose is locked in the 3'-endo conformation which increases binding affinity[183]. This modification also improves serum stability at the 3' end[184]. These LNAs can act as a steric block ASO or in a "gapmer" ASO there is a gap of nucleotides flanked by LNA bases. This gap is to allow for RNase H recruitment[185].

ASOs appear to be safe and numerous clinical trials from phase I to III have and are utilising these agents to silence genes of interest. Vitravene, Macugen and Kynamro are FDA approved agents for the treatment of AIDS related cytomegalovirus retinitis,

neovascular age-related macular degeneration and familial hypercholesterolemia respectively[186–188].

The first clinical trial for gene therapy for HD began this year. It is for the ASO IONIS-HTT_{RX} mentioned above, produced by Ionis and Roche in collaboration with the Cure Huntington's Disease Initiative (CDHI). The phase I/IIa trial is currently recruiting and will establish the safety, pharmacokinetics and pharmacodynamics of the drug in patients with early manifest HD (NCT02519036). It will be administered intrathecally at four-week intervals over a 13 week treatment period.

1.3.3 Exon Skipping

Exon skipping is mediated by ASOs targeted towards the precursor mRNA (pre-mRNA) - synthesised from the template DNA in the nucleus - to alter the splicing of a gene of interest so that an alternate mRNA is produced. An ASO can be designed to target a *cis*-regulatory sequence in the pre-mRNA, an exonic splicing enhancer (ESE)[189]. This binding effectively masks the ESE and prevents the endogenous trans-splicing regulatory factors from binding and through this binding it can alter the splicing of the pre-mRNA to form an alternate mRNA. In a similar fashion to siRNAs and other ASOs, modifications can increase stability. Modification of the ribose 2'-OH to 2'-O-methyl improves resistance to enzymatic digestion and thermal stability with each modification[190].

Exon skipping is perhaps most promising for the treatment of Duchenne Muscular Dystrophy (DMD). In this disease the technique is used to skip an exon with a mutation

to restore a disrupted reading frame generating a largely functional protein[191,192]. This has been used in clinical trials and although a phase III trial by GlaxoSmithKline and Prosensa in 2013 failed to meet its primary endpoint (trial NCT01254019), previous clinical trials showed success in exon skipping and restoration of dystrophin function following intramuscular injection[193,194].

Exon skipping has been used *in vitro* and *in vivo* for HD through engineered skipping of the caspase cleavage sites from which toxic N-terminal fragments are generated[195]. It is yet to be targeted to any other sites in HTT.

1.3.4 CRISPR Interference

The clustered regularly interspaced short palindromic repeats (CRISPR) and CRISPR-associated protein 9 (Cas9) is a newer genetic tool than those described above but its use has expanded in recent years[196]. Derived from the adaptive immune system in bacteria and archaea for nucleic acid editing, it is an RNA programmable DNA nuclease which catalyses double strand breaks[197,198]. A single guide RNA (sgRNA) complementary to the target region is sufficient for the system to recognize its target site[196].

The CRISPR system can be used for permanent knockout via a snip that generates a frame shift DNA mutation or it can be manipulated for a more moderate CRISPR interference (CRISPRi) approach with a catalytically inactive or dead Cas9 (dCas9). This can repress transcription directly via a steric block, and fusion to a translational repressor Krüppel associated box (KRAB) will bind DNA and sterically block RNA polymerase binding or elongation for transcription via heterochromatin mediated gene silencing at the

transcription start site (TSS)[199]. CRISPRi is more reversible than the permanent knockout but requires the sgRNA to be targeted to the TSS which depends on chromatin accessibility at this region.

Due to the recent development of CRISPRi for gene therapy, it has not been used in any clinical trials and to date there are no published studies involving its use for HD *in vitro* or *in vivo*.

1.3.5 Short Hairpin RNA

Short hairpin RNAs (shRNA) are another method of siRNA delivery where shRNA DNA expression plasmids with RNA polymerase promoters are delivered and transcribed within the cell. They are capable of DNA integration and when transcribed contain two complementary 19-22nt RNA sequences linked by a short 4-11nt loop[200]. This mimics the hairpin naturally found in pre-miRNA and the transcribed shRNA sequence is exported to the cytosol where through mimicking endogenous pre-miRNA, it is recognised and cleaved by Dicer into siRNA duplexes products which bind the RISC complex[200–202]. Thus, although it enters the RNAi machinery at an earlier step of the pathway, it follows the mechanism of siRNA mediated silencing in the cytoplasm.

Clinical trials using shRNA include a phase I vaccine with an shRNA directed against both TGF β1 and β2 (NCT01061840) for advanced cancers. For HD there has been success *in vitro* and *in vivo* using viral delivery vectors for shRNA[203].

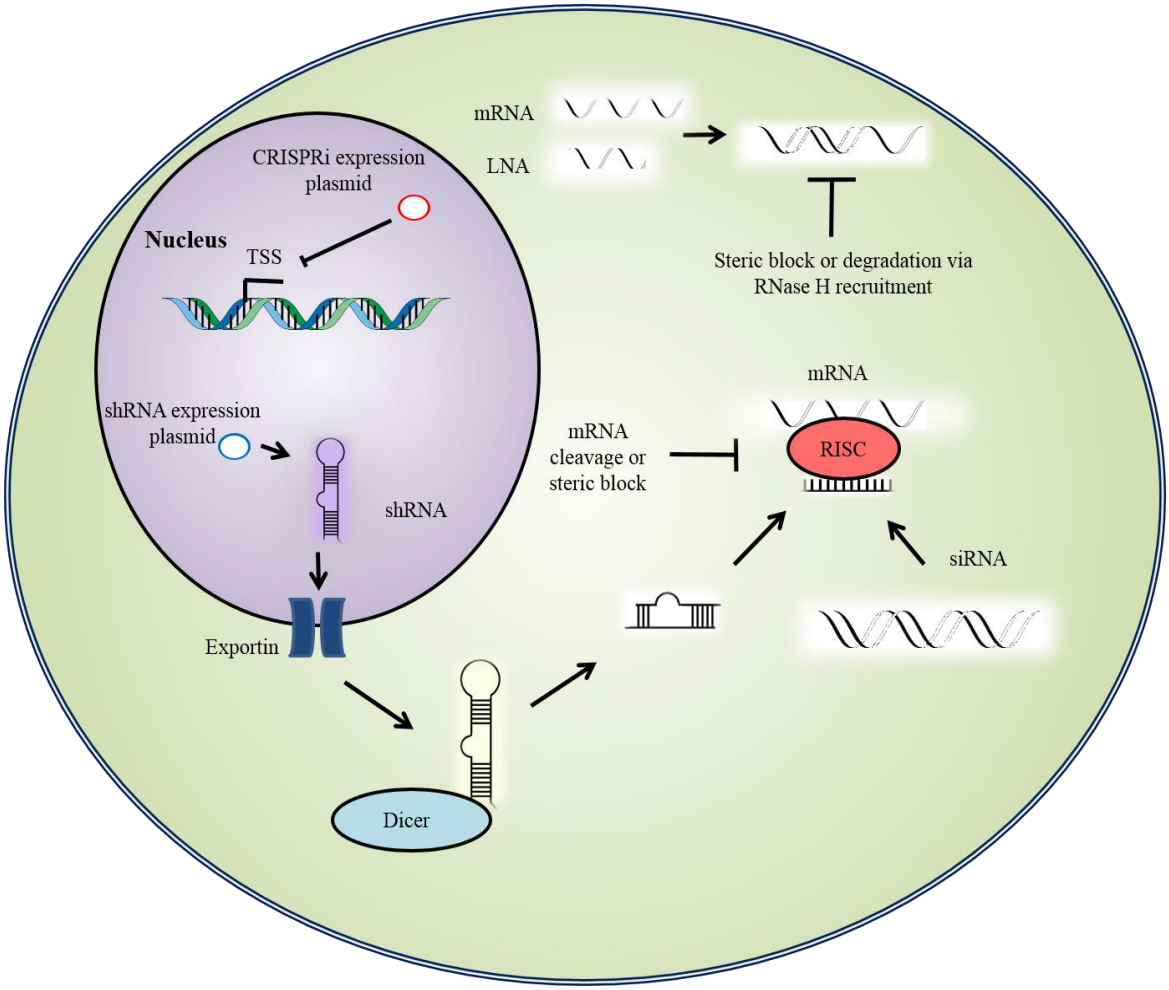


Figure 1.3 Schematic of the Mechanism of Action of Nucleic Acid Based Therapeutics. Diagrammatic summary of the mechanism by which CRISPRi, shRNA, siRNA and LNAs exert their silencing effects. CRISPRi induces a steric block on transcription, shRNA is exported and processed by the cell's endogenous machinery to a double stranded short nucleic acid which mimics miRNA. siRNA also mimics miRNA. The processed shRNA and siRNA induce silencing by recruiting the RISC, target mRNA binding and either degradation of the target mRNA or inducing a steric block of translation. LNAs can bind the mRNA and cause a steric block or in the case of a gapmer with LNA bases limited to flanking regions of the ASO, they can induce cleavage of the mRNA via RNase H.

As described, there are several types of nucleic acid based therapeutics which hold potential for the treatment of HD **(Figure 1.3)**. To date, siRNAs have demonstrated the most potential in a clinical setting when applied to disorders of the eye. For HD they demonstrate safety and tolerability *in vivo* even in primate models[79]. However, ASOs are a step closer to clinical use for HD as a safety and tolerability trial is recruiting for IONIS-$HTT_{RX.}$ The potential for shRNAs and exon skipping oligonucleotides is yet to progress from preclinical development for HD and CRIPSRi as a more novel nucleic acid therapeutic lags behind in development though if its potential can be realised it could hold great promise for diseases such as HD as *in vitro* studies have shown its potential in this short time[199,204,205]. Direct brain injections have been used to administer some of these nucleic acid based therapeutics in preclinical trails but are associated with risks. They cannot be administered systemically however without a carrier due not only to the likelihood of degradation in the serum, but also because these molecules cannot penetrate the blood brain barrier (BBB).

1.4 The Blood Brain Barrier – A Challenge in Delivering Genetic Therapies to the Brain

A common theme among the gene expression modifiers described here is that the availability of a safe and efficient delivery vehicle impedes the translation of therapeutics with proven *in vitro* efficacy to the clinic for the treatment of neurological disorders including HD. Direct brain injection as has been used in preclinical studies is invasive and associated with risks. Even intrathecal injection which will be tested for delivery of IONIS-HTT_{RX} is associated with some risk of nerve trauma, infection, hematoma, air embolism and disc injury[206]. Intravenous injection is a safer route of administration but

the BBB which functions to protect the CNS is also the greatest challenge to successful delivery of therapeutics to the brain.

The BBB is a dynamic physical interface that separates the brain from the periphery to protect the brain from toxic insults and maintain CNS homeostasis so that the local ionic microenvironment surrounding neurons is stable and optimized for signalling, which is necessary for correct neuronal function. The BBB consists of a sealed monolayer of endothelial cells which interact with the basement membrane lending the system structural support, as well as with astrocytes and pericytes, and surround capillaries **(Figure 1.4)**[207,208]. Pericytes promote and maintain BBB formation during development and adulthood and regulate vesicular trafficking in endothelial cells while astrocytic end-feed monitor the junctions between endothelial cells[207,209,210]. These tight junctions between the endothelial cells, and the low rate of transcytosis across these cells renders them almost impermeable so that diffusion is blocked, inhibiting passage of even lipophilic macromolecules over 400Da[211]. Specific nutrients can cross via selective transport systems. There is an urgent need to deliver therapeutics capable of bypassing the BBB. Since the intrinsic properties of the nucleic acid therapeutics are incompatible with this task, a gene delivery vehicle is required. Although several types of delivery vectors have been proposed for this purpose, each is associated with limitations which inhibit clinical development. EVs offer an interesting alternative because they naturally function to transport RNA between cells and it may be possible to manipulate this endogenous function for an immunologically inert gene delivery vehicle[212,213].

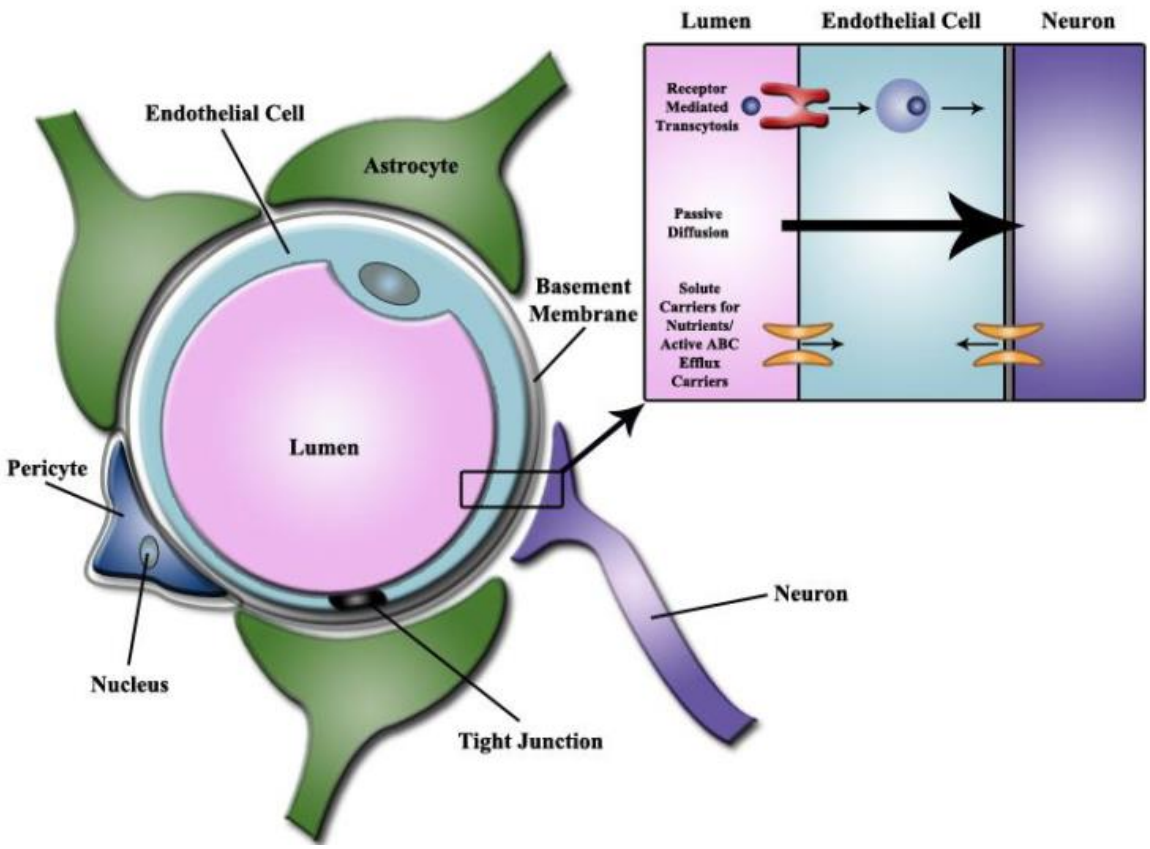


Figure 1.4 Components of the Blood-Brain Barrier. The blood-brain barrier (BBB) is a complex multi-cellular barrier. It protects the central nervous system (CNS) by restricting the passage of molecules from the peripheral blood supply. The BBB consists of a sealed layer of epithelial cells connected by tight junctions. The epithelial cells surround capillaries and interact with pericytes, astrocytes and the basement membrane. Together, these elements shield the brain from toxic insults and maintain CNS homeostasis so that the local ionic microenvironment surrounding neurons is stable and optimized for signalling, necessary for correct neuronal function. Small hydrophobic, lipid-soluble molecules under 400Da may cross the BBB by passive diffusion. However, due to its relatively impermeable nature, specialised transport systems are required for the transfer of most molecules across the BBB. Receptor-mediated transcytosis is one mechanism by which larger molecules may cross. Upon binding of a ligand to a receptor on the endothelial cell the receptor-ligand complex is internalised into a vesicle capable of traversing the cell. Molecules entering the brain in this way include lipoproteins and insulin. Despite our growing understanding of these mechanisms, exactly how drug delivery systems may interact with BBB components to reach the CNS remains largely unknown. Figure adapted from O'Loughlin *et al*., Exosomes and the emerging field of exosome-based gene therapy. Current Gene Therapy. 2012. Aug; 12(4):262-74 with permission.

1.5 Membrane Vesicles

The release of small membrane bound vesicles from cells is increasingly recognized as a model of cell-independent communication. Prior to their discovery, cells were thought to communicate solely via extracellular molecules binding to receptors outside or inside the cell. Historically, when viewed under a microscope, these vesicles were thought to be a result of cell damage or death, but recently, an expanding field of study into these vesicles has shown that they have actually evolved as a universally conserved adaptive cellular response that participate in many physiological and pathological processes and increase the complexity of intercellular communication, transmitting important information as they contain proteins, lipids and nucleic acids capable of altering cell signalling in any cell they meet[212,214].

Currently, this heterogeneous group of intercellular messengers is divided into subgroups based on their biogenesis, biophysical properties and functions, which are summarised in Table 1.3. These include microvesicles, apoptotic blebs, and exosomes. Membrane vesicles share some common characteristics. They have an internal microenvironment which is protected from the extracellular milieu by a lipid bilayer which can be derived from the outer membrane of the host cell, or from intracellular membrane compartments, and are released constitutively or upon stimulation. They maintain the same membrane topology as the parent or source cell whereby the cytosolic side of the lipid bilayer is inside the vesicle, and the luminal part exposed. Maintaining the topology in this way they can extend some of the functions of the parent cell in intercellular communication by activating receptors on target cells, or transfer surface receptors to recipient cells. As exosomes cannot be separated from small MVs by today's methods, for the purposes of

this study small vesicles of under 200 nm diameter will be referred to here as extracellular vesicles (EVs).

1.5.1 Microvesicles

Microvesicles (MVs) are a group of membrane vesicles secreted by budding or shedding from the plasma membrane of most cell types. They usually have a diameter between 50 and 1000 nm[215]. They are also referred to as microparticles, ectosomes, shedding vesicles and exovesicles. Their release can be stimulated by calcium, upon ligand binding and activation or stress, either physical, e.g. shear stress, or chemical e.g. hypoxia[216,217]. Small cytoplasmic protrusions bud from the plasma membrane due to curvature mediated lateral redistribution of membrane components at these microdomains, a calcium influx activates calpain which alters the cytoskeletal structure causing the protrusions to detach from cellular actin ending with fission of the stalk[215]. This shedding is not passive and requires energy input, RNA synthesis and protein translation[218]. The resultant microvesicles contain cytosol and the extracellular side of the membrane is exposed on their surface, in the same orientation and topology as that of their donor cells so that their signalling properties reflect those of their cell of origin[219]. It was originally thought that they were formed as a means for the cell to extrude cellular debris, but MVs are now recognised as capable of performing the metabolic functions of the host cell at a distance.

1.5.2 Apoptotic blebs

Apoptotic blebs/bodies are released directly from the plasma membrane when it buds from disintegrating apoptotic cells. During the process of programmed cell death there is an alteration in cell morphology, shrinkage of the cytoplasm, nuclear condensation, and

the final stage is cell fragmentation into apoptotic blebs, which enclose remnants of the shrinking cell. The number of apoptotic blebs correlates with the degree of apoptosis in cultured cells[220]. These are heterogenous in shape and their size can vary between as low as 50nm to a controversial maximum size of 500nm to 5μm[221,222]. Although sharing some features with MVs, apoptotic blebs can contain cytosolic organelles and possible nuclear fragments while MVs do not[223].

1.5.3 Exosomes

Exosomes are a small relatively homogenous subtype of membrane vesicle of endocytic origin (40-100nm) released from cells upon fusion of a multivesicular body (MVB) containing intraluminal vesicles (ILV) with the plasma membrane. Exosomes are released from all cell types in culture, and are found *in vivo* in various biological fluids[224]. Exosomes contain a common evolutionarily conserved set of proteins which can be used as markers including CD63, CD9, Alix and Tsg101[224]. They also bear a set of proteins which reflect their source and can act as a molecular fingerprint[225]. Once considered to be merely transitional compartments destined for degradation of obsolete cell constituents by the lysosome, it is now recognized that exosomes are a specific subcellular compartment described in mammals and invertebrates with an important role in both physiological and pathological processes. Most research in the use of vesicles for therapeutics focuses on exosomes, so they will be discussed in more detail here.

	Microvesicles	Apoptotic blebs	Exosomes
Size	50-100nm	50-5000nm	50-100nm
Biogenesis	Released from budding of plasma membrane	Released as blebs from apoptotic cells	Released from MVBs
Methods for isolation	Centrifugation at 18000-20000g	Captured from cultures of apoptotic cells. Centrifugation at 1200, 10000 or 100000g	Centrifugation at 100000g, sucrose gradient, ultrafiltration with size exclusion liquid chromatography, kits such as Exoquick, immunoaffinity capture, polymer based precipitation
Markers	Integrins, selectins, CD40, tissue factor and cell-specific markers	contain DNA, histones	CD63, CD9, CD81, LAMP1 and TSG101

Table 1.3 Subcategories of Membrane Vesicles. Biogenesis, isolation methods and markers of the membrane vesicle subgroups. MVs and exosomes cannot be separated fully using today's methods.

1.5.4 Exosome Biogenesis

Unlike MVs and apoptotic bodies which are formed from direct budding of the cell membrane under physiological or apoptotic conditions respectively, exosomes are not formed directly from the plasma membrane. Their release is part of the endosomal trafficking system, a mechanism by which the cell sorts incoming molecules for recycling, storage or degradation by transportation to the lysosome. Endocytic vesicles form at the plasma membrane and fuse to form the early endosome which sorts the endocytosed cargo it receives from the plasma membrane. Endocytic vesicles fuse to

form an early endosome which develops into a late endosome by acidification and alterations in protein content[226]. Continuous inward budding of the limiting membrane of late endosomes into the lumen traps cytosol and on scission form intraluminal vesicles (ILVs). The late endosome is then defined as a multi-vesicular body (MVB)[227].

Upon fusion with a lysosome, the endocytosed cargo is hydrolysed, or upon fusion with the plasma membrane, the ILVs are released as exosomes. This is an active process in live cells and can be constitutive or induced. Exosomes retain the membrane topology of the parent cell. Exosomal membranes contain lipid raft microdomains which are enriched in cholesterol, sphingomyelin and ceramide. A mechanism for selective sorting of membrane associated cargo for degradation in lysosomes versus exportation from the cell in an exosome is regulated by the endosomal sorting complex required for transport (ESCRT) complex which recognizes and sequesters mono-ubiquitinated proteins in the endosomal membranes[228]. There is also an ESCRT-independent sorting mechanism whereby lipid raft microdomains laterally segregate cargo within the endosomal membrane which is coalesced by ceramide, promoting vesicle budding[229]. Exosomes also contain RNA which must be targeted to exosomes via a selective mechanism. The proteins AGO2, a member of the RISC, and its binding partner GW182 have been identified in exosomes from breast cancer cells and could therefore influence miRNA loading in these cells[230]. Some secreted RNAs have been found to share specific sequence motifs and it has been proposed that they function as *cis*-acting elements to selectively target RNAs to exosomes[231].

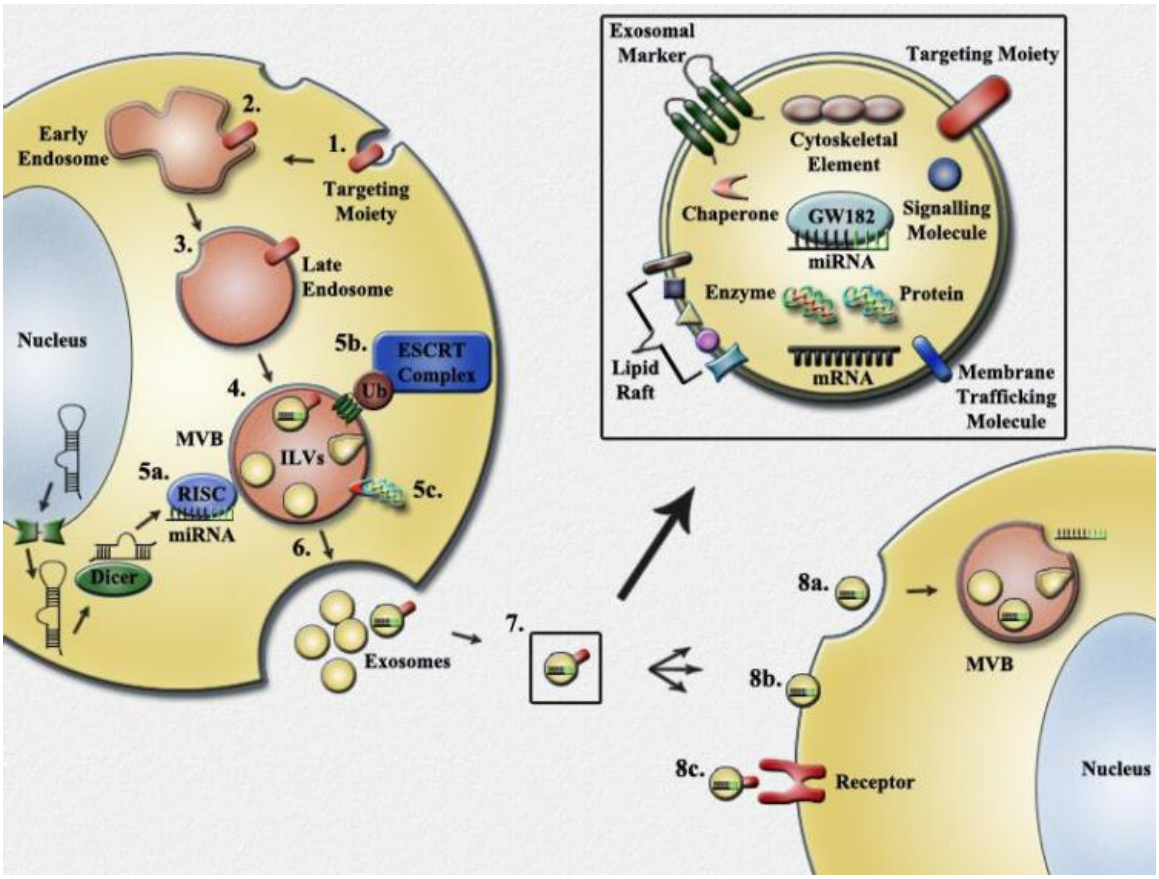


Figure 1.5 Exosome Biogenesis. 1) Small vesicles form following invagination of the plasma membrane. Surface proteins found on the plasma membrane may be transferred to the surface of these small vesicles. 2) Endocytic vesicles fuse to form the early endosome. 3) Following acidification and changes in protein composition the early endosome transforms into a late endosome. 4) Inward budding of the limiting membrane of the late endosome generates intraluminal vesicles (ILVs) and a multivesicular body (MVB) forms from the late endosome. Sorting mechanisms ensure cargos are selectively loaded into ILVs. 5a) After processing in the nucleus, pre-miRNA is exported via Exportin-5 to the cytoplasm and undergoes further cleavage by Dicer to form a miRNA:miRNA* duplex before the guide strand is incorporated into the RNA-induced silencing complex (RISC). Putative sequence motifs within the miRNA may mediate their selective loading into ILVs. 5b) Proteins may be selectively sorted by the ESCRT complex which targets mono-ubiquitinated proteins for inclusion into ILVs. 5c) Chaperone proteins, e.g. heat shock cognate 70 (hsc70), may selectively load proteins into ILVs via the recognition of a short amino acid sequence, such as KFERQ. 6) The MVB fuses with the plasma membrane and ILVs are released as exosomes. 7) Following release, exosomes travel to near and distant cells in biological fluid. Components found in the exosomal surface membrane include lipid rafts (microdomains rich in cholesterol, sphingolipid, glycolipids, lipid raft proteins and externalised phosphatidylserine) and exosomal markers such as tetraspanins (e.g. CD63), which are present across all populations of exosomes. They also contain plasma membrane proteins, including those

involved in endogenous targeting and trafficking, which may be specific to the cell of origin. A wide range of cargos are transported within exosomes. Exosomes may be internalised into recipient cells via a number of potential mechanisms. 8a) Exosomes could be endocytosed into a MVB, following which they may undergo back-fusion, fusing with the limiting membrane and releasing their cargo into the cytoplasm of the recipient cell. 8b) The exosome membrane may fuse with the plasma membrane, releasing the cargo directly into the cytoplasm of the recipient cell. 8c) Receptor-ligand mediated interactions could result in either signal transduction or exosomal internalisation. Figure adapted from O'Loughlin *et al*., Exosomes and the emerging field of exosome-based gene therapy. Current Gene Therapy. 2012. Aug; 12(4):262-74 with permission.

1.5.5 Extracellular Vesicles as Natural Carriers of RNA

The fate of exosomes after binding to their target cells remains to be fully elucidated but they can activate cell surface receptors on a target cell, fuse with the target cell to transfer bioactive exosomal proteins and RNA, or undergo internalisation by endocytosis[232]. Exosomes and MVs can partake in this cell-independent signalling either at close range or at a distance facilitated by their ability to travel in biological fluids.

With regard to gene therapy however, one functionality which is particularly interesting and documented in several studies, is that they are a natural carrier system, transporting mRNA, miRNA and proteins between cells[212]. Furthermore, the RNAs delivered via exosomes are functionally active in the recipient cell. This was evidenced by Valadi *et al.,* in 2007 where 1300 mRNAs and 120 miRNAs were identified in exosomes, most of which were not present in the cytoplasm of the source cells. The RNA from mast cells was shown to be transferrable as incubation of exosomes isolated from murine cells with human mast cells with resulted in expression of donor mouse proteins in the recipient

human cells[212]. This indicates that exosome-delivered mRNA can induce *de novo* translational changes, altering protein production in the target cell.

Skog *et al.* provided further evidence of the transfer of functionally active mRNA from exosomes to recipient cells. Fluorescently labelled MVs from glioblastoma cells were capable of transferring Gaussia luciferase mRNA human brain endothelial cells, with resultant translation to generate the reporter protein in the recipient cells[233]. Angiogenic proteins enriched in these MVs were also capable of stimulating tubule formation in recipient endothelial cells and demonstrated a self-promoting function by stimulating proliferation of human glioma cells[234].

The RNA transferred by exosomes known as exosome shuttle RNA (esRNA) has been implicated in a wide range of processes including protein synthesis through coding for kinases, enzymes and proteins regulating transcription, translation and cell development. Microarray studies show that the mRNA and miRNA profile of exosomes does not necessarily match the composition of the donor cell and thus there must be a selective mechanism of loading of specific mRNAs and miRNAs into exosomes[235]. More recent evidence from Balaj *et al.*, implicates MVs in the transfer of DNA fragments between cells[236]. The ability of exosomes to act as natural transporters of nucleic acids is an exciting aspect of their function which could potentially be harnessed therapeutically through their use as nanocarriers for the transport of exogenous RNA such as RNAi.

1.6 Drug Delivery Vehicles

A transport vehicle is required which can encapsulate, or conjugate with, nucleic acid based therapeutics and traverse the BBB. Current methods are summarised in Table 1.4 and include the use of viral, bacterial and lipid-based vectors. The use of viruses and bacteria in gene delivery harnesses their naturally evolved role in infecting cells to transfer exogenous nucleic acids. Cationic lipid-based vectors which would be attracted to both negatively charged nucleic acids and negatively charged plasma membrane also seemed an ideal candidate for the encapsulation and delivery of nucleic acid based therapeutics. However, these methods all have their own drawbacks which have hampered their development in clinical applications. Furthermore, a method of targeting these vectors without generating an immune response or toxicity has not been found. Recent progress has been made in the field of nanoparticle-based drug delivery including liposomes, carbon nanotubes, polymeric nanoparticles, nanocapsules and protein conjugates, and strides have been made towards increased bioavailability and reduced toxicity[237–239]. However, the foreign nature of these particles in the body makes them candidates for immune stimulation and more studies on their long term safety are required[240,241].

Vector	Advantages	Disadvantages	Refs
Viral Vectors *e.g.* Adenoviruses Adeno-associated viruses Lentiviruses Retroviruses	Some species are non-integrating where the DNA exists as an episomal element avoiding the risk of insertional oncogenesis. Serotypes can be generated with selective target specificity. Virus-like particles, recombinant and gutless forms are less toxic and immunogenic. Some studies report them to be well tolerated.	Non-integrating viral expression may be transient. Some species may integrate DNA into the genome and cause insertional mutagenesis. May cause toxicity and generation of an immune response by antigen-mediated cytotoxicity. Risk of germline transduction. Precise cell or tissue targeting is difficult. Risk of viral recombination. Variable transgene capacity. Some allow only DNA as cargo. Restricted targeting capacity For brain delivery direct injection is used.	23,180,203,242–245
Bacterial Vectors *e.g. Salmonella typhimurim* *Listeria monocytogenes* *Escherichi coli* Bacterial ghosts (non-living bacterial envelopes created by E-mediated lysis of Gram-negative bacteria)	Can be manipulated to deliver shRNAs and DNA plasmids. Can be controlled by antibiotics. Their production is cost-effective. Strains dubbed “probiotic” by manufacturing companies could limit unwanted side effects. Hold promise for diseases of the gastrointestinal tract as the gut has immune tolerance for *E. coli*. May possess intrinsic targeting. Bacterial ghosts can be used for DNA vaccines.	Transgene expression diminishes with time as the DNA released from the bacteria will have immunostimulatory, unmethylated CpG motifs in exogenous plasmid DNA inducing epigenetic silencing of integrated DNA. Can trigger immune response via activation of B-cells and T-cells. Risk of toxicity.	246–248

Vector	Advantages	Disadvantages	Refs
Bacteriophage Vectors *e.g.* Lambda	Can encapsulate DNA, RNA and antisense oligonucleotides. Robust and remain functional at low pH, suitable for oral delivery. Can be manipulated genetically to contain a bacteriophage origin of replication in a plasmid within phage particles. Tissue tropism is inducible by incorporation of targeting ligands in capsid proteins. Phage display allows discovery of novel targeting ligands.	Potent antigens. Cleared by the reticuloendothelial system, limiting their efficacy	249–252
Lipid-based Vectors *e.g.* Lipoplexes, Lipidoids, Cationic liposomes, Anionic liposomes, Stable nucleic acid lipid particles (SNALPs)	May display low IC50 values. Can carry a broad range of therapeutic cargos including small molecules, RNA and large DNA plasmids. SNALPs appear to be well tolerated.	Some are unsuitable for clinical use as cationic complexes attract serum proteins and blood cells, interfering with their activity. Interactions with serum proteins. Quick clearance by mononuclear phagocyte system. Lipoplexes have been associated with toxicity. Efficacy unknown for most tissues. Low efficiency of loading. Short duration of gene expression and rapidly cleared. Can be associated with toxicity.	237–240,253–256
Extracellular Vesicles	Natural transporters of nucleic acids. Can be loaded with exogenous cargos. Can cross biological barriers.	In the early stages of development. Known to be involved in the pathogenesis of several diseases.	212,213,257,258

Vector	Advantages	Disadvantages	Refs
Continued from p61 **Extracellular Vesicles**	Intrinsic and modifiable targeting specificity. Confer anti-inflammatory and immunosuppressive effects. May possess inherent therapeutic potential (*e.g.* in cardiovascular disease). Well tolerated with low immunogenicity. Can be targeted.	Endogenous role not fully elucidated. Biodistribution of targeted EVs not well defined. Protocols for isolation, purification, loading and targeting and require refinement.	

Table 1.4 Currently used Gene Therapy Vectors and Associated Advantages and Disadvantages. List of advantages and disadvantages associated with some commonly used nucleic acid delivery vectors. Table adapted from O'Loughlin *et al*., Exosomes and the emerging field of exosome-based gene therapy. Current Gene Therapy. 2012. Aug; 12(4):262-74 with permission.

1.6.1 Advantages of Extracellular Vesicles as Delivery Vehicles

The success of nucleic acid therapeutics depends on a delivery mechanism that is both safe and efficient. While viral and bacterial vectors risk compromising the health of host cells, exosomes seem to be safe and avoid immunogenicity and the risk of insertional mutagenesis. In many disorders the immune system may already be active, thus in these cases especially an immunologically inert vector is imperative. EVs seem to overcome the hurdles of immunogenicity, even upon repeat administration[213]. In addition, the transfer of exogenous nucleic acids is not entirely novel for this type of vehicle as part of their natural function is delivery of RNAs to the recipient cell. This could render them more efficient at delivery than the synthetic vectors discussed above.

A delivery vehicle must pass capillaries, avoid recognition by phagocytes, bind to their recipient cells, undergo internalisation via endocytosis, then escape the endosome and in some cases (such as CRISPRi) also reach the nucleus avoiding cytoplasmic degradation[213]. Research indicates that EVs can accomplish this whilst shielding therapeutic nucleic acids from degradation[213]. A proposed mechanism for their ability to traverse biological barriers is by internalisation into an MVB then release and re-internalisation into an MVB of a secondary cell[259]. The ability to initiate *de novo* transcriptional and translational changes in recipient cells suggest they are capable of delivering cargo to the correct region of the cell for functionality, which other vectors do not accomplish well. Their unique protein and lipid composition distinguishes them from liposomes, and plays an important role in targeting. The lipid composition is important because, as discussed, the membranes of exosomes are rich in microdomains of cholesterol, sphingomyelin, and externalised phosphatidylserine, which are known biological docking sites for signalling molecules[260]. Evidence that the proteins in the EV membrane are also required comes from analysis of synthetic vesicles comprising ratios of lipids identical to EVs, which are less prone to uptake *in vitro* and the decrease in uptake of EVs following treatment with proteinase K[260].

1.6.2 Therapeutic use of Extracellular Vesicles as Delivery Vehicles for RNAi

Although the study of EVs as delivery vehicles is a relatively new field of research, their potential to transport exogenous RNA has been identified[261,262]. Although not siRNA, miRNA shares common properties and Akao *et al.,* demonstrated that human monocytic THP-1 cells transfected with miR-143 later shed the miR-143 in EVs[261]. It was also demonstrated *in vivo* that miR-143 levels were elevated in the serum and kidney of

xenografted nude mice following intravenous injection of miR-143 pre-transfected THP-1 cells. Although it was not established whether miR-143 retained its functionality, these findings suggest that synthetic miRNA may be packaged into EVs and transported to cells at a distant location. Research by Zhang *et al.*, demonstrated that EVs isolated from the culture medium of THP-1 cells transfected with a fluorescently tagged synthetic miR-150, not only contained the miRNA but were also taken up by human microvascular endothelial HMEC-1 cells[262]. Also, incubation with THP-1 MVs lead to a decrease in expression of a target of miR-150, c-Myb. Thus, this research indicates that exogenous RNAs may be packaged into EVs and delivered, functionally active, into recipient cells *in vivo*. These results suggest that overexpressing a miRNA in a cell can lead to its incorporation in EVs and its functionality upon delivery *in vitro* and *in vivo*.

The first proof-of-concept that the innate ability of EVs to transport RNA may be capitalised on to deliver siRNA *in vivo* has been generated[213]. Immunologically inert EVs lacking immune stimulatory molecules such as MHCII, CD80 and CD86 were isolated from murine bone marrow immature dendritic cells (DCs). The EVs were characterised by nanoparticle tracking analysis, western blotting and electron microscopy. To limit the risk of off-target effects from systemic delivery and to examine targeted delivery of siRNA cargos, a novel targeting strategy was developed. A peptide known to target the brain, specifically a subunit of the nicotinic acetylcholine receptor expressed on neurons and the vascular endothelium of the BBB (rabies viral glycoprotein, RVG), was fused to the extracellular N-terminus of the exosomal surface protein, Lamp2b. DCs were transfected with plasmid containing the Lamp2b fusion protein coding sequence before EV isolation, leading to expression of the protein on the surface of isolated EVs. The surface modified EVs were then loaded via electroporation with exogenous siRNAs.

Lamp2b-RVG targeted EVs loaded with siRNA against GAPDH were administered to neuronal N2A cells to investigate whether they would increase neuronal targeting of the siRNA cargos *in vitro*. The expression of the targeting peptide was successful in providing specific targeting capacities to the EVs. This specific targeting and silencing via Lamp2b-RVG EV-mediated siRNA delivery also generated silencing *in vivo* following intravenous injection of EVs electroporated with GAPDH siRNA. Administration of naked siRNA lead to GAPDH silencing in organs of the mononuclear phagocyte system (MPS) which is associated with drug degradation and excretion, including the spleen, liver and kidney, there was no significant knockdown in these organs following EV-mediated delivery of the siRNA. Instead, GAPDH silencing was achieved in several brain regions which express the RVG target, the nicotinic acetylcholine receptor, including the striatum, midbrain and cortex.

Furthermore, the therapeutic potential of EV-based delivery was exemplified by demonstrating the ability to alter expression of β-secretase, a therapeutic target in AD, both *in vitro* and *in vivo*. Treatment by Lamp2b-RVG targeted EVs electroporated with β-secretase siRNAs of N2A cells *in vitro* yielded dose-dependent silencing. This was found to be significantly aided by the specific targeting by the RVG ligand as pre-treatment of the cells with an antagonist of the acetylcholine receptor, α-bungarotoxin, significantly reduced this silencing. When these EVs were applied *in vivo* intravenously >60% knockdown of cortical β-secretase RNA and protein levels were achieved, which yielded a 55% decrease in β1-42 levels. Combined with the attenuation of silencing by α-bungarotoxin, this indicates that receptor-mediated interactions may be involved in the targeted uptake of EVs across the BBB. Targeted loaded EVs did not induce an immune response as there were no significant changes in inflammatory cytokine markers *in vivo*

nor evidence of the proliferation of T lymphocytes *in vitro*. Importantly for potential clinical development, repeated administration appeared to be well tolerated, with little reduction in silencing efficiency following re-administration which has been identified as an issue and limitation of existing viral delivery methods. Therefore, this study indicates that EV based nucleic acid delivery may provide a safe and effective mean of specifically targeting the brain for therapeutic benefit.

Pan *et al.*, also reported data highlighting the ability of EVs to transport siRNA[263]. This study examined whether EV delivered siRNA could be transferred between hepatic cells to increase the therapeutic benefits of RNAi for hepatitis C virus (HCV) infection. Silencing of HCV replication and expression of the viral entry receptor CD81 was investigated as a means to assess transmission of RNAi *in vitro* in a human hepatic cell line and primary B-lymphocytes transduced with siRNA-expressing vectors. In line with the research described above, human and mouse hepatic cells and primary B-lymphocytes were capable of exchanging small RNAs including siRNA targeting HCV and CD81 partially via EVs. The *in vivo* transmission of siRNA was also analysed in immunocompromised mice engrafted with human hepatoma cells producing CD81 siRNA and EV based suppression of CD81 expression was evident in mouse hepatocytes. In combination with the research outlined above, this suggests that EVs might have therapeutic benefit not only as a direct method to transfer RNAi but also that once delivered, the therapeutic extent of such treatments may be permeated by EV based transmission of RNAi to other cells.

Wahlgren *et al*., applied this technology to human cells[264]. EVs were harvested from plasma from peripheral blood and loaded with mitogen-activated protein kinase 1

(MAPK 1) siRNA by electroporation. The siRNA was delivered to monocytes and lymphocytes resulting in target gene silencing. The siRNA localised primarily to the cytoplasm and interestingly, although no targeting strategy was used, silencing was more prominent in monocytes than lymphocytes suggesting an intrinsic homing capacity of EVs.

Greco *et al*., utilised EVs for the delivery of siRNA directed against polo-like kinase 1 (PLK-1) to bladder cancer tumours and found that the tumour cells displayed elevated levels of uptake compared to normal bladder epithelial cells and the delivered siRNA generated silencing of the target mRNA and protein[265]. In another study in cancer therapeutics, siRNA directed against a prospective therapeutic target, RAD51 was loaded into EVs using electroporation among other strategies, and used to treat HeLa and fibrosarcoma cells[266]. siRNA delivered by the EVs was capable of generating post-transcriptional gene silencing in the recipient cells and resulted in reproductive cell death of recipient cancer cells.

A study using RVG targeted EVs loaded with siRNA directed against α-synuclein has also been conducted[267]. *In vitro* the loaded EVs reduced α-synuclein expression in SH-SH5Y cells and *in vivo* targeted EVs loaded with the siRNA were delivered peripherally into transgenic mice expressing human phosphorylation-mimic S129D α-synuclein. 7 days following injection there was a decrease in α-synuclein mRNA and protein levels in the brain with a resultant decrease in intraneuronal protein aggregates. This study is important in the use of EVs for HD as it demonstrates the reduction of aggregated protein by targeted siRNA loaded EVs.

Together, these studies show that although research into the delivery of therapeutic nucleic acids using EVs is limited so far, EVs may be loaded with nucleic acid based therapeutic cargos to produce functional silencing *in vitro* and *in vivo*.

1.6.3 Exploitation of Intrinsic Therapeutic Role of Extracellular Vesicles

In addition to their role as nucleic acid delivery agents, EVs have other intrinsic properties which may lend themselves to the treatment of certain diseases. If used to deliver exogenous nucleic acids in these diseases the roles could be combined for increased therapeutic effect.

EVs have been shown to mediate anti-inflammatory and immunosuppressive effects. They therefore may have intrinsic therapeutic benefit in the treatment of inflammatory and autoimmune diseases. For example, EVs derived from immature DCs treated with recombinant murine IL-10 could limit the onset of murine collagen-induced arthritis and decrease the severity of previously established arthritis. Similarly, exosomes derived from immature DCs genetically engineered via adenoviral vectors to express IL-4, FasL, indoleamine 2,3-dioxygenase (IDO) or the inducer of IDO, CTLA-4Ig, decreased the inflammatory response in delayed-type hypersensitivity and also partially reversed established collagen-induced arthritis through a mechanism dependent on MHCII[257,268,269]. In these studies, the EVs isolated from the immature DCs were found to be as, if not more, immunosuppressive than the EV source cells. The use of EVs to deliver anti-inflammatory drugs to the brain, bypassing the BBB following intranasal application, has recently been described and further highlights their potential in the treatment of neurological diseases such as HD[270].

Unmodified EVs from mesenchymal stem cells (MSCs) may possess even greater inherent therapeutic potential. For example, paracrine secretions from human embryonic stem cell-derived mesenchymal stem cells (hESC-MSCs) are cardioprotective in the context of myocardial ischemia/reperfusion injury and capable of decreasing infarct size in porcine and murine models[271]. This therapeutic effect was found to be mediated by EVs as conditioned medium as well as purified EVs harvested from hESC-MSCs were capable of decreasing the infarct size in a mouse model of myocardial ischemia/reperfusion injury[258]. Interestingly, this group have also generated an immortalized line of hESC-MSCs via transfection of the oncogene MYC[272]. EVs derived from MYC-transformed MSCs retained the functionality ameliorating infarct size, suggesting that the therapeutic potential of these exosomes had not decreased. While the authors dispel issues regarding the potential risk of transfer of the oncogene to recipient cells by reporting that the MYC protein was not detectable in the exosomes, this warrants further study.

In addition to their immunosuppressive properties, EVs from certain sources have been exploited for their potential to elicit an immune response against cancer cells to reduce tumour size. These EVs are derived from mature DCs, tumours and ascitic fluid and contain MHC-peptide complexes capable of eliciting CD4 and CD8 T cells and may have potential as a cell-free cancer vaccine by priming the immune system to evoke anti-tumour immunity. DC-derived exosomes (Dex) induce antigen-specific T-cell responses by the direct and indirect display of antigens to T-cells[273–275]. Two clinical trials assessing the safety and efficiency of Dex were performed in patients with advanced non-small cell lung cancer and metastatic melanoma[276,277]. The treatments were well-tolerated, indicating that Dex treatment may hold promise. However, later phase II study failed to

reproduce these results though in some patients natural killer T cells were activated[278]. The failure to mount a CD4 or CD8 T cell response was proposed to be due to the late metastatic stage. Hepatotoxicity was noted in one patient.

Tumour-derived exosomes (Tex) may function as antigen delivery systems to pulse and activate DCs to generate EVs but these tumour exosomes can be immune suppressive and counter the desired therapeutic effect in cancer[279–282]. To eliminate the immune suppressive effect, a clinical trial was performed in which patients with colorectal cancer were treated with ascites-derived exosomes (Aex) in combination with the granulocyte-macrophage colony stimulating factor (GM-CSF) to induce anti-tumour activity and generated positive anti-tumour cytotoxic T-lymphocyte responses[283]. Also, EVs derived from tumour cells which have been genetically modified to express either IL-2 or glycolipid-anchored IL-12 indicate that these EVs have increased anti-tumour and anti-immunogenicity effects[257,284]. This indicates that genetic modification of EV source cells to increase expression of desired cytokines in EVs may be therapeutically relevant. Although some of the clinical trials have produced mixed results, these findings indicate that with further study, EV based vaccination therapy for cancer may prove to be a viable treatment strategy and in addition provide evidence that EVs may be delivered safely and in sufficient numbers to produce therapeutic benefit in the clinic.

The immunosuppressive roles of certain EVs could hold potential for HD due to previously mentioned active innate and adaptive immune system in this condition.

1.7 Conclusion

HD is a monogenic neurodegenerative disease caused primarily by a toxic gain of function of mHTT. A therapeutic intervention to reduce the expression of mHTT would act early in the cascade of pathological events and could theoretically prevent the downstream effects of the toxic mutant from taking hold. There has been success *in vitro* and *in vivo* in animal models with nucleic acid based therapeutics which can silence either mHTT selectively or both the mutant and the wild type, but their translation to the clinic is hampered by the lack of safe delivery vehicle. EVs provide a possible solution to this issue but their therapeutic use is limited by a lack of supporting technology including methods to effectively load them with nucleic acid cargo and an understanding of how a targeting strategy might influence their *in vivo* biodistribution.

1.8 Aims

The aims of this thesis were:

1) To identify a nucleic acid cargo which can silence mutant HTT for loading into EVs.
2) To investigate the *in vivo* biodistribution of brain targeted EVs.
3) To evaluate loading of EVs with therapeutic nucleic acid.

CHAPTER 2 MATERIALS AND METHODS

2.1 siRNA and ASO Sequences

2.1.1 siRNAs

Small interfering RNAs (siRNAs) were purchased from Eurogentech or were a kind gift from Novartis. A nonspecific siRNA sequence was used as a negative control for comparison to experimental siRNA activity. The siRNA sequences utilised in this study are provided **(Table 2.1)**.

siRNA	Sense Sequence	Antisense Sequence
siRNA-5'	CpsCCUGGAAAAGCUGAUGACGpsG	UpsUCAUCAGCUUUUCCAGGGsUpsC
siRNA-REP	AACAGCAGCAGCAGCAGCAGC	GCUGCUGCUGCUGCUGCUGUU
Negative Control	AAAUGACGACGCUGGUAUAGC	GCUAUACCAGCGUCGUCAUUU
Cy3-HuR siRNA	GUACGGAAUAGAUAAUUAAUU	Cy3-UUAAUUAUCUAUUCCGUACUU
Cy3-cc-siRNA HuR	Chol-TEG-GfUAfCGGAAfUAGAfUAAfUfUAAfUfU-dTpsdTps	Cy3-fUfUAAfUfUAfUfCfUAfUfUfCfCGfUAfCfUfU-dTpsdT
cc-siRNA HuR	Chol-TEG-GuAcGGAAuAGAuAAuuAAuu-dTpsdTps	fUfUAAfUfUAfUfCfUAfUfUfCfCGfUACfUfU-dTpsdT

Table 2.1 List of siRNAs. siRNA-5' and siRNA-REP target *HTT* upstream or within the CAG repeat respectively. HuR siRNAs target Human antigen R (HuR). Sequences are written in the 5' to 3' direction. chol, cholesterol; fC and fU, 2'-deoxy-2'-fluoro cytidine and uridine respectively; "ps", phosphorothioate linkage.

2.1.2 ASOs

Locked nucleic acid (LNA) antisense oligonucleotides (ASOs) were purchased from Exiqon and designed by Dr. Miguel Varela (Wood Lab), the multi-gene LNA was designed using an algorithm to identify overlapping sequences between genes of interest. This and the "LNA gapmer" are DNA/LNA gapmer antisense oligonucleotides with a phosphorothioate DNA monomer core flanked by modified LNA bases **(Table 2.2)**.

LNA	**Sequence**
LNA-5'	TgcTgcTgcTggAagGacT
LNA-REP	TgcTgcTgcTgcTgcTgcT
LNA gapmer	TgcTgctgctgctgcTgcT
Multigene LNA	CAGtctctcccaCCa
Negative Control LNA	TgcTatAccAgcGtcGtcA

Table 2.2 List of LNA ASOs. LNA nucleotides are in capital letters. The LNAs were synthesised with phosphorothioate backbones. LNA-5' targets a region upstream of the CAG triplet repeat in *HTT* while LNA-REP and LNA gapmer target the repeat. Multigene LNA targets both *HTT* and *mTOR.*

2.1.3 Exon Skipping Oligonucleotides

The exon skipping oligonucleotides were designed with Dr. Graham McClorey (Wood Lab) **(Table 2.3)**. They were designed to skip exon 3, so that the stop codon TGA would be expressed from exon 4 to generate an mRNA fragment predicted to be degraded by nonsense-mediated decay **(Figure 3.6, Chapter 3)**.

Exon Skipping Oligonucleotide	**Sequence 5'-3'**
E.S. oligo A	Ctgaaattctggagaatttct
E.S. oligo B	Tcctgacatctgactctgcg
E.S. oligo C	Tcgtcagccaccatcctgac
E.S. oligo D	Gttgaggcattcgtcagcca
E.S. oligo E	Ccacacggttcttactttga
Negative Control E.S. oligo	Gccaacctcggcttactgaa

Table 2.3 List of Exon Skipping Oligonucleotides. Exon skipping oligonucleotides were designed to induce skipping of exon 3 so that a stop codon would be expressed early in exon 4 and the resultant mRNA fragment would be degraded by nonsense mediated decay. Sequences are modified with 2'O-Me and phosphorothiate backbones.

2.2 Plasmid Sequences for Therapeutic Silencing

2.2.1 CRISPRi Plasmid Sequences

The dCas9 signal guide RNAs (sgRNAs) to target the Huntingtin transcription start site (TSS) were designed by Sabrina Hemen-Ackah (Wood lab) **(Table 2.4)**.

	Target Sequence	**sgRNAs**
dCas9-Htt1	CCGGCGCAGCGTCTGGGACGCAA GGCCGCGTCGCAGACCCTGCGTT	Forward: **CACCG**TTGCGTCCCAGACGCTGCGC Reverse: **AAAC**GCGCAGCGTCTGGGACGCAA**C**
dCas9-Htt2	CCGGGACGGGTCCAAGATGGACG GGCCCTGCCCAGGTTCTACCTGC	Forward: **CACCG**CGTCCATCTTGGACCCGTCC Reverse: **AAAC**GGACGGGTCCAAGATGGACG**C**
dCas9-Htt3	CCTGCGGCCCAGAGCCCCATTCA GGACGCCGGGTCTCGGGGTAAGT	Forward: **CACCG**TGAATGGGGCTCTGGGCCGC Reverse: **AAAC**GCGGCCCAGAGCCCCATTCA**C**

Table 2.4 List of sgRNAs for CRISPRi plasmids. sgRNAs designed to target the Huntingtin TSS to repress transcription. Sequences in bold are part of the sgRNA expression cassette plasmid backbone.

2.2.2 shRNA Expression Plasmids

1 µl of each of four *HTT* SureSilencing short hairpin RNAs (shRNAs) (Qiagen) (sequences in table 2.5) were transformed into four vials of One Shot Stbl3 competent *E. Coli* (Invitrogen) by mixing gently, incubation on ice for 30 minutes, heat-shocking the cells for 45 seconds at 42 °C before a further incubation on ice for 2 minutes. 250 µl of pre-warmed SOC (super optimal broth with catabolite repression) medium (Thermo Fisher) was added per vial, and were shaken horizontally at 37 °C for 1 hours at 225 rpm. 100 µl from each vial was spread on an LB-agar selective plate and incubated overnight at 37 °C. A colony from each plate was selected and grown in 250 ml overnight in LB-broth (Sigma). Plasmid was prepared using the HiSpeed Maxi kit (Qiagen) per manufacturer's instructions.

Clone ID	**Insert Sequence**
shRNA 1	CCACCTGTGTCTCCAGTCAAT
shRNA 2	TTAGTGCCATTCATCGTAATT
shRNA 3	TCATCATTATACAGGGTTTCT
shRNA 4	GAACTGACTTTGCATCATACT
NC shRNA	GGAATCTCATTCGATGCATAC

Table 2.5 List of shRNA Insert Sequence. shRNA insert sequences of HTT SureSilencing shRNAs.

2.3 Brain Targeting Plasmids

2.3.1 Lamp2b-RVG Plasmid for Neuronal Cell Targeting

Where stated, the pEGFP-C1.Lamp2b-RVG plasmid which was a kind gift from Dr. Lydia Alvarez-Erviti, was transfected into the EV source cells so that EVs would express it on their surface. This plasmid had been engineered such that the N-terminal of Lamp2b (Lysosome associated membrane protein 2b) was fused to the acetylcholine receptor ligand Rabies Viral Glycoprotein peptide (RVG) with the removal of eGFP. An additional vector "Lamp2b-empty" was used as a control vector[213]. This vector was designed such that Lamp2b is expressed without any targeting moiety.

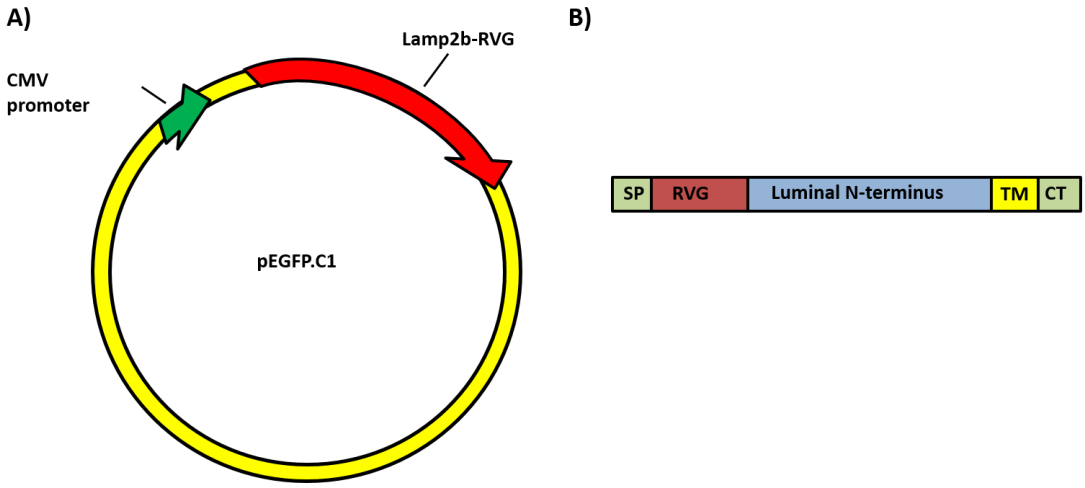
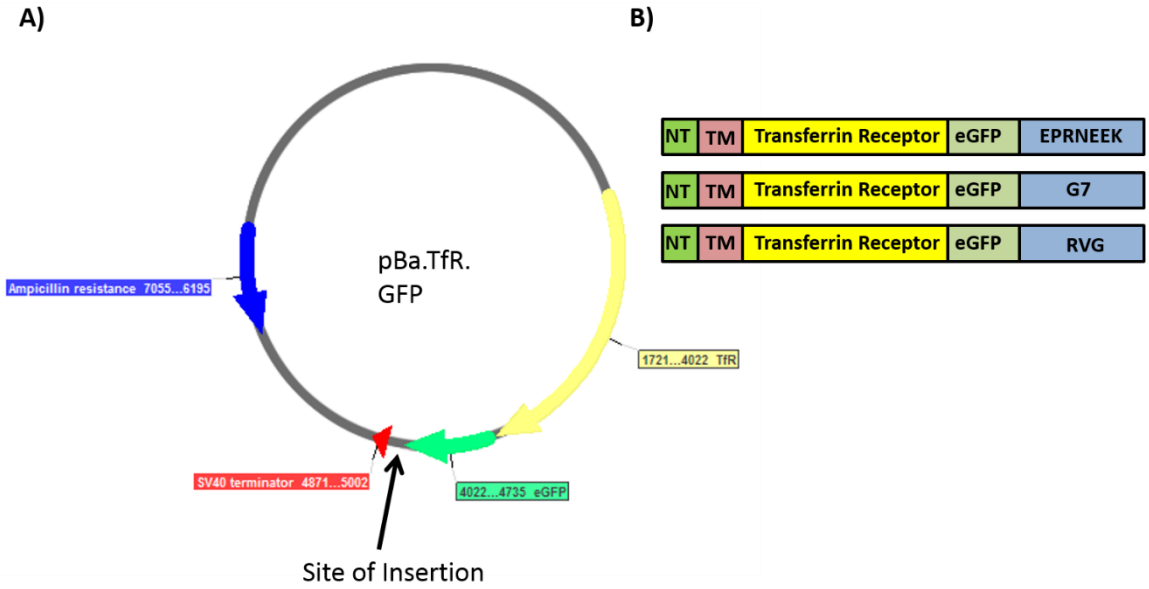


Figure 2.1 Structure of Lamp2B-RVG Targeting Peptide. (A) The Lamp2B-RVG targeting moiety was inserted downstream of the CMV promoter between the *Nhel* and *BamHI* restriction sites in the pEGFP-C1 plasmid. The EGFP sequence was removed. (B) The RVG peptide was cloned into the N-terminus of Lamp2B. SP (signal peptide), TM (transmembrane domain) and CT (C terminus).

2.3.2 Transferrin Plasmids for Neuronal Targeting

The transferrin receptor (TfR) plasmids pBa.TfR.GFP-EPRNEEK, pBa.TfR.GFP-G7 and pBa.TfR.GFP-RVG were designed using the pBa.TfR.GFP (Addgene) backbone. The inserts were designed so that they would be expressed downstream of, and in frame with, TfR.GFP and upstream of the SV40 terminator signal using restriction digest sites for the enzymes RsrII and XbaI, 5'-CG^GWCCG-3' and 5'-T^CTAGA-3' respectively where ^ indicates digestion sites and W is an A or T respectively.



C)

>2142-11: Insertion of 56 bp → TfR.GFP-EPRNEEK

TfR...CTCTCTGGTGACGTTTGGGACATTGACAATGAGTTTGGGGATCCACCGGTCGCCACCATGGTGAGCAAGGGCGAGGAGC
TGTTCACCGGGGTGGTGCCCATCCTGGTCGAGCTGGACGGCGACGTAAACGGCCACAAGTTCAGCGTGTCCGGCGAGGGCGAG
GGCGATGCCACCTACGGCAAGCTGACCCTGAAGTTCATCTGCACCACCGGCAAGCTGCCCGTGCCCTGGCCCACCCTCGTGAC
CACCCTGACCTACGGCGTGCAGTGCTTCAGCCGCTACCCCGACCACATGAAGCAGCACGACTTCTTCAAGTCCGCCATGCCCG
AAGGCTACGTCCAGGAGCGCACCATCTTCTTCAAGGACGACGGCAACTACAAGACCCGCGCCGAGGTGAAGTTCGAGGGCGAC
ACCCTGGTGAACCGCATCGAGCTGAAGGGCATCGACTTCAAGGAGGACGGCAACATCCTGGGGCACAAGCTGGAGTACAACTA
CAACAGCCACAACGTCTATATCATGGCCGACAAGCAGAAGAACGGCATCAAGGTGAACTTCAAGATCCGCCACAACATCGAGG
ACGGCAGCGTGCAGCTCGCCGACCACTACCAGCAGAACACCCCCATCGGCGACGGCCCCGTGCTGCTGCCCGACAACCACTAC
CTGAGCACCCAGTCCGCCCTGAGCAAAGACCCCAACGAGAAGCGCGATCACATGGTCCTGCTGGAGTTCGTGACCGCCGCCGG
GATCACTCTCGGCATGGACGAGCTGTACAAGCGGACCGgaggcggcggcagctgctatggcggcggcgaaccgcgcaacgaag
aaaaataataaaTCTAGATAAGTAATGATCATAATCAGCCATATCACATCTGTAGAGGTTTTACTTGCTTTAAAAAACCTCCC
ACACCTCCCCCTGAACCTGAAACATAAAATGAATGCAATTGTTGTTGTTAACTTGTTTATTGCAGCTTATAATGGTTACAAAT
AA

>Translation

TfR...LSGDVWDIDNEFGDPPVATMVSKGEELFTGVVPILVELDGDVNGHKFSVSGEGEGDATYGKLTLKFICTTGKLPVPWPT
LVTTLTYGVQCFSRYPDHMKQHDFFKSAMPEGYVQERTIFFKDDGNYKTRAEVKFEGDTLVNRIELKGIDFKEDGNILGHKLE
YNYNSHNVYIMADKQKNGIKVNFKIRHNIEDGSVQLADHYQQNTPIGDGPVLLPDNHYLSTQSALSKDPNEKRDHMVLLEFVT
AAGITLGMDELYKRTGGGGSCYGGGEPRNEEK*

NNN: GFP coding sequence

'g': Additional base to make in-frame expression of target insert

D)

>2142-22: Insertion of 38 bp → TfR.GFP-G7

TfR...CTCTCTGGTGACGTTTGGGACATTGACAATGAGTTTGGGGATCCACCGGTCGCCACCATGGTGAGCAAGGGCGAGGAGC
TGTTCACCGGGGTGGTGCCCATCCTGGTCGAGCTGGACGGCGACGTAAACGGCCACAAGTTCAGCGTGTCCGGCGAGGGCGAG
GGCGATGCCACCTACGGCAAGCTGACCCTGAAGTTCATCTGCACCACCGGCAAGCTGCCCGTGCCCTGGCCCACCCTCGTGAC
CACCCTGACCTACGGCGTGCAGTGCTTCAGCCGCTACCCCGACCACATGAAGCAGCACGACTTCTTCAAGTCCGCCATGCCCG
AAGGCTACGTCCAGGAGCGCACCATCTTCTTCAAGGACGACGGCAACTACAAGACCCGCGCCGAGGTGAAGTTCGAGGGCGAC
ACCCTGGTGAACCGCATCGAGCTGAAGGGCATCGACTTCAAGGAGGACGGCAACATCCTGGGGCACAAGCTGGAGTACAACTA
CAACAGCCACAACGTCTATATCATGGCCGACAAGCAGAAGAACGGCATCAAGGTGAACTTCAAGATCCGCCACAACATCGAGG
ACGGCAGCGTGCAGCTCGCCGACCACTACCAGCAGAACACCCCCATCGGCGACGGCCCCGTGCTGCTGCCCGACAACCACTAC
CTGAGCACCCAGTCCGCCCTGAGCAAAGACCCCAACGAGAAGCGCGATCACATGGTCCTGCTGGAGTTCGTGACCGCCGCCGG
GATCACTCTCGGCATGGACGAGCTGTACAAGCGGACCGgaggcggcggcagcggctttaccggctttctgagctaaaTCTAGA
TAAGTAATGATCATAATCAGCCATATCACATCTGTAGAGGTTTTACTTGCTTTAAAAAACCTCCCACACCTCCCCCTGAACCT
GAAACATAAAATGAATGCAATTGTTGTTGTTAACTTGTTTATTGCAGCTTATAATGGTTACAAATAAAGCAATAGCATCA

>Translation

TfR...LSGDVWDIDNEFGDPPVATMVSKGEELFTGVVPILVELDGDVNGHKFSVSGEGEGDATYGKLTLKFICTTGKLPVPWPT
LVTTLTYGVQCFSRYPDHMKQHDFFKSAMPEGYVQERTIFFKDDGNYKTRAEVKFEGDTLVNRIELKGIDFKEDGNILGHKLE
YNYNSHNVYIMADKQKNGIKVNFKIRHNIEDGSVQLADHYQQNTPIGDGPVLLPDNHYLSTQSALSKDPNEKRDHMVLLEFVT
AAGITLGMDELYKRTGGGGSGFTGFLS*

NNN: GFP coding sequence

'g': Additional base to make in-frame expression of target insert

E)

>2142-31: Insertion of 104 bp → TfR.GFP-RVG

TfR...GACAATGAGTTTGGGGATCCACCGGTCGCCACCATGGTGAGCAAGGGCGAGGAGCTGTTCACCGGGGTGGTGCCCATCC
TGGTCGAGCTGGACGGCGACGTAAACGGCCACAAGTTCAGCGTGTCCGGCGAGGGCGAGGGCGATGCCACCTACGGCAAGCTG
ACCCTGAAGTTCATCTGCACCACCGGCAAGCTGCCCGTGCCCTGGCCCACCCTCGTGACCACCCTGACCTACGGCGTGCAGTG
CTTCAGCCGCTACCCCGACCACATGAAGCAGCACGACTTCTTCAAGTCCGCCATGCCCGAAGGCTACGTCCAGGAGCGCACCA
TCTTCTTCAAGGACGACGGCAACTACAAGACCCGCGCCGAGGTGAAGTTCGAGGGCGACACCCTGGTGAACCGCATCGAGCTG
AAGGGCATCGACTTCAAGGAGGACGGCAACATCCTGGGGCACAAGCTGGAGTACAACTACAACAGCCACAACGTCTATATCAT
GGCCGACAAGCAGAAGAACGGCATCAAGGTGAACTTCAAGATCCGCCACAACATCGAGGACGGCAGCGTGCAGCTCGCCGACC
ACTACCAGCAGAACACCCCCATCGGCGACGGCCCCGTGCTGCTGCCCGACAACCACTACCTGAGCACCCAGTCCGCCCTGAGC
AAAGACCCCAACGAGAAGCGCGATCACATGGTCCTGCTGGAGTTCGTGACCGCCGCCGGGATCACTCTCGGCATGGACGAGCT
GTACAAGCGGACCGgaggcggcggcagctacaccatttggatgcccgagaatccgagaccagggacaccttgtgacattttta
ccaatagcagagggaagagagcatccaacgggtaaaTCTAGATAAGTAATGATCATAATCAGCCATATCACATCTGTAGAGGT
TTTACTTGCTTTAAAAAACCTCCCACACCTCCCCCTGAACCTGAAACATAAAATGAATGCAATTGTTGTTGTTAACTTGTTTA
TTGCAGCTTATAATGGTTACAAATAAAGCAATAGCATCACA

>Translation

TfR...DNEFGDPPVATMVSKGEELFTGVVPILVELDGDVNGHKFSVSGEGEGDATYGKLTLKFICTTGKLPVPWPTLVTTLTYG
VQCFSRYPDHMKQHDFFKSAMPEGYVQERTIFFKDDGNYKTRAEVKFEGDTLVNRIELKGIDFKEDGNILGHKLEYNYNSHNV
YIMADKQKNGIKVNFKIRHNIEDGSVQLADHYQQNTPIGDGPVLLPDNHYLSTQSALSKDPNEKRDHMVLLEFVTAAGITLGM
DELYKRTGGGGSYTIWMPENPRPGTPCDIFTNSRGKRASNG*

NNN: GFP coding sequence

'g': Additional base to make in-frame expression of target insert

Figure 2.2 Design of Novel Transferrin Targeting Constructs. A cloning strategy was designed whereby sequences for EPRNEEK, G7 and RVG were inserted into a vector which expresses a GFP tagged transferrin receptor (TfR). The insertions were made downstream of TfR and GFP but upstream of the SV40 terminator signal using restriction sites for the enzymes RsrII and XbaI with digest sites 5'-CG^GWCCG-3' and 5'-T^CTAGA-3' respectively where ^ indicates sites for digestion and W is an A or T. Underlined green "AAG" is the end of the GFP reading frame. The red "g" is a base added to maintain the reading frame of the inserts. The highlighted section in C-E are the inserts. The underlined bases towards the end of the inserts are the stop codons. **(A)** The pBa.TfR.GFP receptor from Addgene showing the site of insertion between the TfR.GFP and the terminator SV40 signal where EPRNEEK, G7 and RVG were designed to be expressed. **(B)** The TfR.GFP.EPRNEEK, TfR. GFP. G7 and TfR.GFP.RVG constructs at the extracellular N-terminus showing the CT (C-terminus), TM (trans-membrane portion), transferrin receptor reading frame, eGFP reading frame and the EPRNEEK, G7 and RVG signalling domain respectively. **(C)** Partial sequence of the pBa.TfR.GFP-EPRNEEK vector showing the insertion. **(D)** Partial sequence of the pBa.TfR.GFP-G7 vector showing the insertion. **(E)** Partial sequence of the pBa.TfR.GFP-RVG vector showing the insertion. Cloning was performed by Mutagenex. This image was created with and adapted from SerialCloner 2.6.1.

2.4 Cell culture

2.4.1 Cell Lines

HEK293 cells (human embryonic kidney cell line), Neuro2A cells (murine neuroblastoma cell line), SH-SY5Y cells (human neuroblastoma cell line) and HD patient-derived fibroblasts line GM04281 with 17 (wild-type) and 68 (mutant) CAG repeats from Coriell Cell Respositories were grown and maintained in Dulbecco's Modified Eagle Medium (DMEM)(Invitrogen) supplemented with 10% Foetal Bovine Serum (FBS)(Invitrogen) and 1% antibiotic/antimycotic (Life Technologies). All cells were incubated at 37 °C in 5% CO_2.

2.4.2 Dendritic cells

All animal procedures were conducted at the Biomedical Sciences Unit, University of Oxford, per the regulations of the Animals (Scientific Procedures) Act (1986) authorised by the UK Home Office. Bone marrow was flushed from the bone cavity of tibias and femurs of 8-10 weeks old C57BL6 mice (Jackson Laboratories) using a G27 syringe into DMEM (invitrogen). Clumps were dissociated by re-suspension and samples were centrifuged for 10 minutes at 280*g*. The supernatant was removed and the pellet re-suspended in red blood cell lysing buffer (Sigma-Aldrich). Following a 5 minute incubation, the suspension was neutralized with DMEM and spun at 280*g* for 10 minutes. Cells were then plated at a concentration of 3 x 10^6 cells per well in a 6 well plate in DMEM, 10% FBS (invitrogen), 1% antibiotics/antimycotic (Life Technologies) and supplemented with 10 ng/ml murine granulocyte macrophage colony stimulating factor

(GM-CSF) (Sigma-Aldrich) to select for dendritic cells (DCs). They were incubated at 37 °C in 5% CO_2.

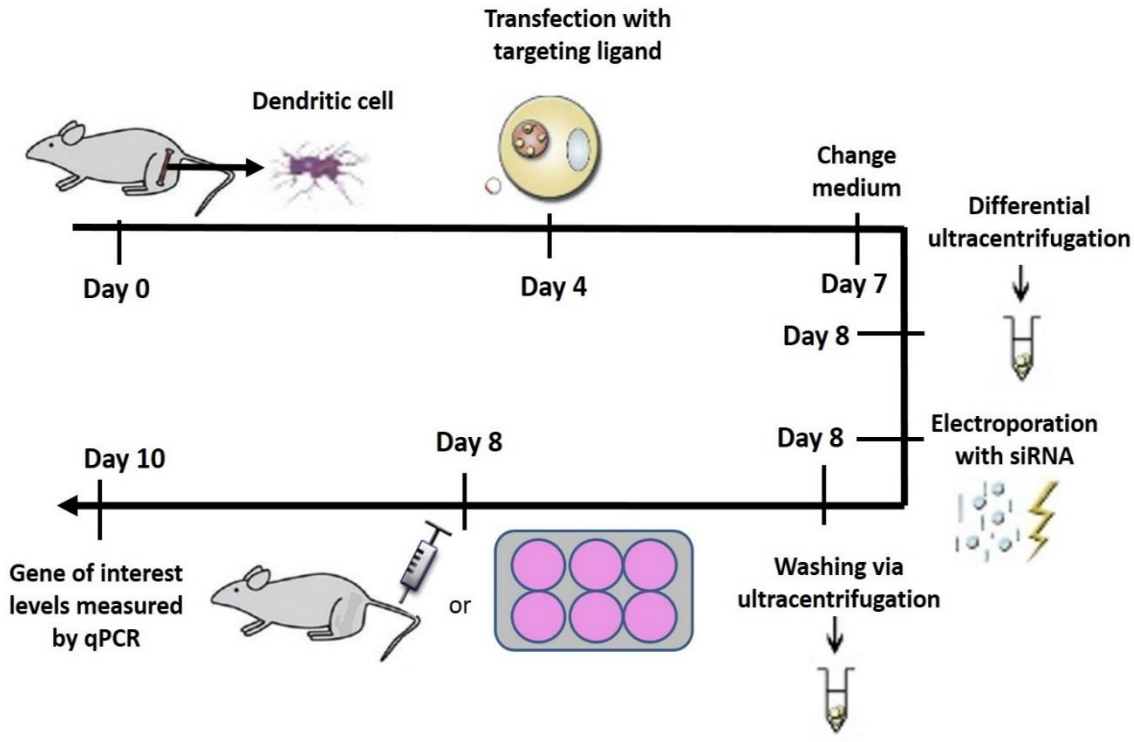


Figure 2.3 Schematic of EV Isolation and Treatment Methods. EVs were isolated from DCs, HEK293s or Neuro2A cells. If isolated from DCs they were transfected with the targeting ligand on day 4, the medium was changed on day 7 to EV depleted medium and conditioned medium was collected on day 8. When EVs were isolated from HEK293 or Neuro2A cells they were plated 24 hours prior to replacing the medium with serum depleted medium which was left on the cells for 48 hours. Conditioned medium from all cell types was used for EV isolation in the same manner, differential ultracentrifugation. Electroporation was performed and a washing step via ultracentrifugation included to eliminate free siRNA. The EVs were then added to cells or injected via the tail vein and 48 hours later RNA was harvested to test for silencing.

2.5 Transfections

2.5.1 Transfections of EV-Secreting Cells

Transfection of DCs with Targeting Plasmids

DCs were cultured for 4 days. On day 4 DCs were transfected with plasmids containing a Lamp2b construct fused to RVG, a vector containing Lamp2b with no targeting moiety (Lamp2b-empty) or mock transfected using TransIT LT1 transfection reagent (Mirus Bio) according to the manufacturer's instructions. 5 μl of the transfection reagent was added to 250 μl of Opti-Mem Reduced Serum Medium (Life Technologies) containing 5 μg of plasmid DNA. Following a 20 minute incubation the mixture was added in a drop-wise fashion to the cells. 4 hours later the medium was changed. DCs were then cultured for a further three days before the medium was replaced with fresh DMEM (Life Technologies) containing FCS (Invitrogen) which had been spun at 120,000*g* for 70 minutes prior to medium preparation to deplete it of EVs. Following 24 hours the cell culture supernatant was collected.

Transfection of Neuro2A Cells with Targeting Plasmids

Neuro2A cells in DMEM (Life Technologies) supplemented with 10% FBS (Invitrogen) were seeded at a density of 5 x 10^6 cells per 15 cm cell culture dish (Corning). 24 hours later they were transfected with the Lamp2b-RVG targeting plasmid. 25 μl of TransIT LT1 transfection reagent (Mirus Bio) was added to 1 ml of Opti-MEM (Life Technologies) containing 25 μg of plasmid DNA. The mixture was incubated at room temperature for 20 minutes and added drop-wise to the cells. Following a four hour incubation of the cells with the transfection reagent and plasmid DNA the medium was

changed to fresh DMEM (Life Technologies) supplemented with 10% FBS (Invitrogen) depleted of EVs and 1% antibiotics/antimycotics (Life Technologies). 48 hours later the cell culture supernatant was collected.

Transfection of HEK293 Cells with Targeting Plasmids

HEK293 cells in DMEM (Life Technologies) supplemented with 10% FBS (Invitrogen) were seeded at a density of 6 x 10^6 cells per 15 cm cell culture dish (Corning). 24 hours later they were transfected with the Lamp2b-RVG, Lamp2b-empty, pBa.TfR.GFP, pBa.TfR.GFP-EPRNEEK, pBa.TfR.GFP-G7 or pBa.TfR.GFP-RVG targeting plasmid. 25 µl of 4 mg/ml PEI was added to Opti-MEM (Life Technologies) and 25 µg of plasmid DNA was added to a separate 500 µl of Opti-MEM, each was mixed and incubated at room temperature for five minutes before mixing. Following mixing and a 15 minute incubation the mixture was added drop-wise to cells. After a four hour incubation of the cells with the transfection reagent and plasmid DNA the medium was changed to fresh DMEM (Life Technologies) supplemented with 10% FBS (Invitrogen) depleted of EVs and 1% antibiotics/antimycotics (Life Technologies). 48 hours later the cell culture supernatant was collected.

2.5.2 Transfection with CRISPRi and shRNA Plasmids

HEK293 or Huntington's patient-derived fibroblasts were seeded at a density of 2 x 10^5 and 1 x 10^5 cells/well respectively in 24 well cell culture plates in 500 µl DMEM supplemented with 10% FBS and incubated for 24 hours. Per well, for each plasmid, the indicated quantity of DNA was mixed with 50 µl of Opti-MEM (Life Technologies). This was incubated for five minutes and added to a mixture of Lipofectamine 2000

(ThermoFisher) and 75 µl Opti-MEM in a ratio of 1:1 w/w compared with the DNA mixture which had also been incubating for five minutes. These were mixed and incubated for 15 minutes together before being added drop-wise to cells. 4 hours later the medium was replaced with fresh DMEM supplemented with 10% FCS and 1% antibiotics/antimycotics. A transfection control was included which contained no DNA. Unless otherwise stated in a duration of silencing experiment, the cells were incubated for 48 hours before the cells were harvested to extract the RNA.

2.5.3 Transfection of siRNAs and Antisense Oligonucleotides

For time course and dose response evaluations of siRNAs and LNA-ASOs (LNAs, multi-gene LNAs and exon skipping oligonucleotides), HEK293 or Huntington's patient-derived fibroblasts as indicated were seeded at 2 x 10^5 cells per well or 1 x 10^5 cells per well respectively in a 24 well plate and transfected using Lipofectamine 2000 (Thermo Fisher) per the manufacturer's instructions. The transfection reactions were set up in a 1:1 weight:weight ratio of RNA:Lipofectamine. The siRNA, LNA or exon skipping nucleotide was mixed with 50 µl per well Opti-MEM (Life Technologies) and incubated for 5 minutes. In a separate reaction tube, Lipofectamine 2000 was mixed with 50 µl per well Opti-MEM and incubated for 5 minutes. The diluted RNA was added to the diluted Lipofectamine and the mixture was incubated for 15 minutes at room temperature. The mixture was then added drop-wise to the cells. 4 hours later the medium was changed to fresh DMEM supplemented with 10% FCS and 1% antibiotics/antimycotics and unless otherwise stated in a duration of silencing experiment, the cells were harvested for RNA extraction following 48 hours.

2.6 Microscopy

To estimate transfection efficiency through visualisation, cells were imaged with an EVOS FL Digital Microscopy (Electron Microscopy Sciences). The images generated were an overlay of GFP and phase images integrated using the computer software.

2.7 Extracellular Vesicle Isolation

Cell culture supernatant from DCs, Neuro2As or HEK293 cells as indicated was collected after 24 (for DCs) or 48 (for Neuro2A and HEK293 cells) hours growth in EV-depleted medium. The supernatant was spun at 300g for 5 minutes to remove dead and floating cells and 3000g for 15 minutes to remove cell debris. This supernatant was then passed through a 0.22 μm filter and was spun at 120,000g for 70 minutes to pellet the EVs in a Beckman Coulter Type 55.2Ti rotor. These were resuspended with a syringe in PBS. All spins were performed at 4 °C.

2.8 Extracellular Vesicle Characterisation

2.8.1 Nanoparticle Tracking Analysis

Nanoparticle tracking analysis (NTA) was carried out with a NS500 nanoparticle analyser (NanoSight) to measure the size distribution of particles. In the case of the biodistribution experiments this was performed following re-pelleting with DiR ($DiIC_{18}(7)$; 1,1'-Dioctadecyl-3,3,3',3'-Tetramethylindotricarbocyanine Iodide). NTA measurements are based on the Brownian motion of nanometre-sized particles which is related to particle size as particle movement is dependent on the temperature and size of

the particle and viscosity of the liquid. Particle size is calculated using the Stokes-Einstein Equation by NanoSight software by the rate of movement of tracked particles. NTA is commonly used for analysis of nanometre-sized particles. A camera level of 15-16 and automatic functions for all post-acquisition settings except for the detection threshold were used. This was fixed at 6. Samples were diluted in PBS between 1:500 to 1:20,000 to achieve a particle count of between 8-13 $x10^8$ particles per ml. The camera focus was adjusted to make the particles appear as sharp dots. Using the script control function, five 30 seconds videos for each sample were recorded; incorporating a sample advance and a 5 seconds delay between each recording. During the analysis, the same settings as for the scattering mode were used except for minimum tracking distance, which was set to 5.

2.8.2 Western Blotting

Pre-cast gels of 3-8% tris-acetate from Invitrogen were used. For EVs, samples consisted of 6.5 µl of resuspended pellets and for cells, 15 µg of protein as measured by Bradford Protein Assay was used. These were made up to 10 µl with 2.5 µl LSD Buffer (4x stock-Invitrogen), 1 µl Reducing Agent (10x stock-Invitrogen) and water. Samples were placed on heat block (70 °C) for 5 mins to denature proteins and were spun down prior to loading. Samples were loaded, as well as 7 µl of HiMark Pre-stained ladder (Invitrogen) and run at 150 V for 1 hour in running buffer (20x NuPage (Invitrogen) diluted to 1x with ddH2O). Transfer onto a nitrocellulose membrane was carried out in NuPage transfer buffer (20x diluted to 1x with 100 ml methanol, 50 ml transfer buffer and 850 ml ddH2O + 0.1 g sodium dodecyl sulphate (SDS)) at 30 V for 100 minutes. Blots were kept overnight in the fridge in neat Odyssey Blocking Buffer (Licor), stained with the primary (from table 2.6) for 1 hour at room temperature. Membranes were then washed 4 x 5 minutes (1x PBS Tween 0.1% + 5M NaCl 20:1 ratio) with an initial quick wash to rinse

out the antibody and incubated in the dark with secondary antibody for 1 hour at room temperature. Infrared dye (IRDye) 680RD goat anti-rabbit IgG (Licor) and IRDye 800CW Goat anti-mouse IgG (Licor) at 1:20,000. 4 x 5 minute (PBS Tween 0.1% + NaCl) washes were again carried out with an initial quick wash to rinse out the antibody. For multiple blotting of the same membrane, the blots were stripped using Restore PLUS Western Blot Stripping Buffer (Life Technologies) for 15 minutes at room temperature. All incubations and washes were performed with shaking. Blots were Imaged with the Odyssey Fc Imagine System (LI-COR Bioscience).

Antibody	Host	Supplier	Product Code	Expected Band Size	Dilution
Anti-Alix	Mouse monoclonal	Abcam	ab117600	96 kDa	1:1000
Anti-β-Actin	Mouse monoclonal	Abcam	ab82618	42 kDa	1:200
Anti-Calnexin	Rabbit polyclonal	Abcam	ab22595	75 kDa	1:1000
Anti-Huntingtin	Mouse monoclonal	Millipore	MAB2166	350kDa	1:1000
Anti-Huntingtin N-terminal	Mouse monoclonal	Millipore	MAB5492	Small fragments	1:1000
Anti-TSG101	Rabbit polyclonal	Abcam	ab30871	49 kDa	1:1000
Anti-GFP	Mouse monoclonal	Abcam	ab38689	~110kDa	1:4000

Table 2.6 List of Primary Antibodies for Western Blot. The antibodies listed were used at the concentrations indicated for a one hour incubation to probe for the specific protein listed.

2.8.2 Transmission electron microscopy (TEM)

10 µl of EVs resuspensed in PBS was added onto formvar-carbon coated 200 Mesh Nickel grids (Agar Scientific). After 20 minutes the grid was blotted with filter paper and

negatively stained using 10 µl 2% uranyl acetate (UA) in distilled water for 1 minute. The UA was then removed and the grids washed with 15 µl of distilled water for 1 minute. The grid was then blotted and left to air-dry for 15 minutes. EVs were then viewed with a JEOL 1010 transmission electron microscope (JEOL, Peabody, MA, USA) using an accelerating voltage of 80 kV and 1 second exposure. This was performed by Dr. Ezzat.

2.9 Measuring Biodistribution of EVs

2.9.1 DiR Labelling

The filtered conditioned medium was incubated with 1 µM fluorescent lipophilic tracer DiR (1,1-dioctadecyl-3,3,3,3-tetramethylindotricarbocyanine iodide) (D12731, Invitrogen) at room temperature for 15 minutes prior to EV isolation by the ultracentrifugation method as described above.

2.9.2 Biodistribution IVIS Measurements

Freshly purified DiR-labelled EVs were injected through the tail vein of C57BL6 or Balb/c mice as indicated. Biodistribution of DiR-labelled EVs was examined using a dose of $1.0x10^{10}$ p/g. The particle count was measured with NTA. For analysis of DiR-EVs distribution, In Vivo Imaging System (IVIS) Spectrum was used. IVIS spectrum contains a high sensitive CCD camera and enables both fluorescence and luminescence measurements. Here, the animals were sacrificed and the organs carefully harvested prior to analysis. The harvested organs were imaged for 1-2 seconds (excitation 710 nm, emission 760 nm). The data was analysed with the IVIS software (Living Image Software

for IVIS®). Adobe Photoshop CS4 and Adobe Illustrator were used to crop out and align the organs images. The animal experiments were approved by The British and Swedish Local Board for Laboratory Animals. The experiments were performed in accordance with the ethical permission and designed to minimize the suffering and pain of the animals. This was performed by Oscar Wiklander and Joel Nordin (Karolinska Institutet).

2.10 Flow Cytometry

HEK293 cells were plated, transfected with targeting plasmids and control plasmids and conditioned medium used to isolate EVs as above. The EVs were added to rpBMECs which had been plated in a 12 well plate coated with collagen (20 µg/cm²) at a density of 1 x 10^5 cells/cm² 10 days prior to the assay in 1 ml endothelial cell growth basal medium (Lonza) culture medium. 6 x 10^{10} EVs/ml were added to each well and incubated for 90 minutes. Cells were washed for 20 minutes in uptake buffer or growth medium, trypsin was used to detach them (300 µl per well) and recordings were made under two conditions; 750 µL uptake buffer (HBSS + 15 mM HEPES) or 750 µL endothelial growth medium (supplemented with 5 % FCS). Staining with 7-amino actinomycin D was added to analyse viability. This was performed at AbbVie by Dr. Christopher Untucht.

2.11 Loading of siRNA by Electroporation into Extracellular Vesicles

2.11.1 For *In Vitro* Use

EV concentration was estimated by Bradford Protein Assay Kit (Sigma Aldrich) per manufacturer's instructions. 10 µg of EVs was used per well in a 24 well plate. EVs corresponding to either 10 or 6 µg of protein per well in addition to 10 µg of siRNA for

high dose experiments or 100 pmol of siRNA (for a final concentration of 200 nM per well) for low dose experiments (corresponding to a ratio of EVs:siRNA of approximately 1:500), were mixed in 400 µl of electroporation buffer (1.15mM potassium phosphate pH 7.2, 25 mM potassium chloride, 21% Optiprep). Electroporation was performed in a 4 mm cuvette at 400 V and 125 µF with a Bio-Rad Gene Pulser (Bio-Rad). The same mixtures which were not electroporated were used as a control. The mixtures were washed by dilution in 2 ml PBS via ultracentrifugation in 2 ml Quick Seal Ultracentrifugation Tubes (Beckman Coulter) at 120,000g for 70 minutes. The EV pellet was either resuspended in 300 µl Opti-MEM or PBS. Of the samples resuspended in Opti-MEM, 100 µl of which was added to three wells of recipient cells which had been seeded 24 hours prior to treatment in 24-well plates at a density of 1 x 10^5 cells per well, 2 x 10^5 cells per well or 5 x 10^4 cells per well for HD fibroblasts, HEK293 cells and Neuro2A cells respectively. These cells were incubated with the treatments for 48 hours before they were harvested for RNA extraction. In the case of the EVs resuspended in PBS, they were used for downstream analysis.

2.11.2 For *In Vivo* Use

Per treated mouse, 150 µg of DC-derived EVs as estimated by Bradford Protein Assay Kit was mixed with 150 µg of siRNA (corresponding to a ratio of EVs:siRNA of approximately 1:1,800). This mixture was electroporated in aliquots of 12 µg EVs and 12 µg siRNA in 400 µl electroporation buffer (1.15 mM potassium phosphate pH 7.2, 25 mM potassium chloride, 21% Optiprep). Electroporation was performed in a 4 mm cuvette at 400 V and 125 µF with a Bio-Rad Gene Pulser (Bio-Rad). Samples from the same group were pooled following electroporation and washed with PBS via ultracentrifugation at 120,000g for 70 minutes. The EV pellet and naked siRNA were

resuspended to 80 µl per mouse in 5% glucose. This was administered intravenously via tail vein injections into 10 week-old C57BL/6 mice. The control group received a tail vein injection of the same volume of 5% glucose. Following 48 hours the mice were sacrificed, tissues dissected, snap frozen in ice-cold isopentane and stored at -80 ºC for analysis at a later stage.

2.12 Loading of Cholesterol-Conjugated siRNA by Treatment of Parent Cell

HEK293 cells were seeded at a density of 2 x 10^5 cells per well of a 24 well plate in DMEM supplemented with 10% FCS. 24 hours later 1 µg of cy3 labelled cc-siRNA was added to each well. Medium was taken from different wells at 30 minutes, 1, 2, 4, 8, 12, 24, 48 and 72 hours following treatment and levels of cholesterol-conjugated siRNA (cc-siRNA) in the medium was assessed by with excitation emission spectrum of 548-570 nm using a Victor3 1420 multilabel fluorescence microplate reader (Perkin Elmer) and compared to the absorbance of a serial dilution of the total cc-siRNA used.

2.13 Loading of siRNA by Mixing Extracellular Vesicles with Cholesterol-Conjugated siRNA

2.13.1 Loading by Mixing - Varying Ratio of Extracellular Vesicles to cc-siRNA

Following NTA analysis as described of EVs derived from Neuro2A cells, EVs were mixed with cc-siRNA in ratios of 1 EV:15 molecules of cc-siRNA, 1 EV: 30 molecules of cc-siRNA, 1 EV:150 molecules of cc-siRNA, 1 EV:300 molecules of cc-siRNA and 1 EV:1500 molecules of cc-siRNA. EV particle analysis was performed by NTA as

described above. Samples were mixed for 30 minutes, at room temperature, in 100 µl, washed via ultracentrifugation at 120,000g for 70 minutes. The fluorescence of the pellet resuspended in PBS for quantification.

2.13.2 Loading by Mixing – Varying Temperature

10 µg of EVs as estimated by Bradford Protein Assay Kit were mixed with cc-siRNA at a ratio of 1 EV:30 cc-siRNA molecules for 30 minutes at 4, 22, 37 and 42 ºC in 100 µl. Samples were then washed via ultracentrifugation at 120,000g for 70 minutes. The fluorescence of the pellet resuspended in PBS for quantification.

2.13.3 Loading by Mixing – Varying Incubation Time

10 µg of EVs as estimated by Bradford Protein Assay Kit were mixed with cc-siRNA at a ratio of 1 EV:30 cc-siRNA molecules at 37 ºC for 30 minutes, 1, 2, 3 and 5 hours in 100 µl. Samples were then washed via ultracentrifugation at 120,000g for 70 minutes. The pellet was resuspended in PBS for quantification.

2.13.4 Loading by Mixing – Varying Incubation Volume

10 µg of EVs as estimated by Bradford Protein Assay Kit were mixed with cc-siRNA for 1 hour at 37 ºC in 100 µl at a ratio of 1 EV:30 cc-siRNA molecules in volumes of 10, 20, 50, 100 and 500 µl. Samples were then washed via ultracentrifugation at 120,000g for 70 minutes. The pellet was resuspended in PBS for quantification.

2.14 Quantification of Loading Using Fluorescence

Percentage loading as measured by fluorescence was assessed by measuring fluorescence with maximum excitation emission spectrum of 548-570 nm using a Victor3 1420 multilabel fluorescence microplate reader (Perkin Elmer). Fluorescence in each sample was compared to a standard curve of Cy-3 siRNA and cc-siRNA alone.

2.15 RNA Quantification

2.15.1 RNA Extraction

Cells

RNA was extracted from cells using the RNeasy mini kit (Qiagen) according to the manufacturer's instructions. Cells were harvested directly from 24 well plates following removal of culture medium and washing with PBS, with 350 µl of Buffer RLT supplemented with β-mercapoethanol (10 µl per 1 ml Buffer RLT). A volume of 200 µl of Buffer RLT was used to obtain RNA from fibroblasts. A pipette was used to ensure disruption of clumps and lysis of cells. An equal volume (350 µl or 200 µl for most cell types and fibroblasts respectively) of 70% ethanol was added to the lysate and the samples were transferred to RNeasy spin columns in 2 ml collection tubes. These were centrifuged at 8,000g for 15 seconds. The flow through was discarded and 700 µl of Buffer RW1 was added to the spin columns. Samples were again spun at 8,000g for 15 seconds and the flow-through discarded. 500 µl of Buffer RPE was added to the spin column and samples were spun at 8,000g for 15 seconds. The flow-through was discarded and a second volume of 500 µl Buffer RPE was added to the spin column. Samples were centrifuged

at 8,000g for 2 minutes. The RNeasy spin column was placed in a new 2 ml collection tube and spun for 1 minute at full speed. The spin column was placed in a new 1.5 ml collection tube and 30 µl of RNase-free water was applied directly to the spin column membrane. The sample was left on the membrane for 1 minute before spinning at 8,000g for 1 minute. The resultant RNA was passed through the spin column again, spun at 8,000g for 1 minute and stored at 4 °C. All spins were performed at 20 °C.

Tissues

Tissues were dissected immediately after mice were sacrificed. They were snap frozen in ice-cold isopentane and stored at -80 ºC. A small piece of each tissue was taken and placed in a 2 ml soft tissue CK14 homogenisation tube containing 1.4 mm ceramic beads (Precellys) with buffer RLT (Qiagen RNeasy kit). The tissue was homogenised with a Precellys 24 homogenizer (Precellys) at settings of 2 x 30 seconds x 6500 rpm. The resultant homogenised tissue was removed and used to extract RNA exactly as described above for cells.

Extracellular Vesicles and Supernatant

When measuring the RNA in EVs and supernatant it was important to preserve small RNA species during the extraction. Therefore, an alternate method using TRIzol LS (Life Technologies) was used for RNA extraction from these samples according to the manufacturer's instructions. 75 µl of resuspended EVs in PBS or supernatant was used per extraction. 225 µl of TRIzol LS was added and samples were incubated for 5 minutes at room temperature. 60 µl of chloroform was added before another 10 minute incubation. Samples were spun at 10,000g for 15 minutes at 4 ºC. The aqueous uppermost layer was

collected and placed in a fresh tube. 1 µl of RNase-free glycogen (Roche) and 150 µl of isopropanol were added to the new tube. After mixing the samples were incubated for 10 minutes at room temperature and spun at 10,000g for 10 minutes at 4 ºC. The supernatant was removed and discarded and the pellet was washed with 300 µl of 75% ethanol, centrifuged at 7,500g for 5 minutes at 4 ºC, allowed to air-dry for 10 minutes. The RNA pellet was then resuspended in 20 µl of nuclease-free water, incubated at 55 ºC for 10 minutes prior to storage at -80 ºC.

2.15.2 Quant-iT RiboGreen RNA Assay

Quant-iT RiboGreen RNA Assay Kit (Life Technologies) was used to measure RNA quantity in EV samples as RNA quantity was low. It was used according to the manufacturer's instructions. A serial dilution of 100 µg/ml of Ribosomal RNA standard (16S and 23S rRNA from *E. Coli*) was performed with TE buffer in a ratio of 1:5. This generated standards ranging from 100 ng/µl to 0 ng/µl. Using a 96-well black microplate (Corning), 100 µl of each standard was added per well in triplicate. 2 µl of each sample was added to 98 µl of TE buffer and added to wells for assessment. The stock Quant-iT RiboGreen reagent was diluted 2,000x with TE and 100 µl of this was added to both the standard and test samples. Absorbance at 530 nM was measured using a Victor3 1420 multilabel fluorescence microplate reader (Perkin Elmer).

2.15.3 cDNA Synthesis

Reverse transcription using the High-Capacity Reverse Transcription Kit (Life Technologies) was used to obtain complementary DNA (cDNA) from RNA samples. RNA quality and quantity was assessed with a NanoDrop 2000c (NanoDrop). Samples

were made up to 10 µl containing 0.5-1 µg of total RNA per well of a 96-well low profile skirted polymerase chain reaction (PCR) plate (Life Technologies). To this, 10 µl of cDNA Reverse Transcription (RT) mastermix was added. The mastermix consisted of 2 µl 10x RT Buffer, 0.8 µl 25x deoxynucleotide triphosphate (dNTA) mix (100nM), 2 µl 10x RT Random Primers, 1 µl MultiScribe Reverse Transcriptase, 1 µl RNase Inhibitor and 3.2 µl nuclease-free water per reaction. The plate was sealed, centrifuged briefly to remove bubbles and placed in a G-Storm Quad Block Thermal Cycler (GMI). The cycler was programmed to run the reaction at 25 °C for 10 minutes, 37 °C for 120 minutes, 85 °C for 5 minutes and to cool to 4 °C. The cDNA was used immediately for qPCR or stored at -20 °C.

2.15.4 Gene Specific Reverse Transcription

For the exon skipping oligonucleotides, a gene specific reverse transcription was performed with primers outside of the region designed to be skipped, table 2.7. Two separate mastermixes were set up. The first contained 2 µl of 25 mM magnesium chloride, 1.5 µl 10x RT Buffer, 4 µl 2.5 mM dNTPs, 0.5 µl RNase Inhibitor, 0.5 µl M-MLV enzyme, 0.75 µl of 10µM reverse primer and 3.75 µl nuclease free H_20 per reaction. Per well, 2 µl containing a total of 200 ng of RNA was added to the master mix, the plate was sealed with a total of 15 µl per well and run at 35 cycles at 94 °C for 30 seconds, 55 °C for annealing for 1 minute and 72 °C extension for 2 minutes in a G-Storm Quad Block Thermal Cycler (GMI). This was then used as the template in the second reaction with 2 µl 25 mM magnesium chloride, 3.5 µl 10x RT buffer, 0.75 µl of 10µM forward primer (Table 2.7), 0.25 µl Taq Polymerase and 28.5 µl of nuclease free H_20 per well. The plate was sealed and placed back in the Thermal Cycler for PCR amplification. Samples were

then electrophoresed on a 2% Tris-acetate-ethylenediamine tetraacetic acid (TAE) agarose gel with ethidium bromide at 90 V for 90 minutes and viewed under UV light.

Forward Primer	**Reverse Primer**
CGACCCTGGAAAAGCTGATG	TCTTCGGGTCTCTTGCTTGT
AAGGCCTTCGAGCTTTGATG	GGGTCTCTTGCTTGTTCGAG
TGGAAAAGCTGATGAAGGCC	CTGCATTTCTGAGGCCGAAC

Table 2.7 Primers for Gene Specific RT-PCR. Gene specific RT-PCR was performed using the above primers to amplify a region including *HTT* exon 3. This region would be larger or smaller depending on the presence or absence (via skipping) of exon 3 and could be separated on an agarose gel.

2.15.5 GeNorm Assays

The 12 gene geNorm Perfect Probe Plus Mouse and Human Kits (PrimerDesign) were used to identify the most stably expressed and therefore appropriate reference genes for *in vitro* and *in vivo* analysis. Using this kit, the expression of 12 candidate reference genes identified from over 30,000 microarray experiments were compared in a representative set of experimental samples. For *in vitro* assessment for HD fibroblasts and HEK293 cells for *HTT* silencing, the samples used were 2 samples each from untreated cells, and 2 from each treatment group cells treated with a mid-range dose of each of the therapeutic nucleic acids. For evaluation of loading the samples used were 2 untreated. 2 treated with siRNA alone, and for cells treated with EVs, 2 samples of EVs + siRNA and EVs alone were also included. For *in vivo* assessment, the samples were cortex and liver from untreated mice, mice treated with siRNA alone and mice treated with RVG-EVs + siRNA. The expression of each of the 12 candidate reference genes was assessed by qPCR using 25 ng of cDNA using the same paramaters as described below for qPCR. The data was analysed with the qbase$^+$ software (Biogazelle) which ranked the candidate reference genes by their gene expression stability (geNorm M) which is the variation of a gene compared with all of the other reference genes following calculation of the standard deviations of the log-transformed expression ratios. Stepwise exclusion of the least stable gene (the gene with highest M value) leaves two genes with the most stable expression. Pairwise variation is sued to calculate the optimal number of reference genes for normalisation (GeNorm V) when $V (n/n+1) < 0.15$.

2.15.6 Quantitative Real-Time PCR

For mRNA

The resultant 20 µl cDNA reaction mixture from cells and EV samples were diluted with 80 µl or 20 µl respectively with nuclease free H_20. 5 µl of this diluted cDNA was used per qPCR reaction with 1 µl FAM or VIC labelled Taqman Gene Expression Assay (20x) (Life Technologies) (Tables 2.8 and 2.9), 10 µl Taqman Fast Universal Master Mix (2x) (Life Technologies), and 4 µl of nuclease free H_20. The StepOnePlus Real-Time PCR system with the relative standard curve method from serial dilutions of cDNA from untreated samples was used to determine the relative fold change for each target's gene expression. The cycling reaction was a 95 °C activation for 20 seconds after which there were forty cycles of 1 second at 95 °C and 20 seconds at 60 °C. The StepOne Software v2.2.2 (Life Technologies) was used to analyse the data. According to the results from the GeNorm Assays, expression was normalised to GAPDH and ACTB.

Gene Name	Assay ID
ACTB	Hs01060665_g1
GAPDH	Hs02758991_g1
Htt	Hs00918174_m1
HuR	Hs00171309_m1
mTOR	Hs00234508_m1

Table 2.8 List of Human qPCR Probes. Taqman probes for human genes used in qPCR analysis.

Gene Name	Assay ID
ACTB	Mm01205647_g1
GAPDH	Mm03302249_g1
HTT	Mm01213820_m1
HuR	Mm00516011_m1

Table 2.9 List of Murine qPCR Probes. Taqman probes for murine genes used in qPCR analysis.

For siRNA

HuR siRNA in samples was denatured with a 5 minute incubation at 95 °C. The reverse primer (GGAAGCCGACAAGTACGGA) was annealed by a 2 minute incubation at 80, 70, 60, and 45 °C. One step RT-PCR was set up using AgpathID One-Step RT-PCR with reaction mixture: 7 µl sample, 12.5 µl Taqman buffer, 10 µM forward primer (FAM-ACTCCCTCCCTCGATTTTTAATTATCTATT), 10 µl reverse primer, 50 µM antiprimer (AAATCGAGGGAGGGAG-BHQ), 1 µl of 25x RT-PCR enzyme and 3 µl water. The incubations were 1 cycle at 40 °C, 1 cycle at 95 °C, and 40 cycles of: 95 °C for 15 seconds and 45 °C for 60 seconds. The StepOnePlus Real-Time PCR system and analysis were used as above.

2.16 Protein Quantification

2.16.1 Protein Extraction

Protein was extracted from cells with Cell Extraction Buffer (Life Technologies) according to the manufacturer's instructions. It was supplemented with Half Protease and Phosphatase Inhibitor Cocktail 100x (Life Technologies) and 1 mM phenylmethyl sulfanyl flouride (PMSF). Cells were harvested by scraping from 6-well plates with 200 µl of the cell extraction buffer mixture. Samples were placed on ice for 30 minutes with vortexing every 10 minutes to lyse the cells. They were then centrifuged at 11,000g for 10 minutes at 4 ºC. The supernatant was removed and the concentration of protein in this resultant cell lysate was measured using the microBCA Protein Assay Kit (Life Technologies) according to the manufacturer's instructions. It was stored at -80 ºC.

2.16.2 Enzyme-Linked Immunosorbent Assays (ELISAs)

Human patient derived fibroblasts were transfected with treatments designed to reduce HTT expression as described above. Cells were detached with trypsin, collected by centrifugation, washed three times in cold PBS (Life Technologies). They were lysed by ultrasonication and centrifigued at 1,500g for 10 minutes at 4 ºC to remove cellular debris. Protein concentration was measured using a Bradford Assay and concentrations normalised by dilution in PBS. A human HTT ELISA kit MBS2021852 (My BioSource) was used to measure HTT protein levels according to the manufacturer's instructions. The kit standard was reconstituted at 100 ng/ml with gentle shaking at room temperature, and diluted to 10 ng/ml. A double dilution series of the standard was set up. Detection reagents A and B were diluted to working concentrations of 1:100 and the wash solution

prepared from 30x concentrate in deionized water. 100 µl of standards, a blank and samples were added to the plate, it was covered with a plate sealer and incubated for 2 hours at 37 ºC. The liquid was removed from each well and 100 µl of Detection Reagent A added before a further 1 hour incubation at 37 ºC. The solution was removed and wells washed with 350 µl of wash solution. This process was repeated twice, the plate inverted and blotted against absorbent paper. 100 µl of Detection Reagent B was added and the plate was incubated for 30 minutes at 37 ºC before washing 5 times. 90 µl of substrate solution was added per well, the plate was protected from light and incubated for 15 minutes at 37 ºC. 50 µl of Stop Solution was added to each well. The absorbance at 450 nm was measured with a Victor3 1420 multilabel fluorescence microplate reader (Perkin Elmer).

2.17 MTS Cell Proliferation Assay

To evaluate cell viability following all treatments to knock down expression of Huntingtin, the CellTiter 96 Aqueous One Solution Cell Proliferation Assay (Promega) was used. Huntington's disease patient derived fibroblasts which had been transfected with each of the treatments according to the methods described above and incubated for 48 hours in a 96 well assay plate with 125 µl medium were treated with 25 µl of the CellTiter Solution Reagent. The cells were incubated for a further 3 hours and their absorbance at 490 nm was measured with a Victor3 1420 multilabel fluorescence microplate reader (Perkin Elmer).

2.18 Statistical Analysis

Statistical analyses of the data were performed using Prism 6.0 (GraphPad Software Inc.). Data was analysed by One-Way Analysis of Variance (ANOVA) followed by Tukey's multiple comparisons post hoc test to assess group statistical significance. For the biodistribution experiments, statistical analysis was performed using the Kruskal-Wallis test and Dunn's post hoc test. Experimental conditions were normalised to a non-specific negative control unless otherwise indicated. All results are expressed as mean ± standard error of the mean (SEM) and differences were considered significant at $p \leq 0.05$. Asterisks indicate significant difference compared to a negative control except where indicated by comparison bars. Asterisk (*) indicates $p \leq 0.05$, double asterisks (**) indicates $p \leq 0.01$ and triple asterisks (***) indicates $p \leq 0.001$.

CHAPTER 3 EVALUATION OF CARGO FOR SUPPRESSION OF HUNTINGTIN EXPRESSION

3.1 Introduction

Huntington's Disease (HD) is caused by an autosomal dominant CAG triplet repeat expansion in exon 1 of the Huntingtin (*HTT*) gene[285]. This is translated into an expanded polyglutamine tract which misfolds and aggregates generating the pathological hallmark of the disorder, intraneuronal inclusions[85]. Therefore, a rational therapeutic strategy for HD is to reduce *HTT* expression, thereby reducing the number of mutant polyglutamine tracts and aggregates and alleviating the neuronal dysfunction to which they contribute[165]. This approach would act early in the cascade of pathological events in HD and if implemented prior to disease manifestation could potentially prevent the disorder from taking hold[165]. The silencing of *HTT* as a treatment for HD has shown promise *in vitro* and *in vivo* in animal models[79,108,151,152,180,286]. Once *HTT* expression is reduced, neurodegeneration is halted[165].

An effective treatment for HD must bypass the blood brain barrier (BBB) and also reach *HTT*, an intracellular target for which conventional drugs such as antibodies cannot reach. The BBB functions to protect the CNS from the external environment but it is also the greatest obstacle to the safe and effective treatment of neurological disorders including HD. In order to treat a neurological disease safely, Alvarez-Erviti *et al*. hypothesised that it might be possible to hijack an EVs endogenous role in intracellular communication of RNA cargo to deliver systemically injected nucleic acid parcelled in a vesicle past the

BBB and to an intracellular location to silence a therapeutic target in Alzheimer's disease (AD)[213].

With the goal of building on previous research and adapting it for HD by the delivery of a therapeutic nucleic acid across the BBB to reduce *HTT* expression, this study firstly analysed potential EV cargos for this approach. The types of cargos investigated were double stranded short interfering RNAs (siRNAs), single stranded antisense oligonucleotides (ASOs) - specifically locked nucleic acids (LNAs) and exon skipping oligonucleotides - and the plasmids clustered regularly-interspaced short palindromic repeats interference (CRISPRi) and short hairpin RNA (shRNA). These were described in Chapter 1, but briefly siRNAs are short double stranded nucleic acids which regulate gene expression through appropriation of the cells ubiquitously expressed endogenous miRNA processing machinery[173]. The guide strand of the siRNA is loaded into the RNA-induced silencing complex (RISC) and undergoes base pairing with the target mRNA directing sequence specific mRNA cleavage or if there is imperfect pairing such as with miRNA, there is an inhibition of translation[171,173–175,287]. LNAs exert their gene expression repression via Watson-Crick binding to the target mRNA and exerting a steric block on translation or induction of RNase H mediated cleavage[288]. Exon skipping oligonucleotides target pre-mRNA, before it is spliced to remove intervening introns[192]. They are complementary to an exonic splicing enhancer (ESE) and their binding increases the likelihood of removal of an exon by inducing altered splicing. shRNAs are longer RNAs which can be delivered as expression plasmids. On expression in the target cell they form shRNA hairpins following cleavage by Drosha, an enzyme in the cell's own repertoire of RNA processing machinery. They are then exported from the nucleus and cleaved by Dicer after which they act in the same way as siRNAs to silence a gene

of interest[200–202,289]. The other plasmid based approach used here to generate *HTT* silencing is CRISPRi. This system borrows from the prokaryotic mechanism of nucleic acid editing in their adaptive immune response[197–199,290]. An sgRNA can be designed which is complementary to a region around the transcription start site (TSS) of the gene of interest, the sgRNA binds the complementary DNA, an enzymatically inactive dCas-9 is recruited and a steric block of transcription follows[205].

The methods to silence *HTT* described above were investigated here for their potency both at the message and protein level and for the duration of silencing they can induce in a HD *in vitro* model; patient-derived fibroblasts. Lastly, their toxicity was measured. The most promising candidates for *HTT* silencing identified in this study were exon skipping oligonucleotides, siRNA and CRISPRi, however due to the slight toxicity of the exon skipping oligonucleotides and perceived difficulty in packaging all of the components necessary for CRISPRi within EVs, in reaching the nucleus and dependency on accessibility of the TSS for CRISPRi silencing, siRNA was chosen as the cargo to bring forward to investigate EV loading in chapter 5.

3.2 Results

3.2.1 Identification of Optimal *In Vitro* Reference Genes for Human Fibroblasts

In this study the chosen HD model system to screen potential nucleic acid cargos for loading into EVs to reduce expression of *HTT* was patient-derived fibroblasts[291]. The HD fibroblast cell line used in this study (GM04281) has one mutant and one wild type allele, with 68 and 17 repeats respectively, which allows testing of both therapeutics directed

against the mutant allele specifically, and those directed against both the mutant and the wild type[292]. HD fibroblasts have been used in many studies to evaluate the efficacy of different therapies aimed at reducing *HTT* expression as they provide a validated model system without the use of an animal model[293].

Initial experiments yielded results with large errors in some samples. Investigation of this variation exemplified a need to evaluate the most stably expressed control genes across samples. To ensure the best read-out following treatment with the nucleic acid therapeutics, geNorm analysis to establish the optimal reference genes for normalisation was performed on the fibroblast line used to test the nucleic acids. GeNorm is a robust method to select both the most stable housekeeping genes for qPCR normalisation and the number of normalisation genes to use, and was performed here to identify the best candidate reference genes to use during qPCR[294]. The geNorm Perfect Probe Human Kit which compares the expression of 12 candidate reference genes in test samples was used to determine both the most stable reference genes and the optimal number of reference genes for qPCR normalisation **(Figure 3.1)**. The qbase$^+$ software associated with the kit identified the most stable reference genes through calculation of the average expression stability value (geNorm M), which is the variation of a gene compared to all other candidate reference genes following stepwise exclusion of the least stable gene. The optimal number of reference genes (geNorm V) was calculated by pairwise variation when $V_{n/n+1} < 0.15$. In this study the optimal reference genes, those with highest stability (lowest geNorm M), were *GAPDH* and *ACTB* **(Figure 3.1)**. The analysis also revealed that a combination of the geometric mean of these genes was optimal for normalisation **(Figure 3.1)**.

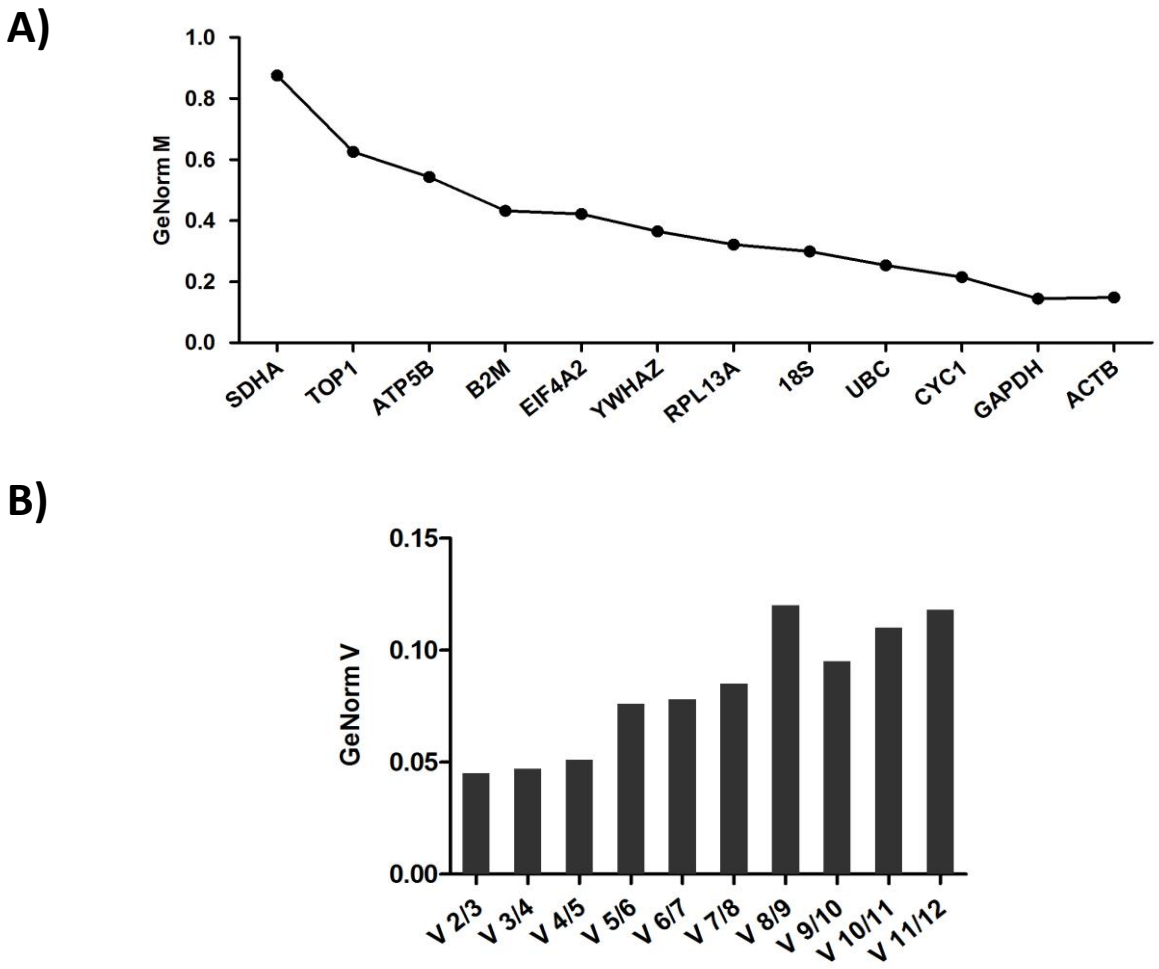


Figure 3.1 Identification of Optimal *In Vitro* Reference Gene for Human Fibroblasts. The expression of 12 candidate reference genes was assessed with qPCR using the geNorm Perfect Probe Plus Human Kit and qbase^{+} software. **A)** The most stable reference genes were identified via calculation of geNorm M (the average expression stability of a gene or the variation of a gene compared to the other candidate genes) of reference genes at each step during algorithmic step-by-step exclusion of the least stably expressed reference genes. The most stable and therefore optimal pair of reference genes for this study are *GAPDH* and *ACTB*, as indicated on the right of the graph with the lowest M. **B)** The optimal number of reference genes for accurate normalisation was assessed by pairwise variation (geNorm V) when V (n/n+1) < 0.15. In this study, a combination of two reference genes (*GAPDH* and *ACTB*) was identified as optimal for *in vitro* normalisation in human fibroblasts.

3.2.2 Identification of Optimal *In Vitro* Reference Gene for HEK293 cells

HEK293 cells were also used in this study for novel treatments to establish efficacy in a system where the cells are easier to grow, maintain and transfect than HD fibroblasts. GeNorm analysis of HEK293 cell samples was performed to determine the most stable and therefore optimal reference genes to use for qPCR normalisation. For this analysis the geNorm Perfect Probe Human Kit was used as above and the qbase^{+} software determined that the most stable reference genes with lowest geNorm M scores indicating highest stability were *GAPDH* and *ACTB* and a combination of their geometric mean was used for optimisation as indicated by the geNorm V score **(Figure 3.2).**

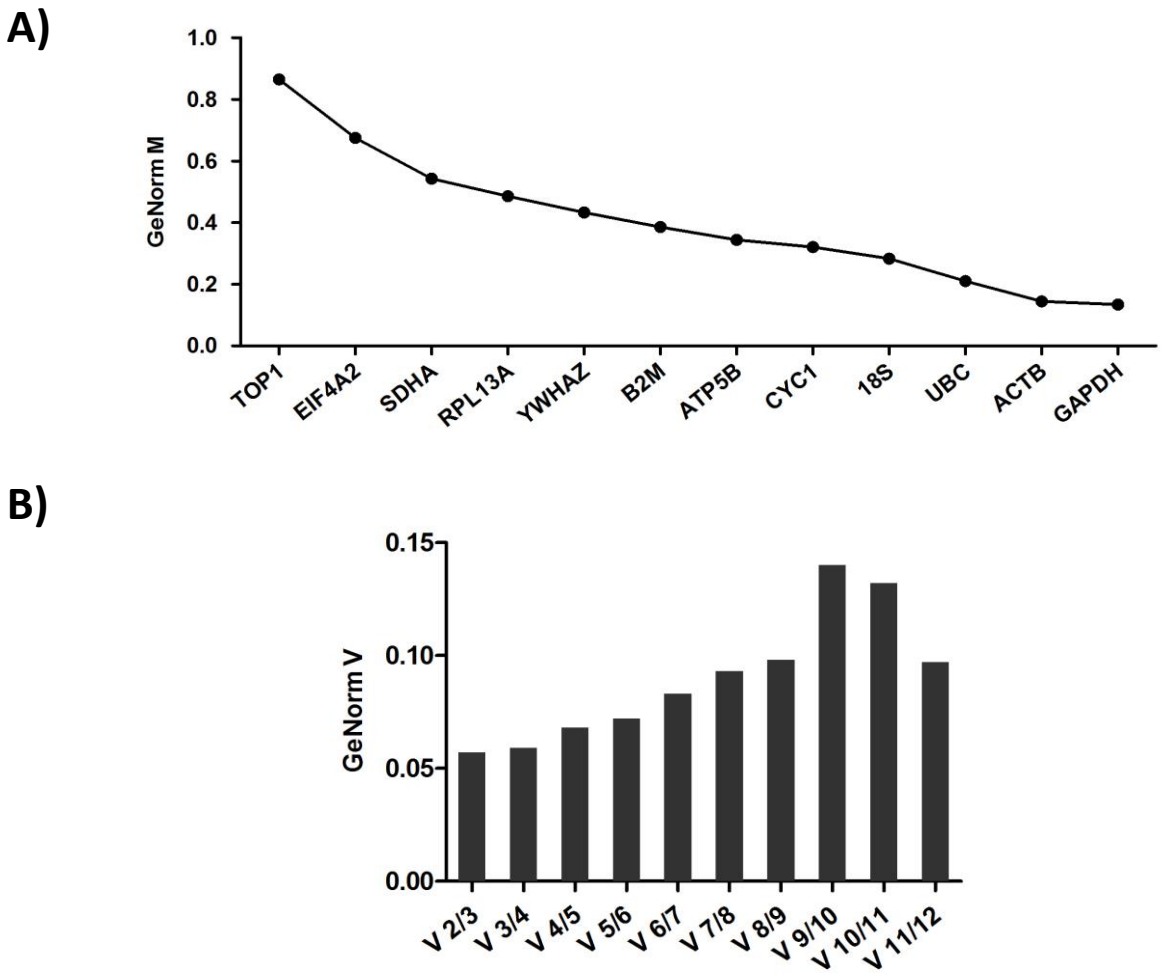


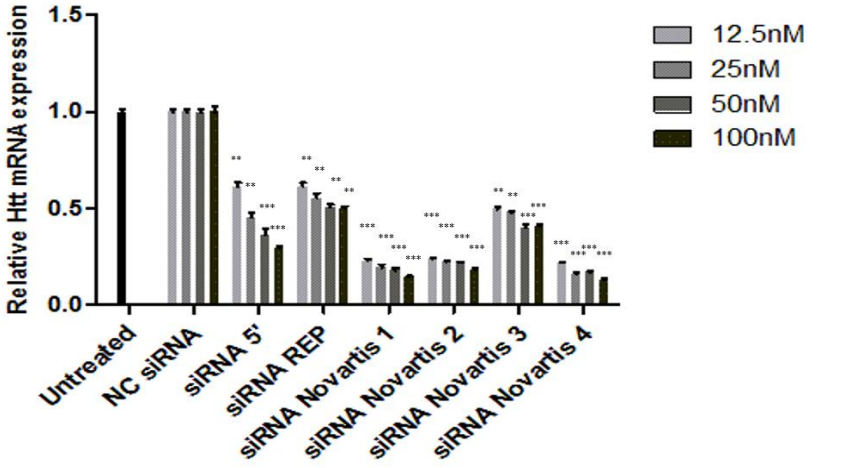
Figure 3.2 Identification of Optimal *In Vitro* Reference Gene for Human HEK293 cells. The expression of 12 candidate reference genes was assessed with qPCR using the geNorm Perfect Probe Plus Human Kit and qbase^{+} software. **A)** The most stable reference genes were identified via calculation of geNorm M (the average expression stability of a gene or the variation of a gene compared to the other candidate genes) of reference genes at each step during algorithmic step-by-step exclusion of the least stably expressed reference genes. The most stable and therefore optimal pair of reference genes for this study are *GAPDH* and *ACTB*, as indicated on the right of the graph with the lowest M. **B)** The optimal number of reference genes for accurate normalisation was assessed by pairwise variation (geNorm V) when V (n/n+1) < 0.15. In this study, a combination of two reference genes (*GAPDH* and *ACTB*) was identified as optimal for *in vitro* normalisation in human HEK293 cells.

3.2.3 Investigation of siRNA Treatments for Huntingtin Silencing

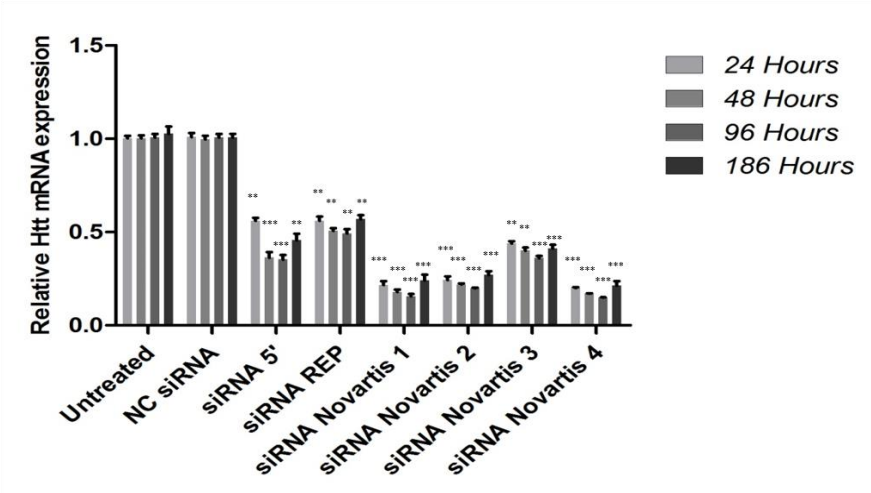
Six siRNAs, double stranded RNAs of 20-25 base pairs which silence genes by recruiting the RISC complex inducing cleavage of the target mRNA or a steric block of translation were transfected individually into HD patient-derived fibroblasts. siRNA-5' targets a region upstream of the CAG triplet repeat. siRNA-REP targets a region within the repeat and is thus allele specific for the mutant *HTT* allele. The remaining four of these siRNAs (siRNA-N1-4) were provided by Novartis. A negative control siRNA was included. To ascertain the potency of the siRNAs they were transfected using Lipofectamine 2000 and following 48 hours the resultant *HTT* mRNA levels normalised to *GAPDH* and *ACTB* were measured at concentrations of 12.5, 25, 50 and 100 nM **(Figure 3.3A)**. To determine the duration of silencing of the siRNAs they were transfected at a concentration of 100 nM into patient-derived fibroblasts using Lipofectamine 2000 and the mRNA expression level of *HTT* normalised to *GAPDH* and *ACTB* was analysed 24, 48, 96 and 186 hours post-transfection **(Figure 3.3B)**.

The most potent siRNAs tested - those that induced the highest level of silencing at the doses tested - were siRNA-N1, siRNA-N2 and siRNA-N4 with *HTT* expression at the highest dose reduced to 14.3, 18.7 and 13.1% respectively **(Figure 3.3A)**. siRNA-5' was also potent, reducing *HTT* expression to 29.5% at 100 nM. siRNA-REP was the least potent siRNA tested with *HTT* mRNA expression remaining at 50.5% following administration of the highest dose tested. The duration of silencing study revealed that all siRNAs directed against *HTT* induced lasting knockdown of *HTT* expression. Silencing was significant for all siRNAs tested at all time points though maximal silencing for each siRNA was at 96 hours showing a trend towards some recovery at 186 hours **(Figure 3.3B)**.

A)


Relative Htt mRNA expression
1.5
1.0
0.5
0.0
12.5nM
25nM
50nM
100nM
Untreated
NC siRNA
siRNA 5'
siRNA REP
siRNA Novartis 1
siRNA Novartis 2
siRNA Novartis 3
siRNA Novartis 4

B)


Relative Htt mRNA expression
1.5
1.0
0.5
0.0
24 Hours
48 Hours
96 Hours
186 Hours
Untreated
NC siRNA
siRNA 5'
siRNA REP
siRNA Novartis 1
siRNA Novartis 2
siRNA Novartis 3
siRNA Novartis 4

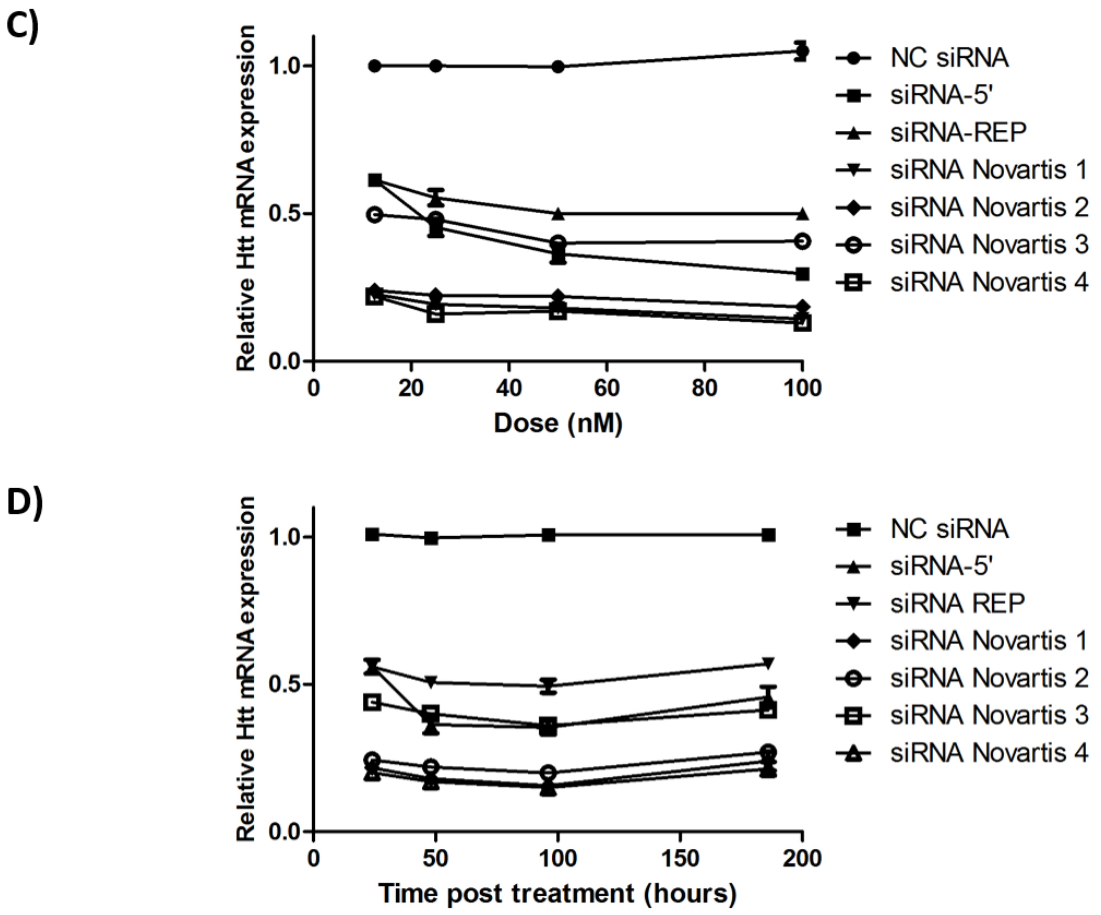


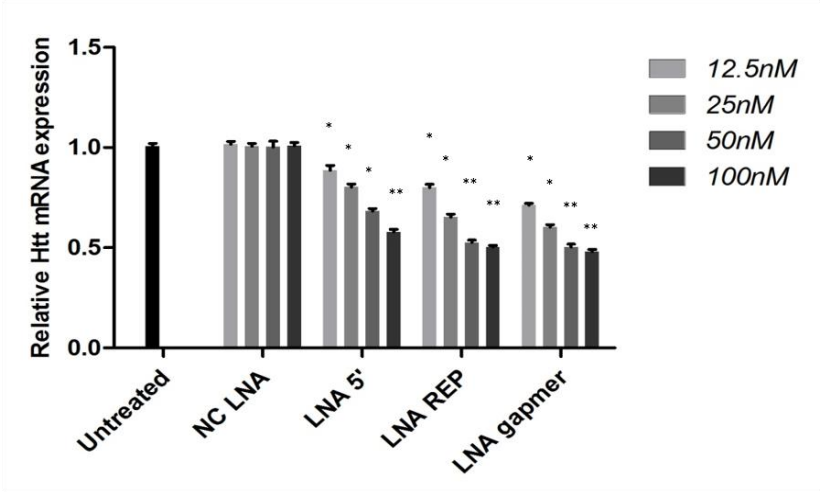
Figure 3.3 Investigation of siRNA Treatments for Huntingtin Knockdown. Patient-derived HD fibroblasts were left untreated, transfected with a negative control (NC) siRNA or transfected with several siRNAs predicted to reduce *HTT* expression in different doses (A and C) and at the same dose following different lengths of time post-transfection (B and D). Graphs indicate the resultant relative *HTT* mRNA levels assessed by qPCR normalised to housekeeping genes *GAPDH* and *ACTB*. siRNA-5' targets a region upstream of the CAG triplet repeat, siRNA-REP targets a region within the repeat and is thus allele specific for the mutant HTT allele. siRNA Novartis 1-4 (siRNA-N1-4) were a gift from Novartis. **A)** Dose response showing relative *HTT* mRNA measured 48 hours after transfection with 12.5, 25, 50 and 100 nM siRNA. **B)** Duration of silencing following transfection with 100 nM of siRNA. **C)** Scatter plot as an alternative display of the dose response data in part A. **D)** Scatter plot as an alternative display of the time course data in part B. Values represent mean + SEM, n = 4. Statistical differences were calculated by one-way ANOVA and Tukey's post hoc test. Significance indicated is compared to negative control. ***p<0.001, **p<0.01, *p<0.05.

3.2.4 Investigation of LNA Treatments for Huntingtin Silencing

LNAs are modified nucleic acids where there is a bridge between the 2'-oxygen and 4'-carbon to increase stability. The LNAs used in this study target either the repeat (LNA-REP) or an area upstream of the repeat (LNA-5'). These ASOs were designed to reduce *HTT* expression through a steric blockade of the binding of ribosomal units for translation. An LNA gapmer was also included. Gapmers contain LNA bases flanking a central DNA region and induce silencing via recruitment of RNase H to cleave the mRNA of a DNA-RNA duplex[295]. These were transfected alongside a non-coding control LNA at doses of 12.5, 25, 50 and 100 nM into patient-derived fibroblasts with Lipofectamine 2000 and *HTT* mRNA expression following 48 hours and normalised to *GAPDH* and *ACTB* was measured **(Figure 3.4A)**. To assess the duration of silencing effects the LNAs were transfected at 100 nM and *HTT* mRNA expression 24, 48, 96 and 186 hours following transfection and normalised to *GAPDH* and *ACTB* was assessed **(Figure 3.4B)**.

Each LNA generated silencing at all doses tested. At the highest dose of 100 nM *HTT* expression was reduced to 58.5, 50.4 and 48.2% for LNA-5', LNA-REP and LNA gapmer respectively **(Figure 3.4A)**. Furthermore, the reduction in *HTT* expression persisted for the full length of the study, though as with the siRNAs there was a trend towards some recovery evident at 186 hours **(Figure 3.4B)**.

A)



B)

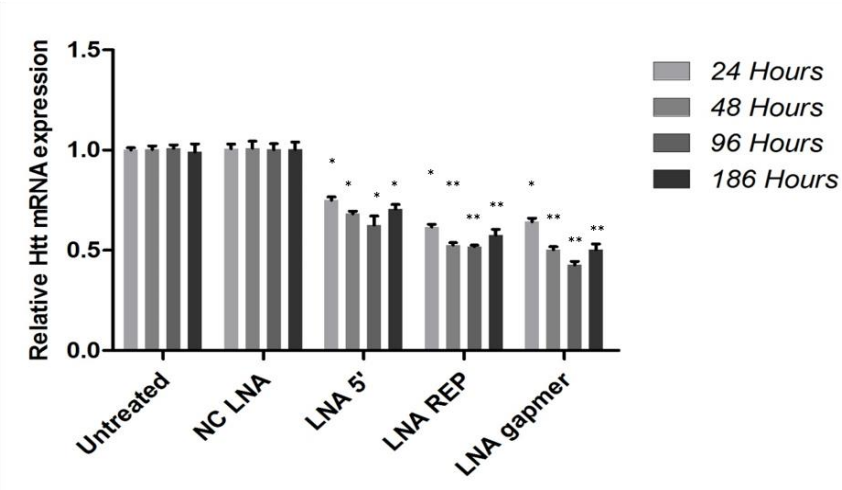


Figure 3.4 Investigation of Antisense Oligonucleotide Treatments for Huntingtin Knockdown. Patient-derived fibroblasts were left untreated, transfected with a negative control (NC) LNA or transfected with several LNAs predicted to reduce *HTT* expression, one targeting an area upstream of the CAG triplet repeat (LNA-5'), one targeting the repeat (LNA-REP) and a gapmer, in different doses (A) and at the same dose following different lengths of time post-transfection (B). Graphs indicate the resultant relative *HTT* mRNA levels assessed by qPCR normalised to housekeeping genes *GAPDH* and *ACTB*. **A)** Dose response showing relative *HTT* mRNA measured 48 hours after transfection with 12.5, 25, 50 and 100 nM LNA. **B)** Duration of silencing following transfection with 100 nM of LNA. Values represent mean + SEM, n = 4. Statistical differences shown were calculated by one-way ANOVA and Tukey's post hoc test. Significance indicated is compared to negative control. ***p<0.001, **p<0.01, *p<0.05.

3.2.5 Investigation of Multigene Oligonucleotides for Huntingtin Silencing

Although HD is caused by a CAG triplet repeat in the *HTT* gene there are other proteins which interact with HTT and could also prove effective as targets for gene therapy in combination with *HTT* targeting. One such candidate is *mTOR* as reducing *mTOR* expression has been shown to reduce the toxicity of polyglutamine expansions in fly and mouse models of HD[296]. A multigene LNA targeting both *HTT* and *mTOR* was designed by Dr. Miguel Varela (Wood lab) with a bioinformatic algorithm to identify overlapping sequences of 13-15 nucleotides between the genes of interest. This was transfected alongside a negative control LNA to patient-derived fibroblasts at doses of 12.5, 25, 50 and 100 nM to assess the potency at silencing both genes normalised to *GAPDH* and *ACTB* **(Figure 3.5A)**. The duration of the silencing effect was measured by recording *HTT* expression normalised to *GAPDH* and *ACTB* 24, 48, 96 and 186 hours after transfection with 100 nM of the LNA **(Figure 3.5B)**.

HTT silencing by the multigene oligonucleotide was not as potent as the best siRNA or LNA but expression was reduced to 74.3% alongside *mTOR* expression of 58.5% at the highest dose, 100 nM **(Figure 3.5A)**. The duration of silencing followed a similar pattern as seen above for the siRNAs and LNAs with strongest silencing observed at 96 hours following transfection **(Figure 3.5B)**.

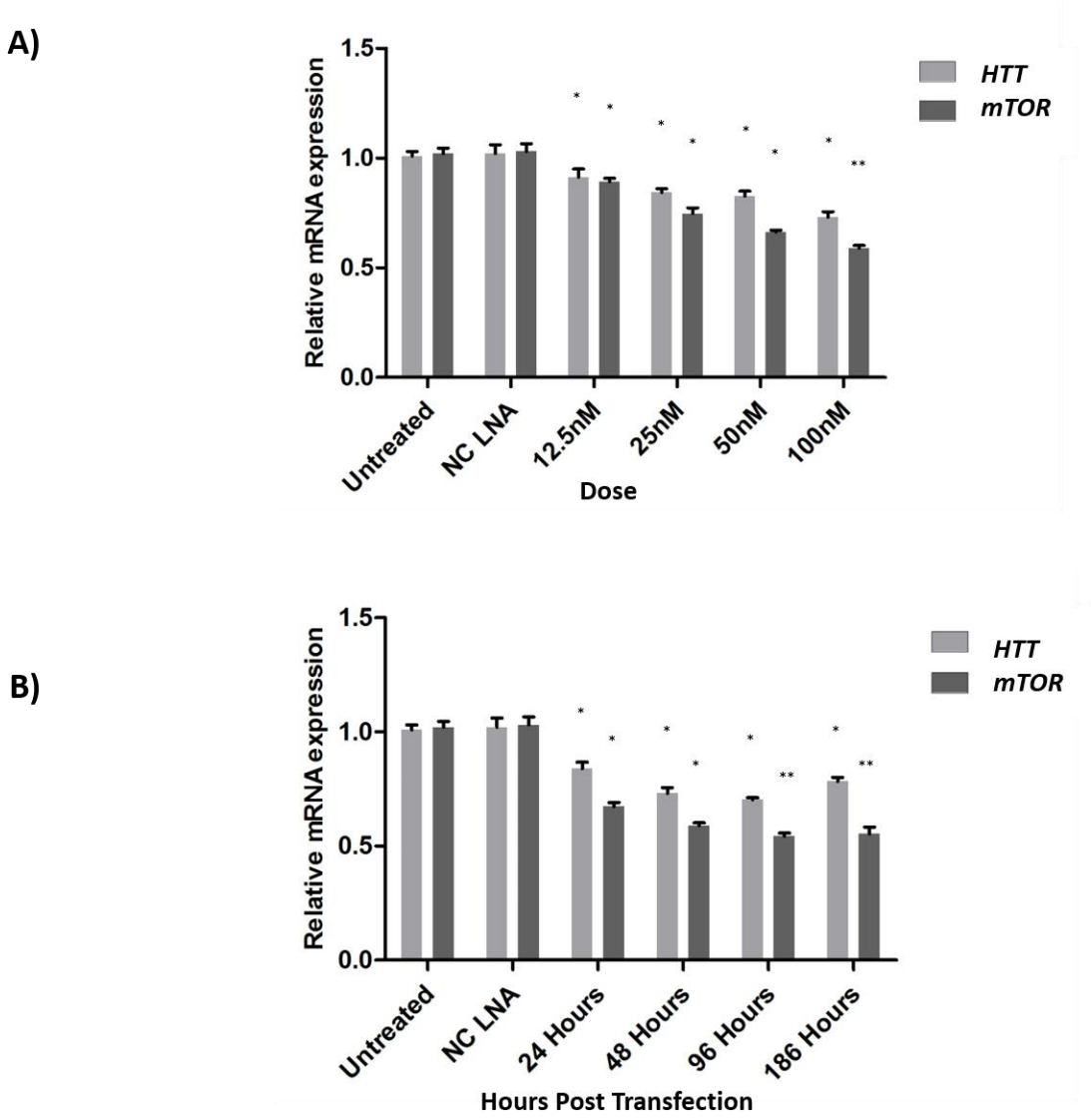


Figure 3.5 Investigation of Multigene Oligonucleotide Treatments for Huntingtin Knockdown. Patient-derived fibroblasts were left untreated, transfected with a negative control (NC) LNA or transfected with a multigene LNA predicted to reduce *HTT* and *mTOR* expression in different doses (A) and at the same dose following different lengths of time post-transfection (B). Graphs indicate the resultant relative *HTT* mRNA and *mTOR* levels assessed by qPCR normalised to housekeeping genes *GAPDH* and *ACTB*. **A)** Dose response showing relative *HTT* and *mTOR* mRNA measured 48 hours after transfection with 12.5, 25, 50 and 100 nM LNA. **B)** Duration of silencing following transfection with 100 nM of LNA. Values represent mean + SEM, n = 4. Statistical differences shown were calculated by one-way ANOVA and Tukey's post hoc test. Significance indicated is compared to the negative control of the same gene. ***p<0.001, **p<0.01, *p<0.05.

3.2.6 Investigation of Exon Skipping Oligonucleotides for Huntingtin Silencing

Exon skipping oligonucleotides, most often used to alter RNA splicing to skip over regions of a gene which are damaged and restore the reading frame, were designed here to skip exon 3 of the *HTT* gene leading to a shift in the reading frame from exon 4. This shift would cause the expression of a stop codon early in exon 4 **(Figure 3.6)**. The short RNA fragments produced are predicted to be degraded by nonsense mediated decay.

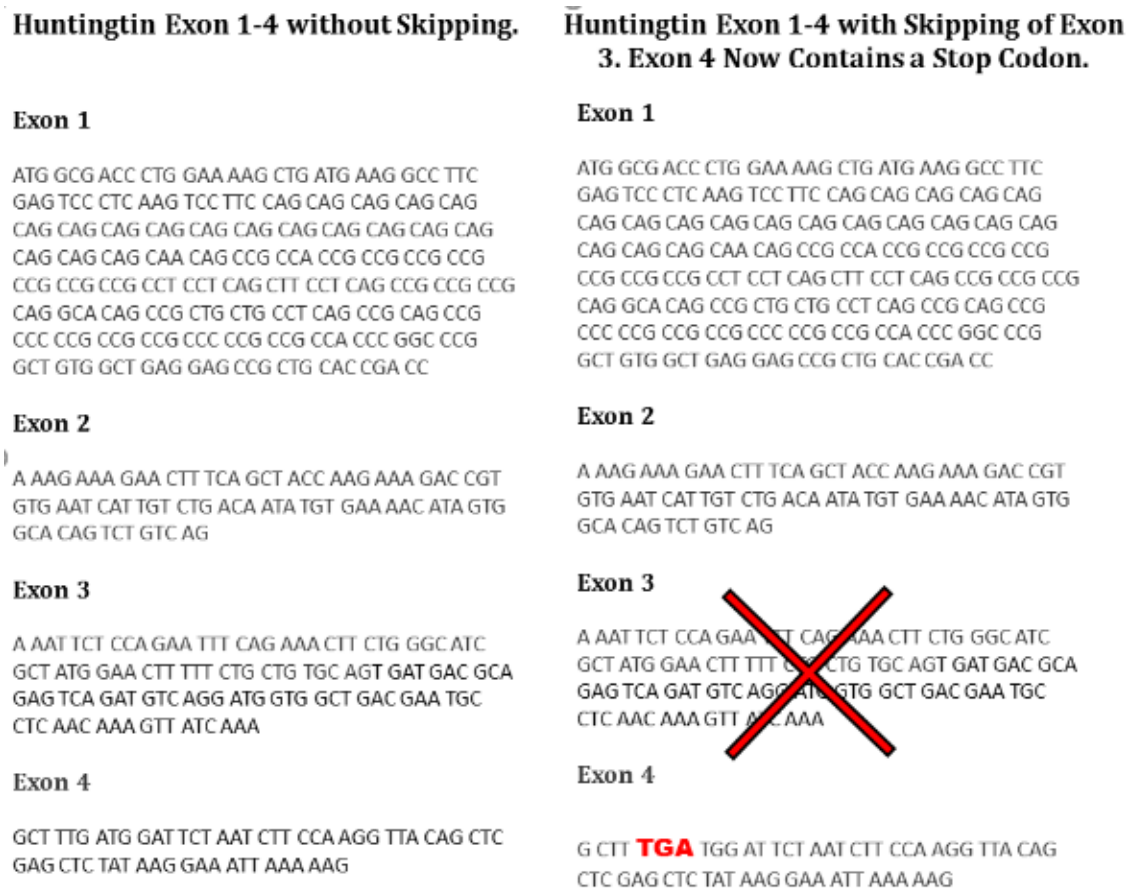
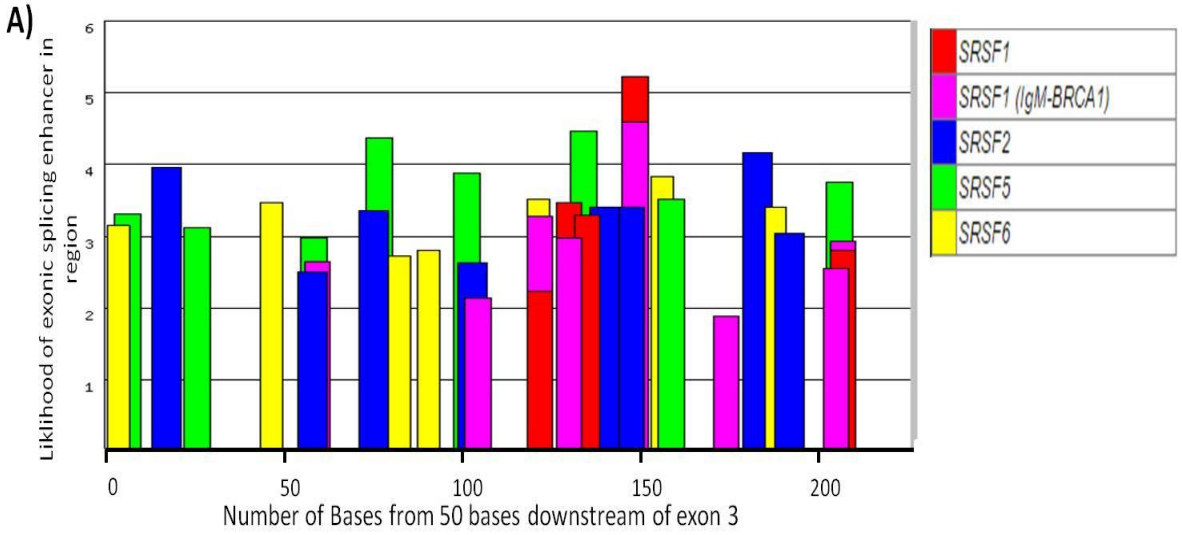


Figure 3.6 Predicted Sequence Following Exon Skipping of Huntingtin Exon 3. Skipping of Huntingtin exon 3 would alter the reading frame resulting in a fragment ending in an in frame TGA stop codon. This fragment should be degraded by nonsense-mediated decay. Stop codon highlighted in red.

Antisense oligonucleotides which could alter the splicing and induce skipping of exon 3 were designed with Dr. Graham McClorey (Wood Lab) using the software tools ESE finder and RESCUE-ESE to locate exonic splicing enhancers (ESEs). These web-based computational resources are based on experimental validation and allow the identification of putative ESEs, the binding sites for serine/arginine-rich (SR) proteins containing RNA-recognition motifs (RRM) which determine sequence-specificity of binding and a C-terminal SR domain rich in SR dipeptides important for protein-protein interactions for recruitment of the core splicing machinery[297].

ESE finder identifies short 6-8 nucleotide motifs for binding a subset of SR proteins and can scan a nucleotide sequence and predict candidate ESEs responsive to the SR proteins SF2/ASF, SC35, SRp40 and SRp55. To do this a functional Systematic Evolution of Ligands by Exponential enrichment (SELEX) selection procedure had been used to determine nucleotide-frequency matrices[298,299]. Briefly, the approach involved replacing a natural enhancer in an IgM minigene with random 20 nucleotide sequences from a library. The pool of minigenes created was utilised to create pre-mRNA transcripts. These transcripts underwent *in vitro* splicing dependent on an ESE and a recombinant SR protein capable of functionally recognizing the ESE. Minigene templates were built with the spliced mRNAs following gel-purification and amplification, cloning, sequencing and progressively enriching sequences bearing the ESE activity motifs allowed the identification of the nucleotide-frequency matrices. There were several predicted ESE motifs in the desired region which consisted of exon 3 and 50 base pairs upstream and downstream of exon 3 **(Figure 3.7)**.

A)


Liklihood of exonic splicing enhancer in region
6
5
4
3
2
1
0
50
100
150
200
Number of Bases from 50 bases downstream of exon 3
SRSF1
SRSF1 (IgM-BRCA1)
SRSF2
SRSF5
SRSF6

B)

SRSF1 threshold: 1.956		SRSF1 (IgM-BRCA1) threshold: 1.867		SRSF2 threshold: 2.383		SRSF5 threshold: 2.67		SRSF6 threshold: 2.676	
Position*/Site/Score		Position*/Site/Score		Position*/Site/Score		Position*/Site/Score		Position*/Site/Score	
117 (-105)	CGCAGAG 2.23323	56 (-166)	CTCCAGA 2.64953	14 (-208)	ggctcctc 3.96065	4 (-218)	tgtcacc 3.30732	2 (-220)	catgtc 3.14477
125 (-97)	CAGATGT 3.46589	100 (-122)	CTGCTGT 2.14309	54 (-168)	TTCTCCAG 2.50039	23 (-199)	tgacagc 3.12112	44 (-178)	tgctta 3.46667
130 (-92)	GTCAGGA 3.28514	117 (-105)	CGCAGAG 3.27618	71 (-151)	AACTTCTG 3.34865	55 (-167)	TCTCCAG 2.97232	79 (-143)	GGCATC 2.71795
143 (-79)	CTGACGA 5.22033	125 (-97)	CAGATGT 2.98016	98 (-124)	TTCTGCTG 2.62582	73 (-149)	CTTCTGC 4.36265	87 (-135)	IATGGA 2.79641
200 (-22)	cagagct 2.80777	143 (-79)	CTGACGA 4.58839	134 (-88)	GGATGGTG 3.39715	97 (-125)	TTTCTGC 3.87671	117 (-105)	CGCAGA 3.51736
		168 (-54)	CAAAgta 1.88465	141 (-81)	GGCTGACG 3.40190	129 (-93)	TGTCAGG 4.45558	151 (-71)	TGCCTC 3.83191
		198 (-24)	ctcagag 2.54670	176 (-46)	gaacggtg 4.16481	153 (-69)	CCTCAAC 3.50997	182 (-40)	tgtgga 3.40507
		200 (-22)	cagagct 2.93671	185 (-37)	ggatgacg 3.03566	199 (-23)	tcagagc 3.75744		

* both positions from 5'end (through 1) and 3'end (through -1) are given

Figure 3.7 Determination of Potential Sequences for Exon Skipping Oligonucleotides to Skip Huntingtin Exon 3 using ESEFinder. Through ESEFinder from where these figures were adapted, weighted matrices were used to identify potential motifs or Exonic Splicing Enhancers (ESEs) within a given target sequence (here *HTT* exon 3 including 50 base pairs upstream and downstream) where splicing factors serine/arginine-rich (SR) proteins are likely to bind. **A)** Graphical representation of the potential exonic splicing enhancer sites within and surrounding *HTT* exon 3. Motif scores indicating the likelihood of an ESE within a region are depicted on the y-axis and base pairs from 50 bases downstream of *HTT* exon 3 on the x-axis. **B)** The sequence motifs for each SR protein including the thresholds above which a score is taken as significant.

RescueESE identifies ESEs through searching for hexanucleotides which are significantly enriched in human exons compared to introns and occur significantly more often in exons with weak non-consensus splice sites than strong consensus splice sites[300]. These sequences had been validated *in vivo* in tests of splicing enhancer activity by introduction into a weak poorly spliced exon within a splicing reporter construct. The reporter minigenes when transfected into cultured cells were transcribed and spliced so the level of inclusion of the test exon could be assayed by qPCR. Point mutations of the putative ESE sequences had been used to confirm the hexamer motifs bearing the ESE activity. 238 hexamers were identified as putative ESEs. The RESCUE-ESE predicted several hexanucleotide ESE motifs within the desired region of 50 base pairs upstream and downstream of exon 3 **(Figure 3.8)**.

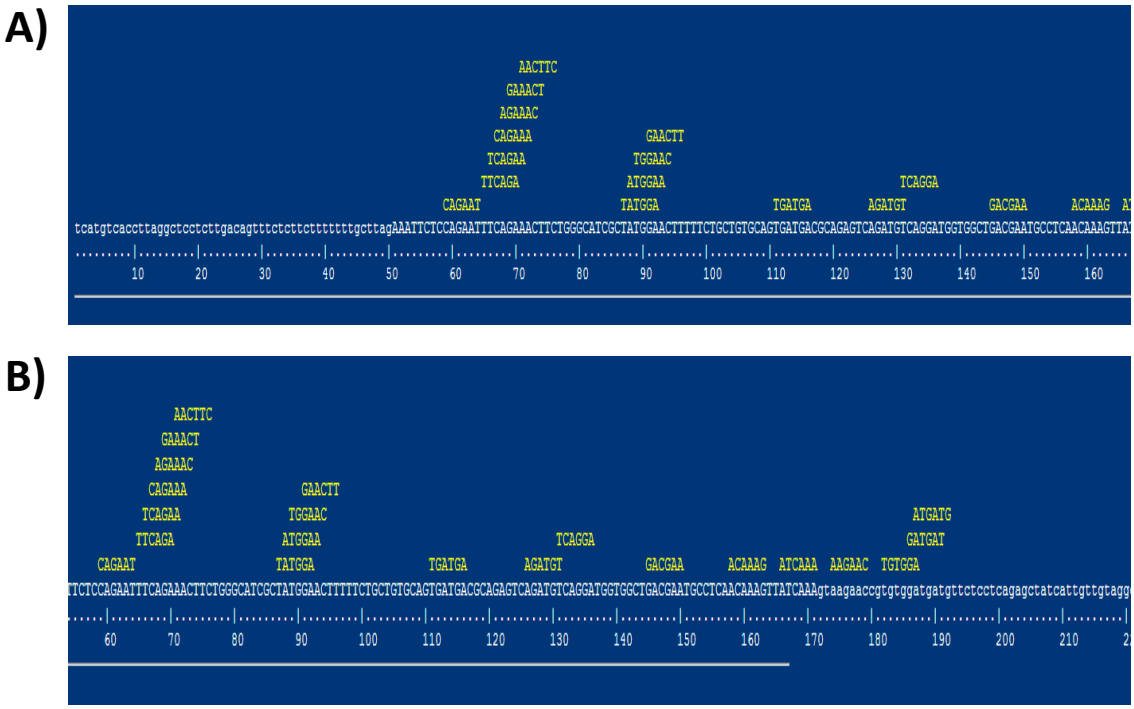


Figure 3.8 Validation of Potential Sequences for Exon Skipping Oligonucleotides for Skipping Exon 3 using RESCUE-ESE. Through MIT's RESCUE-ESE server from where these figures are adapted hexanucleotide sequences within the chosen region of interest (exon 3 and 50 base pairs upstream and downstream of *HTT* exon 3) were identified as potential exonic splicing enhancers (ESEs). Here candidate ESEs are chosen based on sequences identified by their more frequent appearance in exons than introns and in exons with weak splice sites than strong splice sites. Hexamers from these potential ESEs were validated by their ability to increase splicing following introduction into a poorly spliced exon in a splicing reporter construct. Any of these hexamers which appear in the region of interest are shown in A and B where **A)** from base 0 to160 and overlapping **B)** is from base 55 to 220 where base 0 is 50 bases upsteam of *HTT* exon 3.

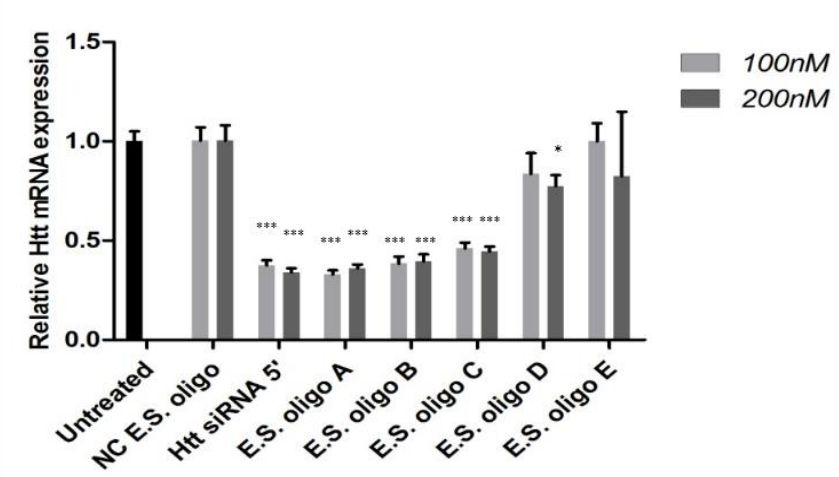
Within *HTT* exon 3 and regions of 50 base pairs upstream and downstream from the exon, the areas containing the highest frequency of candidate ESEs as identified by ESE-finder and RESCUE-ESE were used to design 5 antisense oligonucleotides to bind to these

regions with the aim of enhancing splicing of exon 3 to shift the reading frame so that exon 4 would contain a stop codon.

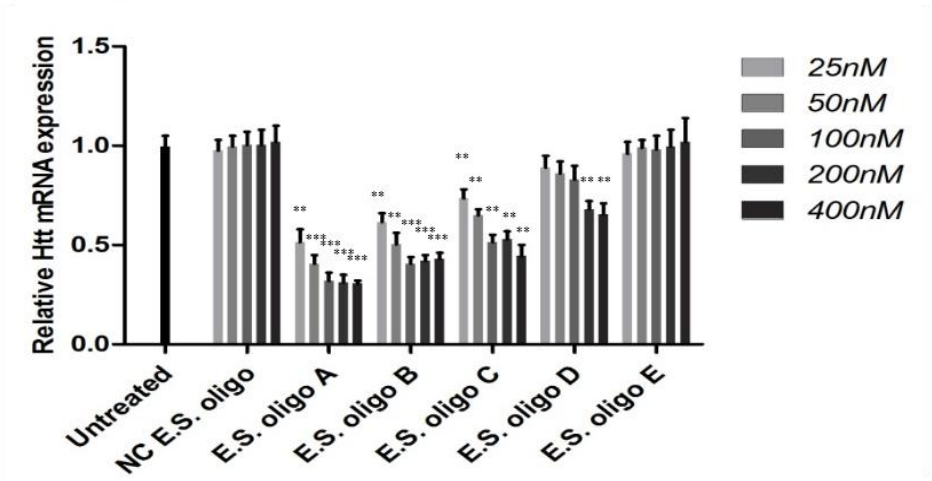
The exon skipping oligonucleotides, alongside a negative control exon skipping oligonucleotide, were transfected firstly into HEK293 cells in an initial pilot experiment to assess their efficacy at two doses, 100 and 200 nM. Following 48 hours the RNA was harvested and qPCR performed to measure *HTT* expression relative to *GAPDH* and *ACTB* **(Figure 3.9A)**.

Silencing was confirmed in HEK293 cells **(Figure 3.9A)** and dose response and duration of silencing studies in patient-derived fibroblasts followed. Cells were transfected with the exon skipping oligonucleotides (E.S. olgio) A - E and a control exon skipping oligonucleotide using Lipofectamine 2000 at more doses than previous experiments in an effort to increase the silencing seen in the pilot study. Here, doses of 25, 50, 100, 200 and 400 nM were used and RNA was analysed following 48 hours. Exon skipping oligonucleotide A showed the strongest silencing, with 30.2% *HTT* expression at the highest dose of 400 nM. Exon skipping oligonucleotides B and C were also promising with relative expression of *HTT* at 43.6 and 45.7% respectively **(Figure 3.9B)**. Furthermore, for the most promising candidate, exon skipping oligonucleotide A, a dose of 100 nM was sufficient for the maximum silencing obtained. A duration of silencing study performed at 100 nM confirmed exon skipping oligonucleotide A as the most potent silencer, this silencing remained high but more variable at 186 hours **(Figure 3.9C)**.

A)


Relative Htt mRNA expression
1.5
1.0
0.5
0.0
100nM
200nM
Untreated
NC E.S. oligo
Htt siRNA 5'
E.S. oligo A
E.S. oligo B
E.S. oligo C
E.S. oligo D
E.S. oligo E

B)


Relative Htt mRNA expression
1.5
1.0
0.5
0.0
25nM
50nM
100nM
200nM
400nM
Untreated
NC E.S. oligo
E.S. oligo A
E.S. oligo B
E.S. oligo C
E.S. oligo D
E.S. oligo E

C)

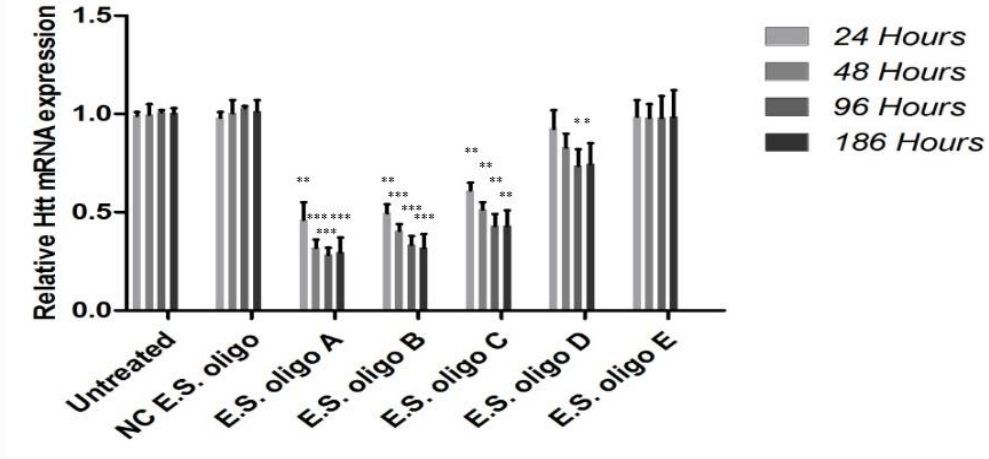

Relative Htt mRNA expression
1.5
1.0
0.5
0.0
24 Hours
48 Hours
96 Hours
186 Hours
Untreated
NC E.S. oligo
E.S. oligo A
E.S. oligo B
E.S. oligo C
E.S. oligo D
E.S. oligo E

Figure 3.9 Investigation of Exon Skipping Treatments for Huntingtin Knockdown. A) In a pilot experiment HEK293 cells were left untreated, transfected with a negative control (NC) exon skipping oligonucleotide or transfected with several exon skipping oligonucleotides predicted to reduce *HTT* expression. B) and C) Patient-derived fibroblasts were left untreated, transfected with a negative control (NC) exon slipping oligonucleotide or transfected with several exon skipping oligonucleotides predicted to reduce *HTT* expression in different doses (B) and at the same dose with RNA expression measured following different durations post-transfection (C). Graphs indicate the resultant relative *HTT* mRNA levels assessed by qPCR normalised to the housekeeping genes *GAPDH* and *ACTB*. **B)** Dose response showing relative *HTT* mRNA measured 48 hours after transfection with 25, 50, 100, 200 and 400 nM LNA. **C)** Duration of silencing following transfection with 100 nM of exon skipping oligonucleotides. Values represent mean + SEM, n = 4. Statistical differences shown were calculated by one-way ANOVA and Tukey's post hoc test. Significance indicated is compared to negative control. ***p<0.001, **p<0.01, *p<0.05.

To confirm exon skipping in these samples, a gene specific reverse transcription-polymerase chain reaction (RT-PCR) with primers upstream and downstream of exon 3 was performed on samples from the dose response study at the highest dose, 400 nM **(Figure 3.10)**. This demonstrated efficient skipping by exon skipping oligonucleotides A, B and C with smaller bands at 630 base pairs indicating low levels of transcript expressing exon 3, and thicker bands at 510 base pairs indicating skipping. There were thin bands at 510 base pairs in samples treated with exon skipping oligonucleotides D and E indicative of low levels of exon skipping. There was no band at 510 base pairs for the control sample showing no skipping took place **(Figure 3.10)**.

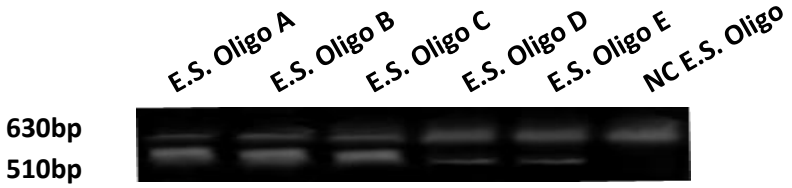


Figure 3.10 Gene Specific Reverse Transcription PCR. Gene Specific Reverse Transcription PCR was performed with primers either side of exon 3 to amplify the area surrounding and including the region predicted to be skipped by the exon skipping oligonucleotides. If the region did not contain exon 3, i.e. with skipping of exon 3, the amplified section would be 510 base pairs long or without skipping 630 base pairs.

This study was designed such that exon 3 would be skipped leading to a shift in the reading frame and a stop codon being expressed in exon 4. This would be predicted not to be translated but rather to be degraded by nonsense mediated decay. However, in HD short N-terminal protein fragments have been shown to form inclusions in animal models so it was important to ensure that no short protein fragments of exon 1-4 were generated using this method of silencing[301]. To this end, protein was extracted from samples which had been treated with the most promising exon skipping oligonucleotide candidate for *HTT* silencing when transfected into patient derived fibroblasts. This was run on a western blot and stained with an antibody which probes for the N-terminal of Huntingtin. Lysate from the brains of mice with the R6/2 mutation which contain short N-terminal protein fragments were used as a positive control[93]. The murine brains used to make this cell lysate were a kind gift from Dr. Roger Barker, Cambridge. No short N-terminal

fragments were seen in the samples from exon skipping oligonucleotide treated cells indicating that any short transcripts were degraded rather than translated **(Figure 3.11)**.

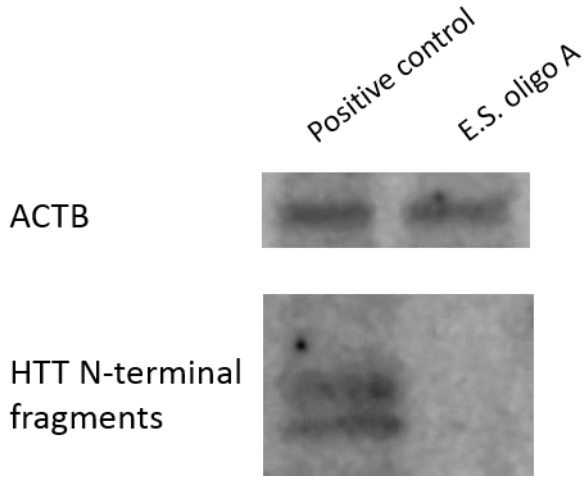


Figure 3.11 Determination of N-terminal Fragment Generation Following Exon Skipping Treatment. Patient-derived fibroblasts were treated with the most efficient exon skipping oligonucleotides which had generated the most knockdown based on mRNA and protein levels in fibroblasts. Following 48 hours protein was harvested from these cells and a western blot was run to identify whether or not N-terminal fragments were present in the sample. The positive control was lysate from R6/2 mouse brains. Protein concentration was measured by Bradford assay and equalised prior to western blot with MAB5492. In order to obtain sufficient protein from fibroblasts for western blot the sample shown was a pooled combination of three treatment groups.

3.2.7 Investigation of shRNAs for Huntingtin Silencing

shRNAs are artificial RNA molecules consisting of a double stranded RNA with a hairpin turn. When expressed the shRNA hairpin mimics pri-miRNA and hijacks a cells machinery so that it is processed by Drosha, exported from the nucleus by Exportin 5,

cleaved by Dicer and like an siRNA it is loaded into the RISC complex to induce RISC mediated cleavage and silencing of mRNA[289]. Four shRNA expression plasmids were analysed in this study for their ability to silence *HTT* by transfection with Lipofectamine 2000 into patient-derived fibroblasts. A non-coding control plasmid was included in the analysis. A dose response experiment where the expression plasmids were transfected at 125, 250, 500, 1000 and 2000 ng and RNA harvested 48 hours later with *HTT* expression normalised to *GAPDH* and *ACTB* revealed that two of the expression plasmids proved effective in *HTT* knockdown, reducing expression to 46.2 and 40.9% for shRNA 1 and 2 respectively, at the highest dose of 2000 ng **(Figure 3.12A)**.

To assess the duration of silencing of the four shRNA expression plasmids 1000 ng were transfected into patient-derived fibroblasts and the relative *HTT* expression to *GAPDH* and *ACTB* was measured 24, 48, 96 and 186 hours following transfection. The two shRNAs which had induced silencing in the dose response study reduced *HTT* expression to 34.7 and 32.2% for shRNA 1 and 2 respectively. In contrast to the silencing generated from siRNA and antisense oligonucleotide treatments above, in this study there was no trend towards recovery of *HTT* expression at 186 hours indicating that shRNAs expression plasmids may induce longer term silencing **(Figure 3.12B)**.

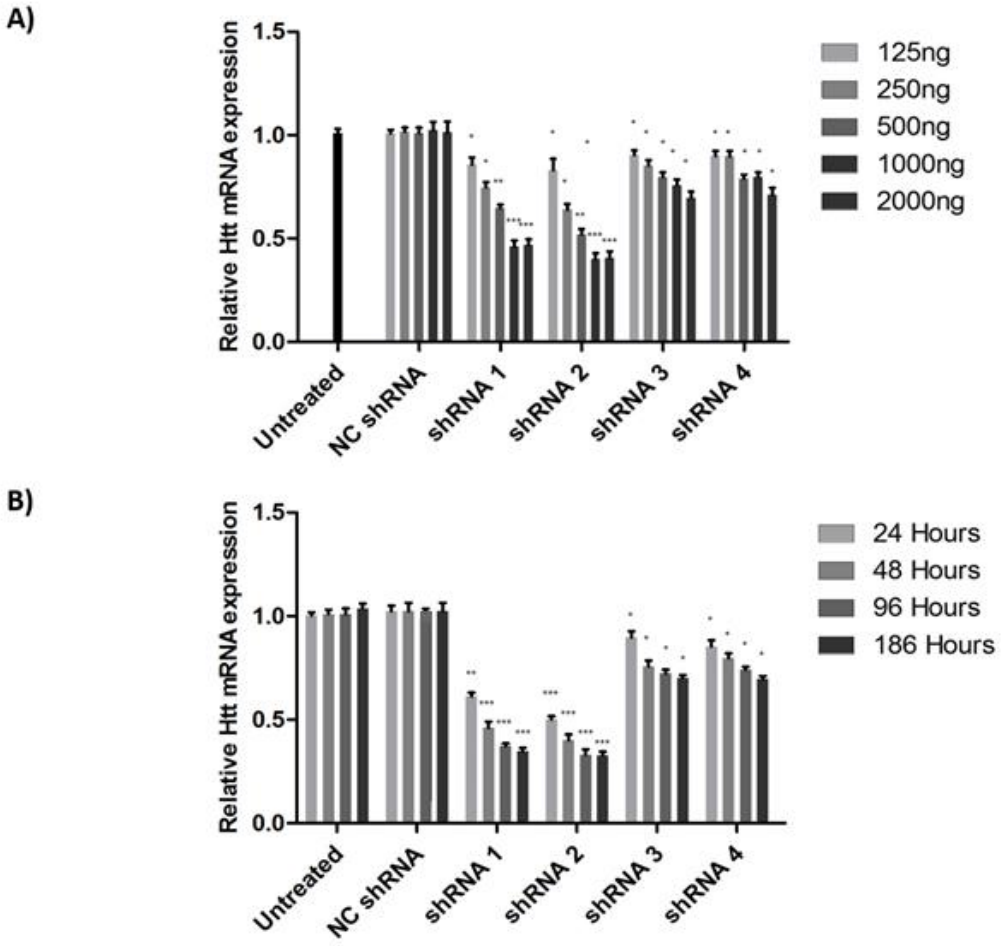


Figure 3.12 Investigation of shRNA Treatments for Huntingtin Knockdown. Patient-derived fibroblasts were left untreated, transfected with a negative control (NC) shRNA or transfected with shRNAs predicted to reduce *HTT* expression in different doses (A) and at the same dose following different lengths of time post-transfection (B). Graphs indicate the resultant relative *HTT* mRNA levels assessed by qPCR normalised to housekeeping genes *GAPDH* and *ACTB*. **A)** Dose response showing relative *HTT* mRNA measured 48 hours after transfection with 125, 250, 500, 1000 and 2000 ng of shRNA plasmid. **B)** Duration of silencing following transfection with 1000 ng of shRNA plasmid. Values represent mean + SEM, n = 4. Statistical differences shown were calculated by one-way ANOVA and Tukey's post hoc test. Significance indicated is compared to negative control. ***p<0.001, **p<0.01, *p<0.05.

3.2.8 Investigation of CRISPR Interference for Huntingtin Silencing

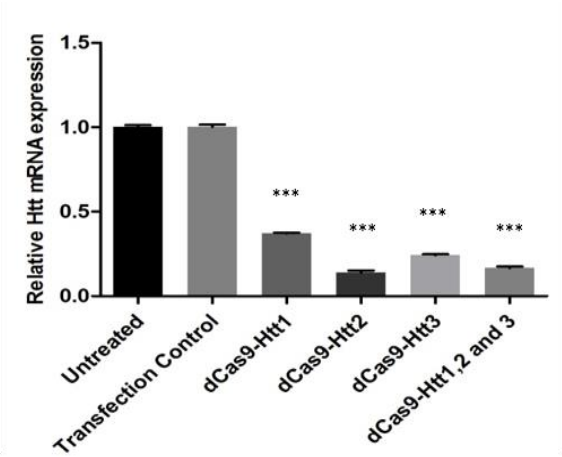
CRISPRi is a method for silencing based on the bacterial CRISPR pathway in the prokaryotic adaptive immune system[197]. Through the design of single guide RNAs (sgRNAs) directed towards the TSS, upstream of the gene of interest and bearing a dCas9-binding hairpin, a catalytically inactive dead Cas9 (dCas9) lacking the endonuclease activity can silence the gene of interest by sterically blocking transcription[204].

Three different sgRNAs were inserted into the plasmid backbone to generate three CRISPRi plasmids, dCas9-HTT1, 2 and 3. Design and cloning were performed by Sabrina Heman-Ackah (Wood lab). These were transfected using Lipofectamine 2000 in an initial pilot study at a concentration of 500 ng per well into HEK293 cells, with a mock transfected sample as a control. Samples transfected with all three constructs in equal weight:weight ratios were also included with a total dose of 500 ng. Silencing in this initial study proved promising as *HTT* expression was reduced to 14.1% following treatment with dCas9-HTT2 **(Figure 3.13A)**.

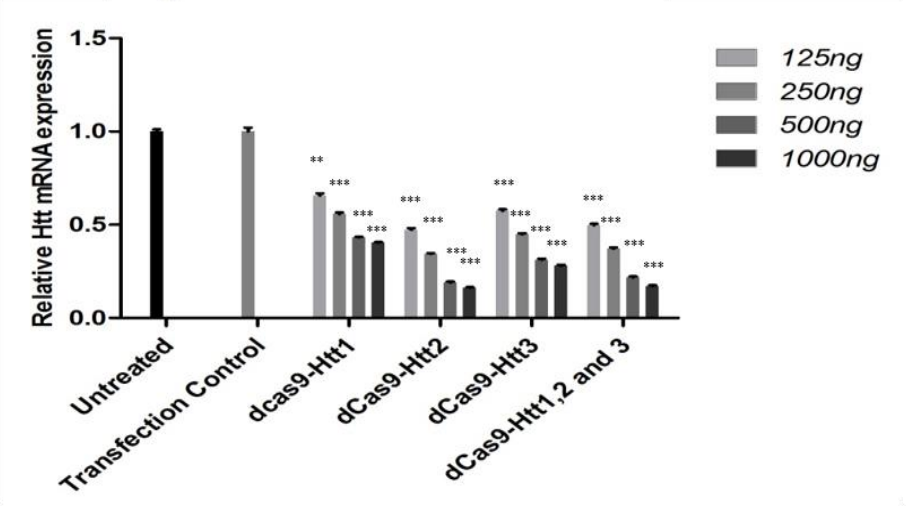
A dose response study in patient-derived fibroblasts was then performed at plasmid concentrations of 125, 250, 500 and 1000 ng per well. Mock transfected control samples and samples transfected with all three constructs with the same weight:weight ratio and the same total plasmid weight as each construct alone were also included. RNA was harvested 48 hours post transfection and *HTT* expression relative to *GAPDH* and *ACTB* was recorded. Silencing was high in some samples as *HTT* expression was reduced to 16.3% on treatment with dCas9-HTT2. There was no difference between silencing in this

sample and silencing in samples transfected with all three plasmids **(Figure 3.13B)**. A duration of silencing study was set up using the same treatment groups with total plasmid concentration per well of 500 ng. RNA was harvested 24, 48, 96 and 186 hours following transfection and *HTT* expression measured relative to *GAPDH* and *ACTB*. As with the shRNA and in contrast to the results from treatments with siRNAs and ASOs, there was no reduction in silencing at 186 hours post transfection for treatment with the most promising CRISPRi candidate, dCas9-Htt2 **(Figure 3.13C)**.

A)


Relative Htt mRNA expression
1.5
1.0
0.5
0.0
***
***
***
***
Untreated
Transfection Control
dCas9-Htt1
dCas9-Htt2
dCas9-Htt3
dCas9-Htt1,2 and 3

B)


Relative Htt mRNA expression
1.5
1.0
0.5
0.0
125ng
250ng
500ng
1000ng
Untreated
Transfection Control
dcas9-Htt1
dCas9-Htt2
dCas9-Htt3
dCas9-Htt1,2 and 3

C)

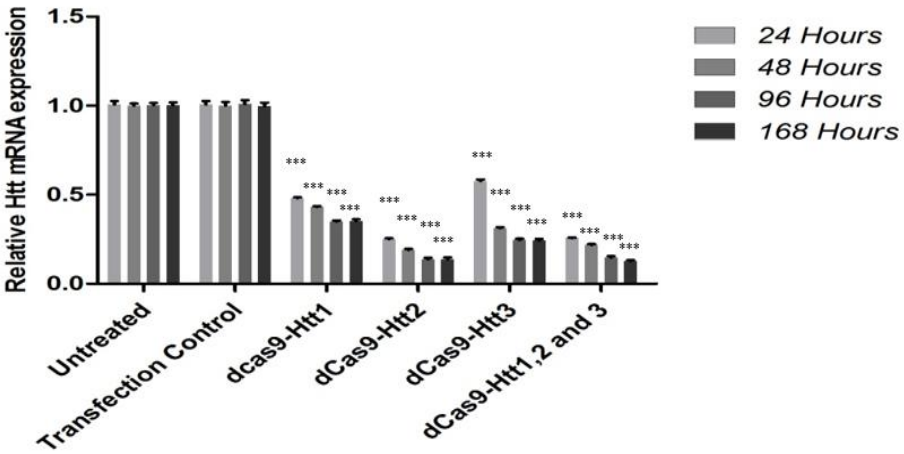

Relative Htt mRNA expression
1.5
1.0
0.5
0.0
24 Hours
48 Hours
96 Hours
168 Hours
Untreated
Transfection Control
dcas9-Htt1
dCas9-Htt2
dCas9-Htt3
dCas9-Htt1,2 and 3

Figure 3.13 Investigation of CRISPRi for Huntingtin Knockdown. A) In a pilot experiment HEK293 cells were left untreated, mock transfected or transfected with several CRISPRi plasmids predicted to reduce *HTT* expression. B) and C) Patient-derived fibroblasts were left untreated, mock transfected or transfected with several CRISPRi plasmids predicted to reduce *HTT* expression in different doses (B) and at the same dose with RNA expression measured following different durations post-transfection (C). Graphs indicate the resultant relative *HTT* mRNA levels assessed by qPCR normalised to housekeeping genes *GAPDH* and *ACTB*. **B)** Dose response showing relative *HTT* mRNA measured 48 hours after transfection with 125, 250, 500, 1000 ng CRISPRi plasmid. **C)** Duration of silencing following transfection with 500 ng of CRISPRi plasmid. Values represent mean + SEM, n = 4. Statistical differences shown were calculated by one-way ANOVA and Tukey's post hoc test. Significance indicated is compared to transfection control. ***p<0.001, **p<0.01, *p<0.05.

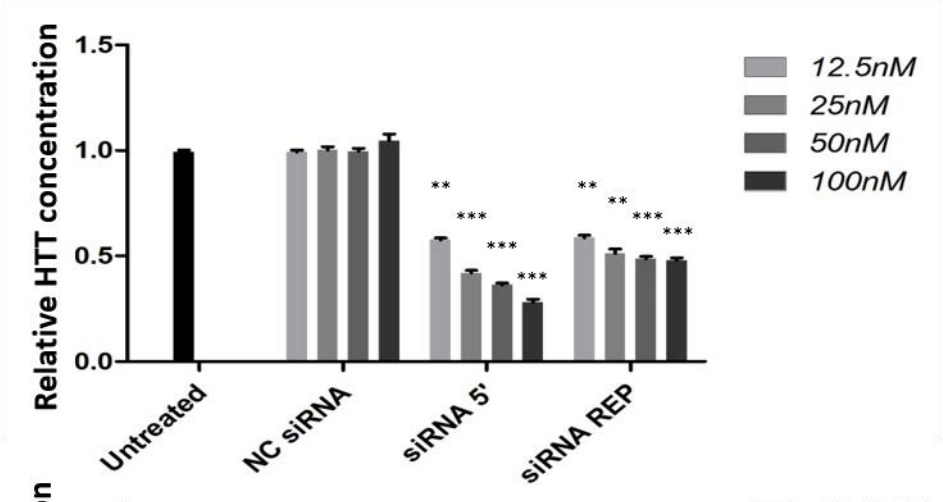
3.2.9 Protein Quantification and Visualisation Following Treatments to Reduce Huntingtin Expression

To validate the previous results of *HTT* mRNA quantification following treatment with siRNAs, ASOs, shRNAs and CRISPRi designed to knockdown *HTT* expression, the HTT protein levels in patient-derived fibroblasts following treatments were measured by ELISA **(Figure 3.14A-F)**. This study was carried out at various doses and protein was harvested from cells 48 hours following transfection with Lipofectamine 2000. For siRNA, LNA and multigene LNA studies of protein expression the doses measured were 12.5, 25, 50 and 100 nM **(Figure 3.14A, B and C** respectively**)**. For exon skipping oligonucleotides a wider range and higher doses were assessed, 25, 50, 100, 200 and 400 nM **(Figure 3.14D)**. CRISPRi plasmids at doses of 125, 250, 500 and 1000 ng were transfected and HTT protein levels after 48 hours analysed **(Figure 3.14E)**. HTT protein

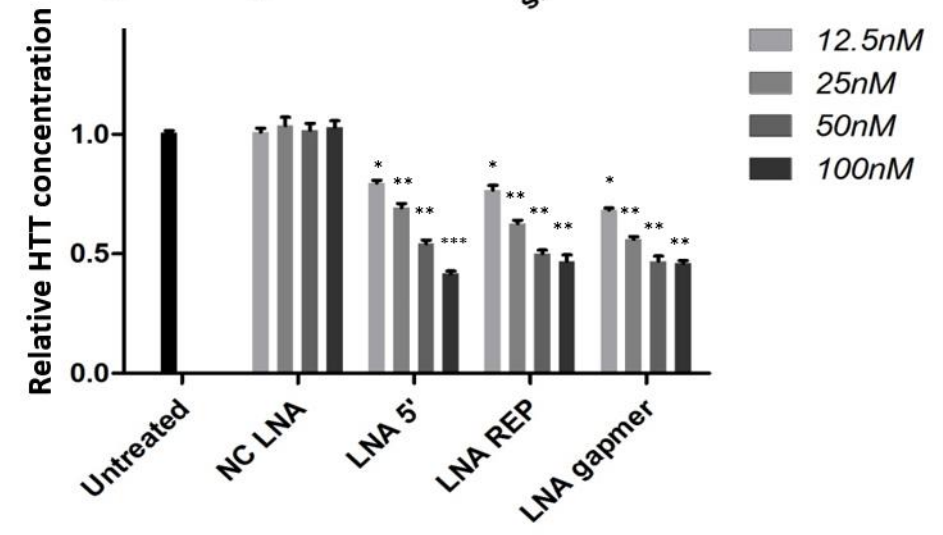
expression following treatment with shRNA expression plasmids at 125, 250, 500, 1000 and 2000 ng were also assessed **(Figure 3.14F)**.

The results from the ELISA study matched that of the qPCR data confirming knockdown of HTT was achieved at a protein level as well as at the mRNA level. The most promising candidate siRNA here was siRNA-5' which reduced *HTT* expression to 28.4% at 100 nM **(Figure 3.14A)**. The LNA which generated the most potent silencing was LNA-5' where *HTT* expression in cells treated with 100 nM was reduced to 41.9% **(Figure 3.14B)**. The multigene LNA proved less potent than other treatments generating with HTT expression even at 100 nM remaining at 64.4% **(Figure 3.14C)**. Exon skipping proved potent with effective silencing achieved at 100 nM by exon skipping oligonucleotide A, reducing HTT expression to 26.9%. The most effective CRISPRi plasmid generated effective silencing, knocking *HTT* expression down to just 17.9% at 1000 ng **(Figure 3.14E).** The shRNA expression plasmids were less effective at *HTT* silencing, with the most effective shRNA, shRNA2 reducing expression to just 41.4%.

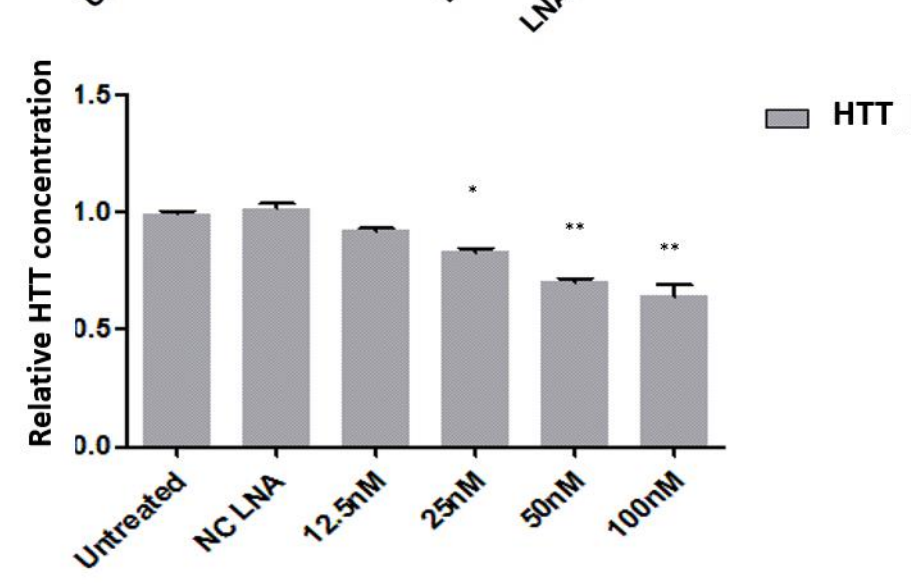
A)


Relative HTT concentration
1.5
1.0
0.5
0.0
12.5nM
25nM
50nM
100nM
Untreated
NC siRNA
siRNA 5'
siRNA REP

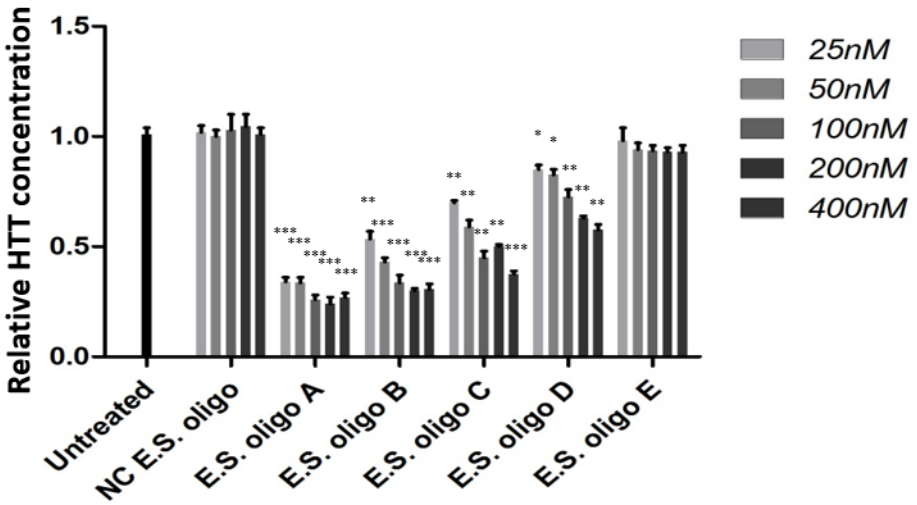
B)


Relative HTT concentration
1.0
0.5
0.0
12.5nM
25nM
50nM
100nM
Untreated
NC LNA
LNA 5'
LNA REP
LNA gapmer

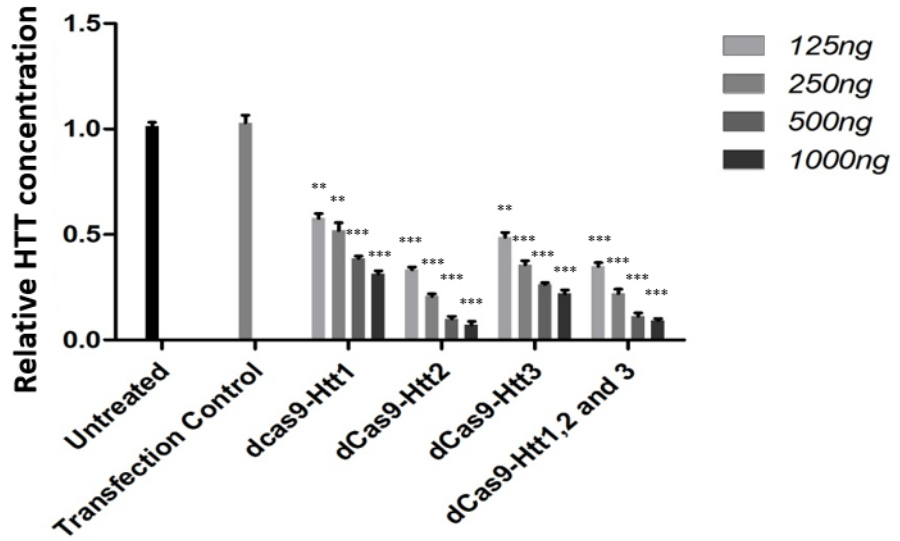
C)


Relative HTT concentration
1.5
1.0
0.5
0.0
HTT
Untreated
NC LNA
12.5nM
25nM
50nM
100nM

D)


Relative HTT concentration
1.5
1.0
0.5
0.0
25nM
50nM
100nM
200nM
400nM
Untreated
NC E.S. oligo
E.S. oligo A
E.S. oligo B
E.S. oligo C
E.S. oligo D
E.S. oligo E

E)


Relative HTT concentration
1.5
1.0
0.5
0.0
125ng
250ng
500ng
1000ng
Untreated
Transfection Control
dcas9-Htt1
dCas9-Htt2
dCas9-Htt3
dCas9-Htt1,2 and 3

F)

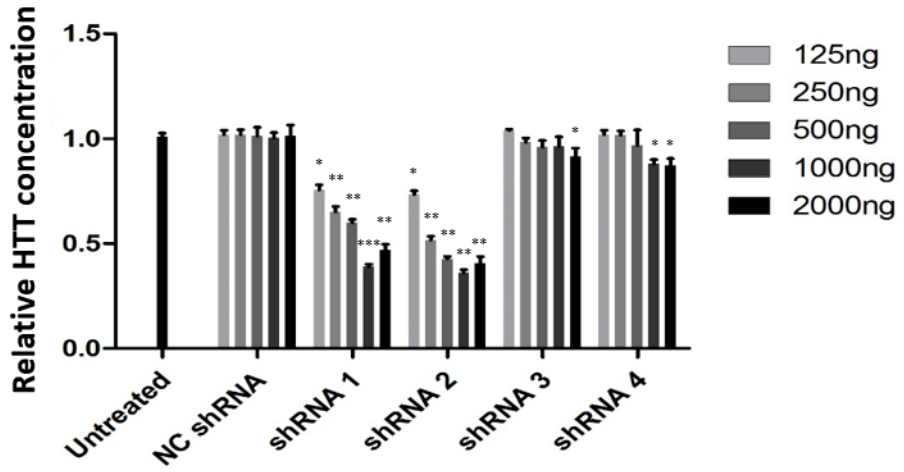

Relative HTT concentration
1.5
1.0
0.5
0.0
125ng
250ng
500ng
1000ng
2000ng
Untreated
NC shRNA
shRNA 1
shRNA 2
shRNA 3
shRNA 4

Figure 3.14 Quantification of Huntingtin Protein Following Treatments for Huntingtin Knockdown. Patient-derived fibroblasts were left untreated, transfected with a negative control (NC) or transfected with **A)** siRNA, **B)** antisense oligonucleotides, **C)** multigene oligonucleotides, **D)** exon skipping oligonucleotides, **E)** CRISPRi plasmid or **F)** shRNA plasmid predicted to reduce HTT expression in different doses. Graphs represent the protein values of HTT measured by Elisa 48 hours post-treatment. Values represent mean + SEM, n = 4. Statistical differences shown were calculated by one-way ANOVA and Tukey's post hoc test. Significance indicated is compared to negative control. ***p<0.001, **p<0.01, *p<0.05.

The information from the protein quantification study using the HTT ELISA provided information which further validated the dose response studies measured by qPCR at the mRNA level. However, the ELISA did not distinguish between the mutant and wild type allele. Reduction of both alleles has been shown to be safe in animal models once it is performed postnatally, up to 45%[79]. Most of the treatments above were designed to silence both the mutant and the wild type allele, but allele specific knockdown is also possible and siRNA-REP, LNA-REP and LNA gapmer were designed to be allele selective and silence just the mutant HTT allele. In order to visualise the allele selectivity of these and not the other treatments, a western blot from protein extracted from patient-derived fibroblasts transfected using Lipofectamine 2000 was performed with the allele selective treatments alongside the most promising candidates from each treatment group, namely siRNA-5', LNA-5', the multigene LNA, exon skipping oligonucleotide A, dCas-Htt2 and shRNA 2 **(Figure 3.15**). This western revealed that siRNA-REP, LNA-REP and LNA gaper are indeed allele selective, with reduction in expression only of the mutant allele, while all other treatments reduced expression of both alleles.

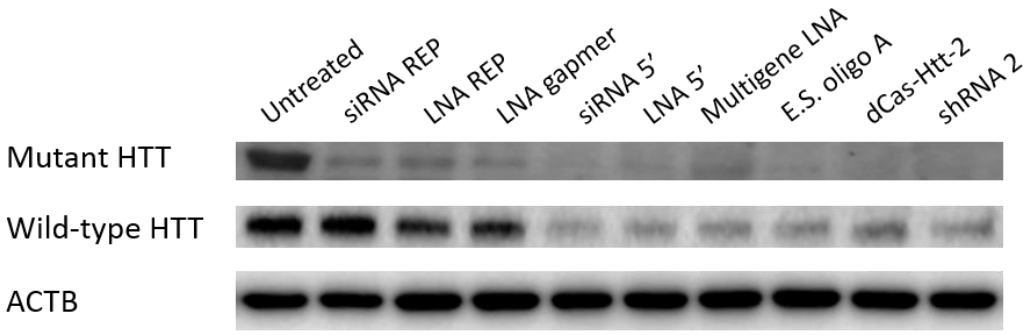


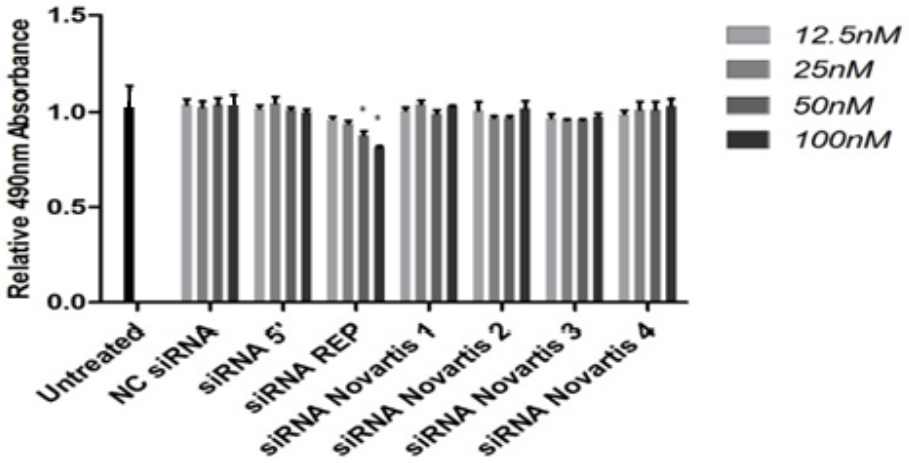
Figure 3.15 Visualisation of Mutant and Wild-type Protein Levels following Treatments for Huntingtin Knockdown. Patient-derived fibroblasts were left untreated or treated with the most promising candidates for HTT knockdown from each category of treatment tested as well as the allele selective nucleic acids; siRNA-REP (100 nM), LNA-REP (100 nM), LNA gapmer (100 nM), siRNA-5' (100 nM), LNA-5' (100 nM), multigene LNA (100 nM), E.S. oligo A (100 nM), dCas-Htt-2 (500 µg) and shRNA 2 (1000 µg). Protein was extracted 72 hours post-transfection and analysed via western blot to separate the mutant and wild-type proteins using antibody mAb2166, and ab82618 for the internal control ACTB. To obtain sufficient protein for western blot each sample is a pooled protein extraction of three treatments to ensure enough protein from fibroblasts.

3.2.10 Measurement of Cellular Toxicity of Treatments to Silence Huntingtin

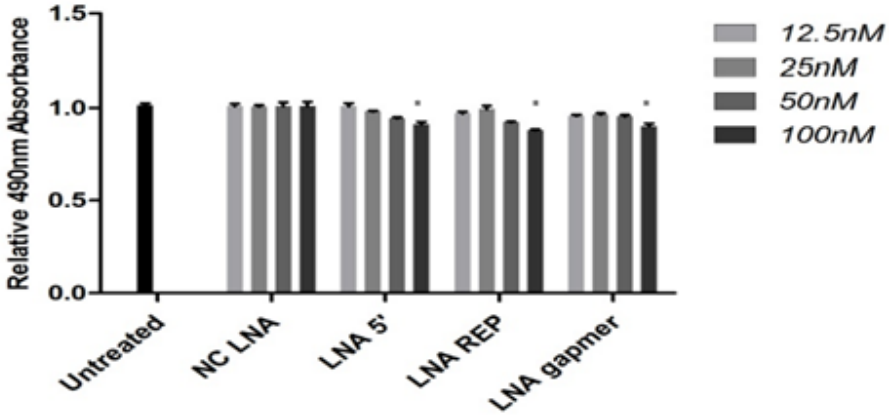
The cellular toxicity of each of the treatment types was measured by MTS assay **(Figure 3.16A-F)**. The MTS viability assay uses a colorimetric method to quantify the toxicity of cellular treatments. It measured the conversion of a tetrazolium compound into formazon by NAD(P)H dehydrogenases in cells which are metabolically active as a measure of cell viability.

siRNA-5’ proved non-toxic however the allele selective siRNA-REP proved toxic, displaying a dose dependent relationship with increased toxicity **(Figure 3.16A)**. The LNA treatments including the multigene LNA also proved slightly toxic particularly at higher doses **(Figure 3.16B and C)**. The exon skipping oligonucleotides also appeared slightly toxic at higher doses but the CRISPRi, and shRNA treatments displayed no measureable toxicity **(Figure 3.16D, E and F respectively)**.

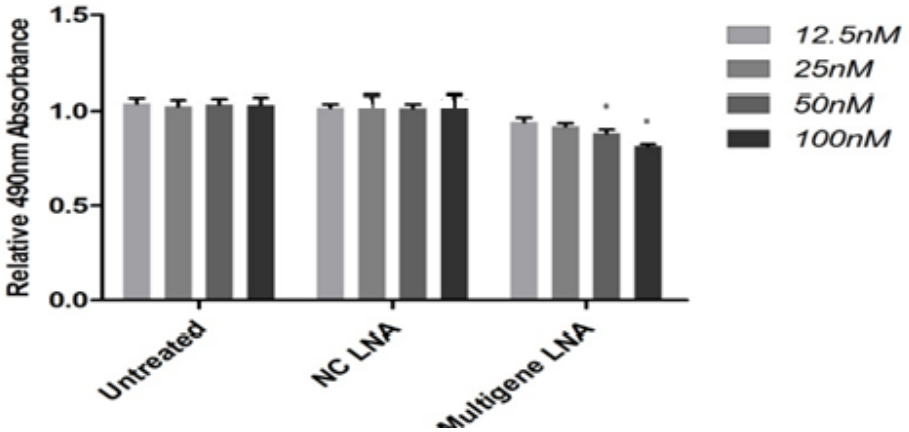
A)


Relative 490nm Absorbance
1.5
1.0
0.5
0.0
12.5nM
25nM
50nM
100nM
Untreated
NC siRNA
siRNA 5'
siRNA REP
siRNA Novartis 1
siRNA Novartis 2
siRNA Novartis 3
siRNA Novartis 4

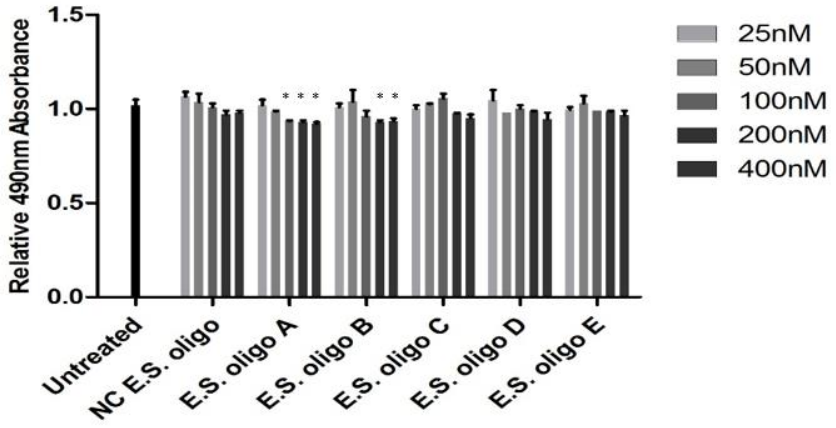
B)


Relative 490nm Absorbance
1.5
1.0
0.5
0.0
12.5nM
25nM
50nM
100nM
Untreated
NC LNA
LNA 5'
LNA REP
LNA gapmer

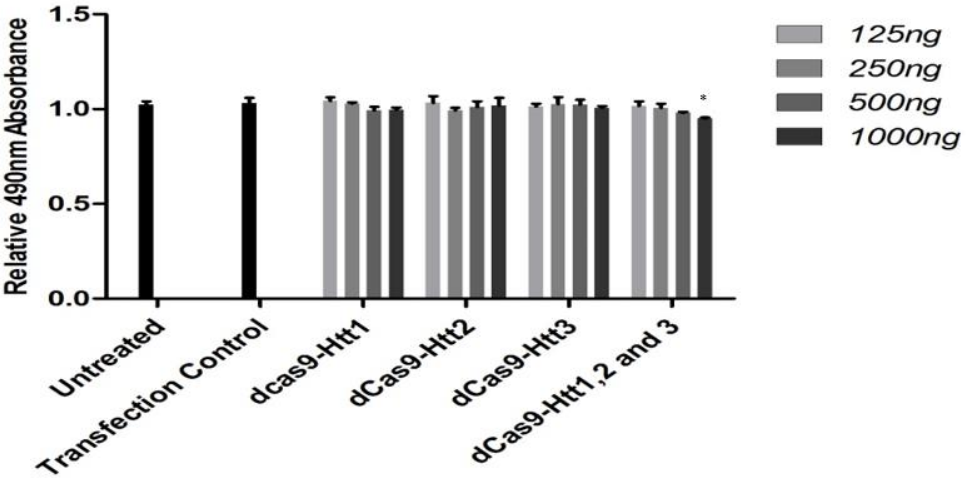
C)


Relative 490nm Absorbance
1.5
1.0
0.5
0.0
12.5nM
25nM
50nM
100nM
Untreated
NC LNA

D)


Relative 490nm Absorbance
1.5
1.0
0.5
0.0
25nM
50nM
100nM
200nM
400nM
Untreated
NC E.S. oligo
E.S. oligo A
E.S. oligo B
E.S. oligo C
E.S. oligo D
E.S. oligo E

E)


Relative 490nm Absorbance
1.5
1.0
0.5
0.0
125ng
250ng
500ng
1000ng
Untreated
Transfection Control
dcas9-Htt1
dCas9-Htt2
dCas9-Htt3
dCas9-Htt1,2 and 3

F)

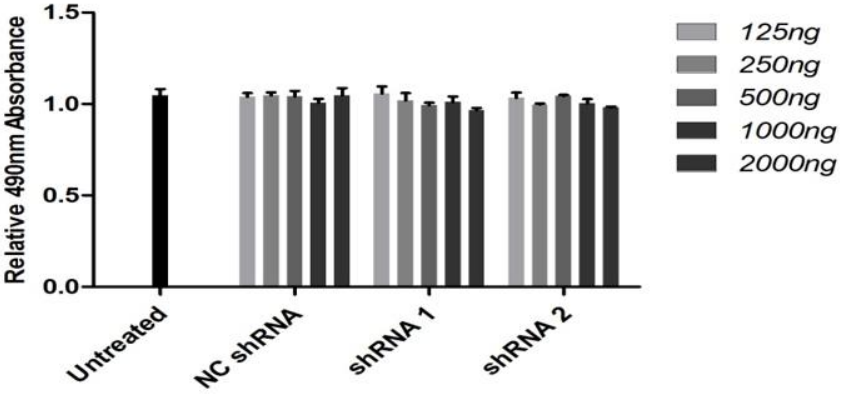

Relative 490nm Absorbance
1.5
1.0
0.5
0.0
125ng
250ng
500ng
1000ng
2000ng
Untreated
NC shRNA
shRNA 1
shRNA 2

Figure 3.16 Investigation of Cell Viability Following Treatments for Huntingtin Knockdown. Patient-derived fibroblasts were left untreated, transfected with the indicated doses of a negative control (NC) and with **A)** siRNA, **B)** antisense oligonucleotides, **C)** multigene oligonucleotides, **D)** exon skipping oligonucleotides, **E)** CRISPRi plasmid or **F)** shRNA plasmid predicted to reduce *HTT* expression in different doses. Cell viability was assayed using an MTS assay 48 hours post-treatment. Values represent mean + SEM, n = 4. Statistical differences shown were calculated by one-way ANOVA and Tukey's post hoc test. Significance indicated is compared to untreated samples. ***p<0.001, **p<0.01, *p<0.05.

3.3 Discussion

This study investigated several methods to silence *HTT*. Specifically, siRNAs, LNAs, a multigene LNA, exon skipping oligonucleotides as well as shRNA and CRISPRi expression plasmids were assessed for their potency and duration of silencing in a validated HD model; patient-derived fibroblasts. The potency of these therapeutic nucleic acids was measured both at the mRNA and protein level and the protein silencing was visualised for the most promising candidates from each group as well as the allele specific nucleic acids. Finally, viability assays were performed to ensure a good safety profile for the therapeutic nucleic acid chosen to continue the study and investigate loading methods in Chapter 5.

There are challenges faced by all nucleic acid therapeutics in translation from *in vitro* to *in vivo* work, one of the most significant of which is safe and effective delivery. As this study aims to evaluate EVs as a delivery vehicle for a nucleic acid cargo, each group of nucleic acid therapeutic investigated here will be discussed with regard to the results generated here but also with reference to its associated merits and drawbacks which must

be considered before selecting a class of nucleic acid to bring forward to load into EVs. Most of these potential cargos face physical barriers posed by the hydrophobic plasma membrane, endosomal escape following endocytosis and some also must compete with the cell's own endogenous RNAi pathways. There are also the issues of degradation by serum RNases, rapid clearance and immune stimulation. Encapsulation in an EV should overcome the issue posed by the inherent negative charge of the nucleic acid and enable entry into the cytoplasm as EVs are thought to facilitate endosomal escape for their cargo[213,259]. EV delivery should also protect the nucleic acids from degradation and not elicit an immune response if harvested from immature DCs which do not bare immune stimulatory factors[213]. Furthermore, in a clinical setting in the future, there is the possibility of a patient's own cells being used as the EV source which would also bypass the immune system.

siRNAs were the first class of therapeutic molecules to be investigated in this study. They induce silencing through incorporation in the RISC complex and induction of mRNA cleavage or a steric block on translation, have previously been used to silence *HTT* and have also been shown to be safe *in vivo* following direct brain injection[180]. In addition, siRNAs have an advantage over the other classes of molecules tested here as there is evidence that they may be loaded into EVs by electroporation for brain delivery[213]. Both an allele specific and non-allele specific siRNA were tested for their efficacy, as were four siRNAs which were gifted from Novartis. These siRNAs were the most potent, eliciting high levels of silencing even at low doses and highlighted the capability of siRNAs to induce strong silencing that persisted for a number of days post-transfection. siRNA-5', an siRNA which targeted a region upstream of the CAG triplet repeat was also potent and had a long duration of silencing. This siRNA, though not allele selective, also

had a good safety profile with no toxicity apparent even at its highest dose in contrast to siRNA-REP, an siRNA directed against the repeat which is allele selective and displayed dose dependent levels of toxicity. This siRNA was also not as potent as siRNA-5', though that could be due to its capacity for allele selectivity and as such would be expected to preferentially silence only one allele.

siRNAs have poor tissue distribution and cellular uptake due to their high hydrophobicity and polyanionic nature, but they have a high level of intercellular potency. The capacity of the intercellular potency of siRNA-5' to overcome the poor bioavailability intrinsic to siRNAs would be aided by delivery in an EV. Furthermore, modifications to the siRNA backbone can increase stability and provide a more favourable uptake profile. For siRNA-5' in this study, phosphorothioate linkages were used to increase nuclease resistance, which if used *in vivo* would be expected to increase the half-life, serum stability of the siRNA and allow improved tissue delivery[176,302,303]. Although high levels of these modifications can lead to toxicity[304], low levels were used here of two modifications per molecule to avoid this and no toxicity was evident from the viability assay.

A variety of ASOs were examined in this study, LNAs mixmers, an LNA gapmer, a multigene LNA and exon skipping oligonucleotides. Of the LNAs, although the LNA mixmers and the LNA gapmer silence through different mechanisms, the former by a steric block and the latter through recruitment of RNase H, all were capable of silencing *HTT*, particularly at higher doses. There was however toxicity apparent from each of these treatments, which was most evident at the highest dose. The multigene LNA, a novel therapeutic for HD, though not as potent as the other treatments, showed promise as it could silence both *HTT* and *mTOR*[296]. It did however exhibit a dose dependent

toxicity. Toxicity here was measured by an MTS toxicity assay which indicates the level of viable metabolically active cells. Although HD patient derived fibroblasts were used in this screening, it remains to be seen whether the toxicity results would be confirmed in primary neuronal cells as cytotoxicity can vary between cell types.

Several exon skipping oligonucleotides were designed to bind to ESEs around exon 3 of the *HTT* gene and stimulate splicing of that exon to induce a shift in the reading frame so that a stop codon is in frame in exon 4. This approach is similar to one used by Sud *et al*., for tauopathies[305]. Out of the five oligonucleotides tested, three were found to induce high levels of silencing at higher doses, and one in particular, exon skipping oligonucleotide A, generated high levels of silencing even at lower doses. Silencing was confirmed by both qPCR and ELISA as with the siRNAs and LNAs but here a gene specific RT-PCR was also performed to visualise exon skipping. This confirmed that exon skipping had occurred in the samples with highest levels of silencing. This silencing was also long lasting.

There was a concern that although the short RNA fragment generated by exon skipping would end in a stop codon in exon 4 and thus would be predicted to be degraded by nonsense mediated decay[306], that instead it might be translated into a short protein fragment which are known to contribute to pathology in HD[81]. Indeed some animal models are based on overexpression of short N-terminal fragments of the human HD gene[93]. To investigate this possibility, a western blot was undertaken with HD patient derived fibroblasts treated with the most promising exon skipping oligonucleotide candidate for HTT silencing, exon skipping oligonucleotide A, and compared to cell lysate from an animal model which overexpresses HTT N-terminal fragments. No protein

band corresponding to short fragments of any size were seen in the exon skipping oligonucleotide treated cells. However, some toxicity was apparent in the samples which had been treated with the most promising candidates for silencing, particularly at the highest doses.

ASOs as single-stranded antisense compounds are generally regarded as having more beneficial cellular uptake and better tissue distribution because they are not as hydrophobic as siRNA, for example on direct brain injection they penetrate further than siRNAs[307]. They also can be modified as in this study by LNA modifications, where the 2'-oxygen is linked to 4'-carbon of the ribose ring via a methylene bridge[308] which increases the binding affinity by locking the nucleic acid in the 3'-endo conformation which is ideal for binding and increases stability in serum[184]. LNA-5' and LNA-REP silence via a steric block of the mRNA but the LNA gapmer recruits RNase H, a ubiquitous enzyme that hydrolyzes the RNA strand in an RNA-DNA duplex hybrid[295]. In the gapmer the chemically modified LNA nucleotides flank a central DNA gap, the LNA bases increase nuclease resistance and binding affinity for the target while the DNA allows for RNase H binding[309]. 2'O-Me modification of the ribose was incorporated into the design of the exon skipping oligonucleotides to increase resistance to enzymatic digestion and improve thermal stability and binding affinity[190]. This increase in binding affinity would improve potency and selectivity. Due to the toxicity displayed by the ASOs in this study however, they were discounted from further work.

Two plasmid based methods of inducing *HTT* knockdown were evaluated: CRISPRi and shRNA. CRISPRi is a technique that borrows from bacteria and uses a system evolved for their adaptive immunity to silence genes[197]. Through the design of a sequence specific

sgRNA directed towards the region surrounding the TSS of a given gene, an enzymatically inactive dCas9 is recruited and transcription is repressed via a steric block[199]. Here, 3 CRISPRi plasmids were examined for their potency and duration of silencing. Although all CRISPRi plasmids generated silencing following transfection, one of these in particular, dCas9-Htt2 was found to be highly potent. In addition, these plasmids demonstrated no detectable levels of toxicity at the doses tested except when the three were used in conjunction with each other. Furthermore, silencing was long lasting with no evidence of recovery at the longest time point tested.

Four shRNA expression plasmids were also evaluated in this study for their potency and duration of silencing. When transcribed, shRNAs contain an RNA hairpin which mimics pri-miRNA and facilitates the hijacking of a cells RNA processing machinery such that the shRNA is processed by Drosha, exported from the nucleus and then incorporated into the RISC complex as an siRNA would be. Four shRNAs were examined and two proved capable of *HTT* silencing, shRNA 1 and 2, though silencing was lower than for other nucleic acid therapeutics.

The two types of plasmids used in this study had an additional task compared to the RNA based therapeutics of accessing the nucleus. The shRNA plasmid, as well as siRNA also has the disadvantage of requiring the appropriation of the cell's endogenous RNA processing machinery and there is potential for this to be saturated. For this reason, if an siRNA or shRNA is brought forward it is vital that it is potent. RNA therapeutics also run the risk of activating an innate immune response evolved to recognise pathogen infection, mediated by interferons (IFNs), Toll-like receptors (TLR) or protein kinase R (PKR) family, but this should be minimised for siRNA due to their short size of under

30bp. This would need to be confirmed *in vivo* however, as these findings have become contentious[310,311].

As mentioned, for CRISPRi, as with shRNA, there is the added challenge of accessing the nucleus, and unique to CRISPRi in this study, access to the TSS is necessary and dependent on chromatin accessibility[312]. The biggest challenge for the use of CRISPRi in this study is the need to deliver all of the components for the required inhibition, as it does not make use of a cell's endogenous machinery. *In vitro* high levels of silencing were observed but as the CRISPR field is in its infancy, whether this would translate *in vivo* for *HTT* or any other gene remains to be seen.

HD is an autosomal dominant disorder and therefore one allele is sufficient to cause the disease phenotype. Homozygous patients are rare and their clinical course is more severe[313]. As discussed in chapter 1, the function of the wild type HTT protein is yet to be fully elucidated though it is known to be involved in a range of cellular physiological functions. Despite the roles it may play, it is thought that its expression is most important prenatally as a partial reduction in *HTT* expression in animal models postnatally has been shown to be safe in several studies, even in primates[286,314]. Allele selective targeting can be achieved through targeting single nucleotide polymorphisms (SNPs) which link with the mutation, or directly targeting the mutant expansion[20,21]. Allele selective inhibition through targeting SNPs is challenging as SNPs vary among the population so such a treatment would need to be tailored[21]. Another method is to target the repeat itself as was done here by targeting the repeat siRNA siRNA-REP and the LNAs LNA-REP and LNA gapmer. This is possible because there may be secondary structures in the mutant expansion which increase accessibility of the mRNA or alternatively the longer stretch

of CAG repeats could allow increased binding sites for an siRNA or LNA[20,315]. Although targeting the mutant specifically is possible, there is evidence that reducing expression of both alleles is a safe and effective means to rescue the phenotype in primate models so may also be effective for symptom recovery or disease prevention in humans[79].

Although theoretically a therapeutic which targets solely the mutant *HTT* allele would be beneficial to rule out any possibility of a negative outcome of silencing the wild type allele, here the allele selective siRNA and LNAs demonstrated toxicity and were ruled out of further work in this study. The antisense oligonucleotides were also not brought forward for loading due to apparent toxicity. The shRNAs were not sufficiently potent and were also not pursued. In terms of silencing potency, the siRNAs, exon skipping oligonucleotides and CRISPRi were the most efficient, in addition the best candidate from the siRNA and CRISPRi group showed low levels of toxicity. However, due to the foreseen difficulty in packaging large plasmids into EVs, in reaching the nucleus and in assuring an accessible TSS, CRISPRi was decided against for loading experiments. Therefore, siRNAs were selected as the best candidates to bring forward to test for EV loading. The potential disadvantages of siRNAs have been negated with siRNA-5' by improved pharmacokinetics through incorporation of phosphorothioate linkages and sequence design to minimise off-target effects which would limit saturation of endogenous RNAi machinery due to higher potency.

Type of Nucleic Acid Based Therapeutic	**siRNA**	**ASO**	**Multigene ASO**	**Exon Skipping ASO**	**CRISPRi**	**shRNA**
Best Candidate in Category	siRNA-5’	LNA-5’	Multigene LNA	E.S. oligo A	dCas9-Htt2	shRNA-2
Maximum Silencing of *HTT* Achieved	70.5%	51.8%	74.3%	69.8%	83.7%	59.1%
Maximum Silencing of HTT Achieved	71.6%	58.1%	37.6%	73.1%	82.1%	58.6%
Toxicity at Dose of Maximum silencing	0.2%	9.2%	18.3%	9.4%	0.4%	0.3%

Table 3.1. Table of Potency and Toxicity Profile of Best Candidate Nucleic Acid Based Therapeutics in Each Category. The best candidates in each category are defined here as the nucleic acid based therapeutics with the most potent silencing combined with minimal toxicity. Listed in this table is the level of silencing or reduction in expression of HTT generated at both the mRNA and protein level as well as the toxicity at the associated doses as measured in HD patient derived fibroblasts.

In summary, the current study undertook to test a number of different methods to reduce *HTT* expression by analysing their potency, duration of silencing and toxicity **(Table 3.1)**. By comparing the results and through consideration of the intrinsic properties of each nucleic acid type, siRNA-5’ which targets a region upstream of the CAG repeat was selected as the cargo to use in EVs. Following cargo selection, the biodistribution of the delivery vehicle and brain targeting must be evaluated and a means to load the EV with the selected therapeutic cargo investigated.

CHAPTER 4 INVESTIGATION OF THE BIODISTRIBUTION OF TARGETED EXTRACELLULAR VESICLES

4.1 Introduction

During the last decade the interest in EV research has grown enormously. Within the field of gene therapy they may offer the possibility of a non-toxic, immunologically inert nucleic acid delivery vehicle which can be administered systemically. However, there are a number of hurdles to pass before their potential as a nanocarrier can be realised in a clinical setting.

EVs are known to play an important role in intercellular communication[316]. They have been shown to be involved in the horizontal transfer of proteins, miRNA, mRNA, DNA and bioactive lipids and are also found in all body fluids indicating their stability *in vivo*. There are different subgroups of EVs based on the subcellular origin and the attention of the gene therapy community has mostly focused on exosomes, a small 40-150nm diameter population of vesicles which form from the inward budding of a late endosomal membrane to form intraluminal vesicles (ILVs) in a multivesicular body (MVB)[317]. When the membrane of the MVB fuses with the cell's plasma membrane these ILVs are released as exosomes[318]. Other EVs may be just as important for gene transfer and include vesicles which bud from the plasma membrane, MVs[319].

For the treatment of neurological disorders such as HD, one of the factors limiting development of a therapeutic and gene delivery vehicle carrier in the clinic is targeting

the brain. The blood brain barrier (BBB), a dynamic physical boundary which acts to protect the brain, separating it from the periphery, is a challenge for drug delivery to the brain. As well as the role of EVs in RNA transfer, another property which can be exploited for their use as a therapeutic delivery vehicle is that they seem to be capable of brain targeting following systemic delivery[213]. The opportunity to deliver a nucleic acid systemically for neurological disorders including HD and bypass this barrier would eliminate the substantial safety concerns of direct brain injection.

Brain targeted EVs have previously been used to deliver Bace1 siRNA to silence a therapeutic target in Alzheimer's disease in the brain[213]. EV source cells were transfected with the targeting construct which consisted of the RVG peptide, a ligand for a subunit of cholinergic receptors, fused to the external portion of Lamp2b, a protein expressed on the surface of EVs used here as a membrane anchor for the brain targeting ligand.

In spite of the accumulated research on EVs in recent years few studies have investigated EV biodistribution leaving much of their *in vivo* trafficking capabilities and potential for targeting unknown[320–325]. Biodistribution is a vital aspect of any therapeutic as the distribution to the required site of action is one of the governing factors on the efficacy and toxicity of a given therapeutic. Targeting to the brain for the treatment of neurological disorders such as HD could increase the potency and efficacy of a treatment and for any brain targeting strategy for EVs it is important to determine how the targeting strategy impacts on the accumulation of the therapeutic or nanocarrier in the brain.

Although completely overcoming the innate distribution profile and natural clearance characteristics of EVs might not be feasible by brain targeting, any shift in biodistribution

generated through EV targeting may be therapeutically relevant. The challenge of targeting a region of interest and reaching an effective dose in this desired location prior to clearance is not limited to gene therapy nor indeed to therapeutics; Any endogenous signalling molecule has to contend with global biological distribution. Any drug delivered systemically will have to avoid clearance by the liver and the reticuloendothelial system (RES). Furthermore, for EV delivery the physicochemical properties of size and charge which enable them to function endogenously *in vivo* as vectors for signalling molecules may obscure any effect that a targeting ligand might have if they prove to be more important for uptake than the targeting moiety. Thus, by analysing the biodistribution of untargeted and targeted EVs valuable information on the suitability of EVs as drug delivery vectors for HD can be gained.

Thus, an important question in the field is how much - if at all - the expression of a brain targeting ligand on an EV surface can alter global biodistribution. To help answer this question this study used the techniques of infrared labelling of targeted EVs enabling them to be tracked, visualised and quantified using the In Vivo Imaging System (IVIS). Using this method, the biodistribution of Lamp2b-RVG targeted EVs was established[326]. Following this, the biodistribution of EVs targeted using new targeting factors anchored via the transferrin receptor (TfR): TfR-EPRNEEK, TfR-G7 and TfR-RVG, were examined. It was found that brain delivery can be increased two-fold on expression of brain targeting ligands. Further analysis of the brain targeting factors *in vitro* in a BBB model system was used to attempt to gather further information on the uptake of these EVs.

For these experiments, design, primary cell extraction, cell culture and targeted EV production was carried out in Oxford, and injections and imaging were performed at the Karolinska Institutet (KI) by Oscar Wiklander (and Joel Norden for the Lamp2b-RVG study). The Lamp2b-RVG targeted biodistribution study was published in 2015[326]. For the *in vitro* study, design, cell culture, and targeted EV production and isolation was also performed in Oxford, but flow cytometry was performed at AbbVie by Dr. Christopher Untucht.

4.2 Results

4.2.1 Investigation of DiR as a Means of Labelling Extracellular Vesicles

$DiIC_{18}(7)$ (1,1'-Dioctadecyl-3,3,3',3'-Tetramethylindotricarbocyanine Iodide), commonly referred to as DiR, a near infrared fluorescent cyanine dye was selected to label EVs *in vivo*. This dye is lipophilic with a high tissue penetrance, low auto-fluorescence and only fluoresces when it is integrated in a lipid-membrane by its two long 18-carbon chains. Designed for non-invasive imaging of cell homing, previous studies have also used this dye to label vesicles for intravenous injection and tracking using IVIS[324].

Prior to commencing the biodistribution study it was necessary to ensure that DiR did not disrupt the size, morphology or expression markers on EVs. In order to do this, EVs were isolated from HEK293 cells by differential ultracentrifugation, labelled with DiR and analysed by western blot for the common EV markers Alix and Tsg101[327], nanoparticle tracking analysis (NTA) to examine their size distribution profile and particle count, and electron microscopy (EM) (**Figure 4.1A-C** respectively).

The EV markers Alix and Tsg101 were both found to be present in DiR labelled EV samples **(Figure 4.1A)**. Furthermore, the NTA profile matched that of unlabelled EVs with a mode of approximately 100 nm in diameter (**Figure 4.1B**). Intact 100 nm vesicles bearing EV morphology were also seen in EM analysis (**Figure 4.1C**).

In this study, free dye emitting a signal would pose a problem *in vivo* as it could bind to serum proteins and circulating cells. For this reason, a sucrose gradient fractionation of DiR-labelled EVs was performed. This showed that the dye is visible when bound to EVs **(Figure 4.1D)**. The DiR fraction also co-localised with the expected density of exosomes (1.11-1.21 g/ml)[316]. In contrast, free DiR alone had a lower buoyant density **(Figure 4.1D)** and fluorescence from this sample was low **(Figure 4.1E)**. This indicates that following DiR labelling of EVs and EV purification via ultracentrifugation, the DiR label is associated primarily with EVs. It is worth noting however that it is impossible to determine exactly the DiR content per vesicle and vesicles with varying lipid content may differentially incorporate varying amounts of the dye. Based on the average yield of EVs from DCs of 1.13×10^9 particles/ml incubated in 26 ml prior to ultracentrifugation with 1 μM DiR, the mixture would contain a ratio of EVs:DiR molecules of $1:5.34 \times 10^5$.

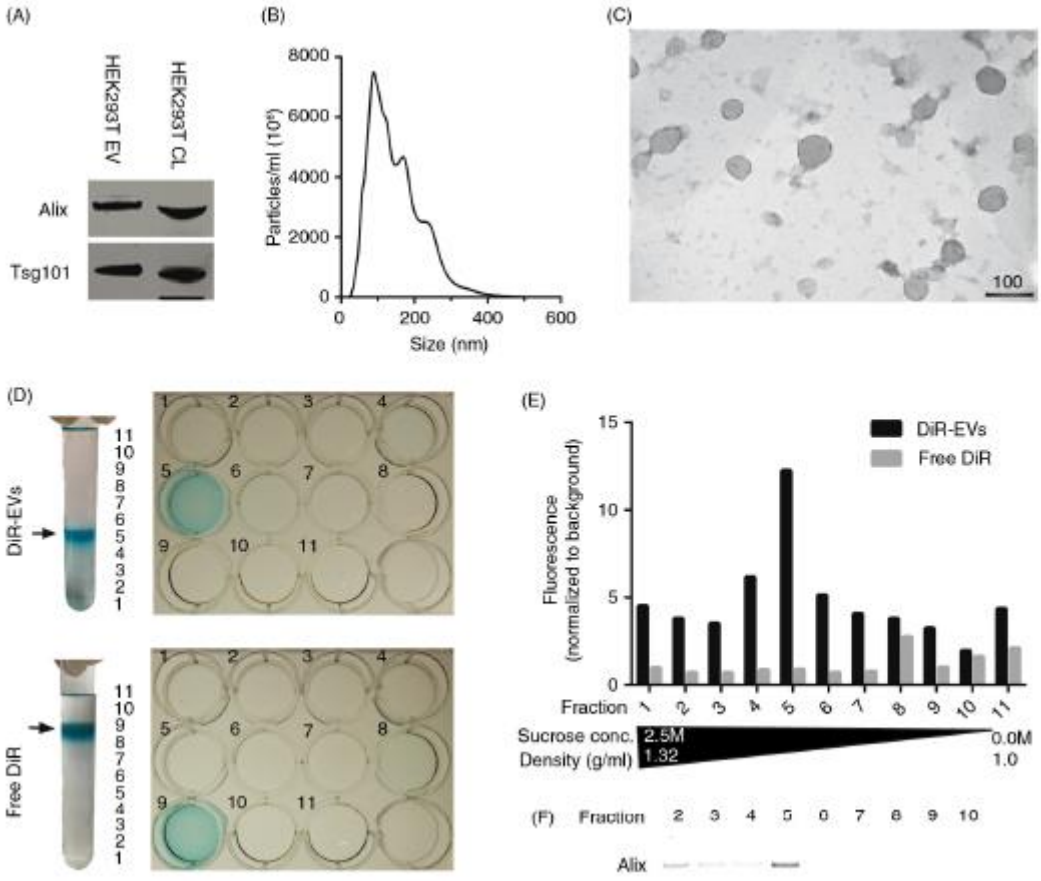


Figure 4.1 DiR Labelling Co-localizes with EVs and does not Affect EV Morphology. A) Western Blot (WB) probed for Alix and Tsg101 on DiR-labelled EVs isolated from HEK293T cells and cell lysate (CL). **B)** NTA profile of DiR-labelled HEK293T EVs showing an EV-like distribution with a mode size of approximately 100 nm. The curve has been normalized to dilution factors. **C)** Electron microscopy picture of DiR-labelled HEK-293T EVs. Scale bar represents 100 nm. **D)** Image depicting DiR-EVs and free DiR sucrose gradients in ultracentrifuge tubes and subsequent 12-well plates containing the different fractions. **E)** Fluorescent values (normalized to background) of the DiR-EVs and free DiR gradients (assayed from the 12-well plates depicted in 1D). **F)** WB stained for Alix for DiR-EVs from fractions 2-10. Figure adapted from Wiklander, Nordin, O'Loughlin *et al*., Extracellular vesicle in vivo biodistribution is determined by cell source, route of administration and targeting. J Extracell Vesicles (4), 26316, 2015.

4.2.2 Biodistribution of Untargeted HEK293 and Dendritic Cell Derived Extracellular Vesicles

Prior to investigating the biodistribution with particular focus on brain delivery of Lamp2b-RVG targeted EVs, it was important to characterise the biodistribution of untargeted DiR labelled EVs. Two cell sources were compared: bone marrow derived DCs and HEK293 cells. DCs were selected because their use has been validated for previous *in vivo* EV gene delivery as when isolated from immature DCs the EVs do not bear markers that activate the immune system[213,328]. HEK293 cells were also investigated as their use offers a more scalable, ethical source of EVs as they are not costly in terms of animal life to produce and they are also easier to transfect[329].

Interestingly, a previous experiment by colleagues in KI showed that perfusion did not affect the biodistribution of dye on injection of HEK293 derived DiR labelled EVs[326]. Thus, perfusion was not performed for this study. The injection of medium alone labelled with DiR was also shown not to affect the biodistribution of labelled EVs[326]. Together with the results from Figure 4.1D-E, this further validates that it is labelled EVs and not free dye being measured. In the same study a dose titration was performed to establish an optimal dose for injection of EVs[326]. It was found that injection of higher doses could alter the relative distribution of injected EVs. Relative liver accumulation decreased from 77% to 60% when treated with $0.25x10^{10}$ particles per gram (p/g) or $1.0x10^{10}$ p/g but did not decrease significantly further on injection of $1.5x10^{10}$ p/g when liver distribution was measured at 56%. One of the hypotheses for this was that the higher dose might saturate the mononuclear phagocyte system (MPS, also known as reticuloendothelial system, RES), so that at higher doses the liver is more efficiently bypassed by the excess of EVs.

The dose of $1.0x10^{10}$ p/g allowed for adequate detection in all organs tested with minimal saturation, so was chosen for the present study.

For the DCs, bone marrow was harvested from the tibias and femurs of 8-10 week old mice. GM-CSF was used to select for dendritic cells which were cultured for 8 days. On day 7 the medium was changed to vesicle depleted medium (vesicle depletion of the medium was performed via ultracentrifugation), conditioned medium was collected and EVs isolated via differential centrifugation 24 hours later. For HEK293 cells, cells were grown to near confluency before the medium was changed to serum depleted medium. After 48 hours the conditioned medium was harvested and EVs were also isolated by differential centrifugation. The vesicles were then labelled with DiR and $1.0x10^{10}$ p/g of each were injected into the tail vein of live mice. Mice were imaged 24 hours post injection using IVIS. IVIS measures the photons per second (p/s) emitted from a user defined region of interest. In order to obtain accuracy in IVIS sensitivity readings in distinguishing from which tissue the fluorescence originated, and to visualise the fluorescence in the brain accurately through the skull, it was necessary to harvest the organs and perform the imaging *ex vivo*.

Overall the distribution of HEK293 and DC derived EVs were similar, but the HEK293 EVs accumulated more in the liver, 60% for HEK293 cells but 46% for DCs. For the spleen the opposite was true, HEK293 derived EVs showed lower distribution with only 12% of signal originating there but 28% for DCs. High levels were also detected in the lungs (7% for DC EVs and 10% for HEK293 EVs) and GI tract (10% for DC EVs, 16% for HEK293 EVs) (**Figures 4.2A, B and C**). Representative IVIS images from the lungs,

spleen and liver of control and DiR labelled DC and HEK293 EV treated mice can be seen in Figure 4.2A.

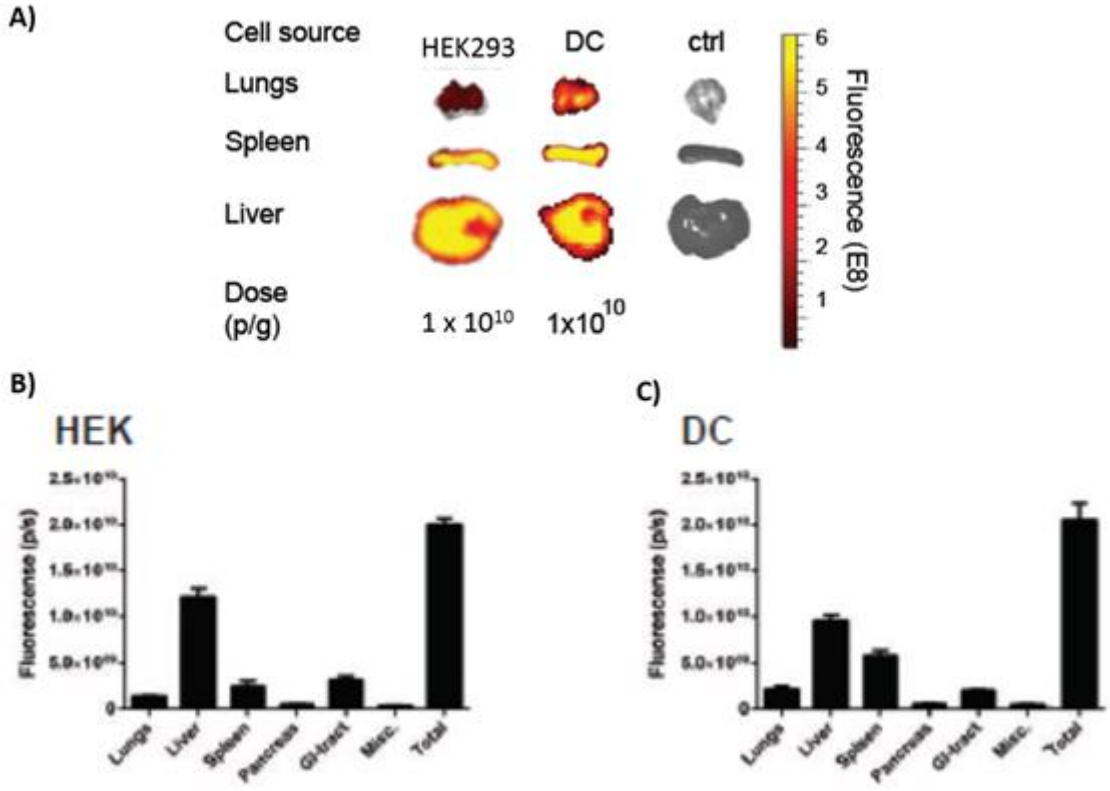


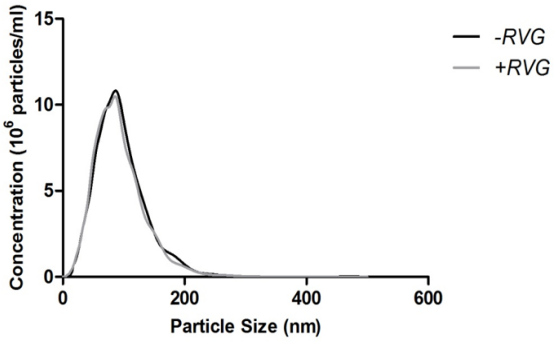
Figure 4.2 Biodistribution of HEK293 and Dendritic Cell Derived EVs. $1.0x10^{10}$ p/g of DiR labelled EVs isolated from bone marrow DCs or HEK293 cells were injected into the tail vein. Organs were harvested 24 hours later and imaged using IVIS. **A)** Representative IVIS images of lungs, spleen and liver 24 hours post-injection of HEK293 or DC EVs and PBS control. **B)** Absolute fluorescent signal in each organ after injection of $1.0x10^{10}$ p/g DiR labelled EVs isolated from HEK293 cells. **C)** Absolute fluorescent signal in each organ after injection of $1.0x10^{10}$ p/g DiR labelled EVs isolated from DCs. Misc.= Brain, heart, kidneys and quadriceps muscle. Values represent mean + SEM, n = 4.

4.2.3 Characterisation of RVG Targeted and Untargeted Extracellular Vesicles

The Lamp2b-RVG peptide has previously been shown to allow for brain targeting *in vivo* with loaded targeted EVs capable of silencing a gene of interest in the brain, but overall biodistribution was not analysed[213]. This targeting was thought to be specific and active in specific uptake as the effect was reduced *in vitro* by α-bungarotoxin, an antagonist of AchRs[213]. Prior to the quantification of brain accumulation and general biodistribution of Lamp2b-RVG targeted DiR labelled EVs, it was necessary to ensure that RVG targeting did not disrupt particle size or the expression of EV markers.

EVs were isolated via differential ultracentrifugation from DCs harvested from the bone marrow of 8-10 week old mice. NTA analysis of size distribution on the EVs identified no change in the diameter, nor in the concentration of vesicles following transfection of EV source cells with the Lamp2b-RVG expression plasmid **(Figure 4.1A and B)**. EVs from these cells also displayed higher levels of the EV markers Alix and Tsg101 than the cell lysate but no marker of contamination from other sources, calnexin **(Figure 4.3C)**. RVG could not be stained for directly as there are currently no antibodies for the peptide**.**

A)



B)

	-RVG	+RVG
Mean size (nm) ± SE	89.7 ± 1.3	88.52 ± 2.1
Mode size (nm) ± SE	85.42 ± 2.4	84.19 ± 3.1
Total Particles ($x10^9$) ± SE	1.13 ± 0.09	1.11 ± 0.08

C)

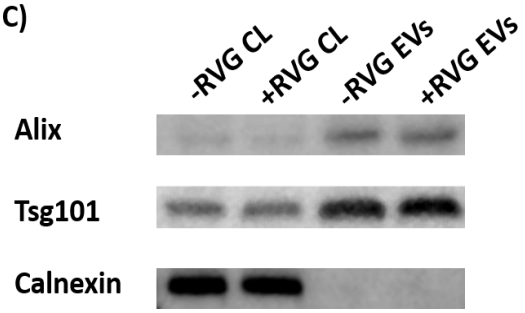


Figure 4.3 Characterisation of Bone Marrow Dendritic Cell Derived Extracellular Vesicles with and without RVG. EVs isolated from bone marrow derived DCs transfected with Lamp2b-RVG or mock transfected were characterised by nanoparticle tracking analysis (NTA) and western blot. **A)** NTA analysis of size distribution histogram of RVG-positive (+RVG) and RVG-negative (-RVG) EVs from bone marrow derived DCs with a peak of 85.42 and 84.19 nm. **B)** Table displaying the mean and mode particle size and total number of particles secreted from bone marrow DCs of RVG-positive (+RVG) and RVG-negative (-RVG) EVs per ml of conditioned medium, n = 3. **C)** Purified EVs and cell lysates (CL) were loaded on a western blot and probed for the exosomal markers, Alix and Tsg101 and the endoplasmic reticulum marker calnexin.

4.2.4 Characterisation of DiR Labelled RVG EVs

To ensure DC derived Lamp2b-RVG targeted EVs maintained the size and markers of DC derived EVs following shipping, NTA and western blot analysis of the EVs was performed prior to injection.

The vesicles displayed similar shaped NTA curves and EV markers as the EVs prior to DiR labelling and shipping **(Figure 4.4)**.

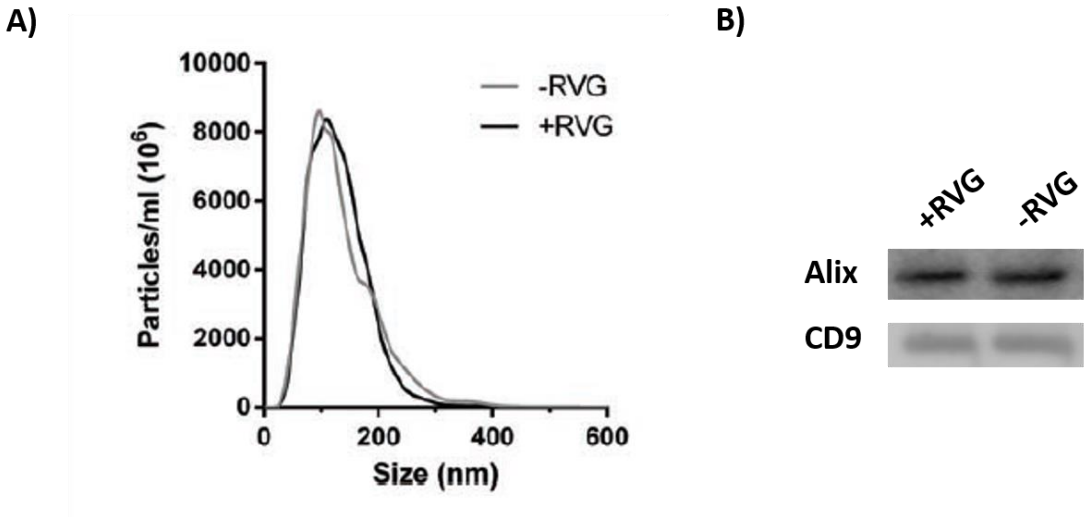


Figure 4.4 Characterisation of DiR labelled EVs Derived from Bone Marrow Dendritic Cells Transfected with RVG. Bone marrow derived DCs were transfected with Lamp2b-RVG or mock transfected and their characteristics were measured by NTA and WB. **A)** NTA profile of DiR labelled RVG-positive (+RVG) and RVG-negative (-RVG) bone marrow derived DC EVs. **B)** WB of DiR labelled RVG-positive (+RVG) and RVG-negative (-RVG) bone marrow derived DC EVs probed for Alix and CD9.

4.2.5 Biodistribution of RVG Targeted Extracellular Vesicles

The RVG peptide, a ligand for a subunit of the nicotinic acetylcholine receptor has been used in several studies which validate it's use as a brain targeting ligand showing that RVG-coupling increases localisation to the brain[213,330–332]. The extent to which targeting through expression of Lamp2b-RVG could alter the biodistribution of EVs was examined by comparing the biodistribution of RVG and non-RVG targeted DC derived EVs. DCs were harvested from the bone marrow of 8-10 week old C57BL6 mice, and transfected on day 4 with the Lamp2b-RVG targeting construct or mock transfected. On day 7 the medium was changed to medium depleted of EVs and on day 8 the EVs were isolated via differential centrifugation. 1.0×10^{10} p/g of DiR labelled RVG and mock transfected EVs were injected via the tail vein of C57BL6 mice and organs imaged *ex vivo* following 24 hours using IVIS.

Overall the distribution pattern was similar for RVG targeted and non-targeted EVs with the highest signal detected in the liver, spleen, GI-tract and lungs **(Figure 4.5)**. However, there was a marked increase in distribution of the RVG targeted EVs to organs bearing a high levels of acetylcholine receptors; the brain, heart and a trend towards increased signal from the muscle **(Figure 4.6)**. 24 hours following injection of DiR labelled Lamp2b-RVG targeted EVs, there was a two-fold increase in accumulation of fluorescence in the brain compared with non-RVG targeted EVs **(Figure 4.6A and B)**.

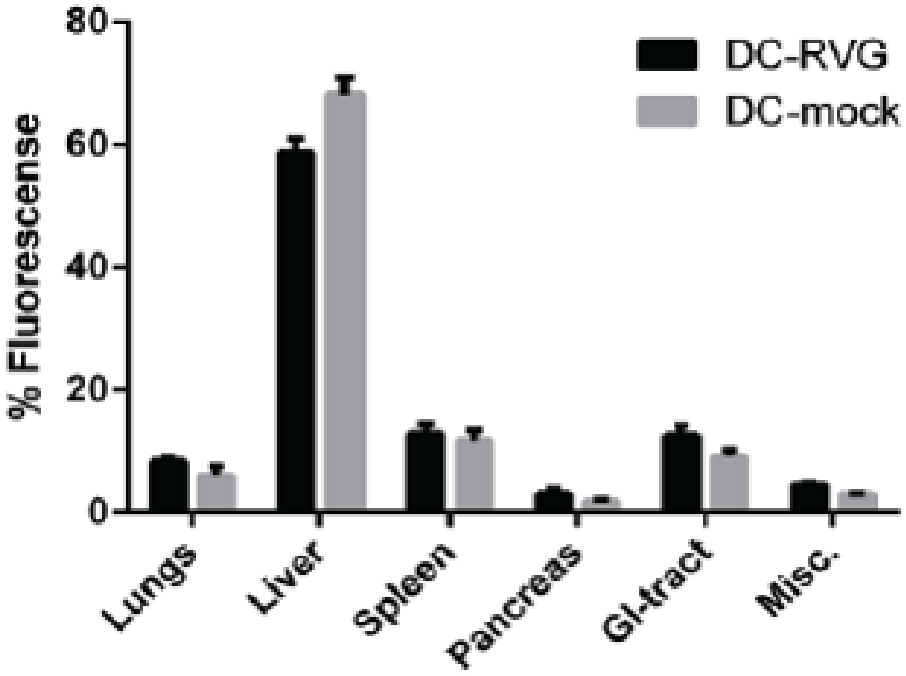


Figure 4.5 Biodistribution of RVG Targeted and Untargeted Bone Marrow Dendritic Cell Derived EVs. Bone marrow derived DCs were transfected with Lamp2b-RVG or mock transfected and 24 hours following injection with of $1.0x10^{10}$ p/g DiR labelled EVs via the tail vein the fluorescence in each organ *ex vivo* was measured using IVIS. The percentage of fluorescent signal in each organ after injection of $1.0x10^{10}$ p/g of RVG (+RVG) and non-RVG (–RVG) DC derived EVs is shown. Misc.= Brain, heart, kidneys and quadriceps muscle. Values represent mean + SEM, n = 4.

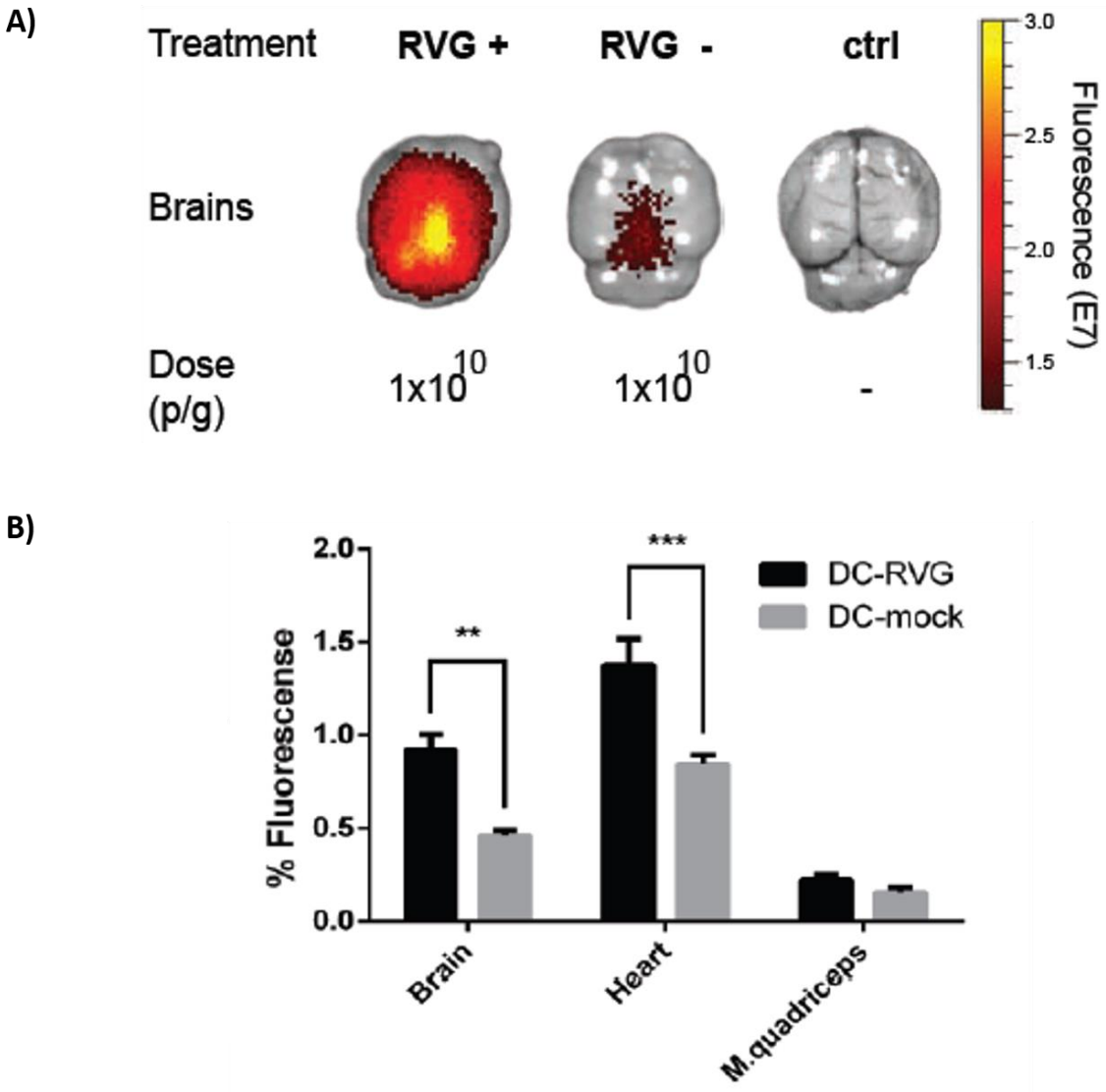


Figure 4.6 RVG increases Targeting to Acetylcholine-Receptor Rich Tissues Including the Brain. Bone marrow derived DCs were transfected with Lamp2b-RVG or mock transfected and 24 hours following injection with of $1.0x10^{10}$ p/g DiR labelled EVs the fluorescence in acetylcholine receptor rich organs was measured. **A)** Representative image of mouse brains, harvested 24 hours post injection of $1.0x10^{10}$ p/g of RVG (RVG +) and non-RVG (RVG -) DC derived EVs. **B)** The percentage of fluorescent signal in the brain, heart and quadriceps after injection of $1.0x10^{10}$ p/g of RVG (DC-RVG) and non-RVG (DC-mock) DC derived EVs. Values represent mean + SEM, n = 4. Statistical significance was calculated using the Kruskal-Wallis test and Dunn's post hoc analysis, ***p<0.001, **p<0.01, *p<0.05.

4.2.6 Investigation of Differences in Biodistribution Arising from Allogeneic and Syngeneic Nature of the Primary Source Cells

An examination of whether the strain of the host from which the source cells are derived has an effect on EV biodistribution could be important for development of EVs as a therapeutic delivery vehicle. If EVs from an allogeneic source result in increased clearance by the RES due to their foreign nature it could highlight a need to prepare therapeutic EVs from a patient's own cells to eliminate the recognition of the EVs as foreign and resultant quicker uptake by the MPS. Any effect on brain delivery would also be relevant for the development of EVs as a delivery vehicle in HD. In this study, DCs were harvested from the bone marrow of tibias and femurs of 8-10 week old C57BL6 mice and grown for 8 days under conditions to select for DCs. On day 4 the cells were transfected with the Lamp2b-RVG targeting plasmid or mock transfected. The medium was changed on day 7 to medium which had been depleted of EVs. Conditioned medium was harvested, EVs were isolated by differential ultracentrifugation and labelled with DiR prior to injection of $1.0x10^{10}$ p/g in Balb/c (allogeneic) or C57BL6 (syngeneic) mice.

Overall the distribution pattern was similar for allogeneic and syngeneic DC derived EVs with and without RVG targeting, except for the liver, spleen and brain **(Figure 4.7 and 4.8A and B)**. In the absence of targeting syngeneic DC EVs showed more targeting to the liver (53%) than allogeneic (46%). When RVG targeting was present these differences were negated (both 55%). In the spleen, in the absence of targeting, DC derived EVs distributed more to the spleen regardless of whether they were from allogeneic or syngeneic sources (29% for allogeneic and 24% for syngeneic) than RVG

targeted EVs. RVG targeting reduced this distribution to 13% for EVs from allogeneic sources and 20% for syngeneic sources.

Interestingly, there were significant differences in the accumulation of EVs from allogeneic and syngeneic sources in the brain. In the absence of targeting, EVs from syngeneic sources distributed more readily to the brain than EVs from allogeneic sources **(Figure 4.8B)**. In fact, this distribution of syngeneic derived EVs was similar to that of allogeneic RVG targeted EVs. The highest brain accumulation was seen in syngeneic RVG targeted EVs, two-fold greater than the same EVs without targeting **(Figure 4.8B)**. In Figure 4.8A are representative images of the brain distribution in control treated animals, animals given injections of allogeneic RVG targeted DC EVs and syngeneic RVG targeted DC EVs showing the increased accumulation of signal in the syngeneic brains.

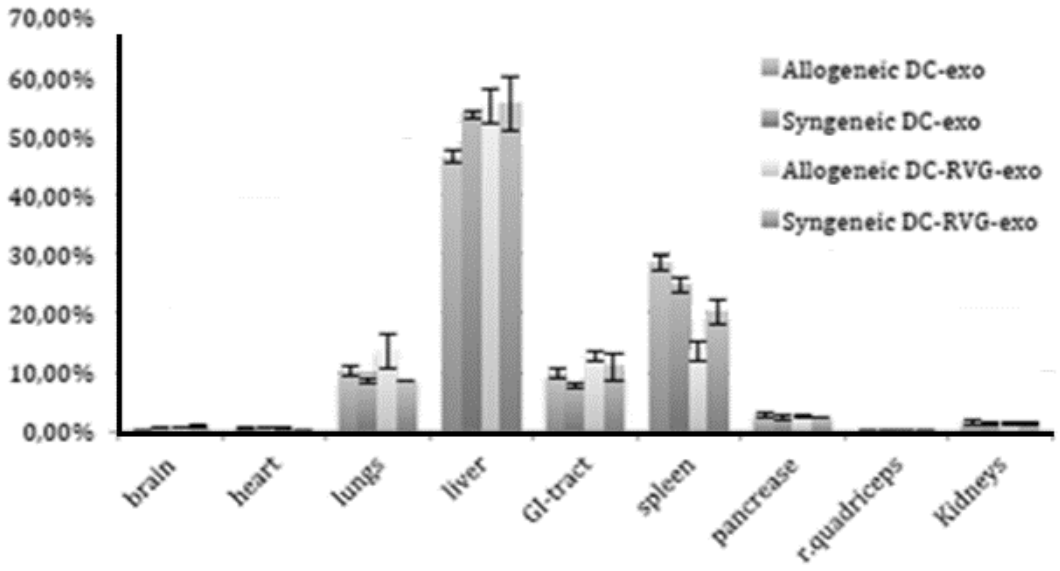


Figure 4.7 Biodistribution of RVG and non-RVG Bone Marrow Dendric Cell Derived EVs in Allogeneic and Syngeneic Recipients. Bone marrow derived DCs from C57BL6 mice were transfected with Lamp2b-RVG or mock transfected and 24 hours following injection via the tail vein into allogeneic (Balb/c) or syngeneic (C57BL5) mice with $1.0x10^{10}$ p/g of DiR labelled EVs the fluorescence in all organs indicated was measured *ex vivo*. The percentage of fluorescent signal in each organ tested after injection of $1.0x10^{10}$ p/g of Lamp2b-RVG (DC-RVG-exo) and non-RVG mock transfected (DC-exo) DC derived EVs is represented. Values represent mean ± SEM, n = 4.

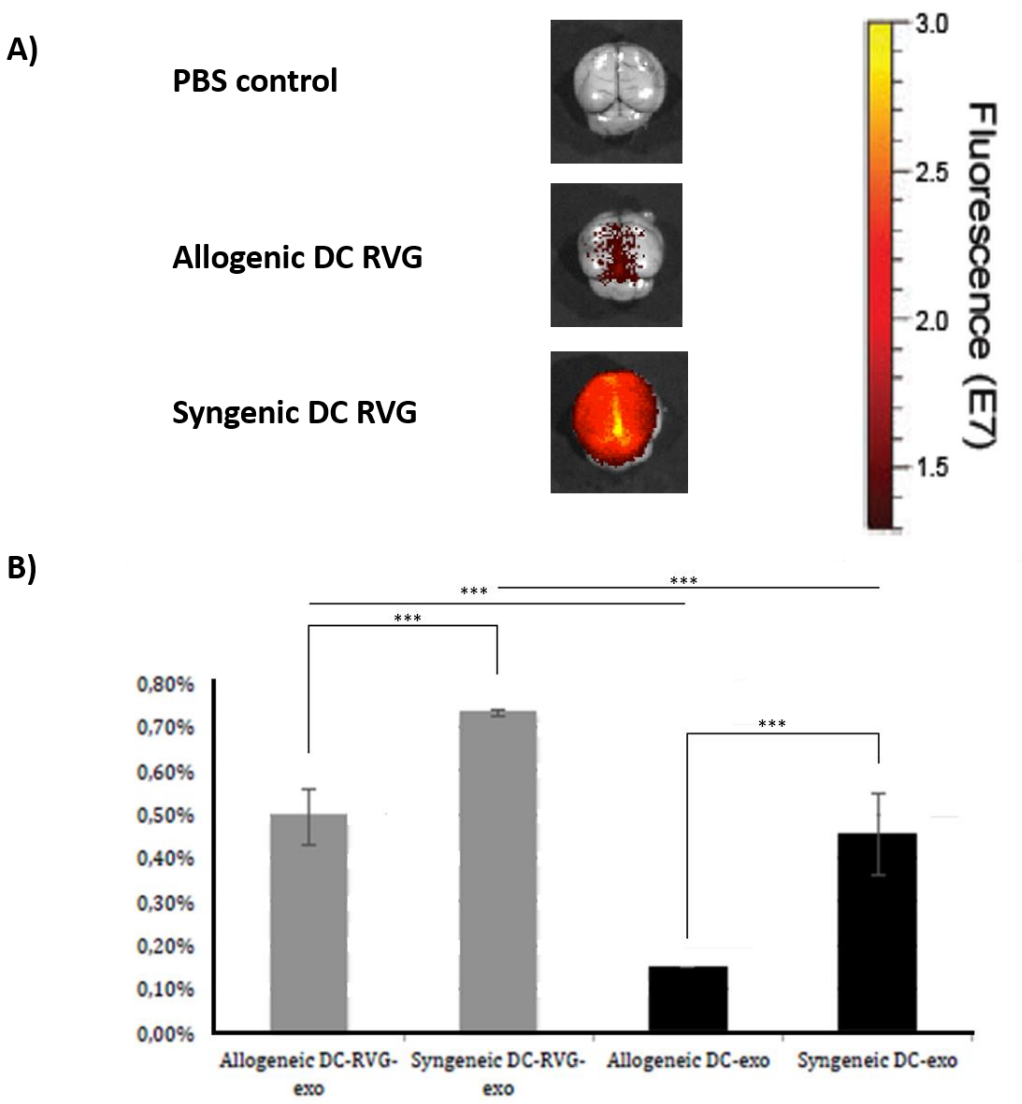


Figure 4.8 Distribution of RVG and non-RVG Bone Marrow Dendritic Cell Derived EVs in Allogeneic and Syngeneic Recipients in the Brain. Bone marrow derived DCs from C57BL6 mice were transfected with Lamp2b-RVG or mock transfected and 24 hours following intravenous injection into allogeneic (Balb/c) or syngeneic (C57BL6) mice with of $1.0x10^{10}$ p/g DiR labelled EVs the fluorescence in all organs indicated was measured. **A)** Representative image of mouse brains of C57BL6 and Balb/c strains, harvested 24 hours post injection of $1.0x10^{10}$ p/g of RVG transfected DCs from C57BL6 mice compared to PBS control. **B)** The percentage of fluorescent signal in the brain of C57BL6 and Balb/c mice after injection of $1.0x10^{10}$ p/g of RVG (DC-RVG-exo) and non-RVG mock transfected (DC-exo) DC derived EVs from C57BL6 mice. Values represent mean ± SEM, n = 4. Statistical significance was calculated using the Kruskal-Wallis test followed by Dunn's post hoc analysis, ***p<0.001, **p<0.01, *p<0.05.

4.2.7 Design of Novel Targeting Peptides

Although a two-fold increased expression was achieved with RVG targeting via transfection of the source cells with the Lamp2b-RVG targeting construct, the brain distribution of RVG targeted EVs was just 1% of the total biodistribution as indicated by the accumulation of fluorescence. This could be because targeting ligands may be able to overcome the innate homing of EVs no more than this, as other factors such as MPS clearance may be the rate limiting factor. Another possibility is that by using Lamp2b as the membrane anchor for the targeting ligand a restriction is being made on potential ligand expression. Lamp2b was chosen originally for exosomal targeting by Alvarez-Erviti *et al.*, because it is found on exosomal and endosomal membranes[333]. Although Lamp2b may be present on other vesicle subtypes, and other subtypes may also be capable of therapeutic gene delivery, it was possible that an alternative protein anchor may be more highly expressed on EVs and its use might increase targeting potential.

In an effort to increase targeting, cell surface proteins that are highly expressed on all EVs were considered. Proteomic analysis was performed by colleagues on EV samples from 10 human and 7 murine cell sources by either ultracentrifugation or ultrafiltration and size exclusion liquid chromatography. This proteomic analysis generated a list of the most common proteins found in EV samples out of which a subset of most abundantly expressed membrane receptors was identified to establish a list of potential proteins to use as anchors for new targeting peptides **(Table 4.1)**. From these results it was evident that Lamp2b was not an ideal transmembrane protein anchor for the fusion of an EV targeting ligand as its expression was over 3 logs lower than the most abundant receptors on EVs. The most abundant receptors however were tetraspannins or had an intracellular C-terminus. Cloning of a targeting ligand in a tetraspannin would have to be performed

in an extracellular loop which could negate the targeting capacity by restricting the tertiary conformation and potentially folding into loops, while a protein with an intracellular C-terminus would preclude cloning of a targeting ligand to that terminus. TfR was chosen as the best candidate for cloning of a targeting ligand from these results as it is highly expressed and the ectodomain is the C-terminus which facilitates more predictable cloning.

Receptor	Average Signal (in log10)	Standard Deviation	Coefficient of Variation
CD81	9.73	0.72	0.07
Itqb1	9.17	0.68	0.07
Mfge8	9.36	0.73	0.08
CD63	8.96	0.71	0.08
CD151	8.25	0.68	0.08
Hspg2	8.86	0.86	0.10
Lgals3bp	9.36	1.01	0.11
Col6a1	8.59	1.02	0.12
Agrn	7.93	1.88	0.24
Tspan1 4	7.79	1.86	0.24
Lamc1	8.31	2.03	0.24
Lamb1	8.02	1.97	0.25
TfRc	7.84	2.02	0.26
CD47	7.44	2.49	0.33
CD82	7.35	2.48	0.34
CD9	7.81	3.30	0.42
Slit2	5.78	3.69	0.64
Lamp2	5.78	4.07	0.70

Table 4.1 Proteomic Analysis of Transmembrane Proteins in EV Samples. A subset of transmembrane proteins with the highest signal in proteomic samples across EV samples derived from several sources. Human and murine cell lines including HEK293 cells, MSCs, Neuro2A cells, NK, C2C12 and B16F10 cells were used as source cells and EVs were isolated by ultracentrifugation or ultrafiltration and size exclusion liquid chromatography. Liquid chromatography tandem mass spectrometry was applied to the samples to determine the most abundantly expressed proteins. The list of most abundantly expressed proteins was cross referenced using QuickGO annotations (a web based browser for gene ontology and annotations) to find the most abundantly expressed receptors. A subset of the resultant transmembrane proteins listed as receptors in QuickGO and most abundant across the various EV samples are shown here. Unpublished data from Wood lab.

The brain targeting ligands EPRNEEK and G7 were chosen for cloning to the ectodomain of TfR for EV brain targeting. EPRNEEK is the critical peptide sequence from *Streptococcus pneumonia*, a pathogen responsible for meningitis, which allows the pneumococcal CpaA domain to bind the laminin receptor on the BBB[334]. A previous study used this peptide conjugated to a type of non-viral gene vector dendrigraft poly-L-lysines (DGLs). The resultant peptide-modified nanoparticles, when loaded with DNA, were capable of eliciting cellular uptake and brain tumour targeting *in vivo* following intravenous injection, demonstrating that EPRNEEK is a good candidate peptide ligand for EV brain targeting[335]. The G7 peptide with sequence H_2N-Gly-$_L$-Phe-$_D$-Thr-Gly-$_L$-Phe-$_L$-Leu-$_L$-Ser(O-β-$_D$-glucose)-$CONH_2$, is a derivative of the synthetic opioid peptide MPP2000, known to be capable of crossing the BBB. The tyrosine in the peptide is replaced with phenylalanine to avoid opioid effects linked to the N-terminal tyrosine[336]. This G7 peptide has also shown promise in brain delivery when conjugated to a biodegradable copolymer nanoparticle poly ($_{D,L}$-lactide-co-glycolide) (PLGA). These copolymers were capable of crossing the BBB following administration via femoral vein injection[337].

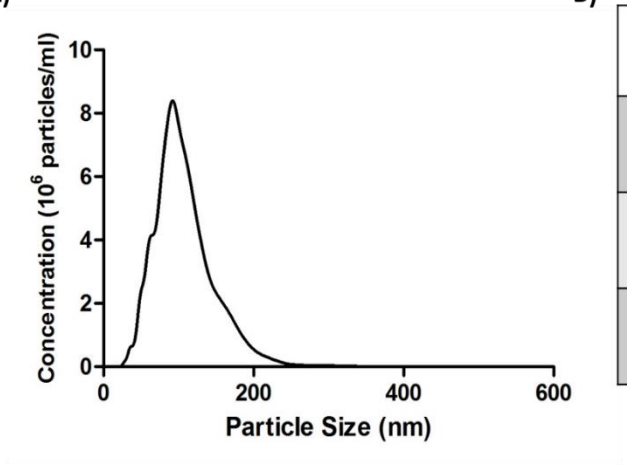
These ligands, as well as RVG, were cloned to the extracellular domain of TfR using the Addgene plasmid backbone pBa.TfR.GFP. The inserts were designed to be expressed following, and in frame with, the TfR peptide coding region and following the GFP coding region, but before the SV40 terminator **(Figure 2.2)**. The GFP was retained as a reporter to allow for estimation of transfection efficiency. The cloning strategy for each vector can be seen in Figure 2.2A-E in Chapter 2.

4.2.8 Characterisation of EVs from HEK293 Cells

To evaluate the new targeting vectors, HEK293 cells were chosen as the EV source cells because their biodistribution is broadly similar to that of DC EVs as was established in section 4.2.2. In addition, they are safe on injection, are more suited to a larger scale study comparing several targeting ligands as they can easily be grown in large numbers, and their use is more ethical in pilot studies as they are not costly in animal life unlike bone marrow DCs.

Although the biodistribution of untargeted HEK293 EVs had been established, it was necessary to characterise the EVs from these cells. NTA and western blot analysis confirmed that HEK293 EVs had a mode of 92.4 nm, a normal EV shaped curve and expressed EV markers Alix and Tsg101 but not the endoplasmic reticulum marker calnexin which would indicate contamination from other cellular sources **(Figure 4.9)**.

A)



B)

	HEK293 EVs	SE
Mean size (nm)	107.42	4.31
Mode size (nm)	92.37	2.06
Total Particles ($x10^9$)	1.21	0.06

C)

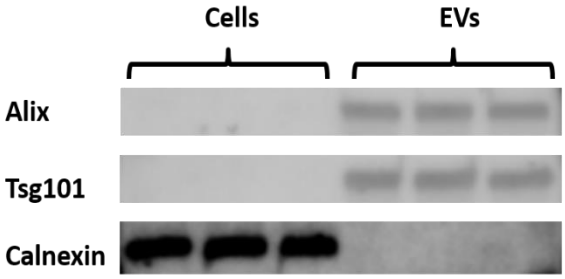


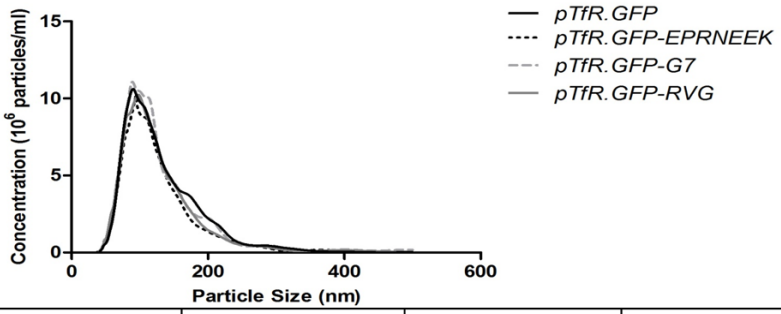
Figure 4.9 Characterisation of HEK293 Derived Extracellular Vesicles. Extracellular vesicles (EVs) isolated from HEK293 cells transfected were characterised by nanoparticle tracking analysis (NTA) and western blot. **A)** NTA analysis of size distribution histogram, n = 3. **B)** Table displaying the mean and mode particle size, total number of particles with standard error secreted from a 15cm dish of HEK293 EVs, n = 3. **C)** Purified EVs and cell lysates (Cells) were loaded on a western blot and probed for the exosomal markers, Alix and Tsg101 and the endoplasmic reticulum marker calnexin.

4.2.9 Characterisation of the EVs Produced by HEK293 Cells Transfected with the Transferrin Receptor-Based Targeting Vectors.

The new targeting vectors designed to express EPRNEEK, G7 or RVG at the ectodomain of TfR were transfected into HEK293 cells using PEI at a previously optimised ratio of 4 µg PEI:1 µg DNA. As a control, the original pBa.TfR.GFP vector was also transfected. Overall the transfection efficiencies were similar for each plasmid.

EVs from these cells were isolated from conditioned medium which had been in contact with the cells for 48 hours via differential ultracentrifugation. NTA analysis and western blot was then performed on EVs collected from each group **(Figure 4.10A-C)**. The NTA size distribution curve was similar for each group **(Figure 4.10A)**, as were the mode sizes of 88.5 nm to 92.0 nm which were within the margin of error **(Figure 4.10B)**. The expression of Alix, Tsg101, and GFP was high in EV samples but the endoplasmic reticulum marker calnexin, as an indicator of contamination, was low **(Figure 4.10C)**. TfR itself could not be stained for as an indicator of the expression level of the fusion constructs as it would not have been clear if the staining resulted from the expressed construct or from TfR naturally occurring on the EV membrane, nor could the ligands be stained for directly as antibodies specific for them do not currently exist.

A)



B)

	pTfR.GFP	pTfR.GFP-EPRNEEK	pTfR.GFP-G7	pTfR.GFP-RVG
Mean size (nm) ± SE	106.04 ± 5.17	116.54 ± 4.41	112.75 ± 5.53	105.71 ± 4.32
Mode size (nm) ± SE	90.56 ± 1.82	88.52 ± 2.13	89.71 ± 2.34	92 ± 2.47
Total Particles ($x10^9$) ± SE	1.06 ± 0.09	0.94 ± 0.09	1.1 ± 0.08	1.02 ± 0.07

C)

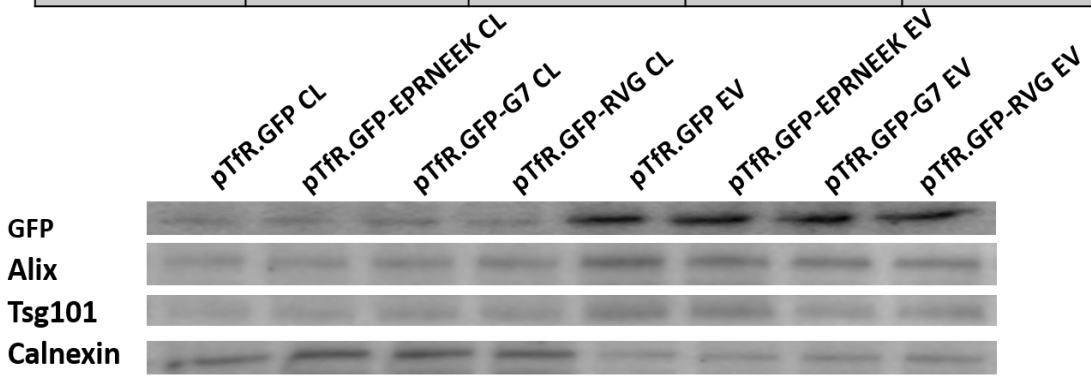


Figure 4.10 Characterisation of EVs from HEK293 Cells Transfected with pBa.TfR.GFP, pBa.TfR.GFP-EPRNEEK, pBa.TfR.GFP-G7 and pBa.TfR.GFP-RVG and confirmation of GFP expression. Hek293 cells were transfected with pBa.TfR.GFP, the original backbone vector used for cloning as well as three new brain targeting vectors; pBa.TfR.GFP-EPRNEEK, pBa.TfR.GFP-G7, and pBa.TfR.GFP-RVG. **A)** NTA distribution pattern of EVs isolated from cells transfected with each vector. **B)** Table showing the mean particle size, the peak and total particle number from a 15cm dish with standard error for each EV preparation, n=3. **C)** A western blot using cell lysate (CL) and EV preparations from HEK293 cells transfected with the original vector pBa.TfR.GFP, and the new vectors pBa.TfR.GFP-EPRNEEK, pBa.TfR.GFP-G7, and pBa.TfR.GFP-RVG., probed for the EV markers Alix and Tsg101, and calnexin.

4.2.10 Investigation of the Biodistribution of Transferrin Receptor Anchored Targeting Vectors

HEK293 cells were transfected with each of the new targeting constructs; pBa.TfR.GFP-EPRNEEK, pBa.TfR.GFP-G7, pBa.TfR.GFP-RVG, as well as the original vector without the cloned inserts - pBa.TfR.GFP - as a control. 4 hours post transfection medium was changed to EV-depleted medium and conditioned medium was harvested following 48 hours. The conditioned medium was used to isolate EVs via differential ultracentrifugation. These were stained with DiR and $1.0x10^{10}$ p/g of EVs from each group were injected to the tail vein. Following 12 hours the organs were harvested and imaged using IVIS *ex vivo* **(Figure 4.11)**.

Similar to the untargeted and Lamp2b-RVG targeted EVs, distribution was highest to the liver, lungs, spleen and GI-tract **(Figure 4.11)**. Although all constructs displayed highest distribution to the liver, there were differences between the groups. EVs from cells transfected with the original control pBa.TfR.GFP plasmid had the highest level of liver distribution, 63% compared to the next highest 53% for pBa.TfR.GFP-RVG and 44% and 43% for pBa.TfR.GFP-G7 and pBa.TfR.GFP-EPRNEEK respectively. Lung distribution was lowest (10%) for EVs from cells transfected with the non-targeting control vector, highest for pBa.TfR.GFP-EPRNEEK at 20%, 16% for pBa.TfR.GFP-G7 and 13% for EVs from cells transfected with pBa.TfR.GFP-RVG. Distribution to the GI-tract bore the same pattern as lung distribution, highest for pBa.TfR.GFP-EPRNEEK and pBa.TfR.GFP-G7 (24% and 23% respectively), lower for pBa.TfR.GFP-RVG (18%) and lowest for pBa.TfR.GFP (12%). Distribution to the spleen was similar for EVs derived from cells transfected with each vector, approximately 10% **(Figure 4.11)**.

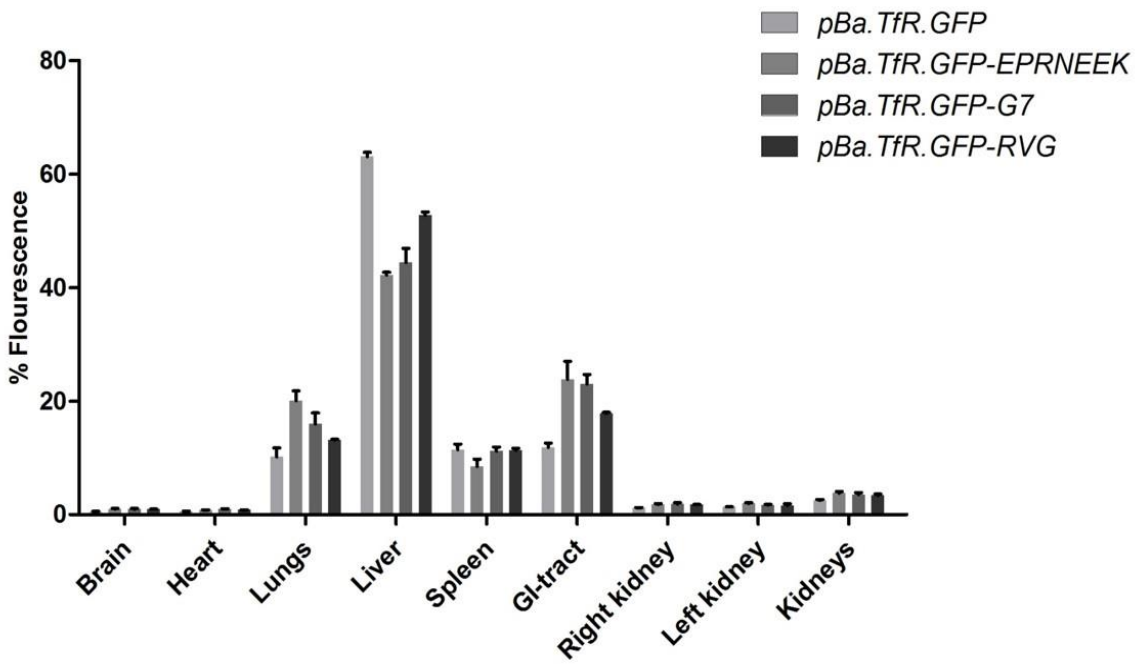


Figure 4.11 Biodistribution of DiR Labelled EVs from HEK293 Cells Transfected with pBa.TfR.GFP, pBa.TfR.GFP-EPRNEEK, pBa.TfR-G7 and pBa.TfR-RVG. EVs were isolated from HEK293 cells which had been transfected with pBa.TfR.GFP, pBa.TfR.GFP-EPRNEEK, pBa.TfR.GFP-G7 and pBa.TfR.GFP-RVG. 12 hours following injection with $1.0x10^{10}$ p/g DiR labelled EVs the fluorescence in each organ was measured *ex vivo*. The percentage of fluorescent signal in each organ after injection of $1.0x10^{10}$ p/g of EVs from each group is shown. Values represent mean + SEM, n = 3 except for the pBa.TfR.GFP-RVG EV treated group where n = 2.

Brain distribution was increased for all of the new constructs when compared to untreated or the control plasmid **(Figure 4.12)**. Representative images from brains from each treatment group can be seen in Figure 4.13A. The increase mirrored that for Lamp2b-RVG for all constructs, it was two-fold **(Figure 4.12B)**.

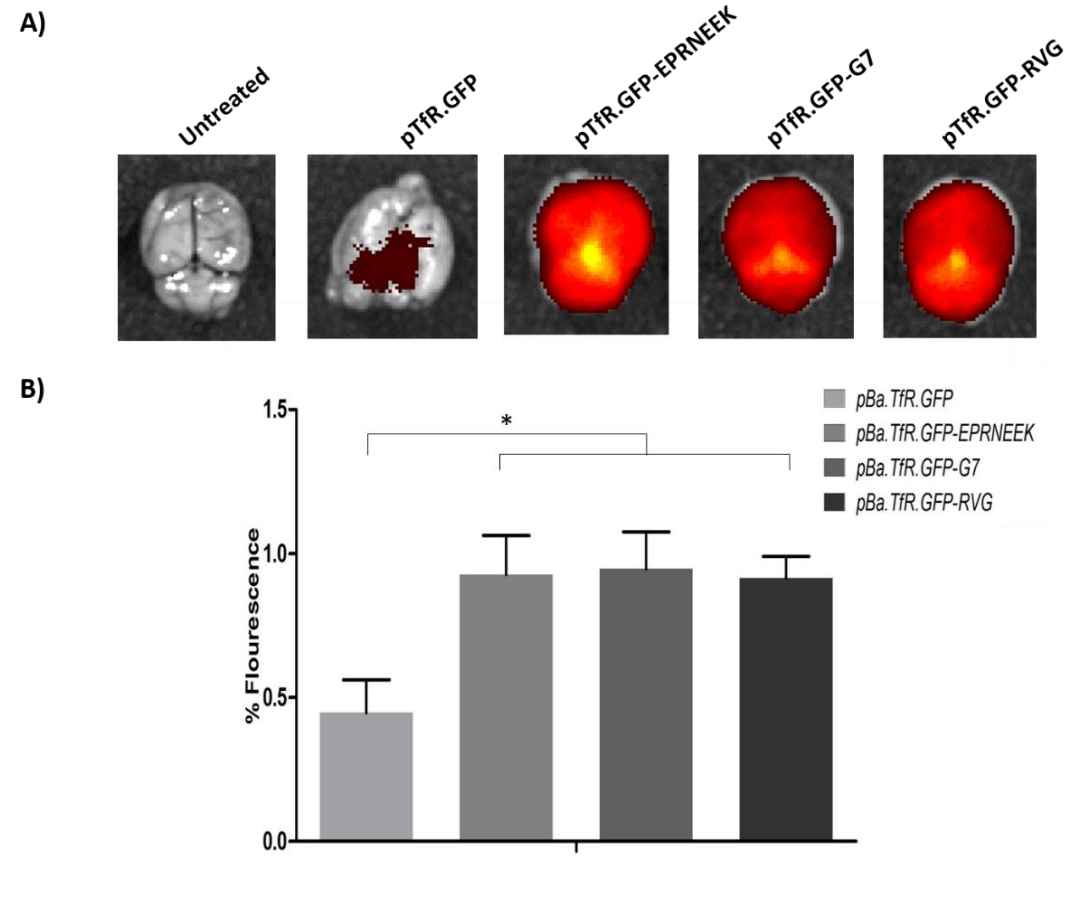


Figure 4.12 Brain Distribution of DiR Labelled EVs from HEK293 Cells Transfected with pBa.TfR.GFP, pBa.TfR.GFP-EPRNEEK, pBa.TfR-G7 and pBa.TfR-RVG. HEK293 cells were transfected with pBa.TfR.GFP, pBa.TfR.GFP-EPRNEEK, pBa.TfR-G7 or pBa.TfR-RVG and 12 hours following injection with $1.0x10^{10}$ p/g DiR labelled EVs the fluorescence in the brain was measured. **A)** Representative image of mouse brains, harvested 12 h post injection of $1.0x10^{10}$ p/g of EVs from HEK293 cells which had been transfected with either pBa.TfR.GFP, pBa.TfR.GFP-EPRNEEK, pBa.TfR-G7 or pBa.TfR-RVG. **B)** The percentage fluorescence signal in the brain 12 hours post-injection. Values represent mean + SEM, n = 3 except for the pBa.TfR.GFP-RVG EV treated group where n = 2. Statistical significance was calculated using the Kruskal-Wallis test followed by Dunn's post hoc test, ***p<0.001, **p<0.01, *p<0.05.

4.2.11 Investigation of Uptake of Extracellular Vesicles from Transferrin Receptor-Based Targeting Vector Transfected Source Cells

To evaluate further the uptake of the new TfR-based targeting vectors, an *in vitro* model system of the BBB was used. There are many BBB models and although no model can currently replicate accurately the properties of the BBB, the use of primary rat progenitor brain microvascular endothelial cells (rpBMECs) isolated from the cerebral cortex as a BBB model can generate useful information on drug delivery to the central nervous system (CNS)[338]. The model grows polarized cell monolayers representative of the BBB[339]. In this study the aim was to examine uptake of EVs harvested from HEK293 cells transfected with each of the targeting vectors through flow cytometry measurements of EV uptake via the GFP in the targeting constructs.

Firstly, a preliminary study in b.END3 cells was performed to establish whether the signal from the GFP was sufficiently intense to measure with flow cytometry, or if a fluorescent label (PKH26) should be added to the EVs to increase the intensity of the signal for detection. EVs from HEK293 cells in the absence of targeting but transfected with pBa.TfR.GFP control vector were isolated from 48 hour conditioned medium via differential ultracentrifugation. In parallel to this, another set of EVs which were also from cells transfected with the same vector were labelled with the lipophilic dye PKH26 and also examined for uptake as a secondary means of visualisation should the GFP signal prove too weak. Dynamic light scattering (DLS) was performed on the EV samples which were unlabelled or labelled with PKH26. Both samples were shown to contain three populations of EVs at different sizes **(Figure 4.13A and B)**. This is likely due to aggregation during transport and for future studies this was eliminated by resuspension

of EVs with a 27G needle prior to use. No uptake could be identified when measured by GFP in flow cytometry, but uptake in the phycoerythrin (PE) channel of PKH labelled EVs showed 9% uptake (measured by the percentage of dye positive cells) when the sample was diluted 1:50 and half that at a 1:100 dilution (**Figure 4.14A and B** respectively). Cell viability was high following all treatments with EVs but reduced slightly for buffer alone **(Figure 4.14C)**. For the uptake study in rpBMECs it was decided to use PKH26 labelling for EVs.

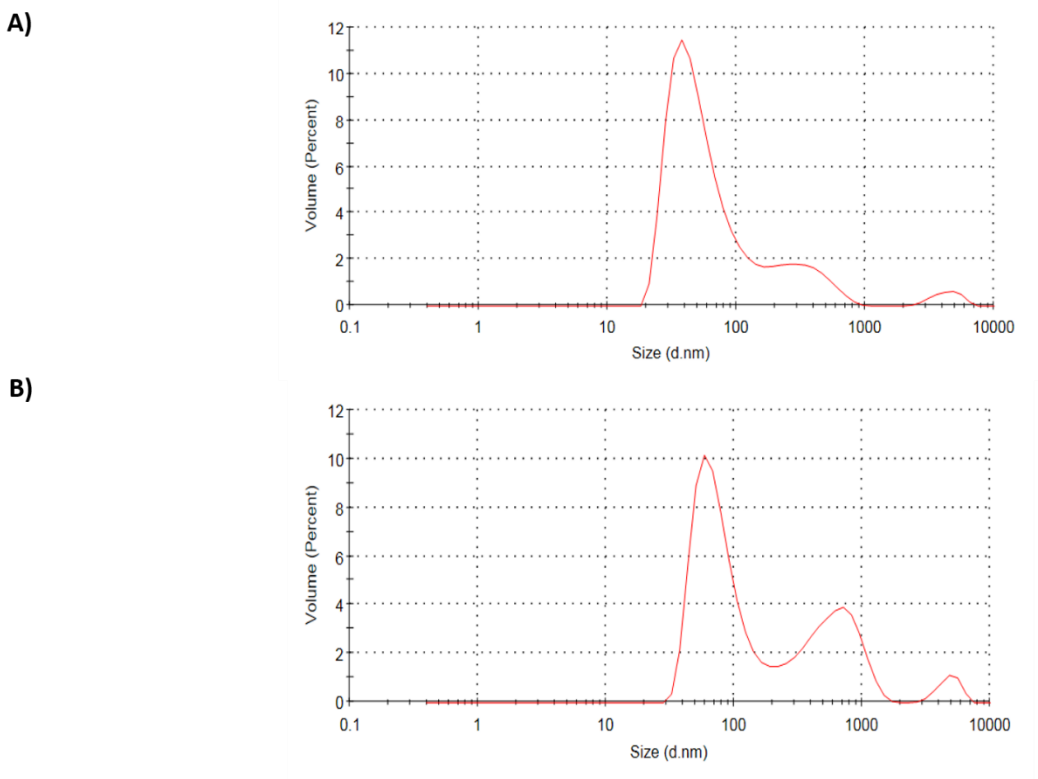


Figure 4.13 Dynamic Light Scattering of PKH26 or non-PKH26 labelled EVs. DLS was performed on EVs from HEK293 cells transfected with pBa.TfR.GFP. **A)** EVs not labelled with PKH26. **B)** EVs labelled with PKH26.

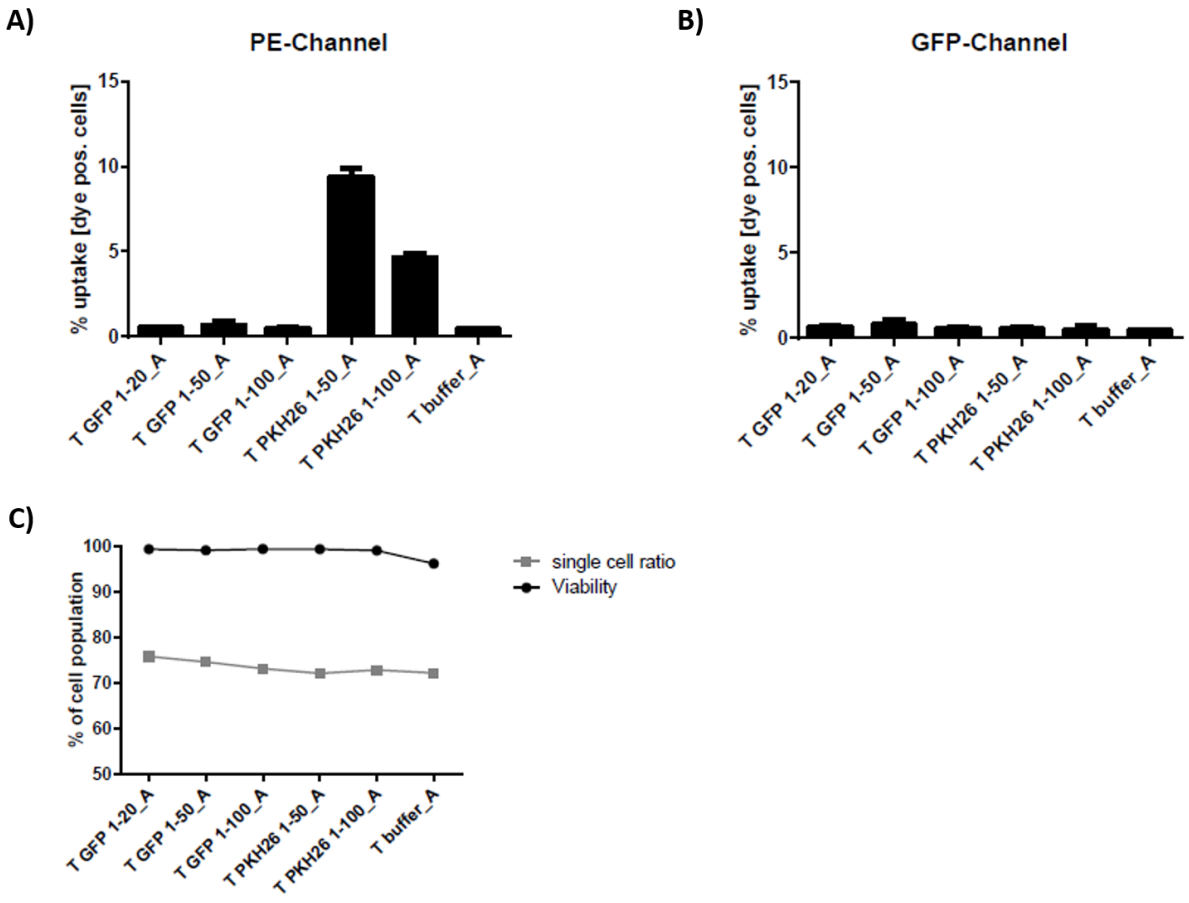
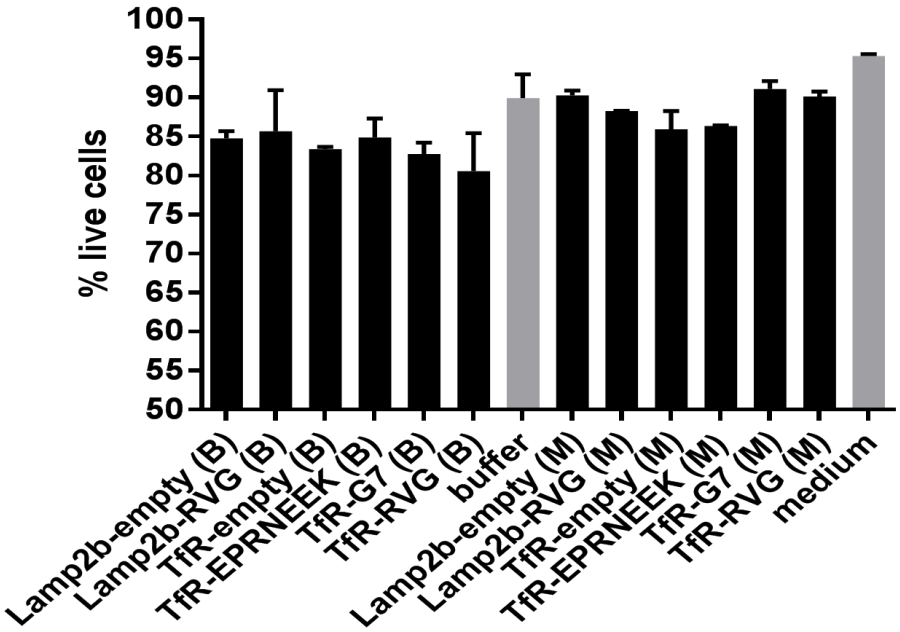


Figure 4.14 Flow Cytometry Uptake Results on b.END3 Cells. Flow cytometry results showing percentage of dye positive cells as an indicator of uptake in b.END3 cells following treatment with EVs harvested from HEK293 cells transfected with pBa.TfR.GFP and unlabelled or labelled with PKH26. Treatments were applied in buffer and dilution factors indicate dilution of the EV sample 1:20, 1:50 and 1:100. **A)** Uptake of unlabelled and PKH26 labelled EVs in the PE-channel. **B)** Uptake of unlabelled and PKH26 labelled EVs as measured in the GFP channel. **C)** Cell viability following treatments. Values represent mean + SEM, n = 3.

HEK293 cells were transfected with each targeting vector and the control pBa.TfR.GFP plasmid (here referred to as TfR-empty) as well as the Lamp2b targeting vector (Lamp2b-RVG) and the Lamp2b vector with no targeting moiety (Lamp2b-empty). 4 hours post transfection the medium was changed to EV-depleted medium. Following 48 hours the EVs were isolated from the conditioned medium using differential ultracentrifugation, labelled with PKH26 used to treat rpBMECs to test for uptake via flow cytometry. The rpBMECs were treated with the EVs resuspended in either buffer or serum depleted medium. In addition to the uptake study, tests of their viability were performed following incubation for 90 minutes. These showed that the uptake in buffer negatively affected cell viability and there were slight differences between constructs **(Figure 4.15A)**. In buffer conditions, there were no significant differences in cell viability between cells treated with the different constructs, however viability was lower overall than in samples treated with the EVs in medium **(Figure 4.15A)**. For cells treated with the EVs from cells transfected with the various constructs in medium, there were negligible differences between treatment groups, but all were slightly lower than medium alone **(Figure 4.15B)**. In contrast to the *in vivo* biodistribution results which showed a two-fold increase in brain distribution on expression of the targeting ligands, the flow cytometry analysis on BBB model cells showed decreased uptake for each targeting ligand compared with the "empty" vectors **(Figure 4.15B)**. The transferrin receptor-based targeting vectors showed increased uptake compared to Lamp2b-RVG.

A)


% live cells
100
95
90
85
80
75
70
65
60
55
50
Lamp2b-empty (B)
Lamp2b-RVG (B)
TfR-empty (B)
TfR-EPRNEEK (B)
TfR-G7 (B)
TfR-RVG (B)
buffer
Lamp2b-empty (M)
Lamp2b-RVG (M)
TfR-empty (M)
TfR-EPRNEEK (M)
TfR-G7 (M)
TfR-RVG (M)
medium

B)

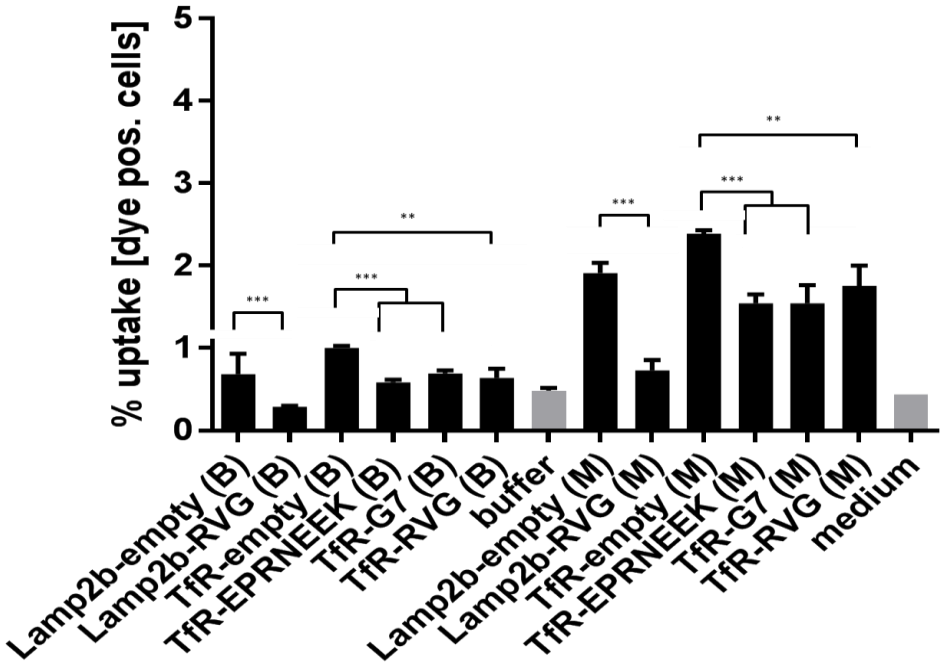

% uptake [dye pos. cells]
5
4
3
2
1
0
***
**
***
***
***
**
Lamp2b-empty (B)
Lamp2b-RVG (B)
TfR-empty (B)
TfR-EPRNEEK (B)
TfR-G7 (B)
TfR-RVG (B)
buffer
Lamp2b-empty (M)
Lamp2b-RVG (M)
TfR-empty (M)
TfR-EPRNEEK (M)
TfR-G7 (M)
TfR-RVG (M)
medium

Figure 4.15 Flow Cytometry Analysis of rpBMECs Treated with EVs from Cells Transfected with Brain Targeting Constructs. Flow cytometry analysis of uptake in rpBMECs in the PE-channel of PKH26 labelled EVs from HEK293 cells transfected with the control vectors Lamp2b-empty and TfR-empty, or brain targeting vectors Lamp2b-RVG, pBa.TfR.GFP-EPRNEEK (TfR-EPRNEEK), pBa.TfR.GFP-G7 (TfR-G7) or pBa.TfR.GFP-RVG (TfR-RVG) following incubation for 90 minutes. Treatments were either in buffer (B) or medium (M). **A)** Cell viability following incubation of cells with each treatment under the indicated conditions of buffer or medium for 90 minutes. **B)** Uptake of EVs from HEK293 cells transfected with each indicated control or targeting vector, measured by percentage of dye positive cells. Values represent mean + SEM. n = 3. Statistical differences were calculated using one-way ANOVA with Tukey's post hoc analysis. ***p<0.001, **p<0.01, *p<0.05.

4.3 Discussion

This study was performed to elucidate the biodistribution of brain targeted EVs compared to untargeted EVs. Specifically, a biodistribution study using DiR labelled Lamp2b-RVG targeted and untargeted EVs was performed. It was confirmed that the DiR labelling did not affect the size distribution, concentration or marker expression of EVs. Following 24 hours after intravenous administration, the distribution profile of Lamp2b-RVG targeted EVs broadly resembled those of untargeted EVs - most accumulated in the RES (the liver, lungs and spleen) - except for organs bearing high levels of cholinergic receptors where an increased accumulation of vesicles was noted for RVG targeted EVs. A two-fold increase in brain delivery was achieved. In an effort to increase this, based on results of a proteomics study and the single transmembrane nature of TfR with an extracellular C-terminus, it was chosen as an alternative membrane anchor to Lamp2b and new targeting peptide ligands EPRNEEK and G7 were investigated for their brain targeting capacity, as well as RVG fused to TfR. Biodistribution was assessed in the same way and a two-

fold increase in brain delivery was observed. To gain further understanding on the uptake of these targeted EVs, rpBMECs were used as a BBB mimic but the targeting ligands caused a slight decrease in uptake compared to the vectors expressing Lamp2b and TfR.GFP with no targeting ligand.

The results of this study must be considered with the other biodistribution studies that have been performed on EVs to date. The choice of reporter here was DiR which has been used by other groups for similar purposes of tracking EVs[323,324]. Data was collected which indicated that free dye was not being tracked, but rather labelled EVs. The results from this study are in line with other studies performed using DiR labelled EVs in that most of the EVs distributed to the liver, spleen and lungs[323]. A difference in organ accumulation between this study and previous work is that some others have noted high accumulation in the kidneys which was not evident in the present study. The disparity here could be due to the source of EVs as EVs were derived previously from tumours, and EVs can bear intrinsic homing capacities derived from the host cells. This homing is evident in the present study from the slight differences between homing when HEK293 and DC derived EV biodistribution were compared. The dose of EVs was also different in this study. In their study, Smyth *et al.,* administered 60 µg based on protein weight but in the present study just 1.0 x 10^{10} p/g was administered. These are difficult to compare as protein quantification can be affected by contamination from other proteins and lipid:protein ratio can vary among EV preparations. As the EVs prepared by Smyth *et al*., were washed in PBS and extracted from a sucrose density cushion there is likely to be low contamination where an estimation of $3x10^{10}$ p/µg of protein can be obtained[340]. Per injection (60 µg protein equivalent) this equates to $1.8x10^{12}$ particles. In the present study, an adult mouse weighing approximately 20 g received an injection containing

approximately $2x10^{11}$ particles. The larger volume of particles used in previous work may have saturated the liver causing more to divert to the kidney. This was avoided here as a dose response study indicated larger doses than those used in this study would cause such saturation. Such a high dose and saturation of this system from liposomes has been shown to result in Kupffer cell failure which could lead to systemic endotoxemia, liver damage, increased rates of infection due to host defence impairment and hepatic failure[341,342].

Another biodistribution study which used near infrared dye labelling on untargeted EVs with DiD and DiI of EVs was the study by Grange *et al*., to evaluate the biodistribution of mesenchymal stem cell derived EVs in nude mice with acute kidney injury[320]. They performed the staining in the same manner as this current study because pre-incubating the EV source cells with the dye produced inferior imaging results. Intravenous injection of the EVs generated results comparable to those reported here. High levels of EVs were detected in the liver, spleen and lungs. Unlike the present study, but similar to the study by Smyth *et al*., kidney accumulation was noted, but only in the diseased mice. Grange *et al*., also faced a similar issue as this present study, in that organs had to be imaged *ex vivo* for accurate determination of signal origin.

Other research on the biodistribution of untargeted EVs has used alternative reporter methods but found similar results as this study for untargeted EVs. Takahashi *et al*., and Lai *et al*., used a Gaussia luciferase fused to the EV surface[321,322]. Takahashi *et al*., found that intravenously administered EVs distributed rapidly accumulating primarily in the liver, lungs and spleen which is also in line with the present study[322]. The distribution pattern of EVs labelled with a fluorescent probe, PKH26, was also analysed and was found to be comparable. The half-life of the EVs were found to be much shorter than that

indicated by fluorescent labelling however, approximately just 2 minutes. Lai *et al*., also found that EVs conjugated to their luciferase probe were eliminated earlier than in estimates based on fluorescent dyes, in 6 hours[321]. The present study used a 24 and 12 hour time point. Lai *et al*., found that there were two phases of exponential decay in their study, EVs with a half-life of 20 minutes and the second phase of 180 minutes. The differences in apparent processing of EVs identified in different studies could be an artefact of their labelling method as an anchor or fusion protein might only be expressed on certain EVs so only a subset of EVs could be labelled whereas a dye is non-selective in its staining. They did however also find accumulation in the spleen, liver and lungs but also the kidney after perfusion which was not performed here as no difference in the biodistribution was seen between perfused and non-perfused animals[326]. Further evidence of the accumulation of EVs in the liver, lungs and spleen was provided using a different reporter system, streptavidin bound to a radiolabelled biotin-lactadherin[343]. Another study which supports the results of EV accumulation in the liver and lungs but not the kidney comes from a study which instead of a reporter, used loaded microRNA to evaluate distribution[344]. Here high levels were also found in adipose tissue which was not tested in the present study.

The variation in biodistribution may arise from the source as cells from different sources may express different tetraspannins and other membrane proteins as well as being composed of varying phospholipid compositions which could lend different homing capacities to EVs obtained from different sources. In addition, as was seen in this study, EVs from different sources have different size distributions as evidenced by NTA which could also contribute to their *in vivo* dynamics. This is apparent here from the slight differences in biodistribution between untargeted EVs derived from HEK293 cells and

DCs. Apart from the cell source biodistribution may also be affected by the isolation methods[345].

Biodistribution of untargeted EVs has been discussed so far, but there is also some research, though limited, on bioengineered targeted EVs. This study provides evidence that although a targeting strategy based on the expression of a neuronal targeting ligand on the ectodomain of an EV anchor protein can increase brain distribution following systemic injection, it is difficult to overcome the innate targeting capacity of EVs. In this study, no more than a two-fold increase in accumulation was achieved using two different anchor proteins and three ligands. This is evidence that targeting is not the rate limiting factor and development of a mechanism to avoid fast clearance may be a more powerful tool in achieving efficacy from EV treatments. The other studies which have looked at targeting include research by Ohno *et al*., where the transmembrane domain of platelet-derived growth factor was engineered to be expressed fused to the epidermal growth factor receptor-binding peptide (GE11) in the source cells[324]. Functional luciferase siRNA activity in the target cells *in vitro* and *in vivo*, let-7a miRNA and DiR labelled EVs were detected in xenograft tumours. In their study delivery was increased 3-fold and their detection methods of DiR labelled EVs visualised with IVIS after 24 hours were the same as the present study.

Other research involving engineered EV targeting is the research on which the Lamp2b-RVG targeting vector was originally used where EVs from DCs transfected with the targeting vector and loaded with Bace1 siRNA by electroporation were capable of inducing knockdown in the brain, but no biodistribution analysis of EV accumulation was performed[213]. In the present study just 1% of the total fluorescence from the injected

labelled EVs was emitted from the brain so alternate methods of targeting were investigated in an effort to increase this. Tian *et al*., also used Lamp2b fused to αv integrin-specific internalizing RGD peptide (iRGD), EVs were then loaded with the chemotherapeutic drug doxorubicin and these targeted EVs were shown to be capable of delivering the drug to the tumour *in vivo* which inhibited its growth[325]. However, the fluorescence was not quantified with and without the targeting ligand.

From the proteomics data described in this chapter, Lamp2b was found to be expressed at a lower and more variable level than other membrane proteins. In addition, Hung and Leonard identified that peptides fused to the N-terminus of Lamp2b are not detected in cells nor on EVs, potentially due to degradation by endosomal proteases[346]. Peptide glycosylation was found to protect against this degradation, increasing EV expression and specific binding. Here it was hypothesised that the use of a different membrane anchor for a targeting ligand may lead to higher levels of expression and increased targeting based on the proteomics data. It is also possible to speculate that because Lamp2b is an endosomal protein, it may be more expressed on exosomes compared to MVs due to their biogenesis in MVBs, and choosing Lamp2b as a membrane anchor may be limiting targeting to expression primarily to one subset of EVs. Although exosomes have been highlighted in the literature as the primary vesicular carriers of RNA (exosome shuttle RNA), EVs other than exosomes are involved in gene transfer, one study found *de novo* reporter protein expression in recipient cells was only achieved via plasmid DNA delivery by larger MVs but not exosomes[319,347]. Furthermore, pDNA, mRNA and siRNA are more effectively loaded into MVs than exosomes, authors suggest that selecting just exosomes could restrict encapsulation of nucleic acid cargos to those with unique signatures[348,349]. However, this group used only centrifugation to distinguish between the

groups and thus it cannot be concluded that only exosomes remain in the "exosome" fraction as small MVs would pellet at the same speed. It is not possible to completely separate these EV subsets using current technology and it could be that MVs do highly express Lamp2b, though nonetheless the proteomics data supported a change in membrane anchor protein. It could also be the case that increasing the EV population of interest to include more MVs, vesicles over 200 nm in diameter, may be beneficial in both targeting and nucleic acid delivery.

In addition to testing an alternative membrane anchor protein for fusion to brain targeting ligands, other ligands were investigated for their targeting capacity. However, greater than two-fold increase in brain accumulation compared to untargeted EVs was not seen with TfR anchored ligands. It is not known whether this two-fold increase would translate into a biological effect if EVs were loaded with a therapeutic for HD as the tissue accumulation does not indicate what is intracellular, however the specific gene silencing achieved by Alvarez-Erviti *et al.*, using systemically delivered Lamp2b-RVG targeted EVs indicates that the targeted EVs are functional at the delivery site[213].

From above, it is clear that although there is some variation in the fate of untargeted and targeted vesicles, in every study which monitored the biodistribution of systemically delivered EVs, the MPS is central in their clearance as in every study described accumulation of EVs is demonstrated in the liver, spleen and lungs. As mentioned above, in a study connected to the data presented here, the dose affected this biodistribution[326]. Between the dose administered here and a dose 50% higher, there was a reduction in distribution to the liver which could be explained by saturation of the MPS/RES and resultant increased bypassing of the liver.

There are many similarities between EVs and liposomes and this may be especially important when considering clearance mechanisms. Liposomes have a similar size as the EVs studied here and have a lipophilic outer layer[350]. They are also known to accumulate in the liver, spleen, GI-tract and lungs. The size and charge may therefore be the most important factors involved in determining the rate of clearance of EVs as Smyth *et al*., observed a similar rapid rate of clearance of intravenously administered EVs as phosphatidylcholine:cholesterol liposomes and EVs formulated with the lipid extracts of exosomes[323].

Other factors influencing RES/MPS system in clearance may also play a role. Smyth *et al.,* performed experiments with mice with impaired adaptive or innate immune systems and revealed that the innate immune system and opsonisation with complement protein C5, a chemoattractant for cells of the RES[351], may be involved in the rate of EV clearance as the rate of EV uptake by cells of the RES in the liver and spleen of mice with impaired innate immune system is slower than Balb/c and nude mice[323]. In the same study, antibodies were ruled out as having a role in EV clearance as there was no difference in rate of EV clearance between Balb/c and nude mice where EVs from a tumour in the Balb/c mice would expose the immune systems of these mice to tumour EVs. Drawing another parallel with liposomes, complement proteins are known to bind to their surface and increase clearance by the RES[352]. Complement proteins have been identified in association with EVs *in vitro* and *in vivo*[353]. In contrast, some studies show that EVs can express CD55 and CD59 which limit complement deposition on them[354]. The former are EVs from tumour cells and the latter are from antigen presenting cells and this could account for the discrepancy.

For most of the aforementioned biodistribution studies it is not possible to rule out the effect of non-self antigenic peptides from the foreign cell source, culture conditions or labelling method on EVs playing a role in the selectivity for MPS clearance. Indeed, in this study there is evidence that the role of foreign cells could alter the biodistribution as untargeted EVs from syngeneic and allogeneic sources show differences in biodistribution. Both distribute readily to the liver and spleen but EVs from syngeneic animals accumulate more in the liver while EVs from allogeneic sources accumulate to a higher level in the lungs but syngeneic derived EVs showed higher levels of accumulation in the brain as indicated by fluorescence. The syngeneic DC derived EVs, though not derived from the animal they would be injected into were derived from the same strain and should minimise this. However, there could still remain some contamination by antigens from the culture process. Future work will need to establish whether it is the properties of EVs such as charge and size or antigens which primarily trigger this processing.

For any future therapeutic use of EVs it would be necessary to engineer a mechanism for avoidance of the RES/MPS system clearance. When selecting a dose for the targeting studies a higher dose could have led to increased brain targeting by saturation of the MPS system and thus bypassing the liver and more effectively targeting the area of interest. However, it is important not to overwhelm the physiological system as MPS saturation can have negative consequences as was described above and was observed by Smyth *et al*., whereby a 400 µg protein equivalent dose of EVs lead to rapid asphyxiation which persisted for 5 minutes post injection[323]. An injection of the same dose of DiR labelled EVs induced death after 3 minutes with an accumulation of EVs found in the lungs potentially due to EV aggregation before or after distribution to the lungs[323]. In another

similarity to the liposome field, this has also been observed with liposomal systems[255]. For future therapeutic use a slow infusion may allow for avoidance of the RES while reducing this risk.

To investigate further the uptake of the targeted EVs in the present study, an *in vitro* analysis of uptake by monitoring the levels of PKH26 labelled EVs via flow cytometry in the BBB model rpBMECs was performed. No model can fully replicate the BBB *in vitro* with high electrical resistance, low paracellular permeability and selective influx/efflux but BMECs have been used in previous studies analysing drug uptake[355]. Here, no increase in uptake was seen, rather a decrease in uptake was evident in cells treated with the targeted ligands compared to the "empty" vectors, that is the vector expressing the anchor protein but no targeting ligand. However, although these results were significant, the physiological relevance may be low, as mentioned the model cannot replicate the BBB. Also, although uptake was slightly reduced, this may be outweighed by any potential tissue specificity which was seen in the *in vivo* study. It is also worth considering that even though the different ligands yielded similar results *in vitro* and *in vivo*, their capacity to reach different areas and cell populations within the brain remains to be investigated. In one study Haney *et al.*, using EVs from macrophages to deliver the antioxidant catalase found EVs in the brain co-localisation with neurons, microglia and endothelial cells[356].

EVs contain proteins and lipid-raft domains that aid efficient fusion, uptake and intracellular processing such as flotillin, Rab, tetraspannins, integrins, which they use endogenously to facilitate intercellular communication, but which can also be exploited for gene therapy[327]. Based on the data collected here and on previous research, it may be

that the tendency towards MPS clearance and short half-lives of EVs limits their suitability as nucleic acid carriers and that targeting can overcome this slightly. Although each brain targeting moiety facilitated a two-fold increased accumulation of labelled EVs in the brain, this accounted for just 1% of the total fluorescence generated from the administered dose of EVs. Further work is necessary to help elucidate the intracellular processing of internalised vesicles and to aid targeted EVs in avoiding the MPS, but another avenue of research that holds promise is the design of EV mimetics, this field may have the capacity to harness the benefits of EVs but make them longer lasting.

In summary, for the first time an increase in accumulation of brain targeted EVs in the brain was visualised. This was shown for EV expression constructs with two different backbones and three targeting ligands. Distribution to the brain was not increased more than two-fold on expression of any targeting moiety. Also, EVs from syngeneic sources were shown to display increased targeting to the brain than EVs from allogeneic sources.

CHAPTER 5 LOADING OF EXTRACELLULAR VESICLES WITH SIRNA

5.1 Introduction

A rational therapeutic strategy for Huntington's disease (HD) is to reduce *HTT* expression, thereby reducing the number of mutant polyglutamine tracts and aggregates and alleviating the neuronal dysfunction to which they contribute[151,165]. As seen in chapter 3, siRNAs offer a means of reducing *HTT* expression in patient derived fibroblasts. Other studies have demonstrated the efficacy of siRNAs *in vitro* and *in vivo* for reduction of *HTT* expression upon direct brain injection with viral vectors[150–152,180].

Despite the success of siRNA for silencing *HTT in vivo*, it has not been brought forward to clinical development. One of the reasons for this is that intracerebroventricular injection is an invasive procedure. A systemic treatment option would avoid the risks associated with direct brain injection. Such a treatment for HD must bypass the blood brain barrier (BBB) and reach *HTT*, an intracellular target. Since RNA can be immunogenic, particularly following a repeated dose, is susceptible to RNase degradation and cannot easily cross membranes due to its negative charge, a carrier is needed for safe *in vivo* delivery, penetration of hydrophobic membranes and facilitation of crossing the BBB. EVs have been suggested as nucleic acid delivery vehicles for the brain as they may have several properties which may overcome these hurdles[213]. They play a natural role as intercellular transporters of RNA capable of eliciting transcriptional and translational changes in target cells[212,347]. Their phospholipid bilayers can allow fusion with a target cell, and this fusion could potentially allow EV cargo to escape the

endosomal and lysosomal pathways which is a major hurdle in the field of gene delivery, and they also seem capable of endosomal escape upon endocytosis[213]. Furthermore, the opportunity. if necessary, to derive these gene delivery vehicles from a patient's own cells could reduce any risk of an immune response.

Alvarez-Erviti *et al*. hypothesised that it may be possible to capitalise on the endogenous role of EVs in intracellular communication for the delivery of exogenous RNA species[213]. Indeed, siRNA directed against a target in Alzheimer's disease (AD), Bace1, loaded into brain targeted EVs seemed to have crossed the BBB when injected intravenously in mice. This lead to the reduction of Bace1 protein levels, thereby suggesting promise for the treatment of AD.

To evaluate whether this strategy could be adapted for the treatment of HD, this study attempted to silence *HTT in vitro* and *in vivo* using similar methods. Electroporation was used to load an siRNA capable of reducing *HTT* expression which had been validated in chapter 3 into EVs. For delivery to neuronal cells, the source cells from which the EVs were isolated were transfected with a Lamp2b-RVG fusion protein expression plasmid for neuronal targeting as used in chapter 4. The efficacy of these EVs loaded with *HTT* siRNA in silencing *HTT* was assessed *in vitro* in several cell types and with two different cellular sources of EVs, and *in vivo* following systemic delivery via tail vein injections. There was difficulty in achieving *HTT* silencing using the established methods of loading. This was investigated and an alternate method of loading based on lipid conjugated siRNA was also evaluated. Cholesterol conjugation of siRNA is known to be capable of generating knockdown *in vivo* alone and when associated with nanoparticles but to date has not been analysed with EVs[357–359].

5.2 Results

5.2.1 Characterisation of Extracellular Vesicles Derived from Different Cell Sources

To evaluate whether the methods used previously to load EVs with siRNA via electroporation could be extended to HD, this study used EVs from different sources, investigated loading by electroporation and analysed the silencing efficiency of the EVs from different cell sources on recipient cells *in vitro* and *in vivo* **(Figure 5.1)**. The primary model system selected for this study was DC derived EVs on patient-derived fibroblasts. Immature DCs were selected as the EVs released by these cells should also be safe to bring forward to *in vivo* work as they do not contain T-cell activators such as MHC-II and CD86[328]. HD fibroblast cells were used in chapter 3 to establish knockdown efficiency of the potential EV cargos as they are a validated model for HD[291,360]. The siRNA selected from chapter 3, siRNA-5' targets both human and murine *Htt* homolog. A murine neuronal cell line - Neuro2A cells - was also selected as recipient cells as the brain is the primary region of interest in this study so the efficiency of silencing in neuronal cells would provide valuable information. As EVs are suspected of displaying homing characteristics to certain cell types, the same neuronal cell line was also used as an EV source in addition to DC derived EVs for the treatment of Neuro2A recipient cells. As a final comparison, HEK293 cells were also included as a recipient cell line as these cells are known to readily take up particles of the size of EVs in this study[329]. A schematic of the experimental plan can be seen in Figure 5.1.

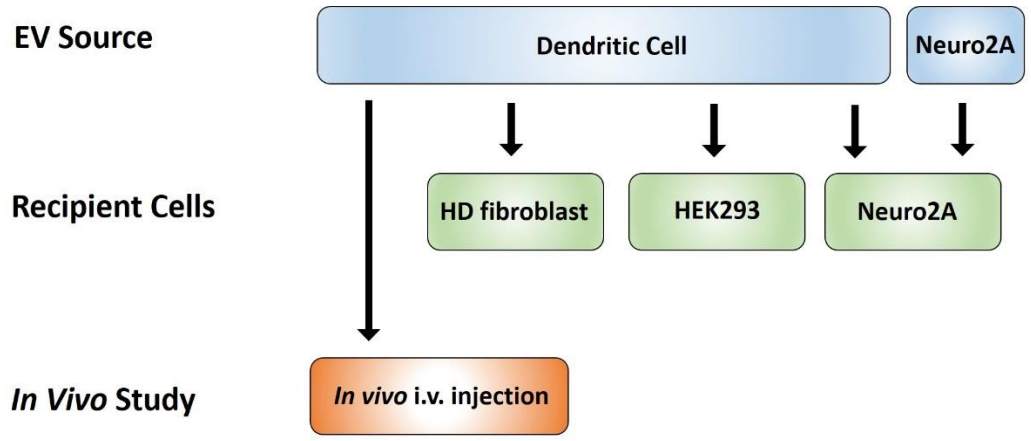


Figure 5.1 Schematic of Experimental Plan to Test Extracellular Vesicle siRNA Delivery. EVs were isolated from two different source cells – DCs and Neuro2A cells. EVs from DCs were tested on the HD model of patient fibroblasts, a murine neuronal line Neuro2A cells and HEK293 cells. EVs from Neuro2A cells were tested for delivery to Neuro2A cells in case of intrinsic neuronal homing. DC derived EVs were also be injected via the tail vein to test for *in vivo* function as they are not immunogenic.

Bone marrow derived DCs were harvested from the bone marrow of the tibias and femurs of 8-10 week C57/BL6 mice. They were cultured for 4 days, left untransfected for the treatment of fibroblast recipient cells, or for use on neuronal cells they were transfected with the neuronal targeting plasmid Lamp2b-RVG (RVG) or a plasmid with the same vector backbone containing the coding region of Lamp2b but without the targeting ligand, this Lamp2b-empty vector was the control plasmid. RVG is a ligand for a subtype of nicotinic cholinergic receptors. On day 7 the medium was changed to fresh DMEM which was supplemented with 10% EV depleted FBS (EV depletion was performed by ultracentrifugation). On day 8 the conditioned medium was collected for EV isolation.

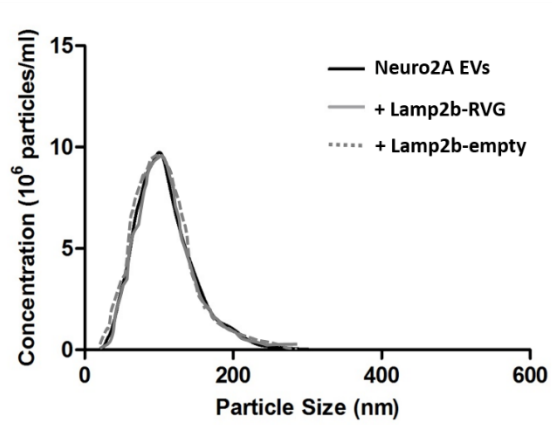
EVs harvested from Neuro2A cells were selected as a neuronal source of EVs in case of any intrinsic homing obtained by the EVs from the parent cells[326]. Neuro2A cells were cultured for 24 hours, transfected with targeting plasmid Lamp2b-RVG (RVG) or the same control plasmid, the vector designed to express Lamp2 but with no targeting ligand "Lamp2b-empty". 4 hours following transfection the medium was changed to OptiMEM and 48 hours later the conditioned medium was removed. EV collection in OptiMEM for 48 hours was chosen here as it was determined by Li *et al.*, as the conditions where Neuro2A cells released the highest yield of EVs[361]. The conditioned medium was collected for EV isolation.

EV isolation was performed in the same way for EVs from both cell types, by differential ultracentrifugation and syringe filtration with 200 nm pores. The pellet was resuspended in PBS and characterised by nanoparticle tracking analysis (NTA) to estimate particle size and concentration of the EVs, and western blot to establish the presence of known EV markers **(Figure 5.2 and 5.3)**.

NTA analysis of bone marrow DCs and Neuro2A cell derived EVs revealed vesicles from all treatment groups had a size and particle count dependent on the cell type from which they originated, but that the size and yield of EVs was unchanged by transfection with the targeting or control plasmids **(Figure 5.2A,B Figure 5.3A,B)**. WB analysis for both DC and Neuro2A derived EVs indicated the presence of the exosomal markers Alix and Tsg101 in the EV populations from untransfected DCs and Neuro2A cells, and those transfected with both control and targeting plasmids, but no calnexin which is present in the cell lysate (CL) samples **(Figure 5.2C, Figure 5.3C)**. The absence of calnexin

staining from EVs derived from both sources indicates a lack of contaminants in all EV samples.

A)



B)

	Neuro2A EVs	+Lamp2b - RVG	+Lamp2b - empty
Mean size (nm) ± SEM	110.61 ± 5.86	111.42 ± 5.69	110.94 ± 7.35
Mode size (nm) ± SEM	99.17 ± 3.52	98.16 ± 3.25	99.53 ± 4.91
Total Particles ($x10^9$) ± SEM	1.78 ± 0.05	1.77 ± 0.04	1.78 ± 0.06

C)

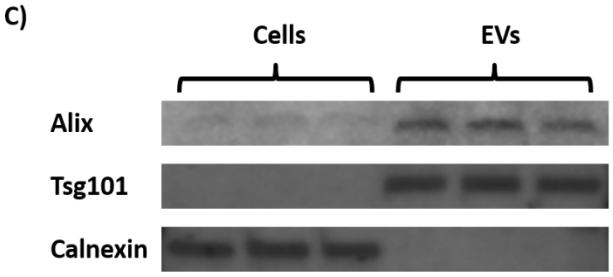
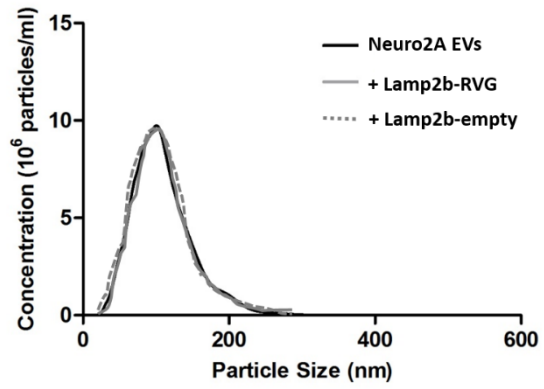


Figure 5.2 Characterisation of Dendritic Cell Derived Extracellular Vesicles. EVs isolated from bone marrow derived DCs following growth in serum depleted medium for 24 hours. They were characterised by nanoparticle tracking analysis (NTA) and western blot. **A)** NTA analysis of size distribution histogram, n = 3. **B)** Table displaying the mean and mode particle size and total number of particles secreted per ml of conditioned medium. **C)** Purified EVs and cell lysates from untransfected, Lamp2b-RVG transfected or Lamp2b-empty transfected cells were loaded on a western blot and probed for the exosomal markers, Alix and Tsg101 and the endoplasmic reticulum marker calnexin.

A)



B)

	Neuro2A EVs	+Lamp2b - RVG	+Lamp2b - empty
Mean size (nm) ± SEM	110.61 ± 5.86	111.42 ± 5.69	110.94 ± 7.35
Mode size (nm) ± SEM	99.17 ± 3.52	98.16 ± 3.25	99.53 ± 4.91
Total Particles ($x10^{12}$) ± SEM	1.78 ± 0.05	1.77 ± 0.04	1.78 ± 0.06

C)

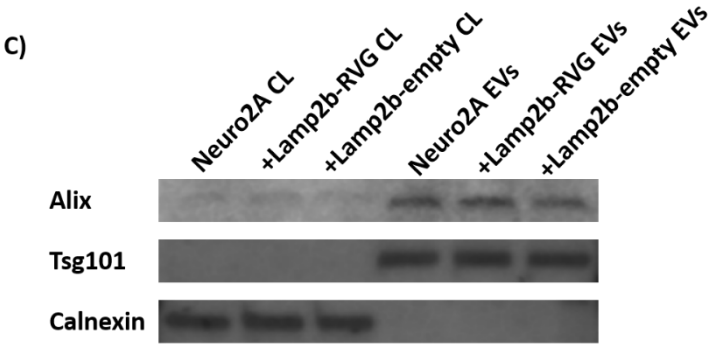


Figure 5.3 Characterisation of Neuro2A Derived Extracellular Vesicles. EVs isolated from Neuro2A cells following growth in serum depleted medium for 48 hours. They were characterised by nanoparticle tracking analysis (NTA) and western blot. **A)** NTA analysis of size distribution histogram, n = 3. **B)** Table displaying the mean and mode particle size and total number of particles secreted from 15cm dish of Neuro2A cells, n = 3. **C)** Purified EVs and cell lysates from untransfected, Lamp2b-RVG transfected or Lamp2b-empty transfected cells were loaded on a western blot and probed for the exosomal markers, Alix and Tsg101 and the endoplasmic reticulum marker calnexin.

5.2.2 Characterisation of siRNA Loading Following Electroporation

Prior to evaluating these characterised EVs for their ability to deliver siRNA *in vitro* and *in vivo*, the efficiency of loading of siRNA into EVs by electroporation was evaluated. It has been reported that loading efficiency varies greatly in spite of optimisation of the experimental parameters of buffer, capacitance and voltage, and previous studies estimate loading efficiencies of between 10 and 55%[213,309,362].

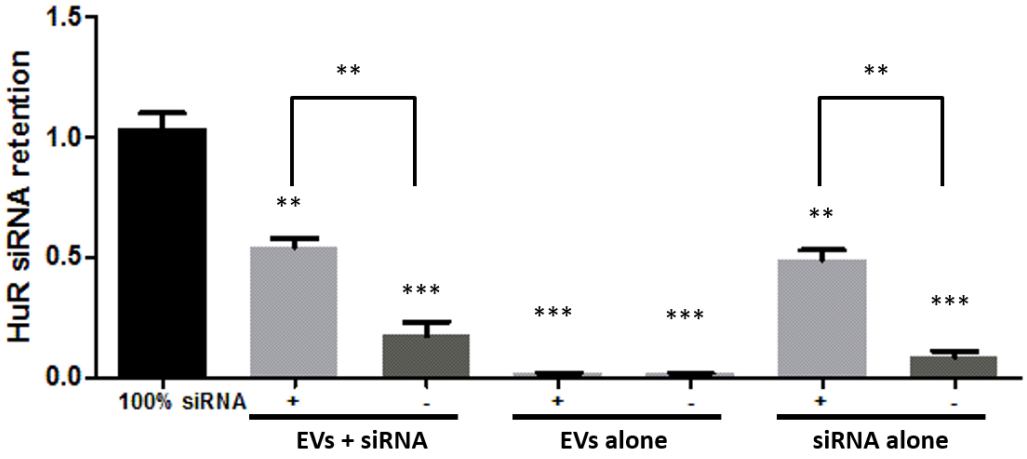
To this end, a fluorescent siRNA directed against a ubiquitously expressed gene was chosen, a Cy3 labelled siRNA against HuR. 6 µg of EVs as estimated by Bradford Protein Assay were mixed with 6 µg of fluorescent siRNA, the ratio used in a previous study for *in vivo* delivery[326]. Samples were included which did not contain EVs, and samples which contained EVs alone, without siRNA. Electroporation at 400 V and 125 µF in electroporation buffer was performed (+) or sampled were left non-electroporated (-). The samples were concentrated by ultracentrifugation and the pellets re-suspended in water to lyse the vesicles. Fluorescence of Cy3 (maximum excitation emission spectrum of 548-570 nm) was measured and compared to a standard curve of dilutions of 100% siRNA, the original quantity of siRNA which had not been loaded or washed by ultracentrifugation. For additional verification of these results, small qPCR was performed on the pellets for the HuR siRNA to determine the quantity of siRNA retained. This was compared to a standard curve of total input siRNA.

Samples containing siRNA and EVs which were electroporated showed siRNA retention of 54.7 and 56.4% as indicated by fluorescence and qPCR respectively. The same samples which had not undergone electroporation retained 21.7% as measured by

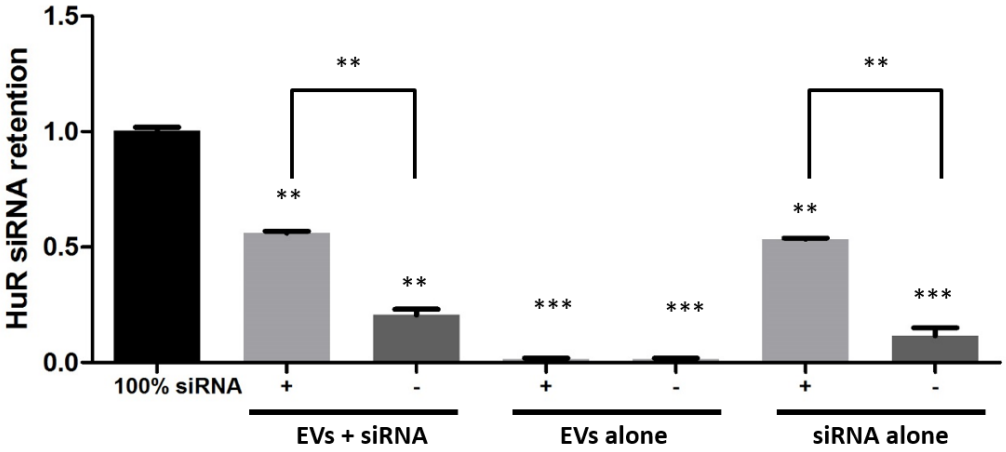
fluorescence and 18.4% as measured by qPCR of the original siRNA **(Figure 5.4A, B)**. Samples which had no siRNA and only EVs displayed no fluorescence but interestingly, samples which contained only siRNA and no EVs and were electroporated retained 49.7 and 53.5% of the original siRNA as indicated by fluorescence and qPCR respectively **(Figure 5.4A, B)**. The same samples containing only siRNA which were not electroporated did not share this retention, with only 9.8 and 12.7% of the original quantity of siRNA retained by fluorescence and qPCR respectively **(Figure 5.4A,B)**.

It was hypothesised that the high level of siRNA retention in samples containing no EVs but which were electroporated could be due to electroporation induced siRNA aggregation. This has been reported by other groups[363]. An EM of gold-labelled siRNA following electroporation shows these aggregates **(Figure 5.4C)**. This siRNA precipitation and aggregation could mask the true level of loaded vesicles in the pellet in electroporated samples containing EVs and siRNA, and in the absence of the control sample with no EVs could lead to overestimation of loading efficiency. This could be responsible for the high levels of loading achieved in previous work[213]. However, in spite of this likely overestimation of loading efficiency, a reduction of Bace1 expression was achieved previously *in vitro* and *in vivo*. In addition, this study verified the use of either small qPCR or fluorescence to quantify siRNA in the pellet as results were similar.

A)


HuR siRNA retention
1.5
1.0
0.5
0.0
**
**
***
***
***
**
**
***
100% siRNA
+
-
+
-
+
-
EVs + siRNA
EVs alone
siRNA alone

B)


HuR siRNA retention
1.5
1.0
0.5
0.0
**
**
**
**
***
***
**
***
100% siRNA
+
-
+
-
+
-
EVs + siRNA
EVs alone
siRNA alone

C)

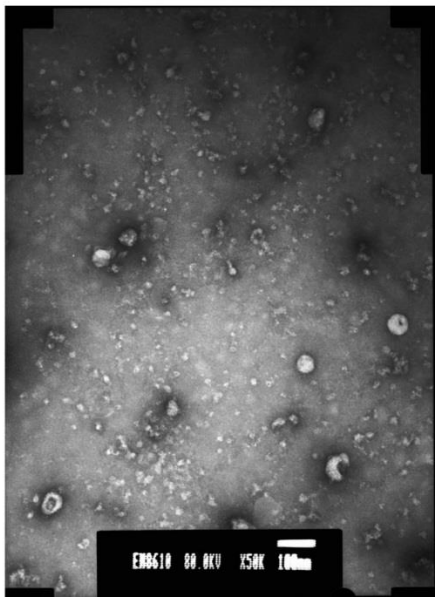

EM8610 80.0KV X50K 100nm

Figure 5.4 Cholesterol Conjugated siRNA Retention Following Electroporation. Neuro2A cell-derived EVs mixed with cc-siRNA, Neuro2A cell-derived EVs alone, or cc-siRNA alone were electroporated (+) or not electroporated (-). Vesicles were concentrated via ultracentrifugation and the percentage of siRNA retained in the pellet was quantified by **A)** fluorescence and **B)** by small qPCR. **C)** EM showing siRNA aggregates in an electroporated sample of siRNA and EVs. EM was performed by Dr. Kariem Ezzat. Values represent mean + SEM. n = 3. Statistical differences were calculated by one-way ANOVA followed by Tukey's post hoc analysis. ***p<0.001, **p<0.01, *p<0.05.

5.2.3 Identification of Optimal *In Vitro* and *In Vivo* Reference Gene

As described in chapter 3, before performing knockdown studies with analysis via qPCR, to decrease variation and obtain accurate results it is necessary to find the optimal reference gene and number of reference genes for normalisation. GeNorm analysis was performed for HD fibroblasts and HEK293 cells in chapter 3. Here, it was used on samples to determine the most stable and therefore optimal reference genes to use for qPCR normalisation *in vitro* in Neuro2A cells and *in vivo*. For this analysis the geNorm Perfect Probe Mouse Kit was used and the qbase$^+$ software determined that for Neuro2A cells the most stable reference genes with lowest geNorm M scores indicating highest stability were *Gapdh* and *Actb* and a combination of their geometric mean was used for optimisation as indicated by the geNorm V score **(Figure 5.5)**. The same result was obtained for *in vivo* samples **(Figure 5.6)**.

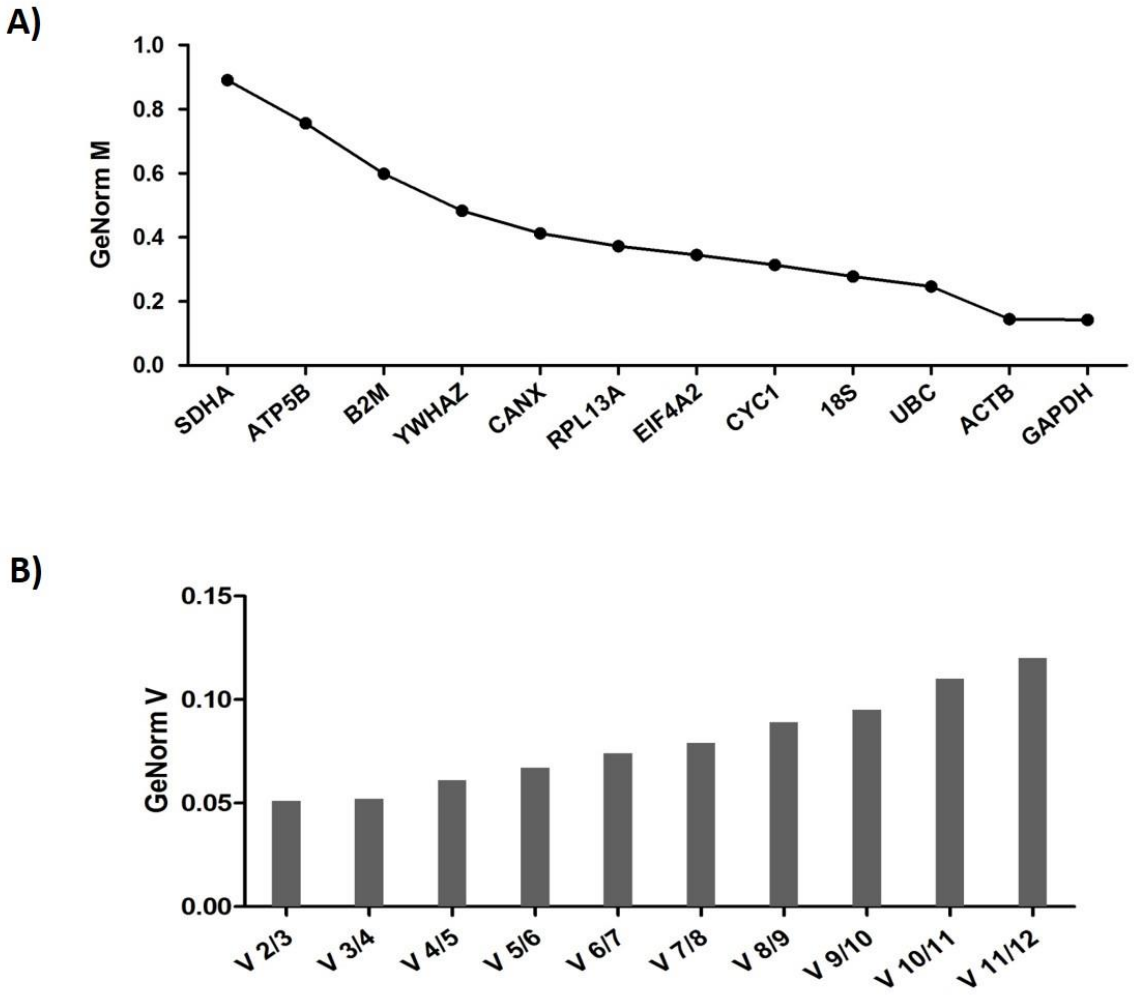


Figure 5.5 Identification of Optimal *In Vitro* Reference Gene for Murine Neuro2A cells. The expression of 12 candidate reference genes was assessed with qPCR using the geNorm Perfect Probe Plus Mouse Kit and qbase^{+} software. **A)** The most stable reference genes were identified via calculation of geNorm M (the average expression stability of a gene or the variation of a gene compared to the other candidate genes) of reference genes at each step during algorithmic step-by-step exclusion of the least stably expressed reference gene. The most stable and therefore optimal pair of reference genes for this study are *Gapdh* and *Actb*, as indicated on the right of the graph with the lowest M. **B)** The optimal number of reference genes for accurate normalisation was assessed by pairwise variation (geNorm V) when V (n/n+1) < 0.15. In this study, a combination of two reference genes (*Gapdh* and *Actb*) was identified as optimal for *in vitro* normalisation in Neuro2A cells.

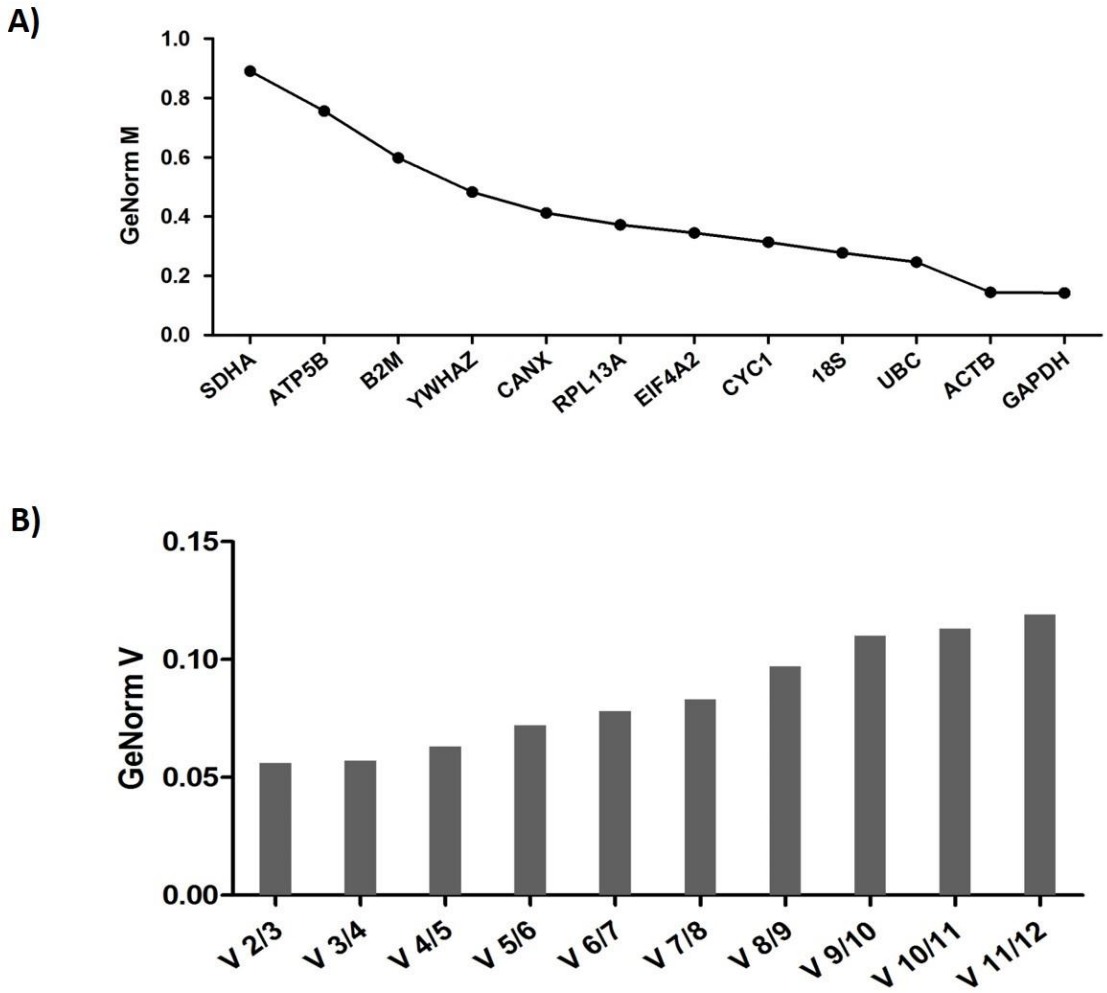


Figure 5.6 Identification of Optimal *In Vivo* Reference Gene. The expression of 12 candidate reference genes was assessed with qPCR using the geNorm Perfect Probe Plus Mouse Kit and qbase^{+} software. **A)** The most stable reference genes were identified via calculation of geNorm M (the average expression stability of a gene or the variation of a gene compared to the other candidate genes) of reference genes at each step during algorithmic step-by-step exclusion of the least stably expressed reference genes. The most stable and therefore optimal pair of reference genes for this study are *Gapdh* and *Actb*, as indicated on the right of the graph with the lowest M. **B)** The optimal number of reference genes for accurate normalisation was assessed by pairwise variation (geNorm V) when V (n/n+1) < 0.15. In this study, a combination of two reference genes (*Gapdh* and *Actb*) was identified as optimal for normalisation *in vivo*.

5.2.4 Dendritic Cell Extracellular Vesicle Delivered siRNA Failed to Silence Huntingtin *In Vitro* in Fibroblasts

The siRNA cargo selected to use with electroporation from chapter 3 was siRNA-5'. Given that previous research had achieved silencing using siRNA loaded EVs by electroporation, despite the likely over-estimation of loading efficiency, this method was used to load DC derived EVs with siRNA-5'. DCs were harvested as described above. The ratios of EVs to siRNA were kept consistent with that of published research for *in vitro* experiments[213]. 6 μg of EVs were mixed with 100 pmoles of siRNA and according to published methods[213], the mixture was electroporated at 400 V and 125 μF in electroporation buffer. To control for the effect of electroporation, control samples were mixed with siRNA in the same way but not electroporated. Following electroporation the electroporated or non-electroporated mixture were washed via ultracentrifugation. The pellet was resuspended in PBS and added to cultured fibroblasts.

No silencing of *HTT* was evident following qPCR analysis 48 hours following treatment with DC EVs loaded with siRNA-5' though the positive control samples, siRNA-5' transfected using Lipofectamine 2000, showed *HTT* knockdown of 80% **(Figure 5.7)**.

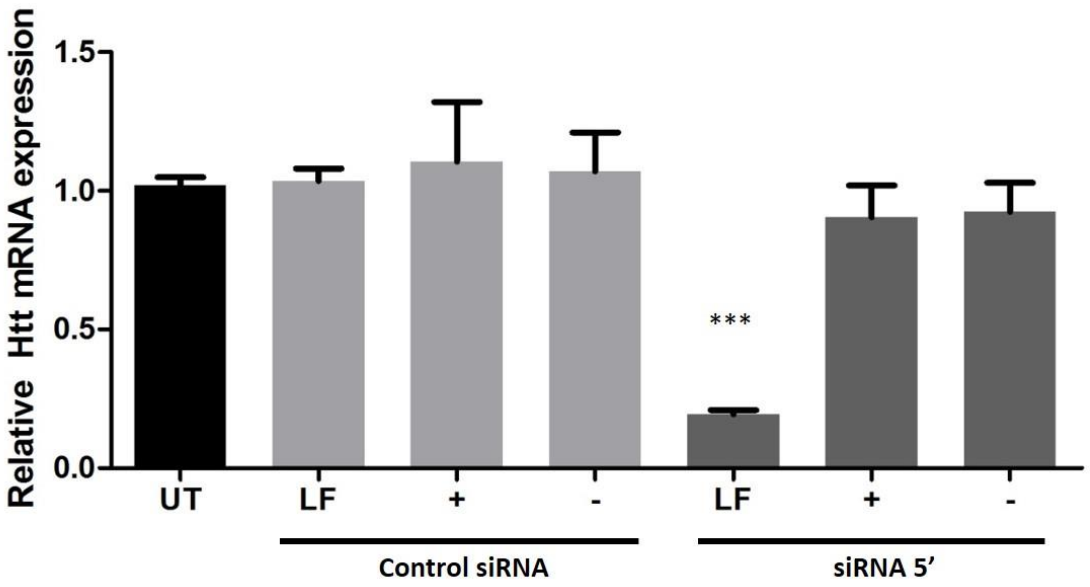


Figure 5.7 Treatment of HD fibroblasts with Dendritic Cell Derived Extracellular Vesicles. *HTT* mRNA expression in HD fibroblasts cells relative to *GAPDH* and *ACTB* was analysed 48 hours after cells were either untreated (UT), transfected with 200 nM control or *HTT* siRNA-5' using Lipofectamine 2000 (LF) or following treatment with 6 µg EVs from DCs, mixed with 100 pmoles (to give a final concentration of 200 nM) control or *HTT* siRNA-5' and unelectroporated (-) or electroporated (+). Values represent mean + SEM. n = 3. Statistical differences were calculated by one-way ANOVA followed by Tukey's post hoc analysis. Statistical significance indicated is compared to control siRNA. ***p<0.001, **p<0.01, *p<0.05.

5.2.5 Dendritic Cell Extracellular Vesicle Delivered siRNA Failed to Silence Huntingtin in Neuro2A cells

It was hypothesised that the neuronal targeting by RVG and neuronal recipient cells Neuro2A cells used in previous work may have been necessary for the successful silencing reported *in vitro* as treatment with an antagonist for the nicotinic acetylcholine receptor attenuated the knockdown of RVG targeted EVs *in vitro*[213]. To test this,

Neuro2A cells were used as the recipient cells, and bone marrow derived DCs were transfected with the targeting plasmid Lamp2b-RVG or control plasmid Lamp2b prior to EV harvesting.

To assess DC derived EV neuronal targeting to Neuro2A cells, DCs were harvested as above, but on day 4 they were transfected with the neuronal targeting vector Lamp2b-RVG, or the control vector Lamp2b-empty which contains the coding region for the Lamp2b protein but no targeting ligand using TransIT-LT1. The medium was changed on day 7 to fresh DMEM supplemented with 10% EV-depleted FCS and 24 hours later EVs were isolated via differential centrifugation. As above, electroporation at 400 V and 125 μF in electroporation buffer was used to load 6 μg of EVs with 100 pmoles of control siRNA or siRNA-5'. The sequence of siRNA-5' targets *Htt* in both human and murine samples. Control samples were mixed with siRNA in the same way but not electroporated. Following electroporation, the electroporated or non-electroporated mixtures were washed via ultracentrifugation. The pellet was resuspended in PBS and added to cultured Neuro2A cells.

No silencing of *Htt* was evident following qPCR analysis 48 hours following treatment with DC EVs loaded with siRNA-5'. The positive control samples, siRNA-5' transfected using Lipofectamine 2000, showed *Htt* knockdown of 76.4% **(Figure 5.8)**.

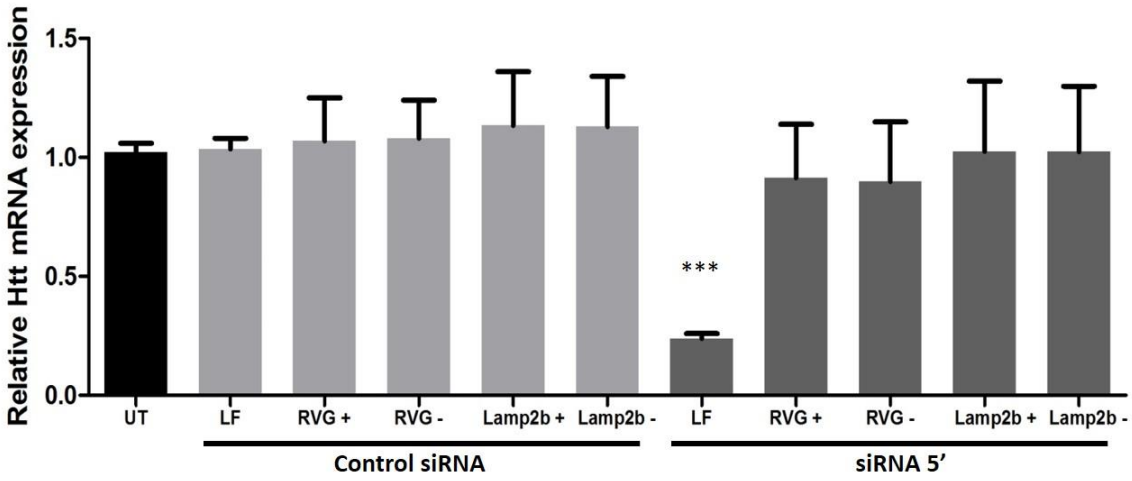


Figure 5.8 Treatment of Neuro2A cells with Dendritic Cell Derived Extracellular Vesicles. *Htt* mRNA expression in Neuro2A cells relative to *Gapdh* and *Actb* was analysed 48 hours following treatment with 6 µg EVs from bone marrow derived DCs which had been transfected with Lamp2b-RVG (RVG) or Lamp2b with no targeting moiety (Lamp2b) and mixed with 100 pmoles (for a final concentration of 200 nM) control or *Htt* siRNA and unelectroporated (-) or electroporated (+). Some cells were left untreated (UT) or had been transfected with 200 nM control or siRNA-5' using Lipofectamine 2000 (LF). Values represent mean + SEM. n = 9. Statistical differences were calculated by one-way ANOVA followed by Tukey's post hoc analysis. Statistical significance indicated is compared to control siRNA. ***$p<0.001$, **$p<0.01$, *$p<0.05$.

5.2.6 Neuro2A cell EV Delivered siRNA Failed to Silence Huntingtin in Neuro2A cells

It was hypothesised that due to their established role in intercellular communication EVs and differences in biodistribution established in chapter 4 between untargeted EVs derived from two different cell sources that EVs may home to particular cell types of

interest. Thus, perhaps EVs derived from Neuro2A cells themselves may be optimal for delivery to Neuro2A cells. Therefore, the experiment was also performed with Neuro2A cells as the source of EVs.

To exploit any potential homing capacity of EVs to their own cell source type, EVs were harvested from Neuro2A cells and used to treat Neuro2A cells. The source cells were transfected with the targeting plasmid; Lamp2b-RVG or the control plasmid; Lamp2b-empty, medium was changed to serum depleted medium and collected after 48 hours for EV isolation via serial ultracentrifugation. Electroporation at 400 V and 125 μF in electroporation buffer was used to load 6 μg of EVs with 100 pmoles of control siRNA or siRNA-5'. Control samples were mixed with siRNA in electroporation buffer in the same manner but not electroporated. Following electroporation, the electroporated or non-electroporated mixtures were washed via ultracentrifugation. The pellet was resuspended in PBS and added to cultured Neuro2A cells.

No silencing of *Htt* was evident in Neuro2A cells following qPCR analysis 48 hours following treatment with Neuro2A EVs loaded with siRNA-5' though the positive control samples, siRNA 5' transfected using Lipofectamine 2000, showed *Htt* knockdown of 77.5% **(Figure 5.9)**.

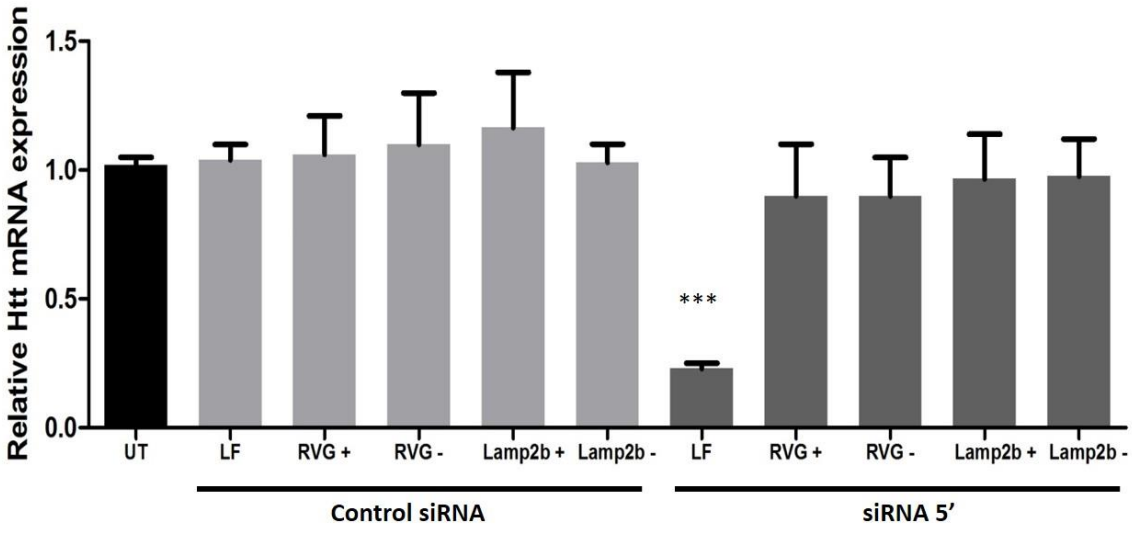


Figure 5.9 Treatment of Neuro2A cells with Neuro2A Cell Derived Extracellular Vesicles. *Htt* mRNA expression in Neuro2A cells relative to *Gapdh* and *Actb* was analysed 48 hours following treatment with EVs from Neuro2A cells transfected with 6 µg Lamp2b-RVG (RVG) or Lamp2b with no targeting moiety (Lamp2b) and mixed with 100 pmoles (for a final concentration of 200 nM) control or *Htt* siRNA and unelectroporated (-) or electroporated (+). Some cells had been left untreated (UT) or transfected with 200 nM control or siRNA-5' using Lipofectamine 2000 (LF). Values represent mean + SEM. n = 9. Statistical differences were calculated by one-way ANOVA followed by Tukey's post hoc analysis. Statistical significance indicated is compared to untreated cells. ***p<0.001, **p<0.01, *p<0.05.

5.2.7 Dendritic Cell EV Delivered siRNA Failed to Silence Huntingtin in HEK293 cells

Since no silencing was achieved with Neuro2A vesicles loaded by electroporation and delivered to Neuro2A cells, an alternate recipient cell type was chosen which is reported as easy to transfect compared to other cell lines and readily takes up particles of the size EVs used in this study (<200 nm), HEK293 cells[329]. As HEK293 cells are not neuronal,

RVG targeting was not used during this study as the EVs should be taken up in the absence of targeting.

To measure the efficiency of *HTT* silencing via EV delivered siRNA in HEK293 cells, EVs were harvested from DCs as described above and 6 μg of EVs was mixed with 100 pmoles of control siRNA or siRNA-5' in electroporation buffer. Samples were electroporated at 400 V and 125 μF or control samples were mixed with siRNA in the same way but not electroporated. Following electroporation, the electroporated or non-electroporated mixture were washed via ultracentrifugation. The pellet was resuspended in PBS and added to cultured HEK293 cells.

No silencing of *HTT* was evident following qPCR analysis 48 hours following treatment with DC EVs loaded by electroporation with siRNA-5' though the positive control samples, siRNA-5' transfected using Lipofectamine 2000, showed *HTT* knockdown of 81.7% **(Figure 5.10)**.

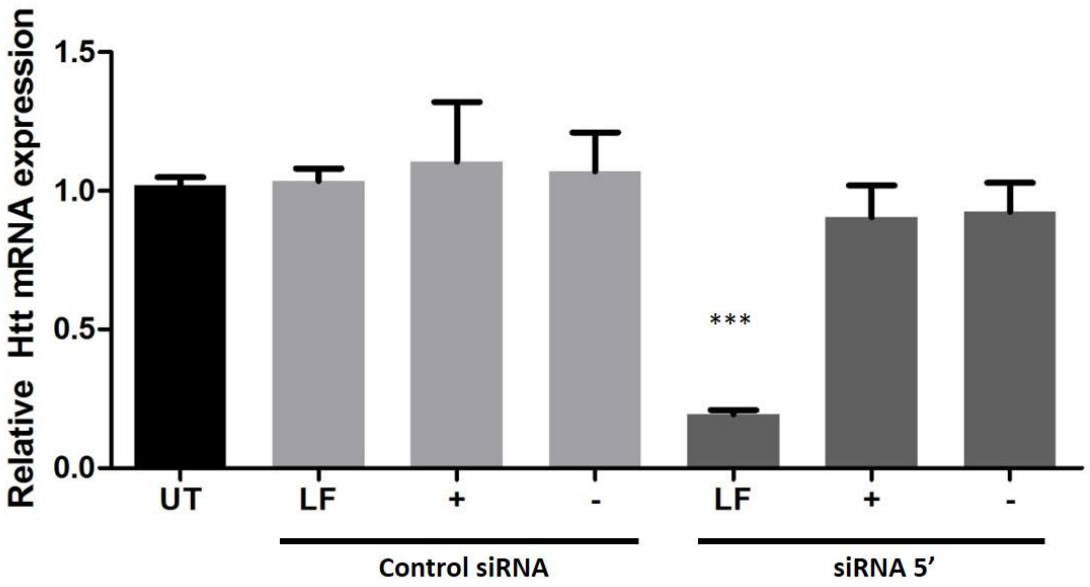


Figure 5.10 Treatment of HEK293 cells with Dendritic Cell Derived Extracellular Vesicles. *HTT* mRNA expression in HEK293 cells relative to *GAPDH* and *ACTB* was analysed 48 hours after cells were either untreated (UT), transfected with 200 nM control or *HTT* siRNA-5' using Lipofectamine 2000 or following treatment with 6µg EVs from bone marrow derived DCs, mixed with 100 pmoles siRNA (for a final concentration of 200 nM) control or *HTT* siRNA and unelectroporated (-) or electroporated (+). Values represent mean + SEM. n = 3. Statistical differences are from one-way ANOVA followed by Tukey's post hoc analysis. ***p<0.001, **p<0.01, *p<0.05.

5.2.8 Dendritic Cell Derived Extracellular Vesicles Failed to Silence Huntingtin *In Vivo*.

In vitro and *in vivo* models have different levels of complexity and in many systems a direct correlation between efficacy does not exist, particularly in the field of siRNA delivery. Often this discrepancy exists in the translation of successful systems from a

simple culture model to complex model animals. Importantly, false negatives also occur where treatments which are effective *in vivo* have shown no efficacy *in vitro*, for example in the field of siRNA delivery by lipid nanoparticles[364]. Within the lab, disparities in the efficacy of EV delivered siRNA *in vitro* and *in vivo* have been observed, the mechanism of which is not yet understood. Due to such disparities and with the aim of evaluating the EV strategy used in previous work for *Bace1* silencing for efficacy in reducing *Htt* expression, an *in vivo* study was performed.

Bone marrow derived DCs were chosen as the cell source for EVs for the *in vivo* study. They had been validated previously and shown to be well tolerated following tail vein injection and they lack immune stimulatory factors such as the lymphocyte stimulatory molecules[328].

The bone marrow DC source cells from C57BL6 mice were transfected with the targeting plasmid; Lamp2b-RVG, shown to increase brain targeting two-fold over EVs from mock transfected cells in chapter 4. Medium was changed to EV depleted medium and collected after 48 hours for EV isolation via serial ultracentrifugation. Electroporation at 400 V and 125 µF in electroporation buffer was used to load (per mouse) 150 µg of EVs with 150 µg of control siRNA or siRNA targeting a region upstream of the CAG triplet repeat in HD, siRNA-5'. Control samples were mixed with siRNA in electroporation buffer in the same manner but not electroporated. Following electroporation, the electroporated or non-electroporated mixtures were washed via ultracentrifugation. The pellets were resuspended in 80 µl of 5% glucose and injected via the tail vein into C57BL6 mice. Naked siRNA in 5% glucose was used as a control.

In contrast to previously published results[213], no significant knockdown was detected in any organ following intravenous delivery of EV loaded siRNA, but a trend towards a reduction in *Htt* mRNA expression in the cortex, striatum and muscle was observed **(Figure 5.11)**.

Due to the failure to obtain silencing of *Htt in vitro* and *in vivo* another method of loading was pursued. It is also worth noting the high level of variation in results following electroporation, indicated by the large error bars in Figure 5.7 to 5.11 even with a large sample size in some experiments.

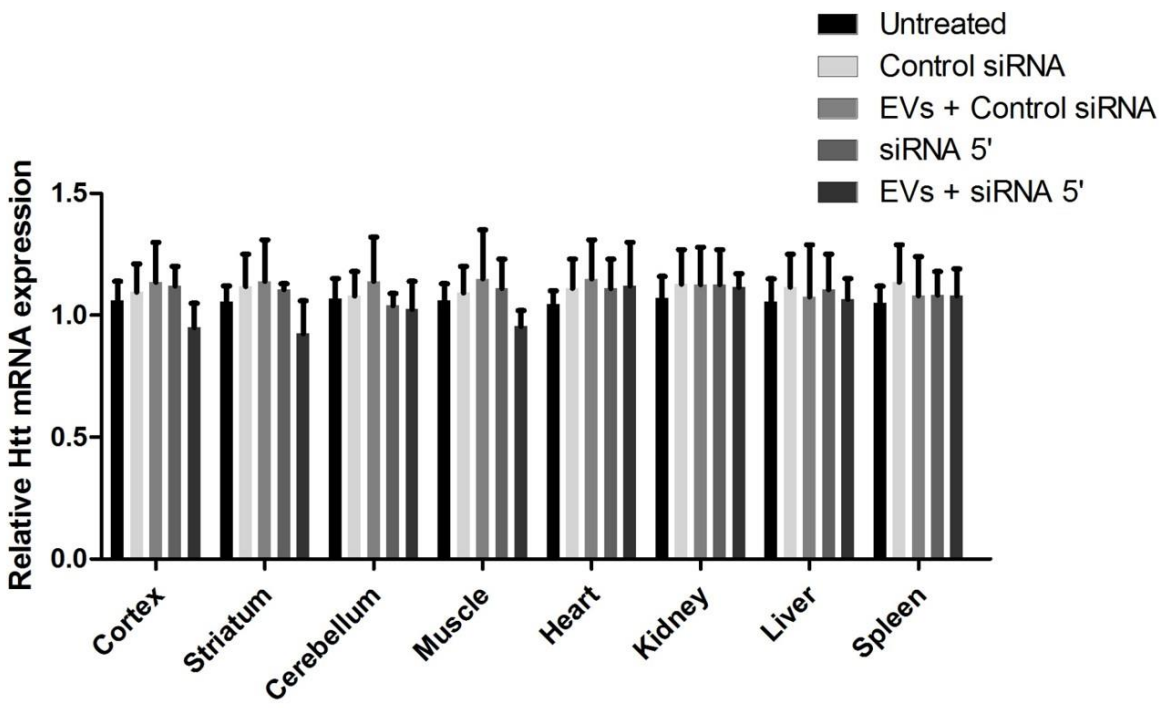


Figure 5.11 *In Vivo* Delivery of siRNA by RVG Targeted DC Derived EVs Loaded via Electroporation. 150 µg of EVs from bone marrow DCs which had been transfected with Lamp2b-RVG and electroporated with 150 µg control siRNA or siRNA-5' were injected into the tail vein of mice. 150 µg of naked control siRNA and siRNA-5' were also injected intravenously. Following 48 hours the organs were harvested and *Htt* expression relative to *Gapdh* and *Actb* was measured. n = 3. Values represent mean + SEM. Statistical analysis by one-way ANOVA did not show any significant differences between treatment groups.

5.2.9 Validation of Cholesterol Conjugated siRNA

Due to the electroporation induced aggregation which can obscure and lead to overestimation of the level of loading by electroporation, and the failure to obtain replicable knockdown *in vitro* or *in vivo* using this loading technique, an alternative method of loading was pursued. Cholesterol conjugated siRNA has been utilised *in vitro*

and *in vivo* for non-toxic effective knockdown of genes of interest. In addition, it has been encapsulated in nanoparticles such as cationic liposomes with an estimated encapsulation efficiency of 80%[365].

It was hypothesised that the lipid conjugation may compensate for, and help to overcome, the electrostatic repulsion between negatively charged siRNA and negatively charged EVs and thus facilitate loading of the siRNA. To test this, a cholesterol conjugated siRNA directed against a ubiquitously expressed mRNA binding protein *HuR* was selected to optimise loading of siRNA into EVs. For the purposes of this study *HuR* was an appropriate target gene as it was expressed at high levels to easily facilitate detection of knockdown. It is an mRNA binding protein and a potential drug target to reduce tumour growth[366].

The *HuR* TEG cholesterol conjugated siRNA (cc-siRNA) was fluorescently labelled with cy3 to monitor loading, modified for stability with 2'-Flouro Us and Cs, phosphorothioate overhangs, and was validated for knockdown efficiency *in vitro* in HEK293 cells via transfection at doses from 12.5 to 200 nM with Lipofectamine 2000. High levels of silencing were achieved, *HuR* expression was reduced to just 16.53% at 200 nM and this silencing was long lasting **(Figure 5.12A,B)**.

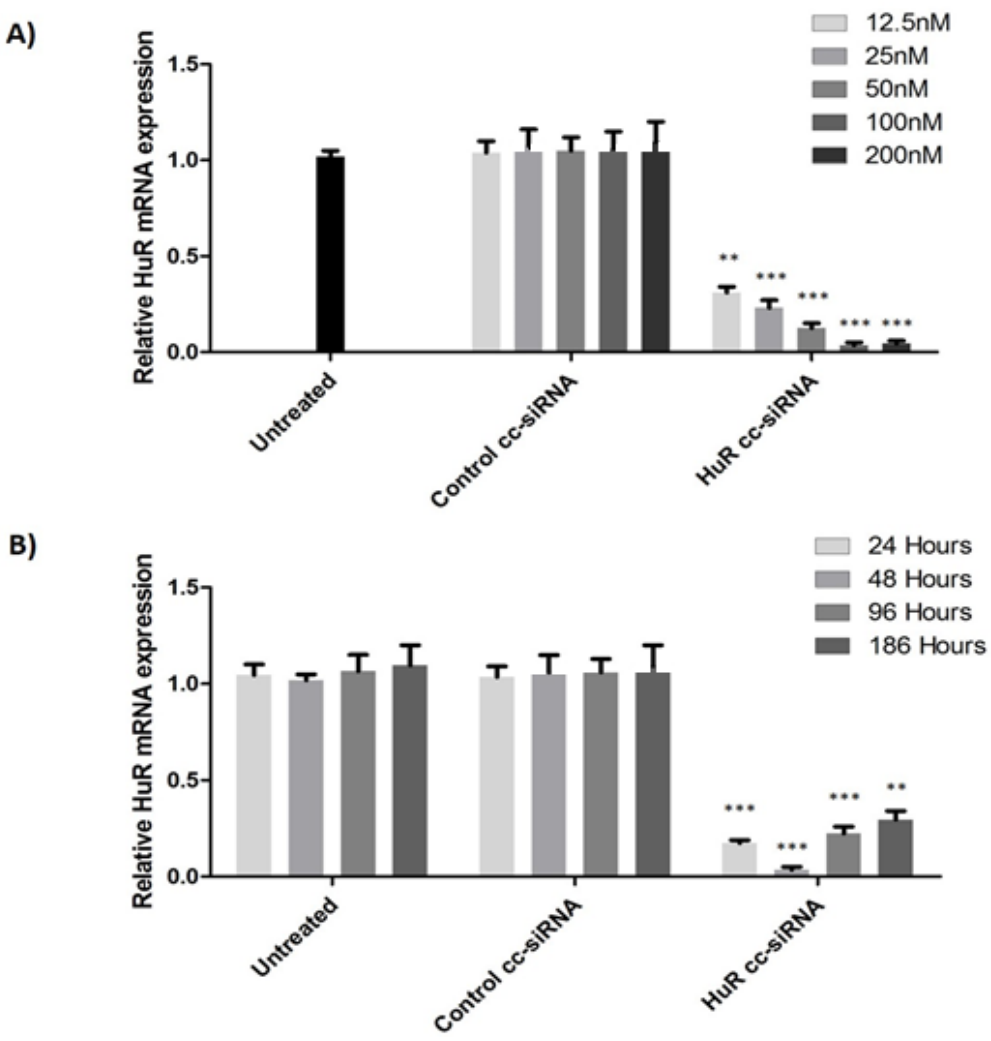


Figure 5.12 Validation of Cholesterol Conjugated siRNA. HEK293 cells were left untreated, transfected with a negative control cc-siRNA or transfected with a cc-siRNA targeted against *HuR* at different doses (A), and at the same dose following different lengths of time post-transfection (B). Graphs indicate the resultant relative *HuR* mRNA levels assessed by qPCR normalised to housekeeping genes *GAPDH* and *ACTB.* **A)** Dose response showing relative *HuR* mRNA measured 48 hours after transfection with 12.5, 25, 50, 100 and 200 nM siRNA. **B)** Duration of silencing following transfection with 100 nM of siRNA. Values represent mean + SEM. n = 3. Statistical differences were calculated by one-way ANOVA followed by Tukey's post hoc analysis. Significance indicated is compared to control siRNA. ***p<0.001, **p<0.01, *p<0.05.

5.2.10 Cells Transfected with Cholesterol Conjugated siRNA will Secrete siRNA

To evaluate loading the source cell as a means of generating cc-siRNA loaded EVs, HEK293 cells were transfected with the HuR cc-siRNA using Lipofectamine 2000. Post-transfection cells were washed with PBS and the medium replaced to remove Lipofectamine-ccsiRNA complexes remaining in the medium. The medium was then removed at time points from 30 minutes to 72 hours and the fluorescence of the medium was measured and compared with a standard curve of cc-siRNA in the same volume of medium **(Figure 5.13)**.

Fluorescent cc-siRNA was present in the culture medium. Highest levels were recorded at 24 hours post-transfection, with a decrease in fluorescence recorded after 48 hours **(Figure 5.13)**. This decrease could be as a result of less secretion or increased uptake and recycling at this time. It is not known whether the secreted cc-siRNA is vesicular but importantly using this method of loading it is impossible to eliminate any transfection reagent which may have been taken up and internalised when the medium was replaced and later secreted. Therefore, this method was not pursued further.

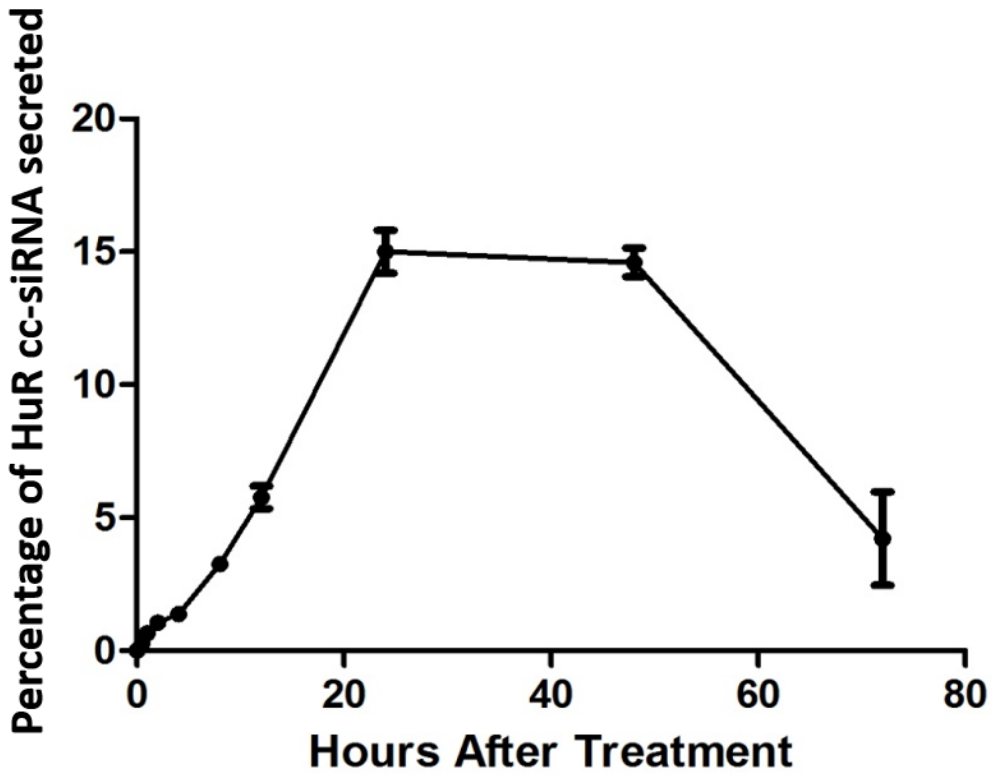


Figure 5.13 Levels of Fluorescent cc-siRNA Secreted in Cell Culture Medium. HEK293 cells were treated with 1 µg HuR cc-siRNA. Cells were washed and the medium replaced. Medium was then taken at time points from 30 minutes to 72 hours following treatment and the fluorescence of the medium was measured and compared to 100% cc-siRNA. Values represent mean ± SEM, n = 3.

5.2.11 Quantification of Loading of Cholesterol Conjugated siRNA Following Electroporation

To evaluate whether the lipid conjugation of an siRNA could help to increase loading with electroporation EVs isolated from Neuro2A cells by differential ultracentrifugation were mixed with cc-siRNA. Neuro2A cells were chosen as the source of EVs because they produce a large amount of EVs, ideal for optimisation studies. The mixtures were either electroporated at 400 V and 125 μF in electroporation buffer or not electroporated **(Figure 5.14)**. The mixtures were then washed by ultracentrifugation, the pellets resuspended in PBS and fluorescence in the pellet was measured and compared to the fluorescence of the total original volume of cc-siRNA in PBS **(Figure 5.14)**.

In the presence of both EVs and cc-siRNA, but regardless of whether or not the samples were electroporated, there was a high (65%) retention of siRNA in the pellet **(Figure 5.14)**. Samples with EVs alone showed negligible levels of fluorescence and in samples with siRNA alone there was, as for non-cholesterol conjugated siRNA, a significant difference between samples which had and had not undergone electroporation. In the electroporated samples 52.4% of the original quantity of siRNA was retained in the pellet as measured by fluorescence, but for the samples which had not been electroporated just 11.9% remained.

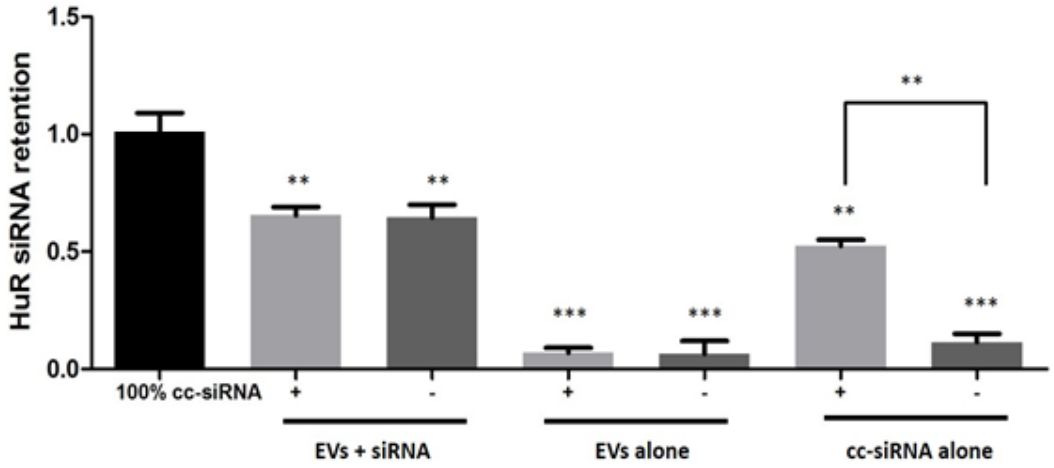


Figure 5.14 Cholesterol Conjugated siRNA Retention Following Electroporation. Neuro2A cell-derived EVs mixed with cc-siRNA, Neuro2A cell-derived EVs alone, or cc-siRNA alone were electroporated (+) or not electroporated (-). Vesicles were concentrated via ultracentrifugation and the percentage of siRNA retained in the pellet was quantified by fluorescence and compared to that of a standard curve of cc-siRNA. Values represent mean + SEM, n = 3. Statistical differences were calculated by one-way ANOVA followed by Tukey's post hoc analysis. Statistical differences, except where indicated by the comparison bar, are compared with 100% siRNA. ***$p<0.001$, **$p<0.01$, *$p<0.05$.

5.2.12 Loading by Mixing Extracellular Vesicles with Cholesterol Conjugated siRNA can Generate Knockdown *In Vitro*

Since it was established that the cc-siRNA associated with EVs in the pellet, EVs mixed with cc-siRNA were analysed for their knockdown capacity. EVs were isolated from Neuro2A cells via differential ultracentrifugation. They were then mixed with the cc-

siRNA in two doses of cc-siRNA, a high dose of 10 µg EVs:10 µg cc-siRNA, or a low dose of 10 µg EVs:1 µg of cc-siRNA. Mixing was performed at room temperature for 30 minutes in 100 µl. After mixing the cc-siRNA targeted against *HuR* or a control siRNA, samples were electroporated or not electroporated, washed by ultracentrifugation and added to cultured HEK293 cells. A positive control of Lipofectamine 2000 transfection was included. 48 hours later *HuR* expression relative to *GAPDH* and *ACTB* was measured **(Figure 5.15)**.

Interestingly, although there was more siRNA per well, in the study with the high dose (1:1 ratio w/w of EVs:siRNA) there were no significant results and a high amount of variation between samples. In the low dose study (10:1 w/w ratio of EVs:cc-siRNA) in the samples which were treated with the mixture which had not been electroporated, but not for the electroporated sample, there was a small but significant reduction in *HuR* expression of 7.5% **(Figure 5.15)**. Although with a larger sample size this effect could potentially be significant for the electroporated sample, it is clear that electroporation is not necessary for the silencing effect. Thus, electroporation was not pursued for further work with cc-siRNA. This study indicated that a large amount of EVs in the mixture may increase silencing capacity of EVs mixed with cc-siRNA and that this protocol has potential for optimisation to increase silencing efficiency by varying the mixing conditions of ratio, temperature, volume and time.

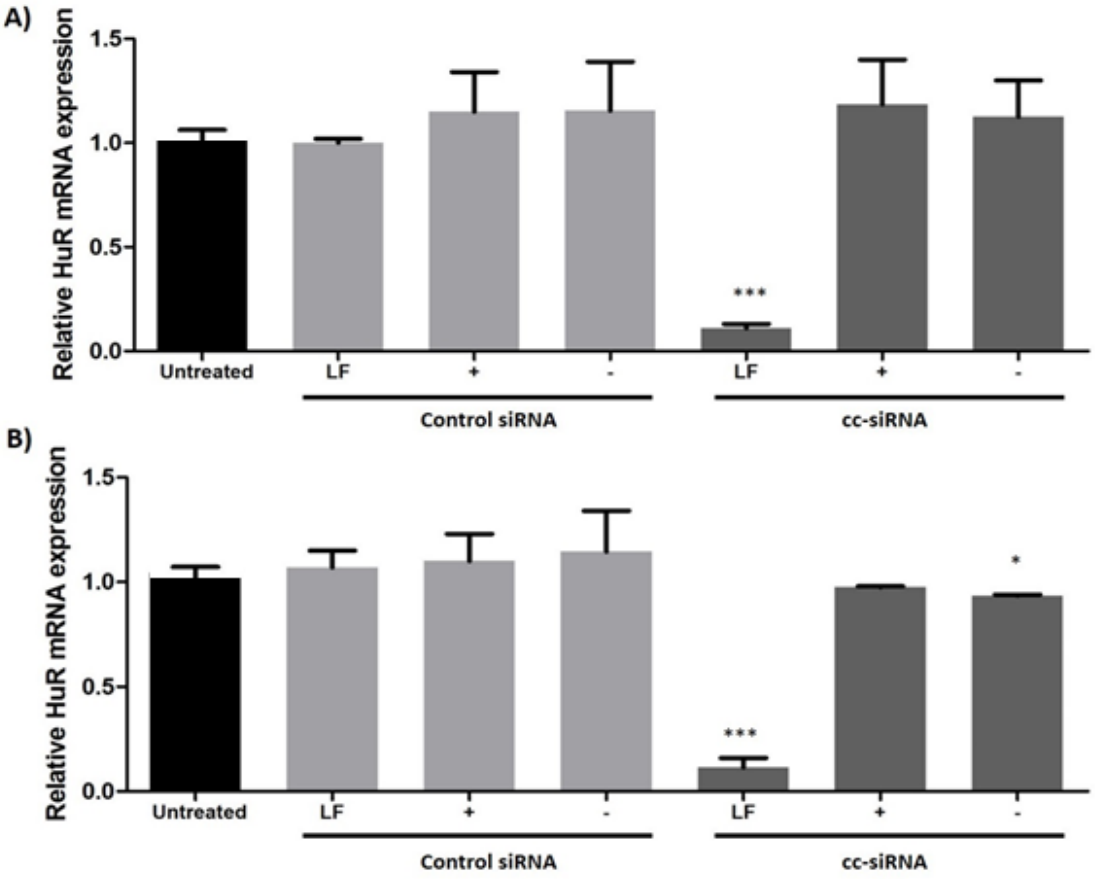


Figure 5.15 Treatment of HEK293 cells with Neuro2A-derived Extracellular Vesicles Mixed with Cholesterol Conjugated siRNA. HEK293 cells were treated with EVs isolated from Neuro2A cells and mixed with cc-siRNA. *HuR* expression relative to *GAPDH* and *ACTB* were measured 48 hours post-treatment with high and low dose EVs mixed with control or HuR cc-siRNA electroporated (+) or not electroporated (-) or transfection with control siRNA or HuR cc-siRNA. A positive control of Lipofectamine 2000 transfected cc-siRNA was included (LF). **A)** EVs were mixed with siRNA in a high dose (10 µg exosomes: 10 µg siRNA) per well. **B)** EVs were mixed with siRNA in a low dose (10 µg exosomes: 1 µg siRNA) per well. Values represent mean + SEM. n = 3. Statistical differences were calculated by one-way ANOVA followed by Tukey's post hoc analysis. Statistical differences indicated are compared with negative control. ***p<0.001, **p<0.01, *p<0.05.

5.2.13 Optimisation of Loading by Mixing by Varying the Ratio of Extracellular Vesicles to Cholesterol Conjugated siRNA

From the above result it was clear that the ratio of EVs to cc-siRNA had an effect on knockdown capacity as a smaller quantity of cc-siRNA had the effect of a slight reduction in HuR expression when associated with EVs but a larger quantity did not, when the amount of EVs (as estimated by weight via Bradford assay) was kept constant **(Figure 5.14)**. To look into this further to optimise the ratio, EVs were isolated from Neuro2A cells via differential ultracentrifugation and a number of different ratios of EVs to cc-siRNA were mixed. The ratios tested were (in terms of 1EV: number of cc-siRNA molecules) EV:cc-siRNA 1:15, 1:30, 1:150, 1:300 and 1:500. A sample with no EVs was also included. All other conditions were kept constant at room temperature in a 100 µl reaction volume with 30 minute incubation time. After the incubation the samples were concentrated by ultracentrifugation and the fluorescence in the pellet measured in comparison to a standard curve of the total original siRNA volume used **(Figure 5.16)**.

In line with the preliminary knockdown study where increased silencing was seen when less siRNA was mixed with a constant quantity of EVs, the higher the ratio of EVs:cc-siRNA the higher the siRNA retention in the pellet as measured by fluorescence. The highest ratio, 1 EV to every 15 cc-siRNA molecules yielded the highest result, with 73.5% of the original quantity of siRNA retained **(Figure 5.16)**. For a ratio of 1 EV:30 cc-siRNA molecules the retention was 60.2% and dropped to 22.3% when there were 150 molecules of cc-siRNA for every EV, and just 11.2% when there were 1,500 cc-siRNA molecules per EV. These mixtures were performed at a constant volume and the electrostatic interactions between the cc-siRNA molecules could explain these

differences. Also, considering the small size of the EVs investigated here with diameters under 200 nm (due to the use of a 200 nm filter in the EV isolation process) not many cc-siRNA molecules would fit per vesicle.

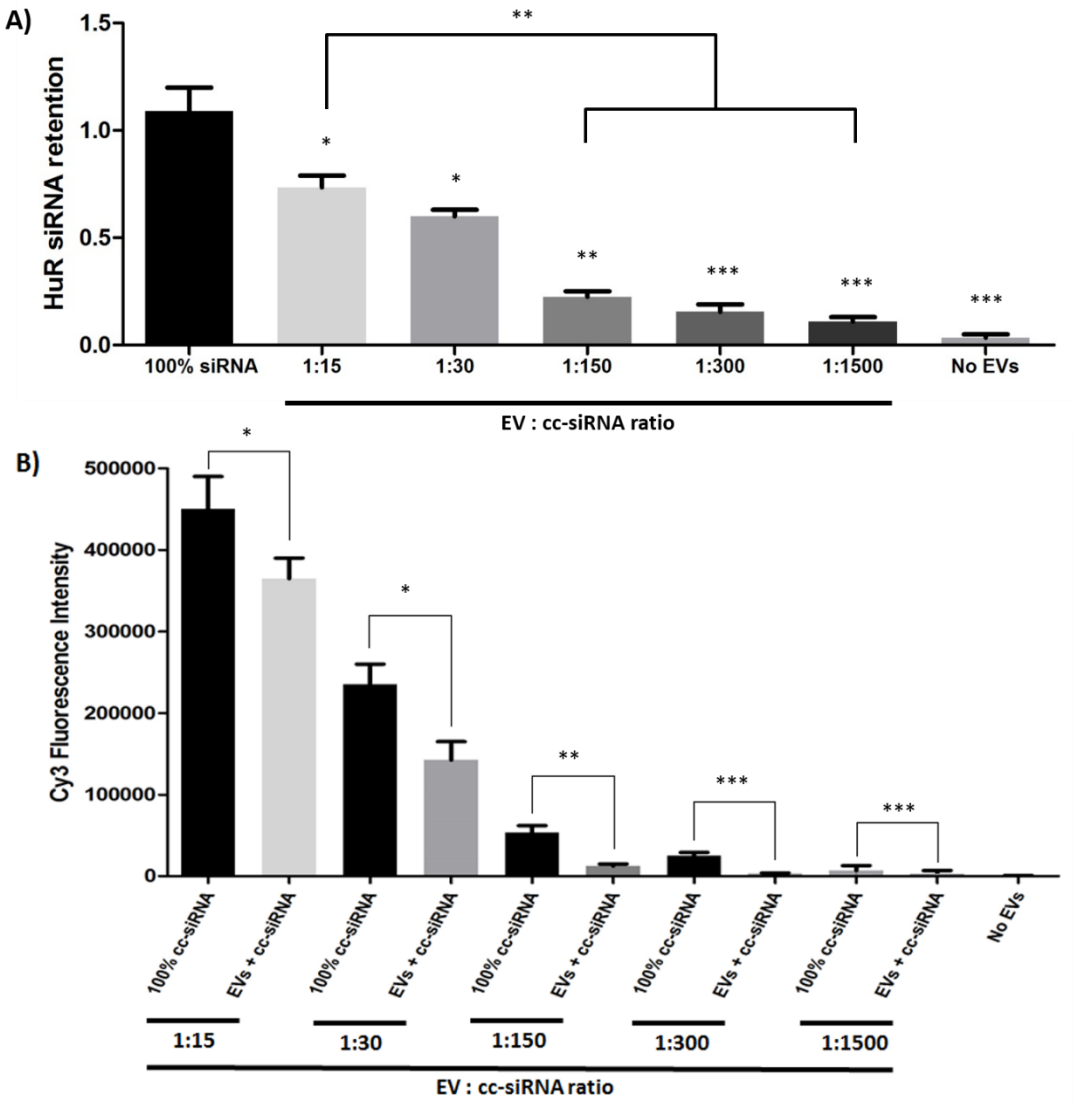


Figure 5.16 siRNA Retention in Pellet with Varying Extracellular Vesicle: Cholesterol Conjugated siRNA Ratio. EVs from Neuro2A cells were mixed with fluorescent cc-siRNA in the ratios 1:15, 1:30, 1:150, 1:300 and 1:1500. Samples were incubated at room temperature for 30 minutes and concentrated by ultracentrifugation. **A)** The percentage of fluorescence retained in the pellet was plotted against that of a standard curve of the original quantity of cc-siRNA as measured by fluorescence. **B)** An alternative representation of the data in absolute values indicating the mean fluorescence intensity of each sample compared to the fluorescent intensity of the total cc-siRNA used. Values represent mean + SEM, n = 3. Statistical differences were calculated by one-way ANOVA followed by Tukey's post hoc analysis. Statistical differences, other than where indicated by comparison bars, are compared with 100% cc-siRNA. ***$p<0.001$, **$p<0.01$, *$p<0.05$.

5.2.14 Optimisation of Loading by Mixing by Varying Incubation Temperature

EVs isolated by differential centrifugation from Neuro2A cells were mixed with a constant amount of cc-siRNA at a ratio of 1 EV:30 molecules of cc-siRNA, in 100 µl for 30 minutes at varying temperatures of 4 °C, room temperature (22 °C), 37 °C and 42 °C, with the hypothesis that increasing temperature and thus the fluidity of the membrane might increase the influence of the lipophilic cholesterol tag on the cc-siRNA and increase association between EVs and cc-siRNA. Temperatures above 42 °C were not tested as the integrity of the membrane would be at risk at high temperatures. This was performed both in the presence and absence of EVs to control for the possibility that increasing the temperature may increase the likelihood of the cc-siRNA forming micelles that might precipitate with the EVs in the pellet. The quantity of cc-siRNA retained in the pellet compared to the original volume of cc-siRNA used was compared after ultracentrifugation and re-suspension of the pellet in PBS **(Figure 5.17)**.

Mixing at 4 °C resulted in a low level (11.7%) of cc-siRNA retention in the pellet indicating low levels of incorporation of cc-siRNA into the vesicles. This was expected as at 4 °C the membrane would be less fluid. There was a significant increase to 60.3% in the amount of cc-siRNA retained in the pellet when the incubation temperature was increased to 22 °C. A 37 °C incubation resulted in 65.8% of the cc-siRNA being pelleted and at 42 °C, 75.4% of the original quantity of cc-siRNA was retained in the pellet **(Figure 5.17)**. In each case, there were only low amounts (3-9%) of cc-siRNA retained in the pellet in the absence of EVs indicating a low relevance of cc-siRNA micelles in the quantity of cc-siRNA in the pellets of the samples containing EVs. At low

temperatures the membrane is less fluid so less cc-siRNA would be expected to associate with EVs. 37 °C was selected as the optimal temperature for future work as biological membranes of the cells investigated here are not designed to withstand temperatures as high as 42 °C so although a more favourable integration of cc-siRNA with EVs seemed to be achieved at 42 °C it was decided not to use this temperature. Interestingly, the cholesterol itself on the cc-siRNA may render the phospholipid bilayer more resilient to the heat stress because of its comparatively rigid 4-ring structure compared to other lipids in the membrane, if incorporated into the membrane rather than the cc-siRNA being internalised and encapsulated[367,368]. If this is the case, the integration of cholesterol in the membrane could itself become a limiting factor of association between the EVs and the cc-siRNA by decreasing membrane fluidity.

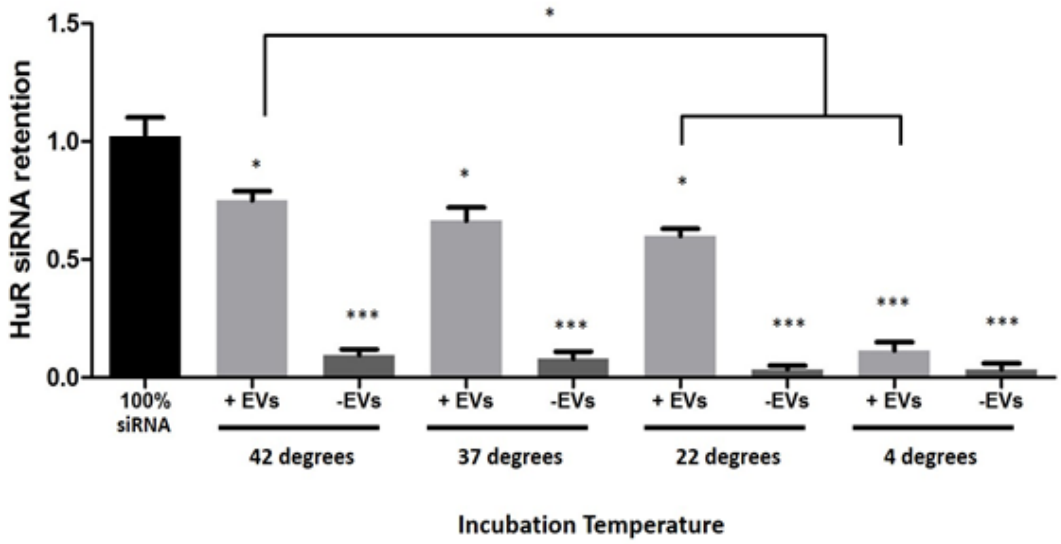


Figure 5.17 siRNA Retention in Pellet Following Mixing of EVs with Cholesterol Conjugated siRNA with Varying Incubation Temperature. EVs from Neuro2A cells were mixed with fluorescent cc-siRNA at a ratio of 1:30 at incubation temperatures of 42, 37, 22 and 4 °C for 30 minutes. Samples were concentrated by ultracentrifugation. The percentage of fluorescence retained in the pellet in samples with (+EVs) and without (-EVs) EVs was compared to that of a standard curve of 100% siRNA and plotted against that or the original quantity of cc-siRNA used as measured by fluorescence. Values represent mean + SEM. n = 3. Statistical differences were calculated by one-way ANOVA followed by Tukey's post hoc analysis. Statistical differences indicated are compared with 100% cc-siRNA. ***$p<0.001$, **$p<0.01$, *$p<0.05$.

5.2.15 Optimisation of Loading by Mixing by Varying Incubation Time

The incubation time of Neuro2A derived EVs mixed with cc-siRNA was then varied while maintaining constant ratio of 1 EV:30 cc-siRNA molecules, in 100 µl at 37 °C. The incubation times tested were 30 minutes, 1 hour, 2 hours, 3 hours and 5 hours. The mixtures were pelleted by ultracentrifugation following the incubation which was

performed in the presence and absence of EVs in case the longer incubation time disposed the cc-siRNA into forming micelles which could lead to over-estimation of the quantity of cc-siRNA associated with EVs in the pellet. The quantity of cc-siRNA retained in the pellet was measured by fluorescence and compared to that of a standard curve the original quantity used **(Figure 5.18)**.

In all samples there was a high level of siRNA retained in the pellet **(Figure 5.18)**. This was lowest (54.2%) for a 30 minute incubation time but increased to 75.3% for a 1 hour incubation time. There was no further increase in siRNA retention with increasing incubation time, though there was an increase in variability with a 5 hour incubation time. Similar to the result from figure 5.16, there was negligible signal from the samples without EVs indicating that formation of micelles were not the reason for the high level of siRNA retention in the pellet. 1 hour was selected as the optimal incubation time as there was no further increase in siRNA retention in the pellet following this time point.

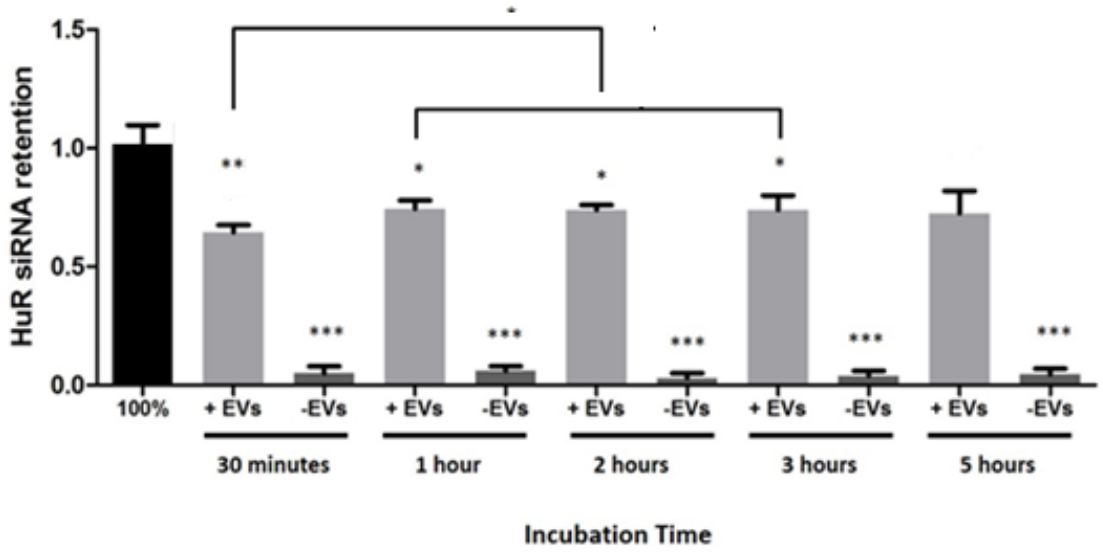


Figure 5.18 siRNA Retention in Pellet Following Mixing of EVs with Cholesterol Conjugated siRNA with Varying Incubation Time. EVs from Neuro2A cells were mixed with fluorescent cc-siRNA at a ratio of 1:30 at incubation temperatures of 37 °C for 30 minutes,1 hour, 2 hours, 3 hours or 5 hours. Samples were concentrated by ultracentrifugation. The percentage of fluorescence retained in the pellet in samples with (+EVs) and without (-EVs) EVs was compared to a standard curve of the original quantity of cc-siRNA used as measured by fluorescence and plotted against 100% cc-siRNA. Values represent mean + SEM. n = 3. Statistical differences were calculated by one-way ANOVA followed by Tukey's post hoc analysis. Statistical differences, except where indicated by comparison bars, are compared to 100% cc-siRNA. ***$p<0.001$, **$p<0.01$, *$p<0.05$.

5.2.16 Optimisation of Loading by Mixing by Varying Incubation Volume

EVs were isolated from Neuro2A cells and mixed with cc-siRNA at a ratio of 1 EV:30 cc-siRNA molecules, at 37 °C, for 1 hour at varying incubation volumes of 10, 20, 50, 100 and 500 µl. Following the incubation, the samples were concentrated via ultracentrifugation to pellet the EVs and any associated cc-siRNA. As with the

optimisation study for incubation time and temperature, this was performed in the presence and absence of EVs to test for the presence of micelles. The quantity of cc-siRNA retained in the pellet was estimated by comparing the fluorescence to that of the original quantity of cc-siRNA used **(Figure 5.19)**.

For each volume tested up to 100 µl there was a stepwise increase in cc-siRNA retention in the pellet as measured by fluorescence **(Figure 5.19)**. In 10 µl 32.8% of the cc-siRNA was pelleted, in 20 µl this increased to 42.1%, at 50 µl 56.7% and in 100 µl 73.5% of the original quantity of cc-siRNA was in the pellet as measured by fluorescence. This decreased to 28.8% with an incubation volume of 500 µl. The electrostatic repulsion between the cc-siRNA and the EVs may be exaggerated in a small volume, but in a large volume the space between the cc-siRNAs and EVs may be a limiting factor. For each volume, there were only low levels of fluorescence in the samples with no EVs, showing that micelles in the pellet are not responsible for the high levels of cc-siRNA retention. As the highest level of siRNA retention was recorded following the use of an incubation volume of 100 µl, it was selected as the optimal incubation volume for further study.

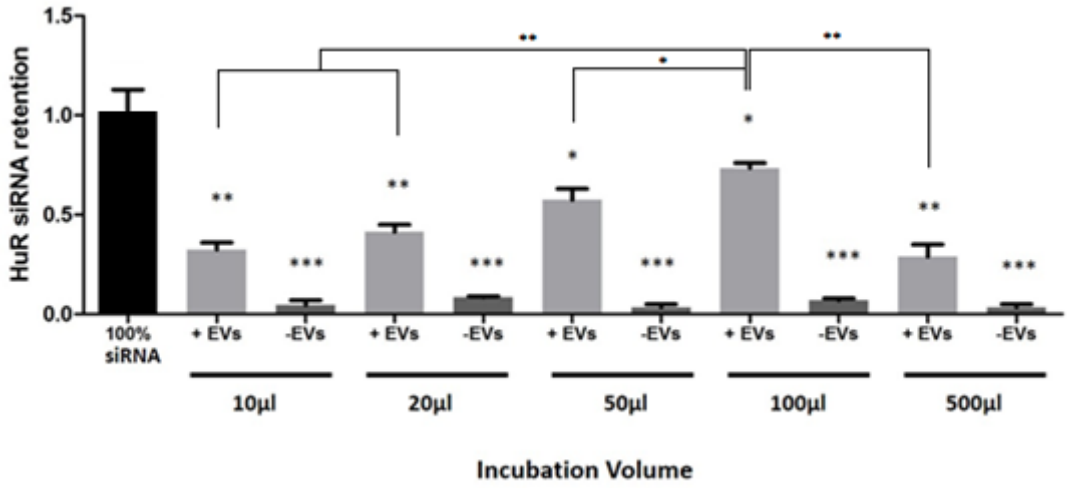


Figure 5.19 siRNA Retention in Pellet Following Mixing of EVs with Cholesterol Conjugated siRNA with Varying Incubation Volume. EVs from Neuro2A cells were mixed with fluorescent cc-siRNA at a ratio of 1:30 at incubation temperatures of 37 °C for 1 hour in volumes of 10, 20, 50, 100 and 500 µl in the presence of EVs (+EVs) or absence of EVs (-EVs). Samples were concentrated by ultracentrifugation. The percentage of fluorescence retained in the pellet in samples with and without EVs was plotted against that of the original quantity of cc-siRNA used as measured by fluorescence. Values represent mean + SEM. n = 3. Statistical differences were calculated by one-way ANOVA followed by Tukey's post hoc analysis. Statistical differences indicated are compared with 100% cc-siRNA. ***$p<0.001$, **$p<0.01$, *$p<0.05$.

5.2.17 Cholesterol Conjugated siRNA Retention Following Loading by Mixing Using Optimised Conditions

EVs were isolated from Neuro2A cells by differential ulracentrifugation. The pellet was resuspended in PBS and mixed with cc-siRNA at the optimised conditions; an EV: cc-siRNA ratio of 1:15 in 100 µl for 1 hour at 37 °C. The EVs were then concentrated by ultracentrifugation and the fluorescence in the pellet measured compared to a standard

curve of total cc-siRNA used and plotted against the fluorescence of 100% of the original quantity of cc-siRNA used **(Figure 5.20)**.

Mixing the cc-siRNA with EVs at the optimised conditions established here increased the loading efficiency to 92.1% compared to 65% in figure 5.14 prior to optimisation of the method. Using these optimised conditions did increase the number of apparent micelles in the samples without EVs however, as 15.7% of the original quantity of cc-siRNA used in the study as measured by fluorescence was retained in the pellet in the absence of EVs compared with 7.5% prior to optimisation. This difference is not as great as the increases in cc-siRNA pelleted with EVs indicating that most of the increase is due to increased association of cc-siRNA with EVs **(Figure 5.20)**.

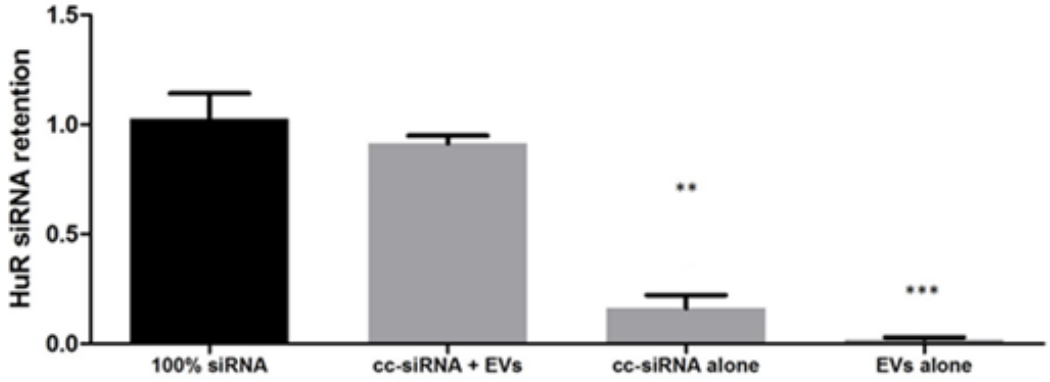


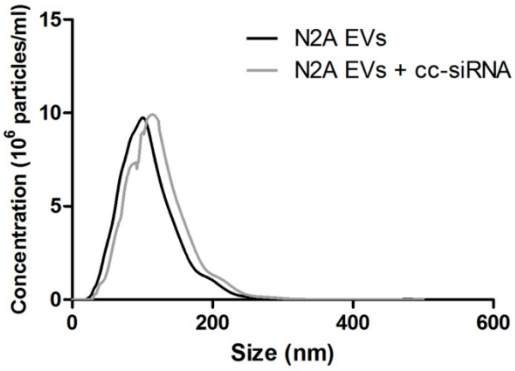
Figure 5.20 siRNA Retention in Pellet Following Mixing of EVs with Cholesterol Conjugated siRNA at Optimised Conditions. EVs from Neuro2A cells were mixed with fluorescent cc-siRNA at a ratio of 1:15 at incubation temperatures of 37 °C for 1 hour in 100 µl. Samples were concentrated by ultracentrifugation. The percentage of fluorescence retained in the pellet in samples with and without EVs was compared to that of a standard curve of that of the original quantity of cc-siRNA used and plotted against 100% cc-siRNA. Values represent mean + SEM, n = 3. Statistical differences were calculated by one-way ANOVA followed by Tukey's post hoc analysis. Statistical differences indicated are compared to 100% cc-siRNA. ***$p<0.001$, **$p<0.01$, *$p<0.05$.

5.2.18 Characterisation of Extracellular Vesicles Following Incubation with Cholesterol Conjugated siRNA

To investigate the effect on EV characteristics the association with the cc-siRNA may have had the size distribution and EV marker expression were analysed after EVs were incubated with cc-siRNA at the optimal conditions established here, concentrated via ultracentrifugation and resuspended in PBS **(Figure 5.21)**. NTA analysis showed a shift in size distribution to slightly larger vesicles, with a mode particle size shift of 98.7 nm

to 109 nm. The shape of the curve remained constant. This could be due to an integration of cholesterol into the membrane.

A)



B)

	N2A EVs	N2A Evs + cc-siRNA
Mean size (nm) ± SE	109.57 ± 4.23	123.63 ± 4.75
Mode size (nm) ± SE	98.73 ± 3.86	109 ± 3.52
Total Particles ($x10^{12}$) ± SE	1.82 ± 0.06	1.83 ± 0.05

C)

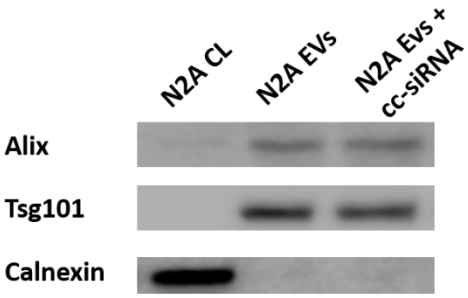


Figure 5.21 Characterisation of Neuro2A-derived Extracellular Vesicles Following Incubation with Cholesterol Conjugated siRNA. Extracellular vesicles (EVs) were isolated from Neuro2A cells following growth in serum depleted medium for 48 hours. Half were mixed with cc-siRNA. Both groups were characterised by nanoparticle tracking analysis (NTA) and western blot. **A)** NTA analysis of size distribution histogram (n = 3). **B)** Table displaying the mean and mode particle size and total number of particles secreted from a 15cm dish of Neuro2A cells (n = 3). **C)** Purified EVs and cell lysates were loaded on a western blot and probed for the exosomal markers Alix and Tsg101, and the endoplasmic reticulum marker calnexin.

5.2.19 Loading by Mixing Extracellular Vesicles with Cholesterol Conjugated siRNA at Optimal Conditions Can Generate Knockdown *In Vitro*

Using the optimal conditions as established here of an EV:cc-siRNA ratio of 1:15, in 100 µl at 37 °C for 1 hour, Neuro2A derived EVs were mixed with cc-siRNA. Following the incubation, the mixture was concentrated by ultracentrifugation, resuspended in PBS and added to plated HEK293 cells. The same procedure was repeated for a control cc-siRNA and a positive Lipofectamine 2000 transfected sample was also included. Following 48 hours the *HuR* expression relative to *GAPDH* and *ACTB* was measured **(Figure 5.22)**.

A small but significant reduction in relative *HuR* expression was obtained from the treatment of EVs mixed with cc-siRNA at the optimised conditions, *HuR* expression was reduced to 89.1% **(Figure 5.22)**. This was at a dose of 100 nM.

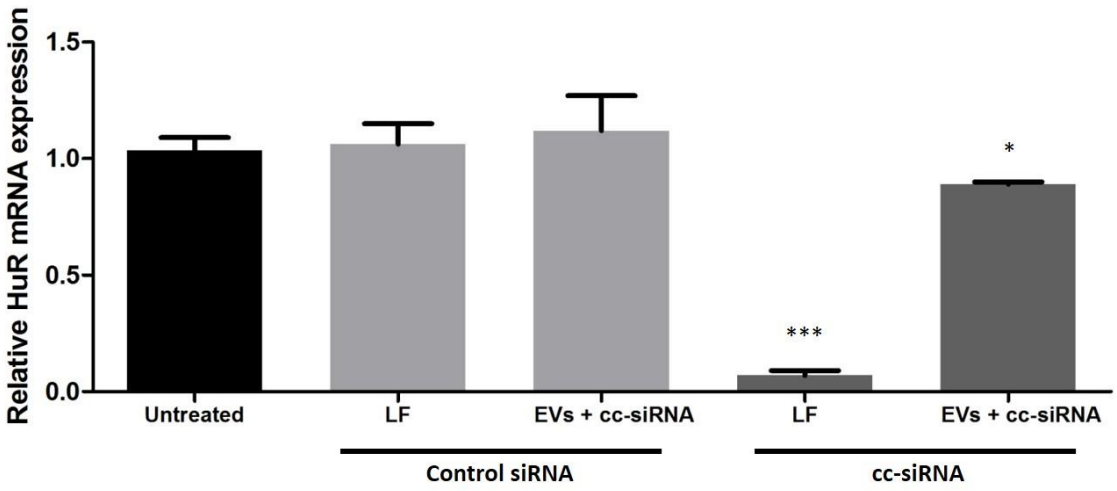


Figure 5.22 Treatment of HEK293 cells with Neuro2A-derived Extracellular Vesicles Mixed with Cholesterol Conjugated siRNA at Optimised Conditions. HEK293 cells were treated with EVs isolated from Neuro2A cells and mixed with cc-siRNA at 100 nM using a ratio of EVs:cc-siRNA of 1:15 at incubation temperatures of 37 degrees for 1 hour in 100 µl. *HuR* expression relative to *GAPDH* and *ACTB* were measured 48 hours post-treatment with EVs mixed with a control or HuR cc-siRNA or transfection with control siRNA or *HuR* cc-siRNA. Values represent mean + SEM. n = 3. Statistical differences were calculated by one-way ANOVA followed by Tukey's post hoc analysis. Statistical differences indicated are compared to control samples. ***p<0.001, **p<0.01, *p<0.05.

5.2.20 Dose Response of Extracellular Vesicles Mixed with Cholesterol Conjugated siRNA at Optimised Conditions

EVs harvested from Neuro2A cells by differential ultracentrifugation were mixed with cc-siRNA at the optimised conditions established here, a 1:15 ratio of EVs:cc-siRNA at 37 °C for 1 hour in 100 µl. The mixture was concentrated and washed by ultracentrifugation and added to plated HEK293 cells in doses of 100, 200, 300, 400 and 600 nM. The same was performed for a control cc-siRNA at the highest dose and a

Lipofectamine 2000 transfected sample was included as a positive control. Another control for gymnosis was also included, in this sample the highest dose of 600 nM of the cc-siRNA alone was added to cells to establish whether the cc-siRNA could enter cells and generate knockdown in the absence of EVs or a transfection reagent **(Figure 5.23)**. 48 hours following treatment the RNA was analysed and *HuR* expression measured relative to *GAPDH* and *ACTB*.

From 100 nM to 600 nM there was a stepwise increase in silencing activity of the EV and cc-siRNA mixture from 89.1% at 100 nM to 43.6% at 600 nM **(Figure 5.23)**. There was approximately a 10% reduction of relative *HuR* expression for every 100 nM increase in concentration. There was also a small but significant reduction in expression in the gymnosis sample indicating that a small amount of the cc-siRNA entered cells and was capable of eliciting silencing in the absence of EVs or a transfection reagent. This effect was small (a 5% reduction in expression) at a high dose of 600 nM.

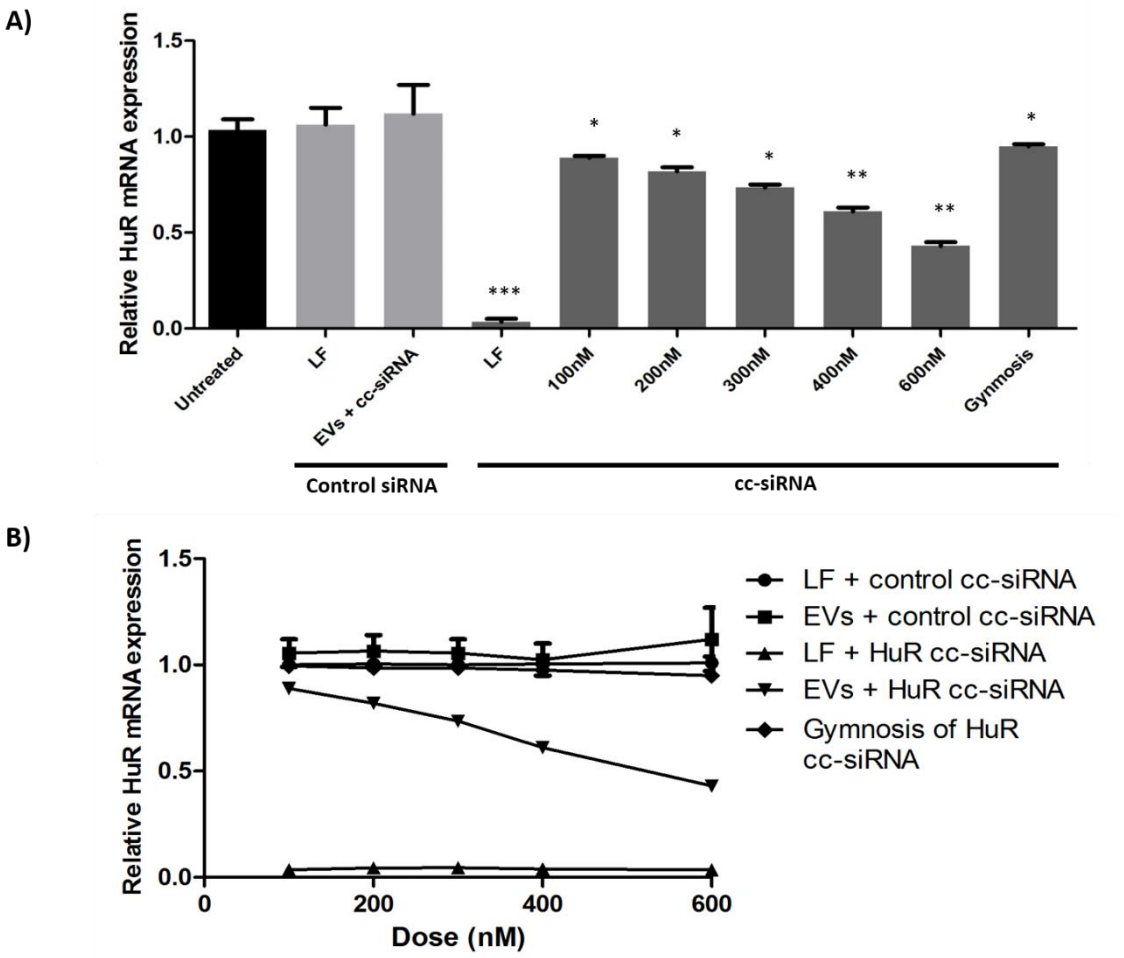


Figure 5.23 Dose Response of Treatment of HEK293 cells with Neuro2A-derived Extracellular Vesicles Mixed with Cholesterol Conjugated siRNA at Optimised Conditions. HEK293 cells were treated with EVs isolated from Neuro2A cells and mixed with cc-siRNA at 100, 200, 300, 400 and 600 nM using a ratio of EVs:cc-siRNA of 1:15 at incubation temperatures of 37 °C for 1 hour in 100 µl. *HuR* expression relative to *GAPDH* and *ACTB* were measured 48 hours post-treatment with EVs mixed with a control or *HuR* cc-siRNA or transfection with control siRNA or *HuR* cc-siRNA. Gymnosis was tested for through the inclusion of samples treated with cc-siRNA in the absence of EVs or a transfection reagent. **A)** Bar graph representation where gymnosis and transfection values represent the expression at 600nM. **B)** Scatter plot representation of the data. Values represent mean + SEM. n = 3. Statistical differences were calculated by one-way ANOVA followed by Tukey's post hoc analysis. Statistical differences indicated are compared with negative control. ***p<0.001, **p<0.01, *p<0.05.

5.2.21 Investigation of Duration of Silencing of Extracellular Vesicles Mixed with Cholesterol Conjugated siRNA at Optimised Conditions

EVs were isolated from Neuro2A cells via ultracentrifugation and mixed with cc-siRNA at the optimal conditions established in this study; at a ratio of 1 EV:15 cc-siRNA molecules, in 100 µl for 1 hour at 37 °C. The mixture was concentrated and washed via ultracentrifugation and the pellets resuspended in PBS and added to plated HEK293 cells at 400 nM. A positive Lipofectamine 2000 positive control was included and a negative control of cc-siRNA was also included. 48 hours later the RNA expression in the samples was analysed and *HuR* expression was plotted relative to *GAPDH* and *ACTB* **(Figure 5.24)**.

There was a stepwise increase in silencing efficiency from 24 hours where *HuR* expression was at 64.2% and 186 hours where it reduced to 40.8% **(Figure 5.24)**.

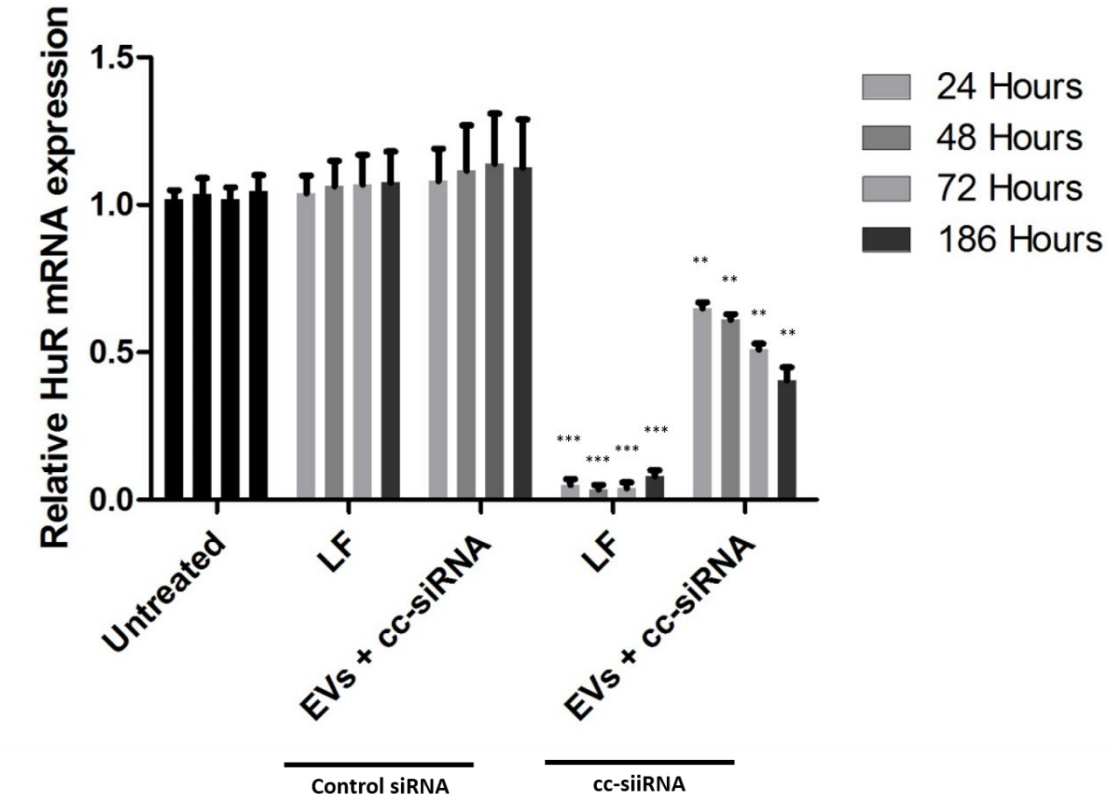


Figure 5.24 Duration of Silencing of Treatment of HEK293 cells with Neuro2A-derived Extracellular Vesicles Mixed with Cholesterol Conjugated siRNA at Optimised Conditions. HEK293 cells were treated with EVs isolated from Neuro2A cells and mixed with cc-siRNA at 400 nM using a ratio of EVs:cc-siRNA of 1:15 at incubation temperatures of 37 °C for 1 hour in 100 µl. *HuR* expression relative to *GAPDH* and *ACTB* were measured 24, 48, 72 and 186 hours post-treatment with EVs mixed with a control or *HuR* cc-siRNA or transfection with control siRNA or *HuR* cc-siRNA, or left untreated. Values represent mean + SEM. n = 3. Statistical differences were calculated by one-way ANOVA followed by Tukey's post hoc analysis. Statistical differences indicated are compared with negative control. ***p<0.001, **p<0.01, *p<0.05.

5.3 Discussion

This study aimed to extend previous findings that EVs may act as nucleic acid delivery vehicles *in vitro* and *in vivo*, specifically to test the silencing efficiency of EV-based siRNA delivery. Firstly, EVs from two cell sources and untransfected or those transfected with the neuronal targeting ligand or control vector were characterised. An siRNA which had been validated and elicited a robust lasting silencing of *HTT* in a dose dependent manner in an *in vitro* model of HD was selected to measure the efficiency of EV-based delivery following loading by electroporation with *HTT* siRNA *in vitro* and *in vivo*. Investigation of the loading method through examination of its efficiency lead to the discovery of aggregates of *HTT* siRNA in electroporated samples. High siRNA retention in the pellet even in the absence of EVs indicated the presence of siRNA aggregates which could be responsible for the high levels of apparent loading reported in previous studies. Furthermore, in contrast to the results on which this study aimed to build[213], EVs loaded with siRNA by electroporation failed to generate knockdown of *HTT in vitro* with a variety of source and recipient cells, or *in vivo* with a high level of variation between samples. An alternate method of loading was then evaluated, using cholesterol conjugated siRNA mixed with EVs. Silencing was obtained using this method *in vitro* and was improved upon by optimising the parameters of co-incubation of the EVs with the cc-siRNA.

Several studies have reported successful delivery of cargo using EVs. As well as Alvarez-Erviti *et al*., who used this technique to bypass the BBB for the delivery of Bace1 siRNA[369], other groups have harnessed this technology to deliver siRNA to inhibit tumour growth *in vitro* and in mouse models[370,371], to deliver siRNA to T cells and monocytes[372], and also to deliver a miRNA inhibitor to glioma cells[362]. The promise of

EVs as a nucleic acid delivery vehicle may only be realised on successful loading of the EVs with the therapeutic cargo of interest. In this study, electroporation was used to create small pores in the EV membrane to allow for diffusion of the *HTT* siRNA inside the EV. Other studies have also reported successful loading of EVs with nucleic acid cargo by electroporation. Shtam *et al*., used this technique to load EVs from HeLa cells with siRNA against RAD51, but delivery was not examined directly following loading by electroporation[371]. Wahlgren *et al*., delivered siRNA to human mononuclear blood cells by electroporation into plasma EVs to successfully silence MAPK1. Furthermore, the siRNA was shown to be inside the EVs and was localised in the cytoplasm of the recipient cells[372]. MSC and HEK exosomes loaded by electroporation with PLK-1 siRNA reduced its expression and cell proliferation at 48 hours[370]. A miRNA inhibitor has also been shown to be loaded by electroporation, EVs from B cells loaded with a miRNA-155 inhibitor caused a reduction of TNFα protein[362].

Despite previous reports of successful generation of silencing in recipient cells following loading of EVs by electroporation, this study failed to see *HTT* silencing in recipient patient fibroblasts, Neuro2A cells or HEK293 cells after treatment with DC or Neuro2A cell derived EVs. Further investigation of the loading efficiency through evaluation of the level of siRNA pelleted following electroporation in the presence and absence of EVs provided evidence of siRNA retention in the pellet when no EVs were present. This indicates siRNA aggregation could lead to over-estimation of loading efficiency in the absence of the experimental control of the siRNA with no EVs. Indeed, these aggregates could be visualised using EM. While increasing the apparent level of loading efficiency this aggregated siRNA could also reduce any resultant biological activity as aggregated siRNA is not available to bind to mRNA. A study by Kooijmans *et al.*, has also reported

this aggregated siRNA following electroporation and its potential contribution to an overestimation of loading efficiency[363]. Precipitation of biological macromolecules following electroporation has also been reported in another study[373], not only can this complicate electroporation but the authors reported that the nucleic acids which had undergone electroporation could be pelleted by spinning at 7,000g for two minutes. As ultracentrifugation was used in this present study to isolate and pellet EVs it is thus not surprising that siRNA following electroporation was also pelleted at 120.000g.

There are some differences between this present study and the studies which have reported successful downstream effects of EVs loaded with siRNA by electroporation. Wahlgren *et al*., incubated samples on ice prior to electroporation and performed extensive optimisation on their electroporation protocol in terms of the buffer, voltage, capacitance, volume and concentration and the conditions they found as optimal were different to those established by Alvarez-Erviti *et al*., which were used in this present study. The methods used by Greco *et al*., (150 V, 100 µF, 0.25 µg/µl siRNA) were also different to the ones used in the present study, though similar to those utilised by Wahlgren[372]. Shtam *et al*., performed electroporation under different parameters with 20 pulses of 700 V, though in their report there was no loading control used, nor were EVs electroporated with siRNA washed to eliminate excess siRNA[371]. Ohno *et al*., were unable to use electroporation to load miRNA inhibitor into EVs[374]. Momen-Heravi *et al*., also performed optimisation of electroporation parameters for miRNA mimic loading and found that an EV density of 0.5 to 1 µg/µl was most effective at encapsulation, but that is lower than the amount used here[5]. They reported a decreased loading efficiency with increased EV concentration which offers one explanation why the methods used here may have failed, but also an alternate method of EV isolation was used, Exoquick rather

than ultracentrifugation, which can precipitate cellular components other than EVs such as serum proteins albumin and apolipoprotein E[375]. Thus, their estimates of EV concentration by protein weight may actually relate to other proteins.

As mentioned, EV quantity estimation by protein quantification is another area where studies can differ and may offer a reason why this study failed to achieve silencing using the same methods as previous work[369]. The nature of the isolation method used, ultracentrifugation, can vary as the resuspension of the pellet is not a standard process and depending on whether a washing step is included or not contaminants from the culture medium may remain and increase the protein yield without a corresponding increase in EVs. In addition, no geNorm analysis was performed in the previous study so determine the optimal reference genes and it is possible that with correction for this, the results could be different[294].

Attempts have been made to overcome the siRNA aggregation in both cytomix buffer and the electroporation buffer used in the present study with mixed results but were not used here as they had not been found to be necessary in the previous study on which this research aimed to build and instead an alternative method was pursued[369]. The aggregation is thought to be due to complex formation between metal ions from the electrodes and hydroxide ions from the buffer[363]. Removing one or both in one study however reduces loading efficiency as measured by siRNA retention in the pellet to 0.05%[363]. The addition of EDTA was used by Momen-Heravi *et al*., to eliminate the effects of the metal ions but in contrast to the results by Kooijmans *et al*, here the EDTA improved loading efficiency as 55% loading efficiency was recorded. Furthermore, using RNase treatment the RNA was shown to be encapsulated and generated functional effects

in recipient cells. Johnson *et al.*, used a buffer containing the disaccharide treholose. This addition prevented any adverse effects on EV integrity following electroporation. EV shape change and aggregation have been reported following electroporation as a result of a destabilized membrane[376]. This could also negatively impact loading efficiency. Addition of treholose[377], lipid complexation or EDTA[362] in an effort to combat siRNA precipitation also reduced this EV aggregation and could explain some of the success when these are added to the electroporation buffers. Thus, for the purposes of this present study, some research indicates that the absence of a chelating agent or other agent which may prevent siRNA and EV aggregation in the electroporation buffer may contribute to the low levels of loading[362], but some research disputes this[363] with regard to EDTA decreasing siRNA retention in the pellet. siRNA aggregation has been shown to decrease with increasing EV concentration[363], which was hypothesised to be due to the capture of multivalent ions on the negatively charged EV membrane or altering buffer conductivity. This same condition of increasing EV concentration has also been shown to decrease loading efficiency however[362].

A theme which is evident from the experiments reported on here as well as others where electroporation is used as a loading method for EVs is variability. Even studies which report successful downstream effects of loaded EVs have this intrinsic inconsistency in results. Wahlgren *et al.*, themselves noted that even following their extensive optimisation, the efficiency varied[372]. Shtam *et al.*, also confirmed the variability of electroporation loading[371]. As stated by Kooijmans *et al.*, equipment, buffers and protocols for loading by electroporation vary between laboratories which could impact on electroporation results[363]. If EVs are to be used as a therapeutic delivery vehicle in a clinical setting, methods must be standardised to eliminate this variability.

A study by Lamichhane *et al*., revealed that the size of EVs is important in encapsulation by electroporation[378]. Larger EVs were more amenable to encapsulation. In the present study EV populations were limited to those with a diameter of under 200 nm due to the use of 200 nm filters. This was performed as the primary population of EVs of interest had been exosomes as being of MVB origin these would be the EVs that would mostly be predicted to express the Lamp2b-RVG targeting factor. Indeed a study by Kanada *et al.,* has reported that a different sub-population of EVs – microvesicles, defined in their study as larger vesicles - may be capable of functional transfer of nucleic acid[379]. Although the latter report focused on DNA, the report by Lamichhane *et al*., of larger EVs having increased potential for loading by electroporation raises the question, should all EVs rather than exosomes be considered as the EVs of interest in drug delivery with methods altered to include slightly larger vesicles. It also highlights the possibility of there being proteins other than Lamp2b which may be better proteins to use as an anchor for targeting moieties which was seen in chapter 4.

In order to prevent the restriction of the use of EVs as gene delivery vehicles by inefficient variable loading, alternative approaches to electroporation must be pursued. Hence, following the failure to silence *HTT* using loading by electroporation, this study focused on a novel method to load EVs, using cc-siRNA mixed with EVs. cc-siRNA has been shown capable of generating knockdown *in vitro* and *in vivo* when delivered alone or in lipid nanoparticles[357,365]. The use of cc-siRNA has not been used with EV delivery to date. A study by Shtam *et al*., used lipid modified siRNA to load by incubation with EVs but the modifications to their so called self delivering RNA were not disclosed[371]. In their study a 30 minute incubation at room temperature was used, and washed EVs loaded with their lipid modified siRNA were capable of delivering the fluorescent siRNA to recipient

cells, however it was not tested if this lipid modified siRNA associated with EVs was capable of generating functional effects in the recipient cell. This strategy when applied to HD also draws parallels with a study by Alderman *et al*., where hydrophobically modified siRNAs (hsiRNA) were used to silence *Htt* in the brain, however EVs were not used and their methods required invasive direct brain injection[380]. The hsiRNA used in their study bears a similarity to the cc-siRNA used here, it is also cholesterol conjugated via TEG, has 2'-flouro modifications to the backbone and a phosphorothioate overhang. It was capable of migrating through the side ipsilateral to the injection site and was found in neurons on that side. This indicates the possibility that if cc-siRNA can reach the brain following EV delivery, it might be capable of migrating to the sites of neurodegeneration in HD.

In the present study, the hydrophobically modified cc-siRNA was initially used to transfect the EV source cells but due to the difficulty in separating any contaminating transfection reagent a new strategy of mixing the cc-siRNA with EVs was devised and optimised to investigate further the loading of EVs with nucleic acid cargo. Biodistribution studies have shown that direct systemic injection of cc-siRNA does not result in localisation of cc-siRNA in the brain[357,358]. Wolfrum *et al*., used radiolabelled cc-siRNA injected systemically in Syrian hamsters. 4 hours post-injection the animals were sacrificed and radioactivity monitored in several tissues and no radioactivity was detected in the brain. The cc-siRNA had bound mostly to high-density lipoprotein (HDL) low-density lipoprotein (LDL) receptors responsible for cc-siRNA transcytosis and albumin but HDL and LDL cannot transport cholesterol across the BBB[358]. The study by Wolfrum *et al*., also highlights the need to associate cc-siRNA with EVs to prevent the cc-siRNA binding to albumin *in vivo*[358]. Another advantage of EV association for cc-

siRNA is endosomal escape, for this the siRNA must be unpackaged from the delivery vehicle prior to crossing the endosomal membrane to reach the cytosol, EVs are thought to be capable of this.

There are several caveats with the use of EV delivered cc-siRNA here which must be considered. One is cholesterol efflux from the cell[381]. If cc-siRNA is expelled from the cell to avoid an excess of cholesterol, it would negatively impact on any silencing *in vivo*. The second is the quantity of EVs needed for this silencing. As seen in this study, the higher the ratio of EVs:cc-siRNA, the higher the level of cc-siRNA retention in the pellet indicating a higher level of cc-siRNA association or encapsulation. Thus, a high quantity of EVs would be needed *in vivo* and as mentioned in chapter 4, large volumes of EVs can overwhelm physiological clearance systems. Another potential caveat is that in the present study it is not known in which direction the cc-siRNA faces, the extracellular environment or in an intraluminal orientation. In this study, there is evidence that the cc-siRNA could intercalate in the membrane as the EVs are slightly larger following mixing with cc-siRNA, though this does not preclude any additional encapsulation. Cholesterol in a membrane can flip-flop[382] but the hydrophobic siRNA may prevent this. Encapsulated cc-siRNA may not be necessary for silencing *in vivo* but for protection from nucleases intraluminal facing insertion into the membrane would be preferable, although the modifications of the siRNA used here would increase nuclease stability. It is also not known what effect insertion of cholesterol may have in the EV membrane. It could alter the signalling properties of lipid rafts in the membrane[383]. These effects would need to be tested *in vivo*.

In summary, the *in vitro* data gathered in this study show that electroporation results in previous studies may have been overestimated due to siRNA aggregates co-pelleting with EVs. EVs loaded with siRNA by electroporation failed to show silencing but cc-siRNAs associate and co-pellet with EVs and can elicit lasting silencing *in vitro* in a dose dependent manner showing this means of therapy shows promise in EV siRNA loading but must be rigorously tested *in vivo*.

CHAPTER 6 DISCUSSION

6.1 Summary of Results

This thesis aimed to identify a non-toxic nucleic acid capable of silencing mutant *HTT* (mHTT), and to investigate EVs as a nucleic acid delivery vehicle by evaluating the biodistribution of brain targeted EVs and examining the loading of EVs with a nucleic acid cargo. To this end, a range of nucleic acid therapeutics designed to reduce *HTT* expression were evaluated for their potency, duration of silencing, and for their effect on cell viability in a HD *in vitro* model. An siRNA was chosen as it had the best safety profile combined with silencing efficacy and potential for loading into EVs without a dependency on accessibility of the nucleus and transcription start site (TSS). EVs were assessed for their suitability as a delivery vehicle in HD in two ways: by testing their biodistribution, and also their loading.

Brain targeted EVs were assessed for their biodistribution following intravenous administration with a focus on brain delivery. Neither a previously validated targeting construct, Lamp2b-RVG, nor new constructs using more highly expressed TfR as a membrane anchor were capable of increasing brain delivery more than two-fold. Lastly, the loading of EVs with siRNA by electroporation was attempted but there was no silencing effect evident following treatment of cells with EVs loaded with siRNA by electroporation. An alternative method of loading by mixing EVs with cholesterol conjugated siRNA (cc-siRNA) was adopted and *in vitro* silencing was achieved.

6.1.1 Silencing Huntingtin

Firstly, a range of different types of therapeutic nucleic acids including siRNAs, LNAs, a multi-gene LNA, exon skipping nucleic acids and the plasmid based approaches shRNA and CRISPRi were analysed for their potency in silencing *HTT in vitro* in a validated HD model. Some of these were designed to be allele specific and silence only the mutant allele or non-allele selective where a reduction in expression of the wild type protein would also be predicted to occur. This has been shown to be well tolerated in primates[79]. The *HTT* silencing efficacy of these therapeutics was assessed at both the mRNA and protein level. Subsequently, the protein silencing of the wild type and mutant allele by the most promising candidates from each category and the allele selective nucleic acids were visualised using a western blot to separate the mutant and wild type protein. The toxicity of each treatment was also recorded.

The most promising therapies with regard to *HTT* silencing were siRNA, exon skipping ASOs and CRISPRi. siRNAs are short double stranded nucleic acids which exert their silencing effect through mimicking miRNA and the use of the cell's endogenous machinery to degrade mRNA or repress translation[174]. CRISPRi is a different method whereby a single guide RNA (sgRNA) binds to complementary nuclear DNA at the TSS inducing a repression of transcription[199]. Exon skipping oligonucleotides bind to the pre-mRNA at exonic splicing enhancers (ESEs) and through their binding they mask the ESEs from trans-splicing regulatory factors and alter the splicing of the target gene[189]. The exon skipping oligonucleotides utilised here were designed such that exon 3 would be skipped, and the resultant protein fragment would contain a premature stop codon and be degraded by nonsense mediated decay[306].

The exon skipping ASOs with highest potency also displayed some toxicity at higher doses. The non-allele selective siRNA displayed no toxicity at any dose, nor did the CRISPRi plasmid which displayed the strongest silencing capacity. Although CRISPRi has shown great potential in the last few years since its application to gene therapy, and is a novel treatment for HD, the applicability of CRISPRi is challenging as it requires accessibility of the TSS which depends on chromatin organisation, and the components could also prove difficult to package into EVs. siRNA has several advantages over CRISPRi and so was selected as the optimal cargo for loading into EVs in this study. These include the benefit of siRNA as a technology which has undergone increased study, has been shown to be safe in clinical trials (NCT00722384, NCT00722384, NCT00259753, NCT00557791) and does not have to reach the nucleus to carry out its therapeutic effect nor rely on the accessibility of the TSS. It does however need mRNA accessibility as secondary mRNA structures can hinder hybridization between the RISC and the target site sequence[384].

This study adds to others which use siRNA for the silencing of mutant *HTT*[79,150–152,180]. They show promise *in vitro* for inducing potent non-toxic silencing, but for the treatment of neurological disorders delivery to the CNS is the biggest hurdle to overcome before they can be considered for clinical use. In animal models delivery has been achieved via direct intrastriatal injection in viral vectors and has been shown capable of correcting both the pathology and the phenotype in HD models[79,150–152,180]. However, direct brain injection is associated with risks. An intravenous delivery option would be less invasive and safer but the blood-brain barrier (BBB) prevents the passage of nucleic acid therapeutics from the circulation into the CNS. EVs targeted to the brain and delivered intravenously or intranasally could provide a solution to this issue because they seem to

be able to penetrate the BBB. Loading of a therapeutic nucleic acid cargo in EVs should increase the stability of the cargo in biological fluids and help to overcome the intrinsic properties of siRNA which limit its clinical use including the short half-life in circulation, its hydrophobicity and its inability to cross membranes[385]. In addition to shielding the siRNA from RNases, EVs capacity for targeting should allow treatments to be administered with fewer off target effects and increased potency by directing the treatment towards where it is needed. Furthermore, previous work has shown they can be loaded with siRNA to silence a target in the brain following intravenous administration[213]. However, prior to this study, no examination of the biodistribution of brain targeted EVs had been performed.

6.1.2 Investigation of the Biodistribution of Brain Targeted Extracellular Vesicles

To assess EVs as a potential delivery vehicle for therapeutic nucleic acids such as siRNA, a biodistribution study of fluorescently labelled brain targeted EVs was performed. EVs from cells transfected with a fusion construct of an EV membrane protein as an anchor (Lamp2b or TfR) and targeting ligand (RVG, EPRNEEK or G7), were labelled with DiR, an infrared fluorescent dye which in combination with IVIS allows tracking of labelled EVs. The labelled targeted EVs were injected intravenously and following 24 or 12 hours the organs were harvested and imaged *ex vivo* for fluorescence.

Untargeted EVs from either DCs or HEK293 cells were found to accumulate mostly in the liver, lungs and spleen, organs of the clearance system, the reticuloendothelial system (RES). There were slight differences between the targeting with EVs from HEK293 cells

accumulating more in the liver and DC EVs in the spleen. The gastrointestinal tract was also a site where EVs accumulated, more for HEK293 derived EVs than DC EVs. The accumulation mostly in organs of the RES indicates that the EVs have been targeted for clearance. This clearance is markedly slower than that reported for siRNA which has a half-life of just 15 minutes in serum due to rapid enzymatic degradation, renal clearance and capture and clearance by distributing to organs of the RES and phagocytosis by the MPS[303,385,386]. Thus, if an siRNA is encapsulated by an EV it should be protected from enzymatic degradation, shielded from RNases increasing its limited blood stability, and preventing renal clearance as they are larger than the <50kDa molecules rapidly excreted through the kidney[326,387,388]. This highlights the promise in the use of EVs as a delivery vehicle for siRNA. However, from this analysis it seems likely that EVs are also cleared by phagocytic cells within the RES, albeit more slowly than siRNA[326,387,388]. Next, the biodistribution of targeted EVs was examined. When the EVs were isolated from cells transfected with a neuronal targeting ligand, the overall biodistribution remained similar, but a two-fold increase in accumulation in the brain was noted on expression of each targeting ligand.

This study adds to others which have also performed biodistribution studies on EVs and built on this knowledge by tracking brain targeted EVs[320–323,343,344]. Other studies have focused on untargeted EVs which offer passive targeting to sites *in vivo* which have increased capillary permeability such as the liver and tumours where the enhanced permeability and retention effects (EPR) allow nanoparticles to be retained[321,323].

These studies have used various means of tracking EVs including fluorescent dyes like the present study[320,323,356], radiolabelled molecules[323,343], genetic engineering for

luciferase expression[321,322], or click chemistry[389]. All of these studies report accumulation primarily in the RES, although the studies with Gaussia luciferase show elimination of signal at 6 hours which is faster than the dye studies. This could be related to the short half-life of Gaussia luciferase in circulation which is reported to be under 30 minutes[390], or this could indicate that the signal recorded from dye studies could originate in part from vesicles which are degraded or recycled, or as with the expression of the brain targeting constructs, it could be that only a subcategory of EVs are expressing the luciferase tag while a fluorescent dye does not discriminate between vesicle subtype nor expression markers. Targeting to other regions has been reported, such as tumours for iRGD-targeted EVs and EVs expressing the EGFR binding peptide GE11[324,325], this targeting as well as the passive targeting reported in those studies was more efficient than the passive tumour targeting noted in the study in which the biodistribution results reported here were published[326].

This present study was the first to visualise increased delivery to the brain by targeted EVs, but a follow up study *in vitro* to assess uptake of fluorescently labelled brain targeted EVs in a model of the BBB failed to show increased uptake by these brain targeted EVs. The disparity in results between those obtained *in vitro* and *in vivo* have been reported previously[391]. This could be because the model, like all BBB models, is not an accurate representation of the complexity of the BBB and could express different levels of the receptors for the target ligands used in this study compared to the BBB, or because just one time point was investigated. Nonetheless, the presence of the targeting moiety did not inhibit uptake to a large extent and there is a possibility that the ligands may increase the specificity of uptake which would explain in part the increased uptake seen *in vivo*. Also, it must be noted that the Lamp2b-empty vector, the vector that overexpresses the

Lamp2b-protein but not the targeting ligand, could increase general uptake as Lamp2b has been reported to act as a cell adhesion molecule[392].

The biodistribution studies here indicate increased brain accumulation upon expression of the targeting ligands but a further study of loaded EVs would be required to test if these brain targeted EVs are intracellular and capable of delivering functional nucleic acid cargo, if endosomal escape is possible following delivery. Other studies indicate that endosomal escape is possible following EV delivery, the study by Ohno *et al*., showed delivery of miRNA by the targeted EVs to tumours and previous work has shown silencing in the brain following delivery of Lamp2b-RVG targeted EVs[213,324]. Also, even though the different ligands yielded the same increase in brain accumulation, they may display alternate neuronal targeting.

6.1.3 Evaluation of Loading of Extracellular Vesicles with siRNA

Based on research which had previously been performed to load EVs with siRNA by electroporation, this method was used to load bone marrow DC and neuronal Neuro2A derived EVs with siRNA[213]. Activity of the loaded vesicles was tested *in vitro* using HD patient derived fibroblasts, Neuro2A cells and HEK293 cells as recipient cells. *In vivo* activity was also analysed. In these experiments no knockdown was achieved by EVs loaded with siRNA via electroporation.

Although some studies have shown a functional effect of siRNA loaded by electroporation, these studies use varying parameters of EV concentration, incubations on ice, voltage and capacitance and some attest to varying electroporation results even

following extensive optimisation[213,264,266,393]. Other groups have reported being unable to load via electroporation at all[324]. Varying results could also arise from differences in individual methods of pellet resuspension, from contamination by proteins from culture media in estimating vesicle amount by protein concentration, from failure to wash the pellet or from the absence of a loading control. To investigate the effect of electroporation on siRNA loading, a fluorescent siRNA was mixed with EVs and electroporated, isolated by ultracentrifugation and the fluorescence in the washed pellet was measured. A control of siRNA alone, electroporated in the absence of EVs and treated in the same way was included and retained high fluorescence in the pellet following ultracentrifugation indicating that previous reports of loading had been overestimated by failing to take into account siRNA aggregation[213]. This result is in line with the siRNA aggregation reported by others[394].

Some groups have taken steps to reduce siRNA aggregation through the addition of EDTA, lipid complexation or to reduce EV aggregation with membrane stabilisation via addition of treholose[394–396]. Given the reports of varying efficiency from electroporation even following extensive optimisation, an alternative loading approach was adopted here using cholesterol-conjugated siRNA (cc-siRNA)[264,393]. Cc-siRNA has been used *in vitro* and *in vivo* for gene silencing[357,359,397]. They have been administered alone, as peptide micelles, as lipid-polymer hybrid nanoparticles (LPNs) and in cationic liposomes[357–359,365,397,398]. When delivered alone, they show broad tissue biodistribution primarily to the liver, heart, lungs, kidneys and adipose tissues 24 hours following injection and bind to high density lipoprotein (HDL), low density lipoprotein (LDL) and serum albumin, but cannot cross the BBB[357,358]. A study using a similar hydrophobically modified siRNA directly injected into the brain was capable of silencing *Htt* in primary neurons and mouse

brain but invasive direct brain injections were used as the lipid modified siRNA could not cross the BBB[380]. Here it was hypothesised that EVs could aid in the delivery of cc-siRNA for gene silencing.

Firstly, to obtain cc-siRNA containing EVs, a transfection method was adopted whereby the source cells were transfected with a fluorescent cc-siRNA and the fluorescence in the medium quantified at various time points. This method of loading has been previously applied for RNA[261,399]. Although cells did secrete the cc-siRNA it was not known if the cc-siRNA was secreted within vesicles, or if some residual contamination from transfection reagent was present. To overcome this challenge, it was decided to test whether EVs could be loaded with cc-siRNA exogenously via co-incubation. This approach where EVs are mixed with a drug has been used for loading the anti-inflammatory curcumin and the chemotherapeutic paclitaxel (PTX), but has only once been used to load siRNA which was lipid modified and the modifications in the publication were not disclosed[266,400,401]. It was hypothesised here that the hydrophobic modification of the cholesterol tag could facilitate loading by mixing. The EVs were mixed with cc-siRNA followed by a washing by ultracentrifugation step to remove free cc-siRNA was adopted and silencing was obtained *in vitro*, though at a low level. Electroporation did not increase association of EVs with cc-siRNA. Control samples of cc-siRNA mixed in the absence of EVs were included to account for the activity that could be mediated by cc-siRNA micelles. The conditions of the mixing were optimised for EV:cc-sirna ratio, incubation time, incubation volume and temperature, and using the optimised conditions cc-siRNA retention in the pellet and silencing efficiency was increased.

It is not known if the increased silencing efficiency observed here would be therapeutically relevant because the dose and outcome (silencing as well as pathological and phenotypic measurements) would require monitoring and optimisation *in vivo*. Due to the high optimal EV:cc-siRNA ratio, a high dose of 1 EV per 15 cc-siRNA molecules was optimal in achieving loading. It remains to be seen what dose would be necessary for *in vivo* efficacy but a potential drawback of the strategy used here could be the number of EVs required. This could limit the therapeutic efficacy as high numbers of EVs could overwhelm a physiological system as has been seen in other studies[323]. As discussed in a dose response study reported on in chapter 4, a high dose will potentially saturate the liver[326]. This could cause endotoxemia and hepatic failure, indeed hepatotoxicity has been noted in one patient of an EV clinical trial[283,326,342]. Also, it was not tested here whether the cc-siRNA was inside or outside the EVs. This was not important for the *in vitro* work presented here but could become important *in vivo* as if the cc-siRNA is not encapsulated it may still be susceptible to RNases, though this would be limited by the heavy modifications to this cc-siRNA. The larger size of the EVs following mixing with cc-siRNA indicates that the cc-siRNA is integrating into the EV membrane rather than being encapsulated. This did not inhibit functionality *in vitro* but future work would establish if this would dampen the *in vivo* silencing potential.

6.2 Challenges in the Treatment of Huntington's Disease

There are a number of different therapies in preclinical and clinical development for the treatment of HD **(Tables 1.1 and 1.2)**. However, most of these therapeutics are directed at stages farther downstream in the pathogenic cascade than directly targeting *mHTT*. Therefore, even if these therapies are successful in the roles for which they are designed, since *mHTT* remains highly expressed, other stages in the cascade may still contribute to

pathogenesis. Thus, unless *HTT* or *mHTT* is targeted directly there is a risk to the patient that some branches of the pathological cascade may continue even following treatment.

In this study, both allele selective and non-allele selective methods to silence *HTT* were investigated. Selective targeting can be achieved through the targeting of SNPs which link with the repeat, or the repeat itself[20,21,293]. Although theoretically the best option may be to reduce expression of the disease allele while leaving the healthy allele untouched, the allele-selective methods used here displayed slight toxicity and were not pursued. In this study it was not possible to establish any negative effects of silencing of the wild type allele. As discussed in chapter 1, wild type HTT is involved in many cellular processes and although some studies have shown that silencing the wild type in an adult is well tolerated even in primate models, others have shown that complete silencing causes cognitive deficits in mice[79,167]. If this treatment were brought forward, careful monitoring of the dose would be required to minimise the risk of any such effect[79].

As mentioned, an ideal therapy for HD would target early in the pathological cascade of events. An siRNA targeted to a region upstream of the CAG triplet repeat was capable of this silencing but the limitations of post-transcriptional gene silencing including saturation of the endogenous RNAi pathway and off-target effects must be considered. The latter can be minimised through optimisation of the sequence and both can be reduced through limiting the dose. *In vivo* analysis for the specific siRNA would need to be performed to determine the optimal dose for efficacy without off target effects and to establish a dosing regimen. A dose limitation would also aid in the minimisation of any potential side effects from silencing the wild type allele. Establishing a dose which reduces wild type HTT to a level shown to be well tolerated in primates but is also capable

of inducing a therapeutic benefit should be possible as even moderate levels of silencing of the mutant allele have been shown to produce therapeutic benefit[79].

Other intrinsic limitations of siRNA include the vulnerability to serum RNases, rapid clearance by the RES, stimulation of the immune system, difficulty in crossing hydrophobic plasma membranes and endosomal escape following endocytosis. Although the resistance to endonucleases can be reduced through modifications such as the phosphorothioate modifications applied to the siRNA used here, and the ability to cross membranes can be aided by modifications such as a cholesterol tag, these limitations still restrict the clinical use of siRNA and could potentially be overcome by encapsulation in EVs. This would protect the siRNA from degradation in the blood stream, from activating an immune response and also facilitate delivery. If targeted using a neuronal ligand, they could also increase brain delivery.

6.3 Challenges in the Development of Extracellular Vesicle Based Therapeutics in a Clinical Setting for the Delivery of RNA

Although the safety of EVs has already been demonstrated in clinical trials, and a phase I trial for delivery of curcumin is enrolling (NCT01294072), their use as a therapeutic delivery vehicle for RNA requires much further study[276,277,283]. The research presented here highlights just some of the hurdles that must be overcome before they can reach a clinical setting including the difficulty in overcoming the intrinsic targeting or homing of EVs and accumulation in organs of the RES as well as the lack of standardised methods of loading. Another issue to be considered is the standardisation of a scalable and

sustainable source of homogenous EVs free from contamination from the isolation and purification procedures.

Here, immature DCs from bone marrow were used as they lack immune modifiers. Neuro2A cells were also used as they secrete a high number of EVs and may have innate homing to neuronal cells and HEK293 cells were also used as their biodistribution was broadly similar to DCs, no negative reaction is evident upon their administration *in vivo*, they are not costly in terms of animal life to produce and they are easy to transfect. Another commonly used source of EVs are mesenchymal stem cells (MSC) as these EVs have intrinsic properties which lend themselves to medicine, for example they have been shown to improve myocardial infarction[258]. With regard to brain delivery, a cell source which is close to the patient's own cells, perhaps derived from their own bone marrow or induced pluripotent stem cells (iPSCs) reprogrammed from their fibroblasts, could be beneficial as one of the novel findings of this study is that differences were noted here in EV brain accumulation between samples which were harvested from allogeneic and syngeneic sources. This would also reduce any risk for potential immunogenicity and the use of iPSCs allows for the potential of differentiation along several pathways which may give rise to EVs with innate homing to the region of interest. Plant derived EVs are being used in the curcumin clinical trial (NCT01294072) in colon cancer and may represent an easily scalable source of EVs which would be interesting to test for HD delivery if the safety measures in the clinical trial are reached.

In this study EVs were targeted through the bioengineering of expression ligands on their surface. However, although increased targeting to the brain was achieved here upon expression of several different brain targeting ligands in the source cells, only 1% of the

administered dose reached the brain. It remains to be seen whether this increase would lead to sufficient delivery of siRNA to the brain for the alleviation of the pathology and symptoms of HD, but previous work has shown it can reduce expression of an AD target, Bace1[402]. Overall the biodistribution between targeted and untargeted EVs was found to be similar. Further study of potential modifications to avoid the RES could facilitate increased targeting to the regions of interest. Other methods of targeting should also be investigated to establish whether the two-fold increase in delivery to the brain obtained in this study can be improved, this could potentially be achieved in the future through antibodies or single-chain variable fragment protein expression directed against receptors that lead to transcytosis[402].

The isolation method would also need to be standardised and scalable to yield a large population of homogenous pure EVs of a clinical grade without contamination. Different methods result in different levels of contamination and vesicles which are more or less intact. Ultracentrifugation was used in this study but shear stress caused by this method can result in vesicle rupture and aggregation[403]. One study has also found that EVs isolated by ultracentrifugation compared with ultrafiltration combined with size exclusion liquid chromatography have a different *in vivo* biodistribution[345]. The EVs isolated by ultrafiltration accumulated less in the lungs but more in the liver than ultracentrifugation. This could be a result of the different methods selecting for alternate subgroups within the EV population. Further work to define EV subpopulations and isolation methods must be performed to investigate this as currently it is impossible to purify and distinguish between EV subpopulations, in part due to a lack of markers specific to a subgroup[404]. This also has the potential to improve targeting over the two-fold increase achieved here if a method of isolating specifically or enriching for the subset

of EVs expressing the targeting ligand to increase the percentage of targeted EVs in a preparation could be achieved. In the future, immunoaffinity purification for specific markers may be able to select for a pure subgroup similar to that used to purify MHC II bearing EVs[354].

As well as the loading methods described here, an alternative method being pursued is manipulation of the endogenous loading mechanisms to select for overexpression of miRNA in EVs. Secreted RNAs share specific sequence motifs which could selectively target RNAs to EVs[348]. Transfection of a cell with RNAs bearing this sequence could increase their packaging into EVs. Research is ongoing into the mechanisms behind RNA selective sorting and how they could be manipulated to facilitate loading[231,348,405]. Unpublished work by Dr. Woffindale in the Wood lab has indicated that loading of miRNA can be enhanced by the co-expression of RNA-binding proteins, particularly when tagged with a membrane-targeting myristoylation domain. However, using methods to overexpress miRNA, the loaded nucleic acid cannot be modified to increase stability as it can with the methods used in this present study. Another proposed method is to load a liposome and subsequently to induce fusion between this loaded liposome and an EV through short membrane-anchored DNA strands mimicking the SNARE proteins[406]. The use of calcium chloride and ethanol which has been used to load DNA into liposomes could potentially be manipulated to load EVs[407]. There are also commercially available kits, for example Exo-Fect from System Biosciences which claim to enable the direct transfection of nucleic acids into isolated exosomes. However, kits such as these present their own difficulties as it is not disclosed what the biologically active component is so it is not known if this will contaminate studies in the same way as a micelle of transfection reagent would[408].

As mentioned, different subgroups of EVs have been reported, and within these categories there may be differences in nucleic acid delivery capacity. For example Kanada *et al*., reported that only MVs were capable of functional transfer of DNA to cells[319]. This would be interesting to study in the context of loading, whether different vesicle subtypes could be more amenable to loading by incubation with cc-siRNA. If the cc-siRNA is integrating into the membrane by the cholesterol tag the membrane composition and fluidity could change and this could be subtype dependent. Before this can be investigated however, improvements in technologies to separate vesicle subtypes must be developed.

The obstacles involved in implementing EVs for medical applications involving RNA delivery may prove difficult to overcome. The source, culture conditions, isolation method, detection/quantification, loading and targeting methods would need to be standardised. However, this study highlights the potential to improve loading efficiency of EVs and to increase their brain delivery. Through further study of EVs and elucidation of the mechanisms by which they can escape the endosome to deliver functional RNA, EV like vesicles could be developed which capitalise on the strengths of EVs without the difficulty in scaling up the production and issues with contamination in the isolation process. These EV mimetics could be more biocompatible and less toxic than existing liposomes and other nanoparticles.

An EV mimetic should have a phospholipid bilayer so that not only can they be internalised into an endosome from which the cargo can escape, but also so they can fuse directly with the target cell plasma membrane, improving internalization of the cargo and eliminating the entry into the endosomal lysosomal pathway[259,409]. Through the study of

both the protein and lipid profile of EVs the optimal membrane components for such a vesicle could be elucidated. To this end, some research has already been performed. The tetraspannin profile can influence the *in vivo* biodistribution and incorporation into cells[410]. EVs have high levels of cholesterol, sphingomyelin and anionic lipids[260,411]. Vesicles formed from the lipid extract of exosomes have been shown to have a similar biodistribution to exosomes and liposomes[323]. Further increasing the cholesterol and sphingomyelin levels and decreasing phosphatidylserine content could potentially decrease clearance by the MPS[341,412]. In addition, in comparison to liposomes which can activate the complement system which increases the rate of clearance, EVs can inhibit complement activation, though the opposite has been seen in EVs derived from tumours[354,412,413].

The idea of an EV mimetic is not novel. Liposomes have been utilised in the field of gene delivery for decades but more recent developments are generating more promising results. Extrusion of monocytes has been used to generate vesicles loaded with chemotherapeutics with a high yield of vesicles bearing EV like properties capable of reducing tumour growth *in vivo*[414]. Another method used to obtain vesicles from cells capitalises on the ability of membranes to self-assemble and involves slicing cells in a microfluidic system. The vesicles generated were capable of encapsulating latex beads[415]. Synthetic vesicles consisting of the lipid fraction of EVs or designed to replicate the lipid composition of EVs and liposomes of phosphatidylcholine and cholesterol display a similar rapid uptake of EVs[323]. Further characterisation of these EV like vesicles is required such as investigation of their immunogenicity, toxicity, biodistribution, targeting and loading capacities for RNA.

Investigation of intrinsic homing and the inclusion of targeting factors on the membrane of EVs or synthetic EVs will be vital to direct the vesicles to the region of interest. In this way a lower dose may be administered to achieve the desired effect. Intrinsic homing of EVs from various sources can be seen here as the biodistribution pattern of EVs from HEK293 cells and DCs, although broadly similar, did display some differences. The targeting strategy employed in this study successfully increased delivery to the brain, but further work to increase this more than the two-fold response seen here and elucidate the rate limiting factors must be performed before it is known which properties of the targeted EVs should be taken forward to synthetic vesicles. It is likely this will involve modifications to evade the MPS. Through targeting, from this study and previous work, it seems that EVs possess the ability to cross the BBB[213]. Future studies on the mechanism behind this would provide the field of nanotechnology with valuable information for the possibility of a systemically delivered treatment for HD.

It should be noted that it is also possible that native EVs within patient brains could actually contribute to the disease mechanism. This has been proposed for the neurological disorders AD, PD and prion diseases and it could be that mHTT is transported between cells in EVs[416–418]. This could potentially contribute to an adverse effect of seeding of mHTT aggregates in recipient cells and would need to be clarified prior to taking EVs or EV mimetics into the clinic. Transcriptomic and proteomic profiling of these EVs from native HD brains compared with EVs from healthy donors would help to determine which endogenous materials may be responsible for these adverse effects to eliminate them from an EV mimetic. It is possible that a treatment to reduce HTT expression would itself prevent this as a decrease in HTT expression would reduce the number of aggregates, limiting the chance they could be passed from cell to cell in an EV.

When considering the role of EVs for HD, it is worth also considering their potential as biomarkers. Although a genetic test is readily available to predict whether or not an individual will develop HD and how many CAG repeats their *mHTT* allele contains, the lack of biomarkers of disease progress halts drug development, as it has for the clinical trials for creatine (NCT00712426) and coenzyme Q10 (NCT00608881). Since EVs can be isolated from plasma their isolation from patients undergoing treatment could potentially yield vital information on the success or failure of any future treatments.

Thus, learning from evolution could guide the development of a more efficient non-toxic gene delivery system. Through the use of EVs themselves, or by mimicking their naturally occurring ability to deliver functional RNA, a mechanism to bypass the BBB and treat HD more effectively may be developed in the future. Artificially created EVs could theoretically be a safe, homogenous and well characterised population capitalising on the innate properties of EVs which make them capable of gene delivery but lacking any components which could mediate adverse effects.

6.4 Concluding Remarks

This thesis adds to a body of knowledge that aims to use silencing *HTT* as a therapeutic strategy for HD. Several different types of nucleic acid based therapeutics were evaluated for their potency, duration of silencing and toxicity and siRNAs were selected as the optimal cargo for loading into EVs. Although siRNAs were selected, CRISPRi and exon skipping ASOs could provide novel treatment strategies for HD, if delivery and toxicity can be overcome.

The work presented here also examined EVs as a delivery vehicle for HD by testing their biodistribution, brain targeting capacity and loading. Brain targeted EVs were found capable of increasing delivery to the brain compared to untargeted EVs, although intrinsic homing and accumulation in organs of the RES for clearance remained after targeting. Loading by electroporation proved challenging as previous reports of loading efficiency may have been overestimated due to siRNA aggregation. However, an alternate method of loading by associating vesicles with cc-siRNA obtained silencing *in vitro* and could be a promising method for further investigation.

To achieve therapeutic effects in the brain in HD, EVs loaded with a therapeutic nucleic acid must reach the brain in sufficient numbers to prevent neurodegeneration. The research documented here indicates that this may be possible in the future as both loading of EVs with cc-siRNA for the silencing of a gene of interest *in vitro,* as well as increased brain targeting were achieved. Through future bioengineering of EV mimetics or mechanisms to avoid fast clearance, as well as further optimisation of loading and targeting parameters, EV based gene therapy may prove to be a promising treatment for HD.

REFERENCES

1. Heemels, M.-T. Neurodegeneration. *Nature* **443,** 767–767 (2006).
2. Gandhi, S. & Abramov, A. Y. Mechanism of oxidative stress in neurodegeneration. *Oxid Med Cell Longev* **2012,** 428010 (2012).
3. Ross, C. A. & Poirier, M. A. Protein aggregation and neurodegenerative disease. *Nat. Med.* **10 Suppl,** S10-17 (2004).
4. Huntington, G. On chorea. George Huntington, M.D. *J Neuropsychiatry Clin Neurosci* **15,** 109–112 (2003).
5. Pringsheim, T. *et al.* The incidence and prevalence of Huntington's disease: a systematic review and meta-analysis. *Mov. Disord.* **27,** 1083–1091 (2012).
6. Karadima, G., Dimovasili, C., Koutsis, G., Vassilopoulos, D. & Panas, M. Age at onset in Huntington's disease: replication study on the association of HAP1. *Parkinsonism Relat. Disord.* **18,** 1027–1028 (2012).
7. Myers, R. H. Huntington's Disease Genetics. *NeuroRx* **1,** 255–262 (2004).
8. Quarrell, O., O'Donovan, K. L., Bandmann, O. & Strong, M. The Prevalence of Juvenile Huntington's Disease: A Review of the Literature and Meta-Analysis. *PLoS Curr* **4,** e4f8606b742ef3 (2012).
9. Quarrell, O. W. J. *et al.* Managing juvenile Huntington's disease. *Neurodegener Dis Manag* **3,** (2013).
10. Walker, F. O. Huntington's disease. *Lancet* **369,** 218–228 (2007).
11. Yanagisawa, N. The spectrum of motor disorders in Huntington's disease. *Clin Neurol Neurosurg* **94 Suppl,** S182-184 (1992).
12. Tabrizi, S. J. *et al.* Biological and clinical manifestations of Huntington's disease in the longitudinal TRACK-HD study: cross-sectional analysis of baseline data. *Lancet Neurol* **8,** 791–801 (2009).
13. Rosenberg, N. K., Sørensen, S. A. & Christensen, A. L. Neuropsychological characteristics of Huntington's disease carriers: a double blind study. *J Med Genet* **32,** 600–604 (1995).
14. Duff, K., Paulsen, J. S., Beglinger, L. J., Langbehn, D. R. & Stout, J. C. Psychiatric Symptoms in Huntington's Disease before Diagnosis: The Predict-HD Study. *Biological Psychiatry* **62,** 1341–1346 (2007).
15. Solomon, A. C. *et al.* Verbal episodic memory declines prior to diagnosis in Huntington's disease. *Neuropsychologia* **45,** 1767–1776 (2007).
16. Gusella, J. F. *et al.* A polymorphic DNA marker genetically linked to Huntington's disease. *Nature* **306,** 234–238 (1983).
17. Gusella, J. F. *et al.* Huntington's disease. *Cold Spring Harb. Symp. Quant. Biol.* **61,** 615–626 (1996).
18. A novel gene containing a trinucleotide repeat that is expanded and unstable on Huntington's disease chromosomes. The Huntington's Disease Collaborative Research Group. *Cell* **72,** 971–983 (1993).
19. Wheeler, V. C. *et al.* Factors associated with HD CAG repeat instability in Huntington disease. *J Med Genet* **44,** 695–701 (2007).
20. Varela, M. A. *et al.* Transfer of genetic therapy across human populations: molecular targets for increasing patient coverage in repeat expansion diseases. *Eur. J. Hum. Genet.* **24,** 271–276 (2016).

21. Pfister, E. L. *et al.* Five siRNAs targeting three SNPs may provide therapy for three-quarters of Huntington's disease patients. *Curr. Biol.* **19,** 774–778 (2009).
22. Zhang, B. *et al.* CCG polymorphisms in the huntingtin gene have no effect on the pathogenesis of patients with Huntington's disease in mainland Chinese families. *J. Neurol. Sci.* **312,** 92–96 (2012).
23. Lee, J.-M. *et al.* CAG repeat expansion in Huntington disease determines age at onset in a fully dominant fashion. *Neurology* **78,** 690–695 (2012).
24. HD iPSC Consortium. Induced pluripotent stem cells from patients with Huntington's disease show CAG-repeat-expansion-associated phenotypes. *Cell Stem Cell* **11,** 264–278 (2012).
25. Rui, Y.-N. *et al.* Huntingtin functions as a scaffold for selective macroautophagy. *Nat Cell Biol* **17,** 262–275 (2015).
26. Atwal, R. S. *et al.* Huntingtin has a membrane association signal that can modulate huntingtin aggregation, nuclear entry and toxicity. *Hum. Mol. Genet.* **16,** 2600–2615 (2007).
27. Ehrnhoefer, D. E., Sutton, L. & Hayden, M. R. Small changes, big impact: posttranslational modifications and function of huntingtin in Huntington disease. *Neuroscientist* **17,** 475–492 (2011).
28. Tartari, M. *et al.* Phylogenetic comparison of huntingtin homologues reveals the appearance of a primitive polyQ in sea urchin. *Mol. Biol. Evol.* **25,** 330–338 (2008).
29. Kim, M. W., Chelliah, Y., Kim, S. W., Otwinowski, Z. & Bezprozvanny, I. Secondary structure of Huntingtin amino-terminal region. *Structure* **17,** 1205–1212 (2009).
30. Dehay, B. & Bertolotti, A. Critical role of the proline-rich region in Huntingtin for aggregation and cytotoxicity in yeast. *J. Biol. Chem.* **281,** 35608–35615 (2006).
31. Southwell, A. L. *et al.* Intrabodies binding the proline-rich domains of mutant huntingtin increase its turnover and reduce neurotoxicity. *J. Neurosci.* **28,** 9013–9020 (2008).
32. Palidwor, G. A. *et al.* Detection of alpha-rod protein repeats using a neural network and application to huntingtin. *PLoS Comput. Biol.* **5,** e1000304 (2009).
33. Li, W., Serpell, L. C., Carter, W. J., Rubinsztein, D. C. & Huntington, J. A. Expression and characterization of full-length human huntingtin, an elongated HEAT repeat protein. *J. Biol. Chem.* **281,** 15916–15922 (2006).
34. Bessert, D. A., Gutridge, K. L., Dunbar, J. C. & Carlock, L. R. The identification of a functional nuclear localization signal in the Huntington disease protein. *Brain Res. Mol. Brain Res.* **33,** 165–173 (1995).
35. Rockabrand, E. *et al.* The first 17 amino acids of Huntingtin modulate its sub-cellular localization, aggregation and effects on calcium homeostasis. *Hum. Mol. Genet.* **16,** 61–77 (2007).
36. Xia, J., Lee, D. H., Taylor, J., Vandelft, M. & Truant, R. Huntingtin contains a highly conserved nuclear export signal. *Hum. Mol. Genet.* **12,** 1393–1403 (2003).
37. Strong, T. V. *et al.* Widespread expression of the human and rat Huntington's disease gene in brain and nonneural tissues. *Nat. Genet.* **5,** 259–265 (1993).
38. Vonsattel, J. P. G. Huntington disease models and human neuropathology: similarities and differences. *Acta Neuropathol* **115,** 55–69 (2008).
39. Nasir, J. *et al.* Targeted disruption of the Huntington's disease gene results in embryonic lethality and behavioral and morphological changes in heterozygotes. *Cell* **81,** 811–823 (1995).

40. Hoffner, G., Kahlem, P. & Djian, P. Perinuclear localization of huntingtin as a consequence of its binding to microtubules through an interaction with beta-tubulin: relevance to Huntington's disease. *J. Cell. Sci.* **115,** 941–948 (2002).
41. DiFiglia, M. *et al.* Huntingtin is a cytoplasmic protein associated with vesicles in human and rat brain neurons. *Neuron* **14,** 1075–1081 (1995).
42. Hilditch-Maguire, P. *et al.* Huntingtin: an iron-regulated protein essential for normal nuclear and perinuclear organelles. *Hum. Mol. Genet.* **9,** 2789–2797 (2000).
43. Velier, J. *et al.* Wild-type and mutant huntingtins function in vesicle trafficking in the secretory and endocytic pathways. *Exp. Neurol.* **152,** 34–40 (1998).
44. Rigamonti, D. *et al.* Wild-type huntingtin protects from apoptosis upstream of caspase-3. *J. Neurosci.* **20,** 3705–3713 (2000).
45. Godin, J. D. *et al.* Huntingtin is required for mitotic spindle orientation and mammalian neurogenesis. *Neuron* **67,** 392–406 (2010).
46. Zuccato, C. *et al.* Brain-derived neurotrophic factor in patients with Huntington's disease. *PLoS ONE* **6,** e22966 (2011).
47. Leavitt, B. R. *et al.* Wild-type huntingtin protects neurons from excitotoxicity. *J. Neurochem.* **96,** 1121–1129 (2006).
48. Rigamonti, D. *et al.* Huntingtin's neuroprotective activity occurs via inhibition of procaspase-9 processing. *J. Biol. Chem.* **276,** 14545–14548 (2001).
49. Zhang, Y. *et al.* Huntingtin inhibits caspase-3 activation. *EMBO J.* **25,** 5896–5906 (2006).
50. Rangone, H. *et al.* Phosphorylation of arfaptin 2 at Ser260 by Akt Inhibits PolyQ-huntingtin-induced toxicity by rescuing proteasome impairment. *J. Biol. Chem.* **280,** 22021–22028 (2005).
51. Perutz, M. F., Johnson, T., Suzuki, M. & Finch, J. T. Glutamine repeats as polar zippers: their possible role in inherited neurodegenerative diseases. *Proc Natl Acad Sci U S A* **91,** 5355–5358 (1994).
52. Steffan, J. S. *et al.* The Huntington's disease protein interacts with p53 and CREB-binding protein and represses transcription. *Proc. Natl. Acad. Sci. U.S.A.* **97,** 6763–6768 (2000).
53. Zuccato, C. *et al.* Huntingtin interacts with REST/NRSF to modulate the transcription of NRSE-controlled neuronal genes. *Nat Genet* **35,** 76–83 (2003).
54. Savas, J. N. *et al.* A role for huntington disease protein in dendritic RNA granules. *J. Biol. Chem.* **285,** 13142–13153 (2010).
55. Caviston, J. P., Ross, J. L., Antony, S. M., Tokito, M. & Holzbaur, E. L. F. Huntingtin facilitates dynein/dynactin-mediated vesicle transport. *Proc. Natl. Acad. Sci. U.S.A.* **104,** 10045–10050 (2007).
56. Zala, D., Hinckelmann, M.-V. & Saudou, F. Huntingtin's function in axonal transport is conserved in Drosophila melanogaster. *PLoS ONE* **8,** e60162 (2013).
57. Gunawardena, S. *et al.* Disruption of axonal transport by loss of huntingtin or expression of pathogenic polyQ proteins in Drosophila. *Neuron* **40,** 25–40 (2003).
58. Wong, Y. C. & Holzbaur, E. L. F. The regulation of autophagosome dynamics by huntingtin and HAP1 is disrupted by expression of mutant huntingtin, leading to defective cargo degradation. *J. Neurosci.* **34,** 1293–1305 (2014).

59. Sun, Y., Savanenin, A., Reddy, P. H. & Liu, Y. F. Polyglutamine-expanded huntingtin promotes sensitization of N-methyl-D-aspartate receptors via post-synaptic density 95. *J. Biol. Chem.* **276,** 24713–24718 (2001).
60. El-Daher, M.-T. *et al.* Huntingtin proteolysis releases non-polyQ fragments that cause toxicity through dynamin 1 dysregulation. *EMBO J.* **34,** 2255–2271 (2015).
61. Modregger, J., Schmidt, A. A., Ritter, B., Huttner, W. B. & Plomann, M. Characterization of Endophilin B1b, a brain-specific membrane-associated lysophosphatidic acid acyl transferase with properties distinct from endophilin A1. *J. Biol. Chem.* **278,** 4160–4167 (2003).
62. Li, X. *et al.* A function of huntingtin in guanine nucleotide exchange on Rab11. *Neuroreport* **19,** 1643–1647 (2008).
63. Harjes, P. & Wanker, E. E. The hunt for huntingtin function: interaction partners tell many different stories. *Trends Biochem. Sci.* **28,** 425–433 (2003).
64. Culver, B. P. *et al.* Proteomic analysis of wild-type and mutant huntingtin-associated proteins in mouse brains identifies unique interactions and involvement in protein synthesis. *J. Biol. Chem.* **287,** 21599–21614 (2012).
65. Zheng, S. *et al.* Deletion of the huntingtin polyglutamine stretch enhances neuronal autophagy and longevity in mice. *PLoS Genet.* **6,** e1000838 (2010).
66. Neveklovska, M., Clabough, E. B. D., Steffan, J. S. & Zeitlin, S. O. Deletion of the huntingtin proline-rich region does not significantly affect normal huntingtin function in mice. *J Huntingtons Dis* **1,** 71–87 (2012).
67. Kalchman, M. A. *et al.* Huntingtin is ubiquitinated and interacts with a specific ubiquitin-conjugating enzyme. *J. Biol. Chem.* **271,** 19385–19394 (1996).
68. Beckerman, M. *Fundamentals of Neurodegeneration and Protein Misfolding Disorders*. (Springer, 2015).
69. Luo, S., Vacher, C., Davies, J. E. & Rubinsztein, D. C. Cdk5 phosphorylation of huntingtin reduces its cleavage by caspases: implications for mutant huntingtin toxicity. *J. Cell Biol.* **169,** 647–656 (2005).
70. Humbert, S. *et al.* The IGF-1/Akt pathway is neuroprotective in Huntington's disease and involves Huntingtin phosphorylation by Akt. *Dev. Cell* **2,** 831–837 (2002).
71. Warby, S. C. *et al.* Huntingtin phosphorylation on serine 421 is significantly reduced in the striatum and by polyglutamine expansion in vivo. *Hum. Mol. Genet.* **14,** 1569–1577 (2005).
72. Schilling, B. *et al.* Huntingtin phosphorylation sites mapped by mass spectrometry. Modulation of cleavage and toxicity. *J. Biol. Chem.* **281,** 23686–23697 (2006).
73. Gu, X. *et al.* Serines 13 and 16 are critical determinants of full-length human mutant huntingtin induced disease pathogenesis in HD mice. *Neuron* **64,** 828–840 (2009).
74. Maiuri, T., Woloshansky, T., Xia, J. & Truant, R. The huntingtin N17 domain is a multifunctional CRM1 and Ran-dependent nuclear and cilial export signal. *Hum. Mol. Genet.* **22,** 1383–1394 (2013).
75. Steffan, J. S. *et al.* SUMO modification of Huntingtin and Huntington's disease pathology. *Science* **304,** 100–104 (2004).

76. Yanai, A. *et al.* Palmitoylation of huntingtin by HIP14 is essential for its trafficking and function. *Nat. Neurosci.* **9,** 824–831 (2006).
77. Jeong, H. *et al.* Acetylation targets mutant huntingtin to autophagosomes for degradation. *Cell* **137,** 60–72 (2009).
78. Zeitlin, S., Liu, J. P., Chapman, D. L., Papaioannou, V. E. & Efstratiadis, A. Increased apoptosis and early embryonic lethality in mice nullizygous for the Huntington's disease gene homologue. *Nat. Genet.* **11,** 155–163 (1995).
79. Grondin, R. *et al.* Six-month partial suppression of Huntingtin is well tolerated in the adult rhesus striatum. *Brain* **135,** 1197–1209 (2012).
80. Andrew, S. E. *et al.* The relationship between trinucleotide (CAG) repeat length and clinical features of Huntington's disease. *Nat. Genet.* **4,** 398–403 (1993).
81. Ratovitski, T. *et al.* Mutant huntingtin N-terminal fragments of specific size mediate aggregation and toxicity in neuronal cells. *J. Biol. Chem.* **284,** 10855–10867 (2009).
82. Davies, S. W. *et al.* Formation of neuronal intranuclear inclusions underlies the neurological dysfunction in mice transgenic for the HD mutation. *Cell* **90,** 537–548 (1997).
83. Arrasate, M., Mitra, S., Schweitzer, E. S., Segal, M. R. & Finkbeiner, S. Inclusion body formation reduces levels of mutant huntingtin and the risk of neuronal death. *Nature* **431,** 805–810 (2004).
84. Sahl, S. J., Weiss, L. E., Duim, W. C., Frydman, J. & Moerner, W. E. Cellular inclusion bodies of mutant huntingtin exon 1 obscure small fibrillar aggregate species. *Sci Rep* **2,** 895 (2012).
85. DiFiglia, M. *et al.* Aggregation of huntingtin in neuronal intranuclear inclusions and dystrophic neurites in brain. *Science* **277,** 1990–1993 (1997).
86. Scherzinger, E. *et al.* Self-assembly of polyglutamine-containing huntingtin fragments into amyloid-like fibrils: implications for Huntington's disease pathology. *Proc. Natl. Acad. Sci. U.S.A.* **96,** 4604–4609 (1999).
87. Li, H., Li, S. H., Yu, Z. X., Shelbourne, P. & Li, X. J. Huntingtin aggregate-associated axonal degeneration is an early pathological event in Huntington's disease mice. *J. Neurosci.* **21,** 8473–8481 (2001).
88. Chen, S., Ferrone, F. A. & Wetzel, R. Huntington's disease age-of-onset linked to polyglutamine aggregation nucleation. *Proc. Natl. Acad. Sci. U.S.A.* **99,** 11884–11889 (2002).
89. Jayaraman, M. *et al.* Slow amyloid nucleation via α-helix-rich oligomeric intermediates in short polyglutamine-containing huntingtin fragments. *J. Mol. Biol.* **415,** 881–899 (2012).
90. Haass, C. & Selkoe, D. J. Soluble protein oligomers in neurodegeneration: lessons from the Alzheimer's amyloid beta-peptide. *Nat. Rev. Mol. Cell Biol.* **8,** 101–112 (2007).
91. Landles, C. *et al.* Proteolysis of mutant huntingtin produces an exon 1 fragment that accumulates as an aggregated protein in neuronal nuclei in Huntington disease. *J. Biol. Chem.* **285,** 8808–8823 (2010).
92. Schilling, G. *et al.* Characterization of huntingtin pathologic fragments in human Huntington disease, transgenic mice, and cell models. *J. Neuropathol. Exp. Neurol.* **66,** 313–320 (2007).
93. Carter, R. J. *et al.* Characterization of progressive motor deficits in mice transgenic for the human Huntington's disease mutation. *J. Neurosci.* **19,** 3248–3257 (1999).

94. Gafni, J. *et al.* Inhibition of calpain cleavage of huntingtin reduces toxicity: accumulation of calpain/caspase fragments in the nucleus. *J. Biol. Chem.* **279,** 20211–20220 (2004).
95. Sathasivam, K. *et al.* Aberrant splicing of HTT generates the pathogenic exon 1 protein in Huntington disease. *Proc. Natl. Acad. Sci. U.S.A.* **110,** 2366–2370 (2013).
96. Tam, S. *et al.* The chaperonin TRiC blocks a huntingtin sequence element that promotes the conformational switch to aggregation. *Nat. Struct. Mol. Biol.* **16,** 1279–1285 (2009).
97. Squitieri, F., Frati, L., Ciarmiello, A., Lastoria, S. & Quarrell, O. Juvenile Huntington's disease: does a dosage-effect pathogenic mechanism differ from the classical adult disease? *Mech. Ageing Dev.* **127,** 208–212 (2006).
98. Frost, B. & Diamond, M. I. Prion-like mechanisms in neurodegenerative diseases. *Nat. Rev. Neurosci.* **11,** 155–159 (2010).
99. Ren, P.-H. *et al.* Cytoplasmic penetration and persistent infection of mammalian cells by polyglutamine aggregates. *Nat. Cell Biol.* **11,** 219–225 (2009).
100. Kazantsev, A., Preisinger, E., Dranovsky, A., Goldgaber, D. & Housman, D. Insoluble detergent-resistant aggregates form between pathological and nonpathological lengths of polyglutamine in mammalian cells. *Proc. Natl. Acad. Sci. U.S.A.* **96,** 11404–11409 (1999).
101. Steffan, J. S. *et al.* Histone deacetylase inhibitors arrest polyglutamine-dependent neurodegeneration in Drosophila. *Nature* **413,** 739–743 (2001).
102. Hodges, A. *et al.* Regional and cellular gene expression changes in human Huntington's disease brain. *Hum. Mol. Genet.* **15,** 965–977 (2006).
103. Cui, L. *et al.* Transcriptional repression of PGC-1alpha by mutant huntingtin leads to mitochondrial dysfunction and neurodegeneration. *Cell* **127,** 59–69 (2006).
104. Nucifora, F. C. *et al.* Interference by huntingtin and atrophin-1 with cbp-mediated transcription leading to cellular toxicity. *Science* **291,** 2423–2428 (2001).
105. Benn, C. L. *et al.* Huntingtin modulates transcription, occupies gene promoters in vivo, and binds directly to DNA in a polyglutamine-dependent manner. *J. Neurosci.* **28,** 10720–10733 (2008).
106. Chandwani, S. *et al.* Induction of DARPP-32 by brain-derived neurotrophic factor in striatal neurons in vitro is modified by histone deacetylase inhibitors and Nab2. *PLoS ONE* **8,** e76842 (2013).
107. Gauthier, L. R. *et al.* Huntingtin controls neurotrophic support and survival of neurons by enhancing BDNF vesicular transport along microtubules. *Cell* **118,** 127–138 (2004).
108. Drouet, V. *et al.* Allele-specific silencing of mutant huntingtin in rodent brain and human stem cells. *PLoS ONE* **9,** e99341 (2014).
109. Balch, W. E., Morimoto, R. I., Dillin, A. & Kelly, J. W. Adapting proteostasis for disease intervention. *Science* **319,** 916–919 (2008).
110. Hay, D. G. *et al.* Progressive decrease in chaperone protein levels in a mouse model of Huntington's disease and induction of stress proteins as a therapeutic approach. *Hum. Mol. Genet.* **13,** 1389–1405 (2004).
111. Vidal, R., Caballero, B., Couve, A. & Hetz, C. Converging pathways in the occurrence of endoplasmic reticulum (ER) stress in Huntington's disease. *Curr. Mol. Med.* **11,** 1–12 (2011).

112. Martin, D. D. O., Ladha, S., Ehrnhoefer, D. E. & Hayden, M. R. Autophagy in Huntington disease and huntingtin in autophagy. *Trends Neurosci.* **38,** 26–35 (2015).
113. Bennett, E. J., Bence, N. F., Jayakumar, R. & Kopito, R. R. Global impairment of the ubiquitin-proteasome system by nuclear or cytoplasmic protein aggregates precedes inclusion body formation. *Mol. Cell* **17,** 351–365 (2005).
114. Bennett, E. J. *et al.* Global changes to the ubiquitin system in Huntington's disease. *Nature* **448,** 704–708 (2007).
115. Martinez-Vicente, M. *et al.* Cargo recognition failure is responsible for inefficient autophagy in Huntington's disease. *Nat. Neurosci.* **13,** 567–576 (2010).
116. Labbadia, J. *et al.* Altered chromatin architecture underlies progressive impairment of the heat shock response in mouse models of Huntington disease. *J. Clin. Invest.* **121,** 3306–3319 (2011).
117. Browne, S. E. Mitochondria and Huntington's disease pathogenesis: insight from genetic and chemical models. *Ann. N. Y. Acad. Sci.* **1147,** 358–382 (2008).
118. Bogdanov, M. B., Andreassen, O. A., Dedeoglu, A., Ferrante, R. J. & Beal, M. F. Increased oxidative damage to DNA in a transgenic mouse model of Huntington's disease. *J. Neurochem.* **79,** 1246–1249 (2001).
119. Saft, C. *et al.* Mitochondrial impairment in patients and asymptomatic mutation carriers of Huntington's disease. *Mov. Disord.* **20,** 674–679 (2005).
120. Dong, X., Wang, Y. & Qin, Z. Molecular mechanisms of excitotoxicity and their relevance to pathogenesis of neurodegenerative diseases. *Acta Pharmacol. Sin.* **30,** 379–387 (2009).
121. Wyss-Coray, T. & Mucke, L. Inflammation in neurodegenerative disease--a double-edged sword. *Neuron* **35,** 419–432 (2002).
122. Pérez-Severiano, F. *et al.* Increased formation of reactive oxygen species, but no changes in glutathione peroxidase activity, in striata of mice transgenic for the Huntington's disease mutation. *Neurochem. Res.* **29,** 729–733 (2004).
123. Singhrao, S. K., Neal, J. W., Morgan, B. P. & Gasque, P. Increased complement biosynthesis by microglia and complement activation on neurons in Huntington's disease. *Exp. Neurol.* **159,** 362–376 (1999).
124. Björkqvist, M. *et al.* A novel pathogenic pathway of immune activation detectable before clinical onset in Huntington's disease. *J Exp Med* **205,** 1869–1877 (2008).
125. Pavese, N. *et al.* Microglial activation correlates with severity in Huntington disease: a clinical and PET study. *Neurology* **66,** 1638–1643 (2006).
126. Shin, J.-Y. *et al.* Expression of mutant huntingtin in glial cells contributes to neuronal excitotoxicity. *J. Cell Biol.* **171,** 1001–1012 (2005).
127. Bradford, J. *et al.* Mutant huntingtin in glial cells exacerbates neurological symptoms of Huntington disease mice. *J. Biol. Chem.* **285,** 10653–10661 (2010).
128. Rosas, H. D. *et al.* Cerebral cortex and the clinical expression of Huntington's disease: complexity and heterogeneity. *Brain* **131,** 1057–1068 (2008).
129. Aylward, E. H. *et al.* Longitudinal change in regional brain volumes in prodromal Huntington disease. *J. Neurol. Neurosurg. Psychiatr.* **82,** 405–410 (2011).

130. Mitchell, I. J., Cooper, A. J. & Griffiths, M. R. The selective vulnerability of striatopallidal neurons. *Prog. Neurobiol.* **59,** 691–719 (1999).
131. Aylward, E. H. *et al.* Regional atrophy associated with cognitive and motor function in prodromal Huntington disease. *J Huntingtons Dis* **2,** 477–489 (2013).
132. Cicchetti, F., Soulet, D. & Freeman, T. B. Neuronal degeneration in striatal transplants and Huntington's disease: potential mechanisms and clinical implications. *Brain* **134,** 641–652 (2011).
133. Coyle, J. T. & Schwarcz, R. Lesion of striatal neurones with kainic acid provides a model for Huntington's chorea. *Nature* **263,** 244–246 (1976).
134. Liu, F. *et al.* Ketamine-induced neuronal damage and altered N-methyl-D-aspartate receptor function in rat primary forebrain culture. *Toxicol. Sci.* **131,** 548–557 (2013).
135. Brouillet, E., Jacquard, C., Bizat, N. & Blum, D. 3-Nitropropionic acid: a mitochondrial toxin to uncover physiopathological mechanisms underlying striatal degeneration in Huntington's disease. *J. Neurochem.* **95,** 1521–1540 (2005).
136. Conner, J. M., Lauterborn, J. C., Yan, Q., Gall, C. M. & Varon, S. Distribution of brain-derived neurotrophic factor (BDNF) protein and mRNA in the normal adult rat CNS: evidence for anterograde axonal transport. *J. Neurosci.* **17,** 2295–2313 (1997).
137. Subramaniam, S., Sixt, K. M., Barrow, R. & Snyder, S. H. Rhes, a striatal specific protein, mediates mutant-huntingtin cytotoxicity. *Science* **324,** 1327–1330 (2009).
138. Swarnkar, S. *et al.* Ectopic expression of the striatal-enriched GTPase Rhes elicits cerebellar degeneration and an ataxia phenotype in Huntington's disease. *Neurobiol. Dis.* **82,** 66–77 (2015).
139. van der Burg, J. M. M., Björkqvist, M. & Brundin, P. Beyond the brain: widespread pathology in Huntington's disease. *Lancet Neurol* **8,** 765–774 (2009).
140. Savani, A. A. & Login, I. S. Tetrabenazine as antichorea therapy in Huntington disease: a randomized controlled trial. *Neurology* **68,** 797; author reply 797 (2007).
141. Nance, M. A. Comprehensive care in Huntington's disease: a physician's perspective. *Brain Res. Bull.* **72,** 175–178 (2007).
142. Mestre, T. A. & Ferreira, J. J. An evidence-based approach in the treatment of Huntington's disease. *Parkinsonism Relat. Disord.* **18,** 316–320 (2012).
143. Priller, J., Ecker, D., Landwehrmeyer, B. & Craufurd, D. A Europe-wide assessment of current medication choices in Huntington's disease. *Mov. Disord.* **23,** 1788 (2008).
144. Groves, M. *et al.* An International Survey-based Algorithm for the Pharmacologic Treatment of Irritability in Huntington's Disease. *PLoS Curr* **3,** (2011).
145. Anderson, K. *et al.* An International Survey-based Algorithm for the Pharmacologic Treatment of Obsessive-Compulsive Behaviors in Huntington's Disease. *PLoS Curr* **3,** (2011).
146. Burgunder, J.-M. *et al.* An International Survey-based Algorithm for the Pharmacologic Treatment of Chorea in Huntington's Disease. *PLoS Curr* **3,** RRN1260 (2011).
147. Gibrat, C. & Cicchetti, F. Potential of cystamine and cysteamine in the treatment of neurodegenerative diseases. *Prog. Neuropsychopharmacol. Biol. Psychiatry* **35,** 380–389 (2011).
148. Wojtecki, L. *et al.* A Prospective Pilot Trial for Pallidal Deep Brain Stimulation in Huntington's Disease. *Front Neurol* **6,** 177 (2015).

149. Cisbani, G. *et al.* Striatal allografts in patients with Huntington's disease: impact of diminished astrocytes and vascularization on graft viability. *Brain* **136,** 433–443 (2013).
150. Stiles, D. K. *et al.* Widespread suppression of huntingtin with convection-enhanced delivery of siRNA. *Exp. Neurol.* **233,** 463–471 (2012).
151. McBride, J. L. *et al.* Preclinical safety of RNAi-mediated HTT suppression in the rhesus macaque as a potential therapy for Huntington's disease. *Mol. Ther.* **19,** 2152–2162 (2011).
152. DiFiglia, M. *et al.* Therapeutic silencing of mutant huntingtin with siRNA attenuates striatal and cortical neuropathology and behavioral deficits. *Proc. Natl. Acad. Sci. U.S.A.* **104,** 17204–17209 (2007).
153. Garriga-Canut, M. *et al.* Synthetic zinc finger repressors reduce mutant huntingtin expression in the brain of R6/2 mice. *Proc. Natl. Acad. Sci. U.S.A.* **109,** E3136-3145 (2012).
154. Chopra, V. *et al.* A small-molecule therapeutic lead for Huntington's disease: preclinical pharmacology and efficacy of C2-8 in the R6/2 transgenic mouse. *Proc. Natl. Acad. Sci. U.S.A.* **104,** 16685–16689 (2007).
155. Tanaka, M. *et al.* Trehalose alleviates polyglutamine-mediated pathology in a mouse model of Huntington disease. *Nat. Med.* **10,** 148–154 (2004).
156. Jia, H., Morris, C. D., Williams, R. M., Loring, J. F. & Thomas, E. A. HDAC inhibition imparts beneficial transgenerational effects in Huntington's disease mice via altered DNA and histone methylation. *Proc. Natl. Acad. Sci. U.S.A.* **112,** E56-64 (2015).
157. Hockly, E. *et al.* Suberoylanilide hydroxamic acid, a histone deacetylase inhibitor, ameliorates motor deficits in a mouse model of Huntington's disease. *Proc. Natl. Acad. Sci. U.S.A.* **100,** 2041–2046 (2003).
158. Di Pardo, A. *et al.* Ganglioside GM1 induces phosphorylation of mutant huntingtin and restores normal motor behavior in Huntington disease mice. *Proc. Natl. Acad. Sci. U.S.A.* **109,** 3528–3533 (2012).
159. Sontag, E. M. *et al.* Exogenous delivery of chaperonin subunit fragment ApiCCT1 modulates mutant Huntingtin cellular phenotypes. *Proc Natl Acad Sci U S A* **110,** 3077–3082 (2013).
160. Sandhir, R., Mahajan, N., Mehrotra, A., Aggarwal, A. & Sunkaria, A. 4-hydroxy tempo improves mitochondrial and neurobehavioral deficits in experimental model of Huntington's disease. *Synapse* **69,** 128–138 (2015).
161. Bouchard, J. *et al.* Cannabinoid receptor 2 signaling in peripheral immune cells modulates disease onset and severity in mouse models of Huntington's disease. *J. Neurosci.* **32,** 18259–18268 (2012).
162. Jiang, M. *et al.* Small-molecule TrkB receptor agonists improve motor function and extend survival in a mouse model of Huntington's disease. *Hum. Mol. Genet.* **22,** 2462–2470 (2013).
163. Simmons, D. A. *et al.* A small molecule TrkB ligand reduces motor impairment and neuropathology in R6/2 and BACHD mouse models of Huntington's disease. *J. Neurosci.* **33,** 18712–18727 (2013).
164. Clément, S., Gargiulo, M., Feingold, J. & Durr, A. Guidelines for presymptomatic testing for Huntington's disease: past, present and future in France. *Rev. Neurol. (Paris)* **171,** 572–580 (2015).
165. Yamamoto, A., Lucas, J. J. & Hen, R. Reversal of neuropathology and motor dysfunction in a conditional model of Huntington's disease. *Cell* **101,** 57–66 (2000).

166. White, J. K. *et al.* Huntingtin is required for neurogenesis and is not impaired by the Huntington's disease CAG expansion. *Nat. Genet.* **17,** 404–410 (1997).
167. Reiner, A. *et al.* Neurons lacking huntingtin differentially colonize brain and survive in chimeric mice. *J. Neurosci.* **21,** 7608–7619 (2001).
168. Molero, A. E. *et al.* Impairment of developmental stem cell-mediated striatal neurogenesis and pluripotency genes in a knock-in model of Huntington's disease. *Proc. Natl. Acad. Sci. U.S.A.* **106,** 21900–21905 (2009).
169. Reiner, A., Dragatsis, I., Zeitlin, S. & Goldowitz, D. Wild-type huntingtin plays a role in brain development and neuronal survival. *Mol. Neurobiol.* **28,** 259–276 (2003).
170. Hu, J. *et al.* Allele-specific silencing of mutant huntingtin and ataxin-3 genes by targeting expanded CAG repeats in mRNAs. *Nat. Biotechnol.* **27,** 478–484 (2009).
171. Leuschner, P. J. F., Ameres, S. L., Kueng, S. & Martinez, J. Cleavage of the siRNA passenger strand during RISC assembly in human cells. *EMBO Rep.* **7,** 314–320 (2006).
172. Wang, Y. *et al.* Nucleation, propagation and cleavage of target RNAs in argonaute silencing complexes. *Nature* **461,** 754–761 (2009).
173. Meister, G. *et al.* Human Argonaute2 Mediates RNA Cleavage Targeted by miRNAs and siRNAs. *Molecular Cell* **15,** 185–197 (2004).
174. Doench, J. G., Petersen, C. P. & Sharp, P. A. siRNAs can function as miRNAs. *Genes Dev* **17,** 438–442 (2003).
175. Fabian, M. R., Sonenberg, N. & Filipowicz, W. Regulation of mRNA translation and stability by microRNAs. *Annu. Rev. Biochem.* **79,** 351–379 (2010).
176. Agrawal, S., Temsamani, J. & Tang, J. Y. Pharmacokinetics, biodistribution, and stability of oligodeoxynucleotide phosphorothioates in mice. *Proc Natl Acad Sci U S A* **88,** 7595–7599 (1991).
177. Allerson, C. R. *et al.* Fully 2'-Modified Oligonucleotide Duplexes with Improved in Vitro Potency and Stability Compared to Unmodified Small Interfering RNA. *J. Med. Chem.* **48,** 901–904 (2005).
178. Tafer, H. Bioinformatics of siRNA design. *Methods Mol. Biol.* **1097,** 477–490 (2014).
179. Ozcan, G., Ozpolat, B., Coleman, R. L., Sood, A. K. & Lopez-Berestein, G. Preclinical and clinical development of siRNA-based therapeutics. *Adv. Drug Deliv. Rev.* **87,** 108–119 (2015).
180. Grondin, R. *et al.* Onset Time and Durability of Huntingtin Suppression in Rhesus Putamen After Direct Infusion of Antihuntingtin siRNA. *Mol Ther Nucleic Acids* **4,** e245 (2015).
181. An assessment of the antisense properties of RNase H-competent and steric-blocking oligomers. Available at: http://www.ncbi.nlm.nih.gov/pmc/articles/PMC306831/. (Accessed: 27th March 2016)
182. Role of RNase H in hybrid-arrested translation by antisense oligonucleotides. Available at: http://www.ncbi.nlm.nih.gov/pmc/articles/PMC281677/. (Accessed: 27th March 2016)
183. Kurreck, J., Wyszko, E., Gillen, C. & Erdmann, V. A. Design of antisense oligonucleotides stabilized by locked nucleic acids. *Nucleic Acids Res* **30,** 1911–1918 (2002).
184. Elmén, J. *et al.* Locked nucleic acid (LNA) mediated improvements in siRNA stability and functionality. *Nucleic Acids Res.* **33,** 439–447 (2005).

185. Zamaratski, E., Pradeepkumar, P. I. & Chattopadhyaya, J. A critical survey of the structure-function of the antisense oligo/RNA heteroduplex as substrate for RNase H. *J. Biochem. Biophys. Methods* **48,** 189–208 (2001).
186. Li, N., Li, Q., Tian, X.-Q., Qian, H.-Y. & Yang, Y.-J. Mipomersen is a promising therapy in the management of hypercholesterolemia: a meta-analysis of randomized controlled trials. *Am J Cardiovasc Drugs* **14,** 367–376 (2014).
187. Roehr, B. Fomivirsen approved for CMV retinitis. *J Int Assoc Physicians AIDS Care* **4,** 14–16 (1998).
188. Solomon, S. D., Lindsley, K., Vedula, S. S., Krzystolik, M. G. & Hawkins, B. S. Anti-vascular endothelial growth factor for neovascular age-related macular degeneration. *Cochrane Database Syst Rev* **8,** CD005139 (2014).
189. Sun, Q., Mayeda, A., Hampson, R. K., Krainer, A. R. & Rottman, F. M. General splicing factor SF2/ASF promotes alternative splicing by binding to an exonic splicing enhancer. *Genes Dev.* **7,** 2598–2608 (1993).
190. Choung, S., Kim, Y. J., Kim, S., Park, H.-O. & Choi, Y.-C. Chemical modification of siRNAs to improve serum stability without loss of efficacy. *Biochem. Biophys. Res. Commun.* **342,** 919–927 (2006).
191. Cirak, S. *et al.* Exon skipping and dystrophin restoration in patients with Duchenne muscular dystrophy after systemic phosphorodiamidate morpholino oligomer treatment: an open-label, phase 2, dose-escalation study. *The Lancet* **378,** 595–605 (2011).
192. McClorey, G., Moulton, H. M., Iversen, P. L., Fletcher, S. & Wilton, S. D. Antisense oligonucleotide-induced exon skipping restores dystrophin expression in vitro in a canine model of DMD. *Gene Ther* **13,** 1373–1381 (2006).
193. Goemans, N. M. *et al.* Systemic administration of PRO051 in Duchenne's muscular dystrophy. *N. Engl. J. Med.* **364,** 1513–1522 (2011).
194. van Deutekom, J. C. *et al.* Local dystrophin restoration with antisense oligonucleotide PRO051. *N. Engl. J. Med.* **357,** 2677–2686 (2007).
195. Evers, M. M. *et al.* Preventing formation of toxic N-terminal huntingtin fragments through antisense oligonucleotide-mediated protein modification. *Nucleic Acid Ther* **24,** 4–12 (2014).
196. Mali, P. *et al.* RNA-guided human genome engineering via Cas9. *Science* **339,** 823–826 (2013).
197. Barrangou, R. *et al.* CRISPR provides acquired resistance against viruses in prokaryotes. *Science* **315,** 1709–1712 (2007).
198. Hsu, P. D. *et al.* DNA targeting specificity of RNA-guided Cas9 nucleases. *Nat Biotech* **31,** 827–832 (2013).
199. Qi, L. S. *et al.* Repurposing CRISPR as an RNA-guided platform for sequence-specific control of gene expression. *Cell* **152,** 1173–1183 (2013).
200. Paddison, P. J., Caudy, A. A. & Hannon, G. J. Stable suppression of gene expression by RNAi in mammalian cells. *Proc. Natl. Acad. Sci. U.S.A.* **99,** 1443–1448 (2002).
201. Sui, G. *et al.* A DNA vector-based RNAi technology to suppress gene expression in mammalian cells. *Proc. Natl. Acad. Sci. U.S.A.* **99,** 5515–5520 (2002).

202. Brummelkamp, T. R., Bernards, R. & Agami, R. A system for stable expression of short interfering RNAs in mammalian cells. *Science* **296,** 550–553 (2002).
203. Huang, B. & Kochanek, S. Adenovirus-mediated silencing of huntingtin expression by shRNA. *Hum. Gene Ther.* **16,** 618–626 (2005).
204. Gilbert, L. A. *et al.* CRISPR-mediated modular RNA-guided regulation of transcription in eukaryotes. *Cell* **154,** 442–451 (2013).
205. Gilbert, L. A. *et al.* Genome-Scale CRISPR-Mediated Control of Gene Repression and Activation. *Cell* **159,** 647–661 (2014).
206. Goodman, B. S., Posecion, L. W. F., Mallempati, S. & Bayazitoglu, M. Complications and pitfalls of lumbar interlaminar and transforaminal epidural injections. *Curr Rev Musculoskelet Med* **1,** 212–222 (2008).
207. Armulik, A. *et al.* Pericytes regulate the blood-brain barrier. *Nature* **468,** 557–561 (2010).
208. Willis, C. L. Imaging in vivo astrocyte/endothelial cell interactions at the blood-brain barrier. *Methods Mol. Biol.* **814,** 515–529 (2012).
209. Daneman, R., Zhou, L., Kebede, A. A. & Barres, B. A. Pericytes are required for blood-brain barrier integrity during embryogenesis. *Nature* **468,** 562–566 (2010).
210. Araya, R. *et al.* BMP signaling through BMPRIA in astrocytes is essential for proper cerebral angiogenesis and formation of the blood-brain-barrier. *Mol. Cell. Neurosci.* **38,** 417–430 (2008).
211. Pardridge, W. M. Blood-brain barrier delivery. *Drug Discov. Today* **12,** 54–61 (2007).
212. Valadi, H. *et al.* Exosome-mediated transfer of mRNAs and microRNAs is a novel mechanism of genetic exchange between cells. *Nat. Cell Biol.* **9,** 654–659 (2007).
213. Alvarez-Erviti, L. *et al.* Delivery of siRNA to the mouse brain by systemic injection of targeted exosomes. *Nat. Biotechnol.* **29,** 341–345 (2011).
214. Deregibus, M. C. *et al.* Endothelial progenitor cell derived microvesicles activate an angiogenic program in endothelial cells by a horizontal transfer of mRNA. *Blood* **110,** 2440–2448 (2007).
215. Cocucci, E., Racchetti, G. & Meldolesi, J. Shedding microvesicles: artefacts no more. *Trends Cell Biol.* **19,** 43–51 (2009).
216. Svensson, K. J. *et al.* Hypoxia triggers a proangiogenic pathway involving cancer cell microvesicles and PAR-2-mediated heparin-binding EGF signaling in endothelial cells. *Proc. Natl. Acad. Sci. U.S.A.* **108,** 13147–13152 (2011).
217. Sanderson, M. P. *et al.* Generation of novel, secreted epidermal growth factor receptor (EGFR/ErbB1) isoforms via metalloprotease-dependent ectodomain shedding and exosome secretion. *J. Cell. Biochem.* **103,** 1783–1797 (2008).
218. Dainiak, N. & Sorba, S. Intracellular regulation of the production and release of human erythroid-directed lymphokines. *J. Clin. Invest.* **87,** 213–220 (1991).
219. Enjeti, A. K., Lincz, L. F. & Seldon, M. Detection and measurement of microparticles: an evolving research tool for vascular biology. *Semin. Thromb. Hemost.* **33,** 771–779 (2007).
220. Aupeix, K. *et al.* The significance of shed membrane particles during programmed cell death in vitro, and in vivo, in HIV-1 infection. *J. Clin. Invest.* **99,** 1546–1554 (1997).

221. Théry, C. *et al.* Proteomic analysis of dendritic cell-derived exosomes: a secreted subcellular compartment distinct from apoptotic vesicles. *J. Immunol.* **166,** 7309–7318 (2001).
222. Hristov, M., Erl, W., Linder, S. & Weber, P. C. Apoptotic bodies from endothelial cells enhance the number and initiate the differentiation of human endothelial progenitor cells in vitro. *Blood* **104,** 2761–2766 (2004).
223. Taylor, M. P. & Kirkegaard, K. Potential subversion of autophagosomal pathway by picornaviruses. *Autophagy* **4,** 286–289 (2008).
224. Simpson, R. J., Jensen, S. S. & Lim, J. W. E. Proteomic profiling of exosomes: current perspectives. *Proteomics* **8,** 4083–4099 (2008).
225. Mathivanan, S. *et al.* Proteomics analysis of A33 immunoaffinity-purified exosomes released from the human colon tumor cell line LIM1215 reveals a tissue-specific protein signature. *Mol. Cell Proteomics* **9,** 197–208 (2010).
226. Stoorvogel, W., Strous, G. J., Geuze, H. J., Oorschot, V. & Schwartz, A. L. Late endosomes derive from early endosomes by maturation. *Cell* **65,** 417–427 (1991).
227. Futter, C. E., Collinson, L. M., Backer, J. M. & Hopkins, C. R. Human VPS34 is required for internal vesicle formation within multivesicular endosomes. *J. Cell Biol.* **155,** 1251–1264 (2001).
228. Hurley, J. H. ESCRT complexes and the biogenesis of multivesicular bodies. *Curr. Opin. Cell Biol.* **20,** 4–11 (2008).
229. Trajkovic, K. *et al.* Ceramide triggers budding of exosome vesicles into multivesicular endosomes. *Science* **319,** 1244–1247 (2008).
230. Gibbings, D. J., Ciaudo, C., Erhardt, M. & Voinnet, O. Multivesicular bodies associate with components of miRNA effector complexes and modulate miRNA activity. *Nat. Cell Biol.* **11,** 1143–1149 (2009).
231. Batagov, A. O., Kuznetsov, Vladimir A & Kurochkin, Igor V. Identification of nucleotide patterns enriched in secreted RNAs as putative cis-acting elements targeting them to exosome nano-vesicles. *BMC Genomics* **12,** S18 (2011).
232. Morelli, A. E. *et al.* Endocytosis, intracellular sorting, and processing of exosomes by dendritic cells. *Blood* **104,** 3257–3266 (2004).
233. Skog, J. *et al.* Glioblastoma microvesicles transport RNA and proteins that promote tumour growth and provide diagnostic biomarkers. *Nat. Cell Biol.* **10,** 1470–1476 (2008).
234. Skog, J. *et al.* Glioblastoma microvesicles transport RNA and proteins that promote tumour growth and provide diagnostic biomarkers. *Nat. Cell Biol.* **10,** 1470–1476 (2008).
235. Ohshima, K. *et al.* Let-7 microRNA family is selectively secreted into the extracellular environment via exosomes in a metastatic gastric cancer cell line. *PLoS ONE* **5,** e13247 (2010).
236. Balaj, L. *et al.* Tumour microvesicles contain retrotransposon elements and amplified oncogene sequences. *Nat Commun* **2,** 180 (2011).
237. Dwivedi, P. *et al.* Pharmacokinetics study of arteether loaded solid lipid nanoparticles: an improved oral bioavailability in rats. *Int J Pharm* **466,** 321–327 (2014).
238. Singh, G. & Pai, R. S. Optimized PLGA nanoparticle platform for orally dosed trans-resveratrol with enhanced bioavailability potential. *Expert Opin Drug Deliv* **11,** 647–659 (2014).

239. Joshi, G., Kumar, A. & Sawant, K. Enhanced bioavailability and intestinal uptake of Gemcitabine HCl loaded PLGA nanoparticles after oral delivery. *Eur J Pharm Sci* **60,** 80–89 (2014).
240. Kumar, V. *et al.* Shielding of Lipid Nanoparticles for siRNA Delivery: Impact on Physicochemical Properties, Cytokine Induction, and Efficacy. *Mol Ther Nucleic Acids* **3,** e210 (2014).
241. Mokhtarzadeh, A. *et al.* Recent advances on biocompatible and biodegradable nanoparticles as gene carriers. *Expert Opin Biol Ther* (2016). doi:10.1517/14712598.2016.1169269
242. Amalfitano, A. *et al.* Production and characterization of improved adenovirus vectors with the E1, E2b, and E3 genes deleted. *J. Virol.* **72,** 926–933 (1998).
243. Marks, W. J., Jr *et al.* Safety and tolerability of intraputaminal delivery of CERE-120 (adeno-associated virus serotype 2-neurturin) to patients with idiopathic Parkinson's disease: an open-label, phase I trial. *Lancet Neurol* **7,** 400–408 (2008).
244. Byrnes, A. P., MacLaren, R. E. & Charlton, H. M. Immunological instability of persistent adenovirus vectors in the brain: peripheral exposure to vector leads to renewed inflammation, reduced gene expression, and demyelination. *J. Neurosci.* **16,** 3045–3055 (1996).
245. Gonzalez, S. C. *et al.* Readministration of adenoviral gene delivery to dopamine neurons. *Neuroreport* **18,** 1609–1614 (2007).
246. Kruis, W. *et al.* Maintaining remission of ulcerative colitis with the probiotic Escherichia coli Nissle 1917 is as effective as with standard mesalazine. *Gut* **53,** 1617–1623 (2004).
247. Paukner, S. *et al.* DNA-Loaded Bacterial Ghosts Efficiently Mediate Reporter Gene Transfer and Expression in Macrophages. *Mol Ther* **11,** 215–223 (2005).
248. Pannell, D. & Ellis, J. Silencing of gene expression: implications for design of retrovirus vectors. *Rev. Med. Virol.* **11,** 205–217 (2001).
249. Jepson, C. D. & March, J. B. Bacteriophage lambda is a highly stable DNA vaccine delivery vehicle. *Vaccine* **22,** 2413–2419 (2004).
250. Larocca, D., Jensen-Pergakes, K., Burg, M. A. & Baird, A. Receptor-targeted gene delivery using multivalent phagemid particles. *Mol. Ther.* **3,** 476–484 (2001).
251. Larocca, D., Witte, A., Johnson, W., Pierce, G. F. & Baird, A. Targeting bacteriophage to mammalian cell surface receptors for gene delivery. *Hum. Gene Ther.* **9,** 2393–2399 (1998).
252. Geier, M. R., Trigg, M. E. & Merril, C. R. Fate of bacteriophage lambda in non-immune germ-free mice. *Nature* **246,** 221–223 (1973).
253. Zimmermann, T. S. *et al.* RNAi-mediated gene silencing in non-human primates. *Nature* **441,** 111–114 (2006).
254. Semple, S. C. *et al.* Rational design of cationic lipids for siRNA delivery. *Nat. Biotechnol.* **28,** 172–176 (2010).
255. Li, S. *et al.* Dynamic changes in the characteristics of cationic lipidic vectors after exposure to mouse serum: implications for intravenous lipofection. *Gene Ther.* **6,** 585–594 (1999).
256. Albanese, A., Tang, P. S. & Chan, W. C. W. The effect of nanoparticle size, shape, and surface chemistry on biological systems. *Annu Rev Biomed Eng* **14,** 1–16 (2012).
257. Kim, S.-H. *et al.* Exosomes derived from IL-10-treated dendritic cells can suppress inflammation and collagen-induced arthritis. *J. Immunol.* **174,** 6440–6448 (2005).

258. Lai, R. C. *et al.* Exosome secreted by MSC reduces myocardial ischemia/reperfusion injury. *Stem Cell Res* **4,** 214–222 (2010).
259. Record, M., Subra, C., Silvente-Poirot, S. & Poirot, M. Exosomes as intercellular signalosomes and pharmacological effectors. *Biochem. Pharmacol.* **81,** 1171–1182 (2011).
260. Subra, C., Laulagnier, K., Perret, B. & Record, M. Exosome lipidomics unravels lipid sorting at the level of multivesicular bodies. *Biochimie* **89,** 205–212 (2007).
261. Akao, Y. *et al.* Microvesicle-mediated RNA molecule delivery system using monocytes/macrophages. *Mol. Ther.* **19,** 395–399 (2011).
262. Zhang, Y. *et al.* Secreted monocytic miR-150 enhances targeted endothelial cell migration. *Mol. Cell* **39,** 133–144 (2010).
263. Pan, Q. *et al.* Hepatic cell-to-cell transmission of small silencing RNA can extend the therapeutic reach of RNA interference (RNAi). *Gut* (2011). doi:10.1136/gutjnl-2011-300449
264. Wahlgren, J. *et al.* Plasma exosomes can deliver exogenous short interfering RNA to monocytes and lymphocytes. *Nucleic Acids Res.* **40,** e130 (2012).
265. Greco, K. A. *et al.* PLK-1 Silencing in Bladder Cancer by siRNA Delivered with Exosomes. *Urology* (2016). doi:10.1016/j.urology.2016.01.028
266. Shtam, T. A. *et al.* Exosomes are natural carriers of exogenous siRNA to human cells in vitro. *Cell Commun. Signal* **11,** 88 (2013).
267. Cooper, J. M. *et al.* Systemic exosomal siRNA delivery reduced alpha-synuclein aggregates in brains of transgenic mice. *Mov. Disord.* **29,** 1476–1485 (2014).
268. Bianco, N. R., Kim, S. H., Ruffner, M. A. & Robbins, P. D. Therapeutic effect of exosomes from indoleamine 2,3-dioxygenase-positive dendritic cells in collagen-induced arthritis and delayed-type hypersensitivity disease models. *Arthritis Rheum.* **60,** 380–389 (2009).
269. Kim, S. H., Bianco, N. R., Shufesky, W. J., Morelli, A. E. & Robbins, P. D. Effective treatment of inflammatory disease models with exosomes derived from dendritic cells genetically modified to express IL-4. *J. Immunol.* **179,** 2242–2249 (2007).
270. Zhuang, X. *et al.* Treatment of brain inflammatory diseases by delivering exosome encapsulated anti-inflammatory drugs from the nasal region to the brain. *Mol. Ther.* **19,** 1769–1779 (2011).
271. Timmers, L. *et al.* Reduction of myocardial infarct size by human mesenchymal stem cell conditioned medium. *Stem Cell Research* **1,** 129–137 (2008).
272. Chen, T. S. *et al.* Enabling a robust scalable manufacturing process for therapeutic exosomes through oncogenic immortalization of human ESC-derived MSCs. *J Transl Med* **9,** 47 (2011).
273. Zitvogel, L. *et al.* Eradication of established murine tumors using a novel cell-free vaccine: dendritic cell-derived exosomes. *Nat. Med.* **4,** 594–600 (1998).
274. Théry, C. *et al.* Indirect activation of naïve CD4+ T cells by dendritic cell-derived exosomes. *Nat. Immunol.* **3,** 1156–1162 (2002).
275. André, F. *et al.* Exosomes as potent cell-free peptide-based vaccine. I. Dendritic cell-derived exosomes transfer functional MHC class I/peptide complexes to dendritic cells. *J. Immunol.* **172,** 2126–2136 (2004).

276. Morse, M. A. *et al.* A phase I study of dexosome immunotherapy in patients with advanced non-small cell lung cancer. *J Transl Med* **3,** 9 (2005).
277. Escudier, B. *et al.* Vaccination of metastatic melanoma patients with autologous dendritic cell (DC) derived-exosomes: results of thefirst phase I clinical trial. *J Transl Med* **3,** 10 (2005).
278. Besse, B. *et al.* Dendritic cell-derived exosomes as maintenance immunotherapy after first line chemotherapy in NSCLC. *OncoImmunology* **5,** e1071008 (2016).
279. Chaput, N. *et al.* Exosomes as potent cell-free peptide-based vaccine. II. Exosomes in CpG adjuvants efficiently prime naive Tc1 lymphocytes leading to tumor rejection. *J. Immunol.* **172,** 2137–2146 (2004).
280. Wolfers, J. *et al.* Tumor-derived exosomes are a source of shared tumor rejection antigens for CTL cross-priming. *Nat. Med.* **7,** 297–303 (2001).
281. Altevogt, P., Bretz, N. P., Ridinger, J., Utikal, J. & Umansky, V. Novel insights into exosome-induced, tumor-associated inflammation and immunomodulation. *Semin. Cancer Biol.* **28,** 51–57 (2014).
282. Andre, F. *et al.* Malignant effusions and immunogenic tumour-derived exosomes. *Lancet* **360,** 295–305 (2002).
283. Dai, S. *et al.* Phase I clinical trial of autologous ascites-derived exosomes combined with GM-CSF for colorectal cancer. *Mol. Ther.* **16,** 782–790 (2008).
284. Yang, Y. *et al.* Increased induction of antitumor response by exosomes derived from interleukin-2 gene-modified tumor cells. *J. Cancer Res. Clin. Oncol.* **133,** 389–399 (2007).
285. Gusella, J. F. *et al.* Huntington's disease. *Cold Spring Harb. Symp. Quant. Biol.* **61,** 615–626 (1996).
286. Boudreau, R. L. *et al.* Nonallele-specific Silencing of Mutant and Wild-type Huntingtin Demonstrates Therapeutic Efficacy in Huntington's Disease Mice. *Mol Ther* **17,** 1053–1063 (2009).
287. Holen, T. Mechanisms of RNAi: mRNA cleavage fragments may indicate stalled RISC. *J RNAi Gene Silencing* **1,** 21–25 (2005).
288. Laufer, S. D., Recke, A. L., Veldhoen, S., Trampe, A. & Restle, T. Noncovalent peptide-mediated delivery of chemically modified steric block oligonucleotides promotes splice correction: quantitative analysis of uptake and biological effect. *Oligonucleotides* **19,** 63–80 (2009).
289. Myers, J. W., Jones, J. T., Meyer, T. & Ferrell, J. E. Recombinant Dicer efficiently converts large dsRNAs into siRNAs suitable for gene silencing. *Nat. Biotechnol.* **21,** 324–328 (2003).
290. Estrella, M. A., Kuo, F.-T. & Bailey, S. RNA-activated DNA cleavage by the Type III-B CRISPR-Cas effector complex. *Genes Dev.* **30,** 460–470 (2016).
291. Marchina, E. *et al.* Gene expression profile in fibroblasts of Huntington's disease patients and controls. *J. Neurol. Sci.* **337,** 42–46 (2014).
292. de Mezer, M., Wojciechowska, M., Napierala, M., Sobczak, K. & Krzyzosiak, W. J. Mutant CAG repeats of Huntingtin transcript fold into hairpins, form nuclear foci and are targets for RNA interference. *Nucleic Acids Res* **39,** 3852–3863 (2011).
293. Fiszer, A., Mykowska, A. & Krzyzosiak, W. J. Inhibition of mutant huntingtin expression by RNA duplex targeting expanded CAG repeats. *Nucl. Acids Res.* gkr156 (2011). doi:10.1093/nar/gkr156
294. Vandesompele, J. *et al.* Accurate normalization of real-time quantitative RT-PCR data by geometric averaging of multiple internal control genes. *Genome Biol.* **3,** RESEARCH0034 (2002).

295. Wu, H. *et al.* Determination of the role of the human RNase H1 in the pharmacology of DNA-like antisense drugs. *J. Biol. Chem.* **279,** 17181–17189 (2004).
296. Ravikumar, B. *et al.* Inhibition of mTOR induces autophagy and reduces toxicity of polyglutamine expansions in fly and mouse models of Huntington disease. *Nat. Genet.* **36,** 585–595 (2004).
297. Kan, J. L. & Green, M. R. Pre-mRNA splicing of IgM exons M1 and M2 is directed by a juxtaposed splicing enhancer and inhibitor. *Genes Dev.* **13,** 462–471 (1999).
298. Cartegni, L., Wang, J., Zhu, Z., Zhang, M. Q. & Krainer, A. R. ESEfinder: A web resource to identify exonic splicing enhancers. *Nucleic Acids Res.* **31,** 3568–3571 (2003).
299. Smith, P. J. *et al.* An increased specificity score matrix for the prediction of SF2/ASF-specific exonic splicing enhancers. *Hum. Mol. Genet.* **15,** 2490–2508 (2006).
300. Fairbrother, W. G., Yeh, R.-F., Sharp, P. A. & Burge, C. B. Predictive identification of exonic splicing enhancers in human genes. *Science* **297,** 1007–1013 (2002).
301. Cooper, J. K. *et al.* Truncated N-terminal fragments of huntingtin with expanded glutamine repeats form nuclear and cytoplasmic aggregates in cell culture. *Hum. Mol. Genet.* **7,** 783–790 (1998).
302. Geary, R. S., Yu, R. Z. & Levin, A. A. Pharmacokinetics of phosphorothioate antisense oligodeoxynucleotides. *Curr Opin Investig Drugs* **2,** 562–573 (2001).
303. Braasch, D. A. *et al.* Biodistribution of phosphodiester and phosphorothioate siRNA. *Bioorg. Med. Chem. Lett.* **14,** 1139–1143 (2004).
304. Harborth, J. *et al.* Sequence, chemical, and structural variation of small interfering RNAs and short hairpin RNAs and the effect on mammalian gene silencing. *Antisense Nucleic Acid Drug Dev.* **13,** 83–105 (2003).
305. Sud, R., Geller, E. T. & Schellenberg, G. D. Antisense-mediated Exon Skipping Decreases Tau Protein Expression: A Potential Therapy For Tauopathies. *Mol Ther Nucleic Acids* **3,** e180 (2014).
306. Brogna, S. & Wen, J. Nonsense-mediated mRNA decay (NMD) mechanisms. *Nat. Struct. Mol. Biol.* **16,** 107–113 (2009).
307. Gagnon, K. T. HD Therapeutics - CHDI Fifth Annual Conference. *IDrugs* **13,** 219–223 (2010).
308. Koshkin, A. A. *et al.* LNA (Locked Nucleic Acids): Synthesis of the adenine, cytosine, guanine, 5-methylcytosine, thymine and uracil bicyclonucleoside monomers, oligomerisation, and unprecedented nucleic acid recognition. *Tetrahedron* **54,** 3607–3630 (1998).
309. Wahlestedt, C. *et al.* Potent and nontoxic antisense oligonucleotides containing locked nucleic acids. *Proc. Natl. Acad. Sci. U.S.A.* **97,** 5633–5638 (2000).
310. Sledz, C. A. & Williams, B. R. G. RNA interference and double-stranded-RNA-activated pathways. *Biochem. Soc. Trans.* **32,** 952–956 (2004).
311. Pebernard, S. & Iggo, R. D. Determinants of interferon-stimulated gene induction by RNAi vectors. *Differentiation* **72,** 103–111 (2004).
312. Wu, X. *et al.* Genome-wide binding of the CRISPR endonuclease Cas9 in mammalian cells. *Nat. Biotechnol.* **32,** 670–676 (2014).
313. Squitieri, F. *et al.* Homozygosity for CAG mutation in Huntington disease is associated with a more severe clinical course. *Brain* **126,** 946–955 (2003).

314. Kordasiewicz, H. B. *et al.* Sustained therapeutic reversal of Huntington's disease by transient repression of huntingtin synthesis. *Neuron* **74,** 1031–1044 (2012).
315. Hu, J. *et al.* Inhibiting Expression of Mutant Huntingtin and Ataxin-3 by Targeting Expanded CAG Repeat RNAs. *Nat Biotechnol* **27,** 478–484 (2009).
316. Valadi, H. *et al.* Exosome-mediated transfer of mRNAs and microRNAs is a novel mechanism of genetic exchange between cells. *Nat. Cell Biol.* **9,** 654–659 (2007).
317. Trajkovic, K. *et al.* Ceramide triggers budding of exosome vesicles into multivesicular endosomes. *Science* **319,** 1244–1247 (2008).
318. Harding, C., Heuser, J. & Stahl, P. Receptor-mediated endocytosis of transferrin and recycling of the transferrin receptor in rat reticulocytes. *J. Cell Biol.* **97,** 329–339 (1983).
319. Kanada, M. *et al.* Differential fates of biomolecules delivered to target cells via extracellular vesicles. *Proc. Natl. Acad. Sci. U.S.A.* **112,** E1433-1442 (2015).
320. Grange, C. *et al.* Biodistribution of mesenchymal stem cell-derived extracellular vesicles in a model of acute kidney injury monitored by optical imaging. *Int. J. Mol. Med.* **33,** 1055–1063 (2014).
321. Lai, C. P. *et al.* Dynamic biodistribution of extracellular vesicles in vivo using a multimodal imaging reporter. *ACS Nano* **8,** 483–494 (2014).
322. Takahashi, Y. *et al.* Visualization and in vivo tracking of the exosomes of murine melanoma B16-BL6 cells in mice after intravenous injection. *J. Biotechnol.* **165,** 77–84 (2013).
323. Smyth, T. *et al.* Biodistribution and delivery efficiency of unmodified tumor-derived exosomes. *J Control Release* **199,** 145–155 (2015).
324. Ohno, S. *et al.* Systemically injected exosomes targeted to EGFR deliver antitumor microRNA to breast cancer cells. *Mol. Ther.* **21,** 185–191 (2013).
325. Tian, Y. *et al.* A doxorubicin delivery platform using engineered natural membrane vesicle exosomes for targeted tumor therapy. *Biomaterials* **35,** 2383–2390 (2014).
326. Wiklander, O. P. B. *et al.* Extracellular vesicle in vivo biodistribution is determined by cell source, route of administration and targeting. *J Extracell Vesicles* **4,** 26316 (2015).
327. Mathivanan, S. & Simpson, R. J. ExoCarta: A compendium of exosomal proteins and RNA. *Proteomics* **9,** 4997–5000 (2009).
328. Quah, B. J. C. & O'Neill, H. C. The immunogenicity of dendritic cell-derived exosomes. *Blood Cells Mol. Dis.* **35,** 94–110 (2005).
329. Maurisse, R. *et al.* Comparative transfection of DNA into primary and transformed mammalian cells from different lineages. *BMC Biotechnol.* **10,** 9 (2010).
330. Mazarakis, N. D. *et al.* Rabies virus glycoprotein pseudotyping of lentiviral vectors enables retrograde axonal transport and access to the nervous system after peripheral delivery. *Hum. Mol. Genet.* **10,** 2109–2121 (2001).
331. Kumar, P. *et al.* Transvascular delivery of small interfering RNA to the central nervous system. *Nature* **448,** 39–43 (2007).
332. Zadran, S., Akopian, G., Zadran, H., Walsh, J. & Baudry, M. RVG-mediated calpain2 gene silencing in the brain impairs learning and memory. *Neuromolecular Med.* **15,** 74–81 (2013).

333. Simhadri, V. R. *et al.* Dendritic cells release HLA-B-associated transcript-3 positive exosomes to regulate natural killer function. *PLoS ONE* **3,** e3377 (2008).
334. Orihuela, C. J. *et al.* Laminin receptor initiates bacterial contact with the blood brain barrier in experimental meningitis models. *J. Clin. Invest.* **119,** 1638–1646 (2009).
335. Liu, Y. *et al.* A bacteria deriving peptide modified dendrigraft poly-l-lysines (DGL) self-assembling nanoplatform for targeted gene delivery. *Mol. Pharm.* **11,** 3330–3341 (2014).
336. Casy, A. F. & Parfitt, R. T. *Opioid Analgesics*. (Springer US, 1986).
337. Costantino, L. *et al.* Peptide-derivatized biodegradable nanoparticles able to cross the blood-brain barrier. *J Control Release* **108,** 84–96 (2005).
338. Franke, H., Galla, H. & Beuckmann, C. T. Primary cultures of brain microvessel endothelial cells: a valid and flexible model to study drug transport through the blood-brain barrier in vitro. *Brain Res. Brain Res. Protoc.* **5,** 248–256 (2000).
339. Trickler, W. J. *et al.* Silver nanoparticle induced blood-brain barrier inflammation and increased permeability in primary rat brain microvessel endothelial cells. *Toxicol. Sci.* **118,** 160–170 (2010).
340. Webber, J. & Clayton, A. How pure are your vesicles? *J Extracell Vesicles* **2,** (2013).
341. Allen, T. M., Austin, G. A., Chonn, A., Lin, L. & Lee, K. C. Uptake of liposomes by cultured mouse bone marrow macrophages: influence of liposome composition and size. *Biochimica et Biophysica Acta (BBA) - Biomembranes* **1061,** 56–64 (1991).
342. Allen, T. M. Mononuclear Phagocyte System Toxicity of drug carriers to the mononuclear phagocyte system. *Advanced Drug Delivery Reviews* **2,** 55–67 (1988).
343. Morishita, M. *et al.* Quantitative analysis of tissue distribution of the B16BL6-derived exosomes using a streptavidin-lactadherin fusion protein and iodine-125-labeled biotin derivative after intravenous injection in mice. *J Pharm Sci* **104,** 705–713 (2015).
344. Bala, S. *et al.* Biodistribution and function of extracellular miRNA-155 in mice. *Sci Rep* **5,** 10721 (2015).
345. Nordin, J. Z. *et al.* Ultrafiltration with size-exclusion liquid chromatography for high yield isolation of extracellular vesicles preserving intact biophysical and functional properties. *Nanomedicine* **11,** 879–883 (2015).
346. Hung, M. E. & Leonard, J. N. Stabilization of exosome-targeting peptides via engineered glycosylation. *J. Biol. Chem.* **290,** 8166–8172 (2015).
347. Lotvall, J. & Valadi, H. Cell to cell signalling via exosomes through esRNA. *Cell Adh Migr* **1,** 156–158 (2007).
348. Bolukbasi, M. F. *et al.* miR-1289 and 'Zipcode'-like Sequence Enrich mRNAs in Microvesicles. *Mol Ther Nucleic Acids* **1,** e10 (2012).
349. Villarroya-Beltri, C. *et al.* Sumoylated hnRNPA2B1 controls the sorting of miRNAs into exosomes through binding to specific motifs. *Nat Commun* **4,** 2980 (2013).
350. Liu, D., Mori, A. & Huang, L. Role of liposome size and RES blockade in controlling biodistribution and tumor uptake of GM1-containing liposomes. *Biochim. Biophys. Acta* **1104,** 95–101 (1992).
351. Shultz, L. D. *et al.* Multiple defects in innate and adaptive immunologic function in NOD/LtSz-scid mice. *J. Immunol.* **154,** 180–191 (1995).

352. Bradley, A. J., Devine, D. V., Ansell, S. M., Janzen, J. & Brooks, D. E. Inhibition of liposome-induced complement activation by incorporated poly(ethylene glycol)-lipids. *Arch. Biochem. Biophys.* **357,** 185–194 (1998).
353. Wang, A. L. *et al.* Autophagy and Exosomes in the Aged Retinal Pigment Epithelium: Possible Relevance to Drusen Formation and Age-Related Macular Degeneration. *PLoS ONE* **4,** (2009).
354. Clayton, A., Harris, C. L., Court, J., Mason, M. D. & Morgan, B. P. Antigen-presenting cell exosomes are protected from complement-mediated lysis by expression of CD55 and CD59. *Eur. J. Immunol.* **33,** 522–531 (2003).
355. Gumbleton, M. & Audus, K. L. Progress and limitations in the use of in vitro cell cultures to serve as a permeability screen for the blood-brain barrier. *JPharmSci* **90,** 1681–1698 (2001).
356. Haney, M. J. *et al.* Exosomes as drug delivery vehicles for Parkinson's disease therapy. *Journal of Controlled Release* **207,** 18–30 (2015).
357. Soutschek, J. *et al.* Therapeutic silencing of an endogenous gene by systemic administration of modified siRNAs. *Nature* **432,** 173–178 (2004).
358. Wolfrum, C. *et al.* Mechanisms and optimization of in vivo delivery of lipophilic siRNAs. *Nat. Biotechnol.* **25,** 1149–1157 (2007).
359. Hattori, Y. *et al.* siRNA delivery into tumor cells by cationic cholesterol derivative-based nanoparticles and liposomes. *Biol. Pharm. Bull.* **38,** 30–38 (2015).
360. Fiszer, A., Mykowska, A. & Krzyzosiak, W. J. Inhibition of mutant huntingtin expression by RNA duplex targeting expanded CAG repeats. *Nucleic Acids Res* **39,** 5578–5585 (2011).
361. Li, J. *et al.* Serum-free culture alters the quantity and protein composition of neuroblastoma-derived extracellular vesicles. *J Extracell Vesicles* **4,** 26883 (2015).
362. Momen-Heravi, F., Bala, S., Bukong, T. & Szabo, G. Exosome-mediated delivery of functionally active miRNA-155 inhibitor to macrophages. *Nanomedicine* **10,** 1517–1527 (2014).
363. Kooijmans, S. A. A. *et al.* Electroporation-induced siRNA precipitation obscures the efficiency of siRNA loading into extracellular vesicles. *J Control Release* **172,** 229–238 (2013).
364. Whitehead, K. A. *et al.* In vitro-in vivo translation of lipid nanoparticles for hepatocellular siRNA delivery. *ACS Nano* **6,** 6922–6929 (2012).
365. Somiya, M. *et al.* One-step scalable preparation method for non-cationic liposomes with high siRNA content. *Int J Pharm* **490,** 316–323 (2015).
366. Bolognani, F., Gallani, A.-I., Sokol, L., Baskin, D. S. & Meisner-Kober, N. mRNA stability alterations mediated by HuR are necessary to sustain the fast growth of glioma cells. *J. Neurooncol.* **106,** 531–542 (2012).
367. Alberts, B. *et al.* The Lipid Bilayer. (2002).
368. Papahadjopoulos, D., Nir, S. & Oki, S. Permeability properties of phospholipid membranes: effect of cholesterol and temperature. *Biochim. Biophys. Acta* **266,** 561–583 (1972).
369. Alvarez-Erviti, L. *et al.* Delivery of siRNA to the mouse brain by systemic injection of targeted exosomes. *Nat. Biotechnol.* **29,** 341–345 (2011).
370. Greco, K. A. *et al.* PLK-1 Silencing in Bladder Cancer by siRNA Delivered with Exosomes. *Urology* (2016). doi:10.1016/j.urology.2016.01.028

371. Shtam, T. A. *et al.* Exosomes are natural carriers of exogenous siRNA to human cells in vitro. *Cell Commun. Signal* **11,** 88 (2013).
372. Wahlgren, J. *et al.* Plasma exosomes can deliver exogenous short interfering RNA to monocytes and lymphocytes. *Nucleic Acids Res.* **40,** e130 (2012).
373. Stapulionis, R. Electric pulse-induced precipitation of biological macromolecules in electroporation. *Bioelectrochem Bioenerg* **48,** 249–254 (1999).
374. Ohno, S. *et al.* Systemically Injected Exosomes Targeted to EGFR Deliver Antitumor MicroRNA to Breast Cancer Cells. *Mol Ther* **21,** 185–191 (2013).
375. Van Deun, J. *et al.* The impact of disparate isolation methods for extracellular vesicles on downstream RNA profiling. *J Extracell Vesicles* **3,** (2014).
376. McConnell, L. C., Miksis, M. J. & Vlahovska, P. M. Continuum modeling of the electric-field-induced tension in deforming lipid vesicles. *The Journal of Chemical Physics* **143,** 243132 (2015).
377. Johnsen, K. B. *et al.* Evaluation of electroporation-induced adverse effects on adipose-derived stem cell exosomes. *Cytotechnology* (2016). doi:10.1007/s10616-016-9952-7
378. Lamichhane, T. N., Raiker, R. S. & Jay, S. M. Exogenous DNA Loading into Extracellular Vesicles via Electroporation is Size-Dependent and Enables Limited Gene Delivery. *Mol. Pharm.* **12,** 3650–3657 (2015).
379. Kanada, M. *et al.* Differential fates of biomolecules delivered to target cells via extracellular vesicles. *Proc. Natl. Acad. Sci. U.S.A.* **112,** E1433-1442 (2015).
380. Alterman, J. F. *et al.* Hydrophobically Modified siRNAs Silence Huntingtin mRNA in Primary Neurons and Mouse Brain. *Mol Ther Nucleic Acids* **4,** e266 (2015).
381. Chen, Y.-H. *et al.* Caveolin-1 Provides Palliation for Adverse Hepatic Reactions in Hypercholesterolemic Rabbits. *PLoS One* **9,** (2014).
382. Bennett, W. F. D., MacCallum, J. L., Hinner, M. J., Marrink, S. J. & Tieleman, D. P. Molecular view of cholesterol flip-flop and chemical potential in different membrane environments. *J. Am. Chem. Soc.* **131,** 12714–12720 (2009).
383. Rosa, P. & Fratangeli, A. Cholesterol and synaptic vesicle exocytosis. *Commun Integr Biol* **3,** 352–353 (2010).
384. Yoshinari, K., Miyagishi, M. & Taira, K. Effects on RNAi of the tight structure, sequence and position of the targeted region. *Nucleic Acids Res.* **32,** 691–699 (2004).
385. Hoerter, J. A. H. & Walter, N. G. Chemical modification resolves the asymmetry of siRNA strand degradation in human blood serum. *RNA* **13,** 1887–1893 (2007).
386. Haupenthal, J., Baehr, C., Kiermayer, S., Zeuzem, S. & Piiper, A. Inhibition of RNAse A family enzymes prevents degradation and loss of silencing activity of siRNAs in serum. *Biochem. Pharmacol.* **71,** 702–710 (2006).
387. Li, S.-D. & Huang, L. Nanoparticles evading the reticuloendothelial system: Role of the supported bilayer. *Biochimica et Biophysica Acta (BBA) - Biomembranes* **1788,** 2259–2266 (2009).
388. *Biotechnology and Biopharmaceuticals: Transforming Proteins and Genes into Drugs*. (John Wiley & Sons, 2013).

389. Smyth, T. *et al.* Surface functionalization of exosomes using click chemistry. *Bioconjug. Chem.* **25,** 1777–1784 (2014).
390. Tannous, B. A. Gaussia luciferase reporter assay for monitoring of biological processes in culture and in vivo. *Nat Protoc* **4,** 582–591 (2009).
391. HALFORD, B. NANOTOXICITY In vivo study of fullerenes contradicts in vitro data. *Chem. Eng. News Archive* **85,** 11a (2007).
392. Kannan, K. *et al.* Lysosome-associated membrane proteins h-LAMP1 (CD107a) and h-LAMP2 (CD107b) are activation-dependent cell surface glycoproteins in human peripheral blood mononuclear cells which mediate cell adhesion to vascular endothelium. *Cell. Immunol.* **171,** 10–19 (1996).
393. Greco, K. A. *et al.* PLK-1 Silencing in Bladder Cancer by siRNA Delivered With Exosomes. *Urology* (2016). doi:10.1016/j.urology.2016.01.028
394. Kooijmans, S. A. A. *et al.* Electroporation-induced siRNA precipitation obscures the efficiency of siRNA loading into extracellular vesicles. *J Control Release* **172,** 229–238 (2013).
395. Johnsen, K. B. *et al.* Evaluation of electroporation-induced adverse effects on adipose-derived stem cell exosomes. *Cytotechnology* (2016). doi:10.1007/s10616-016-9952-7
396. Hood, J. L., Scott, M. J. & Wickline, S. A. Maximizing exosome colloidal stability following electroporation. *Anal. Biochem.* **448,** 41–49 (2014).
397. Hadinoto, K., Sundaresan, A. & Cheow, W. S. Lipid-polymer hybrid nanoparticles as a new generation therapeutic delivery platform: a review. *Eur J Pharm Biopharm* **85,** 427–443 (2013).
398. Qin, B., Chen, Z., Jin, W. & Cheng, K. Development of cholesteryl peptide micelles for siRNA delivery. *J Control Release* **172,** 159–168 (2013).
399. Zhang, Y. *et al.* Secreted monocytic miR-150 enhances targeted endothelial cell migration. *Mol. Cell* **39,** 133–144 (2010).
400. Saari, H. *et al.* Microvesicle- and exosome-mediated drug delivery enhances the cytotoxicity of Paclitaxel in autologous prostate cancer cells. *Journal of Controlled Release* **220, Part B,** 727–737 (2015).
401. Sun, D. *et al.* A novel nanoparticle drug delivery system: the anti-inflammatory activity of curcumin is enhanced when encapsulated in exosomes. *Mol. Ther.* **18,** 1606–1614 (2010).
402. Bryniarski, K. *et al.* Antigen-specific, antibody-coated, exosome-like nanovesicles deliver suppressor T-cell microRNA-150 to effector T cells to inhibit contact sensitivity. *J. Allergy Clin. Immunol.* **132,** 170–181 (2013).
403. Taylor, D. D. & Shah, S. Methods of isolating extracellular vesicles impact down-stream analyses of their cargoes. *Methods* **87,** 3–10 (2015).
404. Gould, S. J. & Raposo, G. As we wait: coping with an imperfect nomenclature for extracellular vesicles. *J Extracell Vesicles* **2,** (2013).
405. Koppers-Lalic, D. *et al.* Nontemplated Nucleotide Additions Distinguish the Small RNA Composition in Cells from Exosomes. *Cell Reports* **8,** 1649–1658 (2014).
406. Stengel, G., Zahn, R. & Höök, F. DNA-induced programmable fusion of phospholipid vesicles. *J. Am. Chem. Soc.* **129,** 9584–9585 (2007).

407. Bailey, A. L. & Sullivan, S. M. Efficient encapsulation of DNA plasmids in small neutral liposomes induced by ethanol and calcium. *Biochimica et Biophysica Acta (BBA) - Biomembranes* **1468,** 239–252 (2000).
408. Peterson, M. F., Otoc, N., Sethi, J. K., Gupta, A. & Antes, T. J. Integrated systems for exosome investigation. *Methods* **87,** 31–45 (2015).
409. Alvarez-Erviti, L. *et al.* Delivery of siRNA to the mouse brain by systemic injection of targeted exosomes. *Nat. Biotechnol.* **29,** 341–345 (2011).
410. Rana, S., Yue, S., Stadel, D. & Zöller, M. Toward tailored exosomes: the exosomal tetraspanin web contributes to target cell selection. *Int. J. Biochem. Cell Biol.* **44,** 1574–1584 (2012).
411. Laulagnier, K. *et al.* Mast cell- and dendritic cell-derived exosomes display a specific lipid composition and an unusual membrane organization. *Biochem J* **380,** 161–171 (2004).
412. Gabizon, A. & Papahadjopoulos, D. The role of surface charge and hydrophilic groups on liposome clearance in vivo. *Biochim. Biophys. Acta* **1103,** 94–100 (1992).
413. Moghimi, S. M. & Hamad, I. Liposome-Mediated Triggering of Complement Cascade. *Journal of Liposome Research* **18,** 195–209 (2008).
414. Jang, S. C. *et al.* Bioinspired Exosome-Mimetic Nanovesicles for Targeted Delivery of Chemotherapeutics to Malignant Tumors. *ACS Nano* **7,** 7698–7710 (2013).
415. Yoon, J. *et al.* Generation of nanovesicles with sliced cellular membrane fragments for exogenous material delivery. *Biomaterials* **59,** 12–20 (2015).
416. Alvarez-Erviti, L. *et al.* Lysosomal dysfunction increases exosome-mediated alpha-synuclein release and transmission. *Neurobiol. Dis.* **42,** 360–367 (2011).
417. Rajendran, L. *et al.* Alzheimer's disease beta-amyloid peptides are released in association with exosomes. *Proc. Natl. Acad. Sci. U.S.A.* **103,** 11172–11177 (2006).
418. Fevrier, B. *et al.* Cells release prions in association with exosomes. *Proc. Natl. Acad. Sci. U.S.A.* **101,** 9683–9688 (2004).